Development of New Photoiniator Systems for Polymerization with Visible Light

Luciano Héctor Di Stefano

UNIVERSITÉ DE HAUTE ALSACE

Year/Année: 2015

THESIS

Defended by/ Presentée par

Luciano Héctor Di Stefano

To obtain the title/ Pour l'obtention du titre de :

DOCTEUR EN CHIMIE-PHYSIQUE

Subject/Sujet :

« DEVELOPPEMENT DE NOUVEAUX SYSTEMES PHOTOAMORCEURS DE POLYMERISATION SOUS LUMIERE VISIBLE. »

Soutenue le 26 Novembre 2015 devant la Commission d'Examen:

Dr. Céline FROCHOT (Rapporteur)

Directeur de Recherche CNRS Laboratoire Réactions et Génie des Procédés (LRGP – ENSIC).

Dr. Claire RICHARD (Rapporteur)

Directeur de Recherche CNRS Institut de Chimie de Clermont-Ferrand (ICCF).

Prof. Xavier ALLONAS (Directeur de thèse)

Université de Haute Alsace, Laboratoire de Photochimie et d'Ingénierie Macromoléculaires (LPIM).

Prof. Christian LEY (Codirecteur de thèse)

Université de Haute Alsace. Laboratoire de Photochimie et d'Ingénierie Macromoléculaires (LPIM).

This thesis work is the result of three years of hard work. It was a process of maturation and personal growth, which could not have been completed without the help of many people who I would like to thank within these pages.

To Professor Xavier Allonas, for admitting me in his research group, giving me this unique possibility. For his kindness and will to helping me in every situation. For his good humor and optimism in all our meetings. This was a never-ending fountain of inspiration and my main source of motivation.

To Professor Christian Ley, for all that he taught me, for being always able to supervise my work and listen to my questions. For the endless and invaluable discussions we had and all the time he devoted to my work during these years. I also want to thank him for the encouragement he gave me all along these three years.

To Doctor Claire Richard and Doctor Céline Frochot, for accepting to evaluate my thesis work and being a part of my jury committee.

To Doctor Olga Tarzi. This thesis would never have been realized without her advice. To the excellent person she is, her wisdom, and her tireless guidance.

To my parents, for letting me become the person I am today. For all the support and freedom they gave me.

To my beloved sisters. Myself would be incomplete without them. They are the most precious thing I have.

To Susana Raggio, who always helped me without any hesitation whenever I was in need of help. A lifetime would not be long enough to give back everything she gave me.

To Professor Silvia Braslavsky. Meeting her in the 25th IUPAC Congress of Photochemistry enlightened me. I admire the immense work she has done for science and I thank her for her invaluable advices.

To Doctor Thomas Rölle. His constant challenges were essential for the development of the work here presented. For his help and good predisposition to answer my needs. For his outstanding energy and unmatched good humor.

To Prof. Patrice Bordat, who made the Astrazone Orange calculations, which were essential to understand the photophysics of this compound.

To all the inspirational people who marked my decisions and helped me chose to follow the path I am going through.

To Julien Christmann, Hatice Sahin and Morgane Bischoff, who contributed to this work and whom I appreciate very much.

To the technical staff of the LPIM, especially to Mlle. Marjolaine Bessieres, for her invaluable help inside the laboratory and her good predisposition.

To my colleagues. To the ones who were there the first day I stepped in the laboratory and to the ones who are there now. All of them will be a part of me wherever I go, and I hope a part of me will be with them as well.

To Caroline Rocco, Vincent Charlot and Diane Fischer, who transited their pathway through the LPIM along with me. I am happy to have shared those times together with three amazing people as they are.

To my friends in Mulhouse, especially to Lucía Blas, Diego Alvite, Carol Seguras, Patxi Garra and Beatriz García, for all the weekends and holidays spent together and for making me feel in Mulhouse as if I were home.

To my Argentinian friends I met in Mulhouse, especially to Matías Callara, María Laura Paz, Tamara Di Carlantonio and Nair Tomas who made me feel that Argentina was just around the corner.

To my friends in Argentina, who made me feel that I will always feel home wherever I am with them.

To my flat mates, who always supported me and heard my stories every day back home.

To all the amazing people I met during these three years. To all of them who helped me to discover the many things that I have learned during this period of time.

Abstract

Photopolymerization is a technology that is gaining more and more importance due to its numerous applications and its advantages compared to thermic polymerization. This chemical process requires compounds called photoinitiators, which absorb light and produce the initiation of the radical polymerization.

The development of photoinitiating systems (PIS) which are able to absorb visible light have an increasing interest due to its industrial applications, such as holographic recording.

During this thesis, many PIS were studied, from its photophysical properties to its application in acrylate polymerization.

There are many different types of photoinitiators. The most classical ones are Type I PI, which are molecules that overcome homolytic cleavage from their excited state, generating initiating radicals immediately after photon absorption. Type II PI, in contrast, are composed by two molecules: one that absorbs the photon, and other that will react with the excited state of the first via electron transfer or hydrogen transfer, generating radicals that will be able to initiate polymerization. In last place, there are the most efficient Photocyclic Initiating Systems (PCIS) whose mechanism is more complicated and will be widely discussed within these pages. A state of the art of the PIS available up to date is made in the first chapter.

Given the importance of the properties of the molecules involved in the photoinitiating process, the studies of the photophysical properties of a Photoinitiator, the Astrazone Orange (AO), are shown. It was found that this molecule suffers an isomerization process from its excited state, which then comes slowly back to the more stable conformer. This process being viscosity-dependent makes AO a suitable photoinitiator for polymerization with visible light in highly viscous media.

The last three chapters of this thesis are devoted to the study of a novel technique called Pulsed Laser Polymerization (PLP). This technique consists in the irradiation of the samples with a short duration pulsed laser, which allows the separation of the initiation steps of the polymerization reaction from the steps of propagation and termination.

A simple Type I PI was used as a model to study the properties of this technique of polymerization. The monomer conversion was registered by RT-FTIR and analyzed. To a better understanding of these results, a mathematical model was developed. Thanks to it, it was possible to collect valuable information about propagation and termination rate constants (k_p and k_t, respectively), the variation of viscosity with conversion and other aspects relatives to PLP mechanism.

Furthermore, the efficiency of many visible light PIS was studied by PLP. Their performance was compared and studied and contrasted with the classical continuous irradiation mode (CW). The characteristics that a PIS must have in order to show efficient polymerization in PLP mode were found and discussed.

Finally, the effect of formulation viscosity in PLP and CW was analyzed by diluting the sample with different amounts of DMSO. In PLP, it was seen that the highest conversion is found for the most concentrated samples, while the opposite effect is noticed in CW. This result is attributed to the different conditions given by the difference in irradiation methods.

Résumé

La photopolymérisation est une technologie qui gagne de plus en plus d'importance de par ses nombreuses applications et ses énormes avantages par rapport à la polymérisation thermique tels que le respect de l'environnement, des coûts économiques maitrisés car la technologie est mise en œuvre à température ambiante et ne requiert qu'une faible consommation d'énergie. De plus, elle n'utilise pas ou très peu de solvants, d'où la réduction d'émission de produits polluants. Le processus de polymérisation photochimique présente également l'avantage d'être très rapide : en effet les réactions de photopolymérisation sont souvent rapides voire même quasi instantanées. De plus le procédé de polymérisation devient photolatent : la polymérisation impliquant les formulations actives seulement en présence de lumière, la réaction peut être déclenchée « quasi à la demande ». Ce processus chimique nécessite des composants nommés « photoamorceurs », lesquels absorbent la lumière et produisent le démarrage de la réaction de polymérisation. En particulier, le développement de systèmes photoamorceurs capables d'absorber de la lumière visible a un intérêt croissant pour différentes applications industrielles, notamment l'holographie. Dans la cadre de cette thèse, des diverses systèmes photoamorceurs contenant un colorant et un ou deux co-amorceurs, qui après réaction avec les états excités des colorants génèrent les radicaux actifs, ont été étudiés, depuis leurs propriétés photophysiques fondamentales et moléculaires, jusqu'aux applications et performances pour la polymérisation des résines acrylates.

Cette thèse est articulée autour de six chapitres. Dans le premier chapitre une introduction et une étude bibliographique des différents systèmes photoamorceurs développés ces dernières années sont présentées et comparés. Les chapitres deux et trois sont consacrés à l'étude des propriétés photochimiques et photophysiques réalisés sur des photoamorceurs absorbant de la lumière ultraviolette et visible respectivement. Les techniques utilisés dans ces chapitres incluent, mais ne sont pas limités à, la spectroscopie d'absorption UV-Vis stationnaire, la fluorescence, la photolyse éclaire (LFP), la fluorescence résolue en temps par comptage de photon unique (TC-SPC), la spectroscopie ultrarapide nanoseconde et femtoseconde, la spectroscopie de résonance paramagnétique électronique (EPR), entre autres.

Le chapitre deux porte sur l'étude de la photophysique d'un colorant de type cyanine : l'astrazone Orange R (AO R). La photophysique de ce colorant n'est pas connue et une étude exhaustive a été menée avec des spectroscopies ultra rapides (femtoseconde) ainsi que par modélisation moléculaire. Malgré sa photophysique compliquée ce colorant, fonctionne comme un photoamorceur très efficace dans la région bleue du spectre électromagnétique.

Les chapitres suivants forment une deuxième partie de la thèse dédiée à l'étude des mécanismes d'amorçage de photopolymérisation, dont le chapitre quatre aborde le cas d'irradiation le plus « traditionnel », qui est l'irradiation en mode continu (ou CW). Est ensuite abordé l'étude de la polymérisation sous irradiation pulsée ultra-courte : dans cette partie la source d'irradiation continue classique est remplacée par un laser Nd :Yag qui produit des impulsions lumineuses d'une durée de quelques 9-10 nanosecondes. Cette polymérisation avec laser pulsé ou PLP est très originale et sera étudiée par spectroscopie infrarouge à transformée de Fourier résolue en temps (RT-FTIR).

Dans le chapitre trois, donc, on retrouve les études réalisés avec différents types de systèmes photoamorceurs visibles. Ainsi, les propriétés des colorants capables d'absorber de la lumière visible à différentes longueurs d'onde ont été étudiées dans des systèmes photoamorceurs à deux et trois composants. Aussi, l'efficacité supérieure des systèmes à trois composants de type photocycliques (PCIS selon ses sigles en Anglais) a été montrée et démontrée par photolyse éclaire. La figure 4 montre le schéma de réaction d'un système photocyclique typique.

On trouve aussi dans le chapitre trois, un modèle cinétique complet correspondant au mécanisme qui a été developé. Il permet de modéliser et calculer les rendements quantiques en radicaux, c'est-à-dire l'efficacité des systèmes photoamorceurs utilisés simplement par la connaissance des constantes de vitesse des processus ayant lieu pendant le photoamorçage de la polymérisation. Ce modèle a été validée par des expériences de quantification de la photolyse du colorant dans des solutions contenant des systèmes photoamorceurs.

Pendant la réalisation de cette thèse, un projet de recherche avec la compagnie allemande Bayer Material Science a été développé. Ce projet porte sur l'utilisation d'impulsions laser nanoseconde pour amorcer des réactions de polymérisation instantanées. Le chapitre quatre introduis une étude théorique et le développement d'un modèle mathématique de la polymérisation pulsée (PLP). Pour conforter le modèle aux résultats expérimentaux des mesures avec un photoamorceur très simple, le TPO, ont été réalisées. Les principaux caractéristiques de ce type d'irradiation sont présentés ainsi que ces différences et similitudes avec l'irradiation CW. Comme dans le chapitre précédent, un modèle théorique est présentée ici, cette fois avec l'objective de clarifier le mécanisme qui a lieu en PLP et qui fait que cette méthode d'irradiation soit si diffèrent de la méthode « traditionnelle » d'irradiation ou CW.

Le chapitre numéro cinq aborde les études réalisées avec des systèmes photoamorceurs absorbant lumière visible (en particulier, de la lumière verte) dans ce cadre contractuel. Dans ce contexte, plusieurs systèmes à trois composants ont été étudiées et leurs réactivités ont été comparés et analysés afin de trouver les systèmes à trois composants les plus efficaces pour la PLP.

Dans le dernier chapitre, l'effet de la viscosité des formulations photosensibles sur l'efficacité de polymérisation CW et PLP a été étudié. Pour ces études, un système trois composant de référence absorbant de la lumière verte, à base de Safranine (le colorant), de borate (le donneur d'électron) et d'une triazine (l'accepteur d'électron) (SFH^+/CGI 909/TA) a été utilisé. Il sera montré que la viscosité à un impact négatif lors d'une irradiation continue alors qu'en PLP l'augmentation de la viscosité entraine une augmentation de l'efficacité des processus de photopolymérisation.

Table of Frequently Used Abbreviations

A: Redox Additive.

AA: Acrylamide.

AO: Astrazone Orange.

APTB: Alcoxypyridinium Tetrafluoroborate salt.

BP3B: Tris(tertbutylphenil)-butylborate.

CGI 909: Tetrabutylammonium tris(3-chloro-4-methylphenyl)(hexyl)borate.

Co: Co-initiator.

CQ: Camphorquinone.

CV : Crystal Violet.

CW: Continuous Irradiation Mode.

C% : Monomer Conversion Percent.

ΔC% : Monomer Conversion Percent per Pulse.

DMSO : Dimethylsulfoxide.

DPI : Diphenyliodonium.

EDB : Ethyl 4-dimethylaminobenzoate.

EMP : 1,3,5.7.8-pentamethyl-2.6-diethylpyrromethene difluoroborate.

EPP: 2.6-diethyl-8-phenyl-1.3.5.7-tetramethylpyrromethene difluorborate.

EV: Ethyl violet.

HABI: Hexaarylbisimidazole.

HMP: 1.3.5.7.8-pentamethylpyrromethene difluoroborate.

I 250: Methylphenyl, isobutylphenyl iodonium salt

ITX: Isopropylthioxanthone

KOP: Orthogonal kinetics.

k_p: Propagation rate constant.

k_t: Termination rate constant.

LFP: Laser Flash Photolysis.

MMA: Methylmetacrylate.

NPG: N-Phenylglycine.

P3B: Triphenylbutylborate.

PCIS: Photocyclic initiating system.

P_{in}: Number of inhibition pulses.

PIS: Photoinitiating system.

PLP: Pulsed laser polymerization.

PMMA: Polymethylmetacrylate.

RB: Rose Bengal.

R_c: Conversion rate.

R_p: propagation rate.

RT-FTIR: Real-time-Fourier transformed Infrared spectroscopy.

Rh 2074: Methylphenyl, isopropylphenyl iodonium salt

SFH^+: Safranine O.

SR 349: Sartomer 349 diacrylate.

SVD: Singular value decomposition.

TBA: Tetrabutylammonium.

TBB: Tetrabutylborate.

TPB: Tetraphenylborate.

TX: Triazine derivative X.

List of Figures, Tables and Schemes.

Table of contents

INTRODUCTION.

Photopolymerization is a brunch of science that faces nowadays a big development, due to its numerous potential applications, which gives it industrial interest for the developing of new materials.

This technique is differenced from traditional, thermic polymerization by the use of light instead of heat in order to initiate the reaction. This allows to a temporal and spatial control of the reaction, and is a greener, more eco-friendly technology, for it saves the use of great amounts of solvents.

In order to initiate polymerization with light, there is the need of the use of a photoinitiating system (PIS) in the formulation. There are many different types of PIS, from the traditional type I and II, to the more performant Photocyclic Initiating Systems (PCIS). The development of PIS allowed the improvement of UV light in polymer synthesis to the use of safer visible light of different wavelengths, from violet to red. The photophysics and photochemistry of the PIS used has a direct impact in the efficiency of polymerization. Thus, the study of the physico-chemical properties of compounds used as PIS is of primary importance to the development of photopolymerization technique.

At the same time, two different irradiation methods are used in photopolymerization. The first one, or continuos irradiation (CW), is the traditional method used for polymer synthesis and in industrial processus. The second one, Pulsed Laser Polymerization (PLP), is a method that was developed and used with mechanistic purposes only to the date.

During LPIM's long term collaboration with Bayer Material Science in Leverkusen, the idea of using PLP technique as a synthetic route was suggested. As no work was registered to the initial date of the present work, this possibility was studied in an extensive way setting, thus, the main objective of this thesis work, which was to study all the conditions needed in order to obtain performant results using PLP.

With this in mind, the first step was to characterize PLP experiments and to compare them with CW experiments. The efficiency of photopolymerization is affected by many parameters, but it depends mostly on the energy of irradiation, the PIS used and the viscosity of the formulation, since many of the processus involved in polymerization are controlled by diffusion. The study of the effect caused by all these parameters in the most extensive way possible is the main aim of this three-year term research.

During the first PLP experiments performed in the course of this thesis, a very challenging subject was the possibility to obtain reaction parameters from the conversion curves obtained under our work conditions. For this, a model was needed that could be contrasted with the already existent

ones. This was one of the toughest and more ambitious objectives that could be achieved all along this work.

Of course, another interesting objective was to keep on studying the photophysics and photochemistry that were used in the PIS, contributing to the extensive amount of work that can be found in the literature. Most of the studies performed were centered on Astrazone Orange R, which had previously shown surprising properties as a photosensitizer.

The photochemistry studies of PIS include the study of their reactivity and the generation of species that are able to initiate polymerization. This is why a part of the work was devoted to the understanding of complex PCIS.

This manuscript is divided in six chapters, where different aspects of the study of photopolymerization will be boarded.

Chapter One.

Background of Photoinitiators.

1. 1. Introduction.

Photopolymerization is basically described as a chemical reaction whereby organic materials exposed to electromagnetic radiation combine to form high-molecular-weight polymer molecules[1,2]. Historically, photopolymerization was first used over 4000 years ago during the time of ancient Egypt in the mummification process[3].

As the number of applications of visible light-induced photopolymerizable materials increase, the need for development of efficient photoinitiators that can be activated under visible-light irradiation conditions becomes more and more evident. In brief, the general categories of photopolymer applications are electronic materials[1], printing materials[4], optical and electro-optical materials[5,6], fabrication of devices and materials[7], adhesives and sealants[8], coatings[9] and surface modifications[10,11].

Photopolymer resins usually contain a photoinitiator or a more complex photoinitiating system (PIS), a mixture of monomers and oligomers, some additives, and fillers[12]. The most versatile process is the free radical photopolymerization which offers the most important choice of monomers and oligomers as well as a large number of potential PIS. The efficiency of one PIS is determined by its absorption properties, its quantum yield of initiating radicals and the reactivity of the radicals generated toward the monomer[13]. It is well known that the PIS is the corner stone of photopolymerization process and numerous works have been devoted to the development of PIS for specific applications ranging from metal coating to laser direct imaging. Holography also represents an interesting and growing field due to an increasing demand in security and data storage [14–16].

Different polymer chemistry has been studied as reactive medium to produce holograms. Due to intrinsic drawbacks for most of them, it turns out the free radical photopolymerization is the best chemical reaction which allows the recording of holograms with a good efficiency and a good durability[16]. Therefore, the major interest focuses on the PIS usable for free radical photopolymerization.

In this chapter, the conventional Type I and Type II PIS are briefly described. A particular attention is paid to three-component PIS that have emerged as an improvement over Type I and Type II initiating systems. The spectroscopic studies of some of these systems outline the possible presence of a photocyclic reaction. Such behavior allows the recovery of the dye after photoreaction, leading to

higher probability of radical production. The efficiency of these systems is higher than conventional systems, a fact which places these systems as good candidates for holographic recording.

1. 2. Type I Photoinitiators.

Regarding the formation of initiating radicals, the photoinitiation proceed essentially through two mechanisms, which differentiates photoinitiators in two big groups: Type I and Type II. Type I photoinitiators are those that overcome a homolytic cleavage after irradiation absorption, as indicated in figure 1.1. The result is the generation of two radicals per reacting photoinitiator molecule that could eventually initiate polymerization by reacting towards acrylate double bonds.

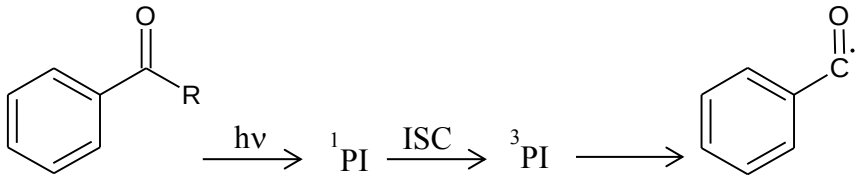

Figure 1.1: Typical mechanism of Type 1 PI initiated photopolymerization.

The most efficient Type I photoinitiators are benzoin ether derivatives, benzylketals, hydroxylalkylphenones, α-aminoketones and acylphosphine oxides. The high rate of cleavage and quantum yield of radicals explain the efficiency of type I PIS[13,17]. However, most of Type I photoinitiators are only active under UV irradiation[17,18].

Only a limited set of available Type I PIS absorbs in the blue or green region. An example of these kind is a bisbenzoylphosphine oxide derivative, Irgacure 819, which exhibits an absorption spectrum extending up to around 410–420 nm. One of the main features of this class of acylphosphine is the high photobleaching ability that increases the photoinitiation efficiency. This is especially useful when curing films and coatings with high thickness. However, this type of acylphosphine oxide is known to suffer from oxygen inhibition, a fact which limits their applications[19].

To overcome the irradiation wavelength limitation that type I PI have, big effort was devoted to the development of PI able to absorb within the visible light spectra. Titanocene derivatives represent one of the few examples of visible photoinitiators that are directly photolyzed upon light exposure[20-21]. In 1999, Schilling *et al.*[20] described the use of titanocene CG-784 in experiments where several high-index organic monomers were incorporated into acrylate oligomer-based

formulations, irradiating at 546 nm. The effectiveness of titanocene as photoinitiator in the polymerization of tetraethyleneglycol dimethacrylate (TEEGDM) under visible light was studied in comparison with the pair camphorquinone/dimethylaminoethyl methacrylate, CQ/DMAEMA. The reactions were carried out both in the presence of oxygen and in an inert atmosphere, and with different titanocene concentrations and incident light intensity. It was observed that in both atmospheres the polymerization reaction commenced rapidly and its initial rate was comparable with that obtained in the presence of the classic initiation systems. However, after reacting for a few seconds, this process suffered abrupt deactivation, being this more evident with low titanocene concentrations.

More recently, a visible light photoinitiator based on acylgermanium structure was developed. This compound absorbs visible light at wavelengths up to 550 nm, and exhibits high reactivity. The main drawback relies on the availability of the molecule (proprietary structure) and the high price due to synthesis[22].

1. 3. Type II Photoinitiators.

In contrast to type I, the formation of initiating radicals from type II PIS requires a photoinitiator which reacts (in general from its triplet state) with a coinitiator (figure 1.2). Typical Type II PIS with good absorption features in the UV–blue region are benzophenones[23-30], thioxanthones[31–36], camphorquinone[37–39], benzyls[24, 40] and ketocoumarins derivatives[38–40]. For visible light PIS, many dyes were reported as photosensitizers such as coumarins[40], xanthenic dyes[44–46], cyanine dyes, thiazine dyes[44] and pyrromethene dyes[47–49]. The coinitiator is generally a hydrogen donor which forms an initiating radical after photoreaction. By contrast, the ketyl radical formed on the photoinitiator moiety is generally inactive with respect to the double bonds, or even acts as a terminating agent toward the polymerization reaction[11,50–52].

Although Type I PIS can exhibit high quantum yields of radicals, their main drawback is due to the spectral limitation in the UV to blue region. By contrast, Type II PIS are versatile initiators for UV curing systems and visible light photopolymerization. The combination of different dyes and coinitiators provides tremendous flexibility in the selection of irradiation wavelength from the UV to the red region. These type II PIS, however, show limited efficiency compared with Type I systems.

This section will be devoted to give a wide panorama of all the relevant Type II PI available nowadays for radical polymerization and to review the most relevant studies made in the field in the last years.

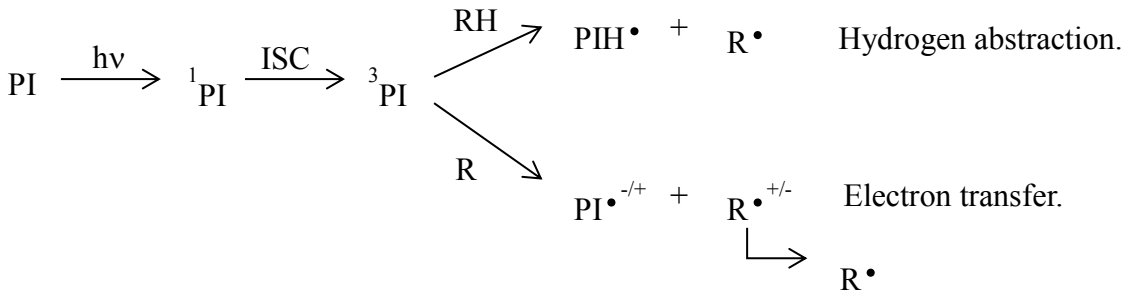

Figure 1.2: Typical mechanism of Type 2 PI initiated photopolymerization.

1. 3. 1. Dye/Amine Systems.

The most common pairs of compounds used as Type II photoinitiators are the dye/amine and dye/borate salt systems, i.e., systems that use an electron donor as coinitiator. This subsection will be devoted to the first group.

Regarding holographic applications, Mallavia *et al.*[44] studied an ion pair formed by Methylene Blue and Rose Bengal as photoinitiator in formulations of acrylamide and polyvinylalcohol tested as holographic recording materials in the form of dry films, under irradiation at 633 or 514 nm. Triethanolamine (TEA) was added as an electron donor. This mixture was used in holography, and turned out to be more efficient than a 1:1 physical mixture of the two dyes. Rose Bengal with *N*-methyl-*N*,*N*-diethanolamine (MDEA) was also used as a photoinitiating system to study the photopolymerization of acrylates based wood coatings under visible light[45].

A large amount of studies shows that amines act as excellent electron donors for polymerization in several systems containing synthetic dyes. Already in 1994, for example, an eosin ester possessing an *O*-benzoyl-α-oxooxime group in the C-2' carboxylate was synthesized[46] by reaction of the dye disodium salt with benzyl chloride. To study the behaviour of the new ester as a photoinitiator for the polymerization of 2-hydroxyethyl methacrylate (HEMA), a photopolymerizable mixture containing the dye, HEMA, MDEA, and ethylene glycol dimethacrylate (EGDMA) was evaluated as a photosensitive recording material for holography, irradiating at 514 nm. The ester

proved to be a more efficient photoinitiator than the starting dye. The performance of this ester and the corresponding ester of Rose Bengal as photoinitiators were studied at 525 nm, together with different photophysical and redox properties[53]. Same studies were carried out adding N,N-dimethylaniline as coinitiator under visible light irradiation. The polymerization rate observed for this PIS was 4.5 times bigger than that reached with eosin ester alone[54].

Several dyes containing an azomethine moiety have been synthesized (figure 1.3) and evaluated as photoinitiators for free radical polymerization of acrylates as well, using NPG as electron donor[55]. Considering the structure of the compounds, the replacement of the substituent in the pyrazolone skeleton causes a significant red shift in the electronic absorption spectra but does not affect photoinitiation ability. The opening of the pyrazolone skeleton causes a blue shift in the absorption spectra without affecting the photoinitiation ability. Moreover, an important increase in the photoinitiation efficiency and an increase in the quantum yield of the bleaching process were observed when the twisting motion of the C=N bond is severely hindered. Elimination of the motion of C=N bound by coplanarization of the azomethine moiety with other parts of the dye, decreases the degree of branching and consequently the molecule is stabilized in its excited state. The red shift of the absorption spectra maximum of the dye allows the initiation of acrylate polymerization using both argon-ion and He-Ne lamps.

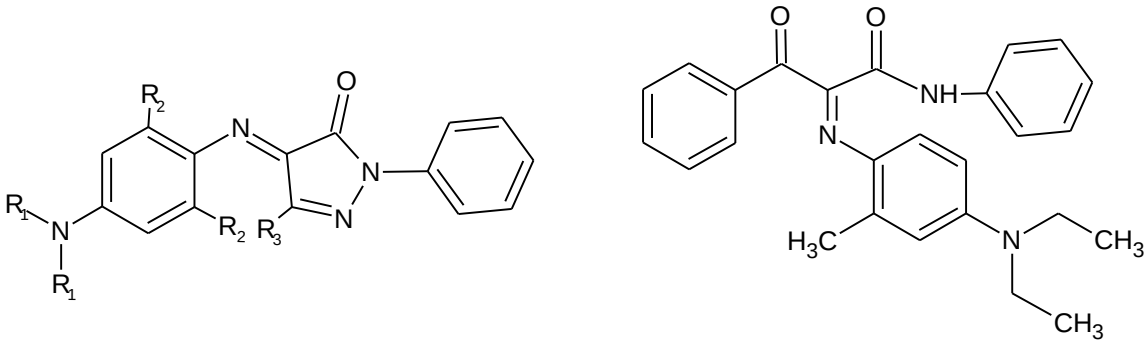

Figure 1. 3. Dyes with the azomethine moiety used with the amine NPG as type II photoinitiators. (a) general structure, where R_1, R_2 and R_3 are alkyl substituents; (b) dye with the pyrazolone skeleton ring opened.

In a similar approach, dyes containing benzylideneimidazopyridine moieties (BIPDs) were synthesized. The structure was afterwards modified by eliminating the motion of a C=C bond by coplanarization of the styrylium residue with other parts of the dye, in order to enhance the photoinitiating ability. The dye obtained, quinoline[2,3-b]-2,3-dihydro-1H-imidazo[1,2-a]pyridinium bromide (QDIPB), showed high sensitivity when used with different electron donors such as NPG to

polymerize 2-ethyl-2-(hydroxymethyl)-1,3-propanediol triacrylate (TMPTA) by irradiation with an argon-ion laser[56].

The photochemical bleaching of the following xanthene dyes, erythrosin B (ErB), eosin Y (EY), rose bengal (RB), rhodamine B (RoB) and fluorescein (F) was studied in the presence of the electron donor triethanolamine (TEA). The bleaching kinetics followed the order ErB > EY > RB > RoB > F. The authors of this work also present the influence of expose intensity and concentration of the xanthene dye on the photochemical bleaching process and their holographic recording properties[57].

The mentioned studies, along with another outrageous number of them, illustrate the improvement on versatility of photosensitizers and, thus, of irradiation sources that could be achieved by using an amine as coinitiator.

1. 3. 2. Dye/Borate salt Systems.

As well as it has been for amines, numerous combinations of dyes and borate salts have been reported to be efficient PIS. Below, several examples of this kind of Type II PI will be summarized.

Many commercial dyes such as methylene blue, rhodamine B, pyronine GY, safranine O, crystal violet, rose Bengal and cresyl violet have been used combined with tetramethylammonium hexyltris(m-fluorophenyl)borate (figure 1. 4) for imaging applications[58]. The results reported demonstrate that the derived dye/borate photoinitiators are highly reactive over the whole visible range of the electromagnetic spectrum and, thus, tunable to a variety of light sources.

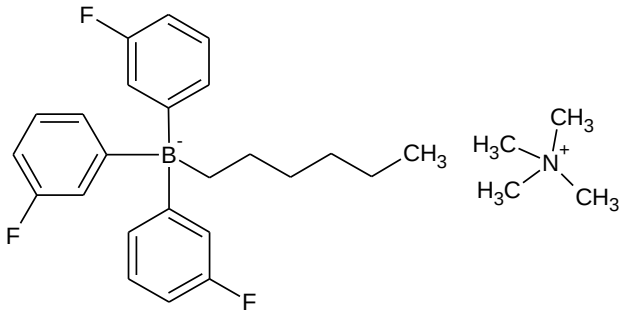

Figure 1. 4. structure of tetramethylammonium hexyltris(m-fluorophenyl)borate, borate salt used in holography.

Valdes-Aguilera *et al.* [59] synthesized six esters of decarboxylated rose bengal and employed them as photoinitiators at 514 nm. Photoreduction of the dyes by triphenyl n-butyl borate ion in ethyl acetate yielded decarboxylated rose bengal (RB) as well as products that do not absorb in the visible region. The yield of RB is approximately 8 % of total dye consumption and is produced by cleavage of the radical anion formed in the initial electron-transfer step. Photopolymerization of polyol acrylates initiated by the RB esters plus electron donor resulted in thin films as well as in thick samples, indicating that the order with respect to light intensity is 0.5 at both low and relatively high conversions (40%). The ratio $k_p/k_t^{0.5}$ depends on the identity of the RB ester employed as photoinitiator. The initiating radical is derived from the electron donor, whereas the radical released by cleavage of the semireduced dye acts as the predominant termination agent of polymer chains.

In another work, several new tetraorganoborate salts have been synthesized and tested as coinitiators with 2,4-diiodo-6-butoxy-3-fluorone (DIBF, figure 1.5) for the photopolymerization of acrylic monomer mixtures[60]. The rate of photopolymerization has been found to be a function of chemical structure of the borates. Stability, solubility, and reactivity of these borates as coinitiators for photopolymerization have been investigated. Diphenyldialkylborates have been found to be the best among the studied coinitiators.

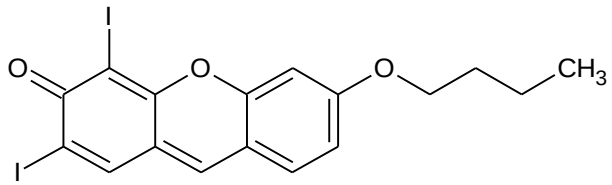

Figure 1. 5. structure of 2,4-diiodo-6-butoxy-3-fluorene, DIBF. Diphenyldialkylborates showed to be the most efficient coinitiators among all the borate salts studied with DIBF in Dye/ Borate salts PIS.

Another type of dye, 3,3'-carbonylbis(7-diethylaminocoumarin), was used as a sensitizer to produce visible light polymerization (488 nm) of an acrylate in poly(methyl methacrylate) (PMMA) film using a series of dialkylphenacylsulfonium butyltriphenylborate initiators[61]. The rates of polymerization (*Rp*) and the degrees of conversion increased when the reduction potential of the sulfonium cations of the sulfonium borates increased.

Furthermore, Lan and Schuster[62] discovered that a solution of 1,4-dicyanonaphtalene and alkyltriphenylborate salt, when irradiated, yielded the formation of alkyl free radicals through the carbon-boron bond cleavage. This observation was later applied to the formation of cyanine borates[63,64].

Kabatc *et al.* [65, 66], reported the preparation of three series of cyanine butyl triphenyl borate salts and the experiments performed with these dyes as initiators of photoinitiated free radical polymerization, *via* the photoinduced electron transfer process. To illustrate the influence of the primary process on the rate of photoinitiated polymerization, the fluorescence lifetime of the tested dye containing non-electron donating counterion, as well as electron donating borate ion were measured. The experimental data revealed that the relationship between the rate of the electron transfer and the free energy for this reaction display the typical "normal Marcus region" kinetic behaviour and they show that the relationship between the logarithm of the rate of polymerization and the logarithm of the rate constant for the electron transfer is linear in character. Therefore, the rate of photopolymerization is a function of the free energy change of the electron transfer (ΔG_{el}). This type of relationship was observed only for cyanines with no substituent in the *meso* position. These observations allow the conclusion that in the case of *meso*-cyanines the fluorescing state of the dye is not the state that is reduced by the borate.

Another example of the photoinitiating system dye/borate is the one formed by 3-ethyl-2-(*p*-(*N*,*N*-dimethylamino)styryl)benzothiazolium iodide and 3-ethyl-2-(*p*-pyrrolidinestyryl)-benzothiazolium iodide acting as light absorbers, *n*-butyltriphenylborate (Bo^-) anion being the electron donor, and alkoxypyridinium (AP^+) cation acting as ground-state electron acceptor (figure 1.6). Both Bo^- and AP^+ in polymerizing formulations were present either as Bo^- tetramethylammonium salt (TBAB) and AP^+ tetrafluoroborate salt (APTB), respectively, or as an ion pair composed of Bo^- anion and AP^+ cation (AP^+Bo^-). The most performant photoinitiating ability is observed for the system in which borate anion and pyridinium cation form an ion pair. It is postulated that an enhancement of photoinitiation ability observed for an ion pair is caused by a specific spatial organization of the reactants allowing the secondary reactions, yielding free radicals, in three-component encounter complex to occur. From a combination of either alkoxypyridiunium or alkyltriphenylborate salts with suitable sensitizer or properly designed dye and alkyltriphenylborate salt, two radicals can be generated per one absorbed photon, thus enhancing the overall polymerization efficiency[67]. This is the principle of the photocyclic initiating systems (Section 1.4).

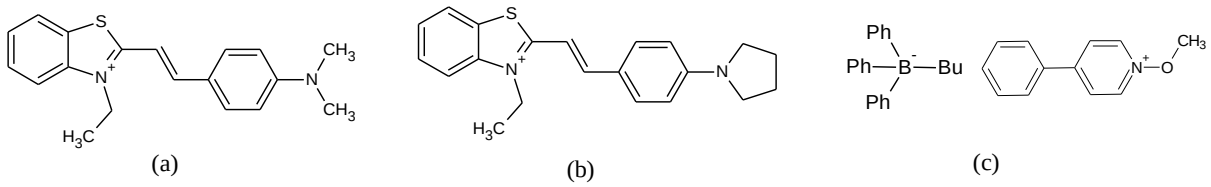

Figure 1. 6. Structures of (a) 3-ethyl-2-(*p*-(*N*,*N*-dimethylamino)styryl)benzothiazolium iodide, (b) 3-ethyl-2-(*p*-pyrrolidinestyryl)-benzothiazolium iodide and (c) *n*-butyltriphenylborate alkoxypyridinium. The mixture of either (a) or (b) with (c) showed the most performant photoinitiating ability among all the studied systems.

More recently, in 2006, the same group introduced asymmetric cyanine dyes combined with borate anions as visible-light photoinitiators. The kinetics of polymerization of trimethylolpropane triacrylate was studied by a microcalorimetric method. Asymmetric cyanine borates were found to be effective photoinitiators, and both the initiator and coinitiator concentration as well as the light intensity strongly affected the progress of photopolymerization, leading to an increase in the polymerization rate[68].

A new series of heterobicationic hemicyanine dyes were also prepared by this group[69]. The dyes paired with butyltriphenylborate anions proved to be very efficient photoinitiators of the free-radical polymerization of trimethylolpropane triacrylate when irradiated with an argon-ion laser. The tested heterobicationic chromophores showed significantly enhanced photoinitiation ability in comparison with their monocationic analogue when coupled with n-butyltriphenylborate anions. This was attributed to an artificially increased concentration of the n-butyltriphenylborate anion (acting as an electron donor) in proximity to the electron accepting excited cyanine dye chromophore.

Later, Jedrzejewska and co-workers[70] compared the reactivity of several photoinitiating systems composed of a positively charged cyanine as a dye (Cy^+) and *n*-butyltriphenylborate anion (Bo^-) as a ground state electron acceptor. Through Stern-Volmer experiments they determined that the dye cation and the donor anion form a ground state complex (ground state ion pair) and that an artificial increase of the electron donor concentration in close proximity to the cyanine moiety is needed. Photoinitiating systems containing two borate anions in one molecule show better photoinitiation ability and the degree of monomer conversion depends on the structure of the cation additionally attached to the dye. They also tested initiators composed of two identical chromophores covalently linked to each other, with results that strongly depended on the structure of the modified dye.

In 2007, Kabatc *et al.*[71] reported the synthesis of 6-bromo-3-ethyl-2-styrylbenzothiazolium *n*-butyltriphenylborates and evaluation as photoinitiators of free radical polymerization. The resulting styrylbenzothiazole dyes (hemicyanine dyes) paired with n-butyltriphenylborate anion (SBrB2), are shown to be efficient photoinitiators for free radical polymerization of trimethylolpropane triacrylate (TMPTA) induced with the visible emission of an argon-ion laser. The introduction of the bromine into benzothiazolium residue causes a small red shift of the electronic absorption maxima, changes the reduction potential of the dye and, finally, increases the photoinitiation ability of the dye.

Gould *et al.*[72] described reactions of photoinitiated polymerization with the electron transfer occurring between the excited state of the dye and N-alcoxypyridinium salts, acting as ground state electron acceptors. The electron transfer process from excited dyes to N-alkoxypyridinium salts leads to reductive cleavage of the N-O bond to give an alkoxy radical that can be used to initiate polymerization. The bond-dissociation energy (BDE) obtained from calculation based on DFT were in agreement with predictions from a thermochemical cycle. These data show a difference of ca. 290-315 kJ/mol between the BDE of the pyridinium and that of the pyridyl radical and indicate that the fragmentation of the radical is highly exothermic. The energetic requirements for the photoinduced electron transfer are discussed in terms of a simplified model that shows that the initiation efficiency of the radical polymerization can be correlated with a single parameter, the reduction potential of the sensitizing dye. Dyes including cyanine, styrylpyridinium, rhodamine, squarylium, coumarin and oxanol, with absorption bands spanning the entire visible region were effective in initiating photopolymerization of acrylate monomers in this system. The photoresponse can be doubled through coupling of the reductive cleavage of the N-alkoxypyridinium with oxidative cleavage of the C-B bond of an alkyltriarylborate, a process that utilizes the potential stored in the oxidized dye following electron transfer to the pyridinium salt. This is also an example of a 3-C PIS, which will be further discussed in section 1.4.

Toba *et al.*[74] investigated photoinitiating systems of dimethylphenacylsulfonium butyltriphenylborate (DMPSB) as a donor-acceptor initiator and styryl dyes for free radical polymerization of an acrylate with visible lasers (488, 514 and 647 nm). When polymerized with pentaerythritol triacrylate, the sensitivity value of the photosensitive layer contaning DMPSB was higher than that of tetrabutylammonium butyltriphenylborate (TBAB) as an electron donating initiator or dimethylphenacylsulfonium tetrafluoroborate (DMPS) as an electron accepting initiator. The sensitivity values of the photosensitive layer containing the photoinitiator systems showed a close relation to the free energy changes between the excited singlet styryl dyes and DMPSB.

In 2009, Jedrzejewska *et al.*[75], studied the behavior of a series of Styrylbenzimidazolium dye–borate complexes, which were found to be very effective PIS for the polymerization of vinyl monomers. However, the efficiency of the system was found to be dependent on the structure of the dye.

The same year, Kabatc *et al.*[76] reported the synthesis of three-cationic carbocyanine dyes, which were tested as photoinitiators using n-butyltriphenylborate as counter-ion. Conversion rate was compared with that obtained for the correspondent mono-cationic carbocyanine dye. The highest rate of polymerization was found for the three-cationic system at a concentration of PI of about one order of magnitude than that of the mono-cationic system. The following year, the same group reported the synthesis of new bicationic dyes[77]. This new cromophoric, polycharged derivatives were found to be much more efficent than the identical monochromophoric ones.

In 2011, mechanistic studies suggested that the photoinitiating ability of the Dye/borate salt couples were controlled by both the driving force of the electron-transfer process between the electron donor and the electron acceptor, and the reactivity of the free radical that resulted from the secondary reactions occurring after the photoinduced electron-transfer process[78]. Later in the same year, this group studied the relationship between reactivity and structure for a series of borate salts, founding that the reactivity increased with the number of alkyl groups per boron[79].

1. 3. 3. Dye/Onium salt Systems.

Not all of the co-initiators are electron donors. Electron acceptors can also play the role of co-initiators by quenching the excited state of the photosensitizer. Among the electron acceptors used in polymerization, onium salts are one of the most popular ones.

Kaneko *et al.*[80] informed that crystal violet lactone (CVL, 3,3-bis[4-(dimethylamino)phenyl]-6-(dimethylamino)-1(3*H*)-isobenzofuranone) and other lactone dye precursors form coloured triphenylmethyl cations when irradiated with UV light in the presence or absence of [4-(octyloxy)phenyl]phenyliodonium hexafluoroantimonate (OPPI, figure 1. 7). In selected monomers in the presence of iodonium salt, colour formation and polymerization occur simultaneously. The excited singlet state lifetimes of the precursors were estimated from quantum yields for the disappearance of CVL in the presence of OPPI and are similar to those observed for fluorescence quenching, occuring mainly by electron transfer. On the basis of the transient absorption spectra, it can be concluded that triarylmethane cations are generated from the lactone precursors in the presence of OPPI in acetonitrile with a pseudo first order rate constant of 10^4 s^{-1}. Colour formation in the absence of OPPI

is suggested to occur from the excited singlet states of the lactone via a biradical formed by photoinduced β-bond cleavage.

The photosensitive initiating system composed of 7-diethylamino-3-(2'-benzimidazolyl)-coumarin dye (DEDC) and the initiator diphenyliodonium hexafluorophosphate (DIHP) were used to initiate the polymerization of Methylmethacrylate (MMA)[81]. When exposed to visible light, coumarin dye/iodonium salt undergoes quick electron transfer from DEDC to DIHP with the production of free radicals. The visible light induced reaction between DEDC and DIHP is mainly through the excited singlet state of DEDC and a little sensitive to O_2.

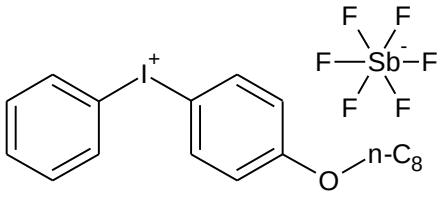

Figure 1. 7. Structure of OPPI, an iodonium salt coinitiator.

Mono-, and diphenyliodonium salts of eosin dye (EoEt (Ph_2I) and Eo($Ph_2I)_2$) were synthesized and studied as a sensitization system for visible photopolymerization in comparison with the corresponding bimolecular systems ($EoNa_2$/Ph_2ICl)[82]. The photochemical activity of the unimolecular system is much higher than that of the bimolecular one. The photobleaching rate decreases in the order Eo($Ph_2I)_2$ > $EoNa_2$ /2(Ph_2 ICl) > EoEtNa/2(Ph_2ICl). Photocrosslinking rates of acrylate polymers in dry film indicate that the diiodonium salt is more efficient than mono salt and that no reaction occurs in the case of bimolecular system of eosine and iodonium.

Also, several dimethylamino-substituted chalcone (i.e., dimethylaminobenzal acetophenone, figure 1.8) derivatives were used as visible light sensitizers for radical photopolymerization initiated by diphenyliodonium tetrafluoroborate (I) [73]. Initiating radical species were produced from the chalcone-sensitized photolysis of I through single electron transfer. The authors inform that the activity of the chalcone decreased as a function of the substituent attached to the aromatic ring in the order: OCH_3 > H > Cl.

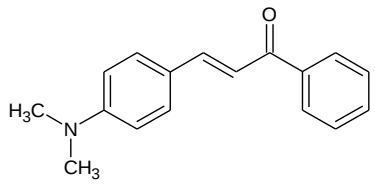

Figure 1. 8. Structure of dimethylaminobenzal acetophenone. Derivatives of this molecule were used as photosensitizers with diphenyliodonium salts.

A new photosensitizer, 4-(4'-dimethylaminostyryl)benzophenone, was synthesized and characterized spectrophotometrically[83]. The combination of this compound and diphenyliodonium tetrafluoroborate, showed a good photoresponse at near UV and visible light regions. The photolysis of the two component system occurs rapidly *via* electron transfer and leads to a simultaneous photobleaching of the photosensitizer and cleavage of the iodonium salt to generate phenyl radicals. The photobleaching rate constant detected was 30.7 ($mol^{-1}.L.s^{-1}$). The photopolymerization of MMA was carried out in N_2 purged acetonitrile solution. The kinetic results obtained showed that the polymerization rate is proportional to the concentration with exponents of 0.46, 0.32, and 1.0 for the iodonium salt, the dye and MMA respectively. Considerable rate increment was obtained by adding thiol compounds.

Iodonium butyltriphenylborate salts were found to be more efficient than iodonium tetraphenylborate salts when used as photoinitiators for the polymerization of acrylates. It was found from a study of the photoreaction of iodonium borate salts with the model monomer MMA, that iodonium butyltriphenylborate salts simultaneously produce a butyl radical from the borate anion and an aryl radical from the iodonium cation upon irradiation. Both radicals initiate polymerization. Iodonium tetraphenylborate salts were found to release an aryl radical from the iodonium cation only. Iodonium borate salts exhibit strong absorption below 300 nm with tail absorption above 400 nm, being efficient photoinitiators even when used with visible light. When a photosensitizer such as 5,7-diiodo-3-butoxy-6-fluorone is employed, iodonium butyltriphenylborate salts are rendered much more efficient for visible light photopolymerization[84].

Timpe *et al.* studied a series of ketone-iodonium salt systems as photoinitiators for radical polymerization[85]. 4,4'-bis(dimethylamino)benzophenone (Michler's ketone), xanthone, thioxanthone, acridone and 10-methylacridone sensitize the decomposition of diphenyliodonium salts via electron transfer processes. They found that owing to the long lifetime of the excited singlet state, at high concentrations of iodonium salts, both the singlet and triplet states can function as electron donors.

There are many other electron acceptors that are currently used as coinitiators. Nevertheless, as they have been more widely used as redox additives in 3-C PIS, they will be presented in section 1.4.

1. 3. 4. Other Two-component Systems.

A dye-linked initiator consisting of a merocyanine dye, which has an absorption maximum at 460 nm, and a substituted bis(trichloromethyl)-1,3,5-triazine initiator was prepared in order to achieve an efficient photopolymerization in the visible-light region. The relative photoinitiating efficiency of dye-linked initiators in photopolymerization of acrylate monomers was evaluated and the results clearly indicated that the dye-linked photoinitiator exhibited a marked increase in the photoinitiating efficiency of photopolymerization of acrylates compared to a simple mixture of the dye/initiator in photopolymer coatings particularly at a lower concentration of the initiator. This was explained in terms of the active quenching sphere of the dye/initiator system. Superior photosensitivity in the linked compound at a lower concentration indicates that this would be particularly useful as a visible-light photoinitiator in holographic recording photopolymers[86].

A different bimolecular photoinitiator system, which exhibits maximum sensitivity at 518 nm and consists of a sensitizer dye, pyrromethene 567 (PM567), and a radical generating reagent 3,3',4,4'-tetrakis(tert-butylperoxycarbonyl)benzophenone (BTTB) was reported[87]. The photosensitization of BTTB through the excitation of PM567 induces high polymerization rates, in spite of low quantum yield of photoreduction of the dye. On the contrary, different experiences have revealed that PM567 or BTTB, separately, are unable of initiating the polymerization of 2-hydroxyethyl methacrylate (HEMA) over extensive periods of time at 40ºC. The polymerization efficiency of the photoinitiator system PM567/BTTB, was analyzed by following the bulk polymerization kinetics of monomer HEMA by differential scanning photo-calorimetry.

Suzuki *et al.*[88] studied the sensitization mechanism of a photoacid generator (PAG), *N*-(trifluoromethanesulfonyloxy)-1,8-naphthalimide (NIOTf) by a pyrromethene sensitizing dye, such as 1,3,5,7,8-pentamethyl pyrromethene BF_2 complex (HMP), 2,6-diethyl-1,3,5,7,8-pentamethyl-pyrromethene BF_2 complex (EMP), and 2,6-diethyl-8-phenyl-1,3,5,7-tetramethylpyrromethene BF_2 complex (EPP), by means of absorption and fluorescence spectroscopies, product analysis and nanosecond laser flash photolysis. For all the systems pyrromethene/NIOTf, the fluorescence quenching was nearly diffusion-controlled. This reaction involves an electron-transfer process from the excited singlet state of the pyrromethene derivative to NIOTf, as supported by the negative values of the Gibbs free energy change and the observation of the pyrromethene radical cations. The triplet state of the pyrromethene dyes was found to be unreactive toward NIOTf. Photoacid generation quantum yields for the sensitization were also measured and they showed a correlation with the electron-transfer rate constant from the dye singlet excited state. The system EPP/NIOTf was applied

to printing technology with an appropriate binder polymer bearing an acetal protection group. By controlling the exposure energy and the post-exposure baking (PEB) process, a printing plate was obtained with a high resolution.

Bipyrromethene-BF_2 complexes, which are dyes derived from pyrromethene, have been studied in photopolymers with hydrophobic binder, where the dye can act as sensitizer and initiator at the same time. Ortuño *et al*.[89] introduced the use of pyrromethene in a hydrophilic binder photopolymer to change the redox initiation system in photopolymers with xanthene dyes. In this way the authors avoided the use of triethanolamine as the redox initiator, typical in hydrophilic binder photopolymers, which is related to the existence of diffusion phenomena in the recorded hologram. Using a pyrromethene derived dye and 4,4'-azobis(4-cyanovaleric acid) as initiator they obtained photopolymer layers with high thickness, good optical quality, absorption levels very close to xanthene dyes, and with the capability to record diffraction gratings with low noise level.

1. 4. Three-Component Photocyclic Initiating Systems.

To overcome the lack of reactivity of conventional systems under visible light, many groups have developed more complex PIS in which not only the intrinsic problem of reactivity of the Type II system is circumvented but also the dye is recovered after reaction, as it is shown in figure 1.9. leading to so-called 3-C PIS or photocyclic initiating systems (PCIS). Indeed, the photopolymerization efficiency of Type II PIS can be greatly improved by addition of a third additive, which yields to an additional formation of initiating radicals by reaction with one photoproduct arising from the photochemical reaction[90–94]. The use of PIS based on three components offers tremendous flexibility in the selection of the light sources and the determination of the actinic wavelength because a wide variety of dyes can be used. Three different kinds of additives can be used: latent species that create reactive centers after reaction, molecules that are oxidized and molecules that are reduced. Many works have shown that these PIS lead to increased rate of polymerization and final monomer conversion than the corresponding Type II PIS[48, 49, 95, 96].

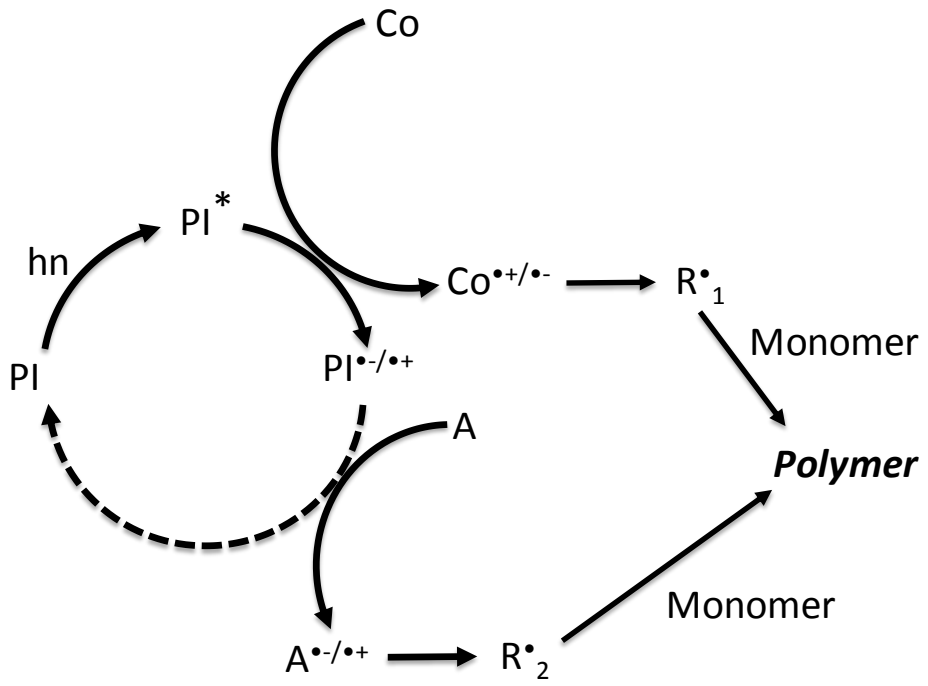

Figure 1.9. PCIS Mechanism. After excitation, the photosensitizer (PI, generally a dye), reacts with the Coinitiator (Co) and with the redox additive (A) successively, after which reactions the PI can be partially recovered. The coinitiator and redox additive generate initiating radicals.

The first class of molecules, latent species that leads to the formation of reactive centers after reaction, contains chain transfer agents such as S–H, P–H, Si–H or Ge–H based molecules. They have found only limited applications[97] which will not be further discussed, because our main interest is fast, efficient polymerization.

Molecules that are oxidized during the process are electron donors. Amine derivatives such as N-methyldiethanolamine[25, 26], or triethylamine[94] are the common electron donor reported to date for the PIS in the literature. The aromatic amines such as N-phenylglycine (NPG) already mentioned in the previous section, are used to avoid the toxicity of alkyl amines[38]. Triarylalkyl borates, sulfur- or tin-containing compounds have also been reported as well as, although to a lower extent, amides, ethers, ferrocene, metallocenes, ureas, salts of xanthanates, salts of tetraphenylboronic acid, etc. As can be expected, the oxidation potential of the donor plays a key role in the mechanism of electron transfer.

Among the additives that are reduced during the process, the most commonly used are iodonium salts, triazines, and HABI derivatives. All of these were studied among the present thesis work and their use as redox additives will be detailed in the following subsections.

1. 4. 1. 3-C PIS proposed mechanisms.

Many studies reported the photopolymerization efficiency, kinetics and mechanistic reactivity of this type of systems[43, 47–50, 90–94,123–129]. The mechanisms which have been proposed for three-component systems can be summarized into two general classes: parallel reactions in which two coinitiators react with the excited dye independently; and sequential reactions in which two of the three components first react together followed by the reaction of the third component with one of the photoproducts. In all the proposed mechanisms, the dye absorbs the light and prompts the photoreaction either through the excited singlet state or through the triplet state. In the case of parallel reactions, the total yield of radicals depends on the reactivity of each coinitiator with the excited state, an obvious fact which does not deserve further discussion.

More interesting are the sequential reactions in which the photoreaction could be an electron transfer or a hydrogen transfer with the coinitiator (Co) (Scheme 1.3). An initiating radical is formed from the coinitiator and the dye turns into its reduced or oxidized form. In the presence of the third component (A), a redox reaction takes place between the additive and the reduced or oxidized form of the dye. This reaction yields two advantages: the additive (A) leads to the formation of supplementary initiating radical, and the ground-state dye is recovered and can be involved in further photoreaction. Therefore, a real cyclic photoreaction occurs until complete depletion of reactants.

1. 4. 2. Triazine derivative based 3-C PIS.

The use of triazine derivated based three-component PIS has been widely studied in the last years. Not only his role of ground-state electron acceptor, but also the possibility of free radical production by this species, made them a great complement for enhancing the efficiency of respectives two-component systems.

Grotzinger *et al*.[97] investigated the addition of a bis(trichloromethyl)-substituted-1,3,5-triazine (figure 1. 10) to a dye/amine photoinitiating system, finding that this addition leads to an increased efficiency of polymerization under visible light irradiation. The dyes used were phenosafranine, eosin and rose bengal; whatever the investigated dye/amine mixture, the addition of triazine led to a strong synergistic effect: the inhibition time decreased and the polymerization rate increased significantly when the three components were used jointly. Results show that triazine acts mainly as an inhibitor scavenger. The involved inhibitor is the reduced dye, arising from the first

photochemical reaction between the excited states of the dye and the amine. The same authors evaluated six designed three-component systems containing a dye (i.e acridine orange, erythrosine B, safranin O, fluorones DIBF and TIHF), an amine and a triazine derivative (2-(4-methoxyphenyl)-4,6-bis(tricholomethyl)-1,3,5-triazine, triazine A, TA), for the initiation of the photopolymerization of multifunctional acrylates under visible light[98]. Dyes showing very poor efficiency in dye/amine photoinitiating systems, such as acridine orange, show very interesting reactivity in the presence of TA. Moreover, the maximum of absorption of the dye (493 nm in acetonitrile) matches very well the 488/514 nm emission lines of Ar^+ laser that is used in imaging applications and could be very useful in such applications. This article suggests that consideration of the thermodynamic aspect of the processes can be successfully applied as a first approach, to provide screening of potentially efficient photoinitiating systems.

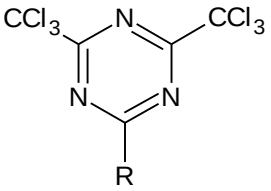

Figure 1. 10. Structure of bis(trichloromethyl)-substituted-1,3,5-triazine. A large amount of molecules containing this structure are used as coinitiators nowadays.

The efficiency of the photonitiating system rose bengal/MDEA, used in the photopolymerization of acrylates based wood coatings under visible light, was compared to the system rose bengal/MDEA/2-(4´-methoxy-1´-naphtyl)-4,6-bis(trichloromethyl)-1,3,5-triazine, showing a faster conversion than the two-component system[45].

3-C PIS consisting of a cyanine dye, borate salt, and a 1,3,5-triazine derivative (as coinitiator) for photopolymerization of acrylates in the blue and green regions of the spectrum were investigated by Kabatc *et al*[99]. Polymerization kinetic studies based on a microcalorimetric method revealed a significant increase in polymerization rate when the concentration of n-butyltriphenylborate salt or the 1,3,5-triazine derivative were increased. The authors conclude that the primary photochemical reaction involves an electron transfer from the n-butyltriphenylborate anion to the excited singlet state of the dye, followed by the reaction of the 1,3,5-triazine derivative with the resulting dye radical to regenerate the original dye. This reaction simultaneously produces a triazinyl radical anion derived from the 1,3,5-triazine, which undergoes the carbon-halogen bond cleavage yielding radicals active in initiation of a free radical polymerization chain.

In 2009, Kabatc *et al.* reported the synthesis of a novel N-ethyl-2-styrylquinolinum Iodides dye[100]. A three-component photoinitiating systems, possessing styrylquinilinum borate salt and 1,3,5-

triazine derivative was used as a PIS for free radical polymerization, obtaining two and ten times faster rates in comparison to parent two-component system.

The following year, the same author published a paper[101] in which a thiol derivative was used instead of borate salts as an electron donor, obtaining a rate of polymerization that was twice as fast as te one obtained with the correspondent two-component system.

Furthermore, the synthesis of eight new multicationic monomethine dyes was tested as PIS using borate salts in a two-component system, and then with the aggregation of triazine derivatives[102]. As expected, the addition of the triazine derivatives enhanced the photoinitiation ability of the system.

In the same year, Tarzi *et al.*[48] tested the aptitude as PIS of pyrromethene/amine/triazine derivative systems. Surprisingly, for the two-component systems, better results were obtained for triazine A, than for ethyl-4-dimethylaminobenzoate (EDB), nevertheless, the best results were obtained for the three-component system.

Kabatc also utilized 2,4-Bis-(trichloromethyl)-6-(4-methoxy)phenyl-1,3,5-triazine (XL-353) in the visible light photoinitiating systems[105]. The addition of halomethyl 1,3,5-triazine to two-component dye photoinitiating systems resulted in a very efficient acceleration of the rate of free radical polymerization of acrylate monomers.

1. 4. 3. Onium salt based 3-C PIS.

Already presented above, onium salts have also been used as electron acceptors in a great number of formulations.

Methylene blue has been used in a three-component system, with an electron donor (*N*-methyldiethanolamine) and diphenyliodonium chloride (DPI), and 2-hydroxymethylacrylate as a monomer[50, 104]. Kinetic studies based upon photodifferential scanning calorimetry revealed a significant increase in polymerization rate with increasing concentration of either the amine or the iodonium salt. However, laser-induced fluorescence experiments showed that while increasing the amine concentration dramatically increases the rate of dye fluorescence decay, increasing the DPI concentration actually slows consumption of the dye. The authors conclude that the primary photochemical reaction involves electron transfer from the amine to the dye and suggest that the iodonium salt reacts with the resulting dye-based radical (which is active only for termination) to regenerate the original dye and simultaneously produce a phenyl radical (active in initiation) derived from the diphenyliodonium salt. The addition of MDEA produces faster photobleaching.

The mechanistic study of the above mentioned three-component radical photoinitiator system, is extended by investigating the influence of oxygen on the rate of the consumption of methylene blue dye[105]. The mechanism involves electron transfer/proton transfer from the amine to the dye as the primary photochemical reaction. Oxygen quenches the triplet state of the dye, leading to retardation of the reaction. In a sealed reactor, a retardation period (attributed to the presence of oxygen) was observed, followed by rapid exponential decay of the MB fluorescence after the oxygen was depleted. On the basis of the impact of the amine and iodonium concentrations on the fluorescence intensity and the duration of the retardation period, the proposed mechanism includes an oxygen-scavenging pathway, in which the tertiary amine radicals formed in the primary photochemical process consume the oxygen *via* a cyclic reaction mechanism. The iodonium salt is an electron acceptor, acting to reoxidize the neutral dye radical back to its original state and allowing it to reenter the primary photochemical process.

In another approach of the use of methylene blue as the photosensitizer in a three component system, a series of electron donors were used[106]. The Rehm-Weller equation was used to verify the thermodynamic feasibility for photo-induced electron transfer from the electron donors to the dye. Comparison of the photopolymerization rates of each two-component initiator system (containing the photosensitizer and amine) to those of the corresponding three-component system (with the addition of DPI), allowed fundamental information regarding the role of the DPI to be obtained. It was concluded that the DPI enhances the photopolymerization kinetics in two ways: (1) it consumes an inactive MB neutral radical and produces an active Ph radical, thereby regenerating the original methylene blue, and (2) it reduces the recombination reaction of the MB neutral radical and amine radical/cation.

Fouassier *et al.*[107] have studied the system eosin-amine-iodonium salt. The iodonium salt had no effect on the initiation step of the polymerization reaction for acrylates but sharply decreased the termination reactions.

Padon *et al.* also studied, in an analogous way, the three-component system comprised of eosin Y, MDEA, and DPI[108]. The Eosin may be oxidized by the DPI to produce an eosin radical, which may be reduced by the amine back to its original state. This reaction has the effect of regenerating the original eosin dye, and secondly, it produces an active amine radical in place of the presumably less active dye radical. Because of the difference in reaction rates for the pairwise reactions, this amine-mediated dye regeneration reaction may be the primary source of active radicals in the three-component system.

The same authors also studied a similar system with neutral Eosin Y, N-methyldiethanolamine, and diphenyliodonium chloride for the polymerization of 2-hydroxyethyl methacrylate[109]. The fastest reaction occurred when all three components were present (the next fastest was with the dye/amine pair, and the slowest was with the dye/iodonium pair). However, laser-induced fluorescence experiments showed that the reaction between eosin and iodonium bleaches the dye much more rapidly than the reaction between eosin and the amine. Although a direct eosin/amine reaction can produce active radicals in the three-component system, this reaction is largely overshadowed by the eosin/iodonium reaction, which does not produce active radicals so effectively.

The photopolymerization of acrylamide (AA) initiated by the synthetic dye safranine-T in the presence of triethanolamine (TEOHA) as co-initiator was investigated in aqueous solution[110]. The addition of diphenyliodonium chloride (DPIC) to the system has a marked accelerating effect on the polymerization rate. In the absence of DPIC, an inhibiting effect of TEOHA is observed at high concentrations of the amine. This effect is suppressed by the presence of the onium salt. At the same time, the photobleaching of the dye caused by the amine is suppressed by the presence of AA or DPIC. The presence of the onium salt increases the yield of the triplet state of the dye. Also the yield of radicals in the quenching of the dye triplet by TEOHA increases by the presence of DPIC. The semi-reduced form of the dye decays faster in the presence of DPIC, thus, suggesting a possible way of generating extra active radicals at the same time that the dye is regenerated.

Harada *et al.*[111] reported the polymerization of acrylate monomers by means of a three component system containing thioxanthene dye (TX), NPG, and diphenyliodonium salt (DPI). This system is approximately five times more sensitive than the two component systems containing TX, i.e., TX/NPG and TX/DPI systems. Afterwards, they studied the photoinitiating system by spin resonance spectroscopy[112], observing that the phenyl radical produced by electron transfer from $TX^{-\cdot}$ to DPI as well as the phenylaminomethyl radical of decarboxylated NPG initiates the polymerization.

Another photosensitive organic material, based on a three-component photoinitiating system formed by 3-3'-carbonyl-bis-7-diethylaminocoumarin, NPG and DPI was used to polymerize an acrylic monomer (phenoxy diethylenglycol acrylate), observing a better performance than the corresponding two component systems dye/NPG or dye/DPI. Reflection holograms could also be recorded with this system at λ = 488 nm (Ar^+ laser) with diffraction efficiency $\approx$ 51% and refractive index modulation 0.013[113].

A combination of dihydropyridine-iodonium salt was used to photopolymerize acrylates and methacrylates by Timpe *et al.*[114]. In a photoassisted reaction, by exposure of 9-phenyl-10-methylacridinium salt to blue light (λ = 405, 436 or 460 nm) in the presence of a 1,4-dihydropyridine derivative as electron donor and diphenyliodonium salt as electron acceptor, phenyl radicals are

formed. These radicals initiate the polymerization of MMA in acetonitrile solutions or of bulk multifunctional acrylate monomers usually used in industrial formulations. The phenoxy molecular structure of the monomer gives rise to an electron transfer reaction responsible for the formation of initiating radicals. Other dyes can also be used as light-absorbing components in such ternary systems. Systems having tetrabromomethane instead of the iodonium salt as electron acceptors exhibit the same polymerization efficiency.

The combination dye/amine/onium proved to be very efficient to induce polymerization also when used with thioxanthones and ketocoumarins as photoinitiators[93].

In the recent years, Kim *et al.*[115] compared the efficiency of two different systems containing DPI salt and an electron donor species. The first using CQ, thus involving a photo-reducible series initiation mechanism, while, in the second, the use of Porphrin Dye (Zn-tpp) implies a photo-oxidizable series mechanism. It was found that the latter was a much more efficient system than the former one.

In 2011, Cook and Chen[116] studied the reactivity of systems using CQ as photosensitizer, together with diphenyliodonium hexafluorophosphate (Ph_2IPF_6) and different amines. For every amine tested, the 3-C PIS was found to be around five times more effective than any of the respective 2-C PIS, which means that the addition of the third component to the formulation produces the same results of the addition of 25 times the amount of CQ. These results were independent of the monomer used.

1. 4. 4. HABI derivative based 3-C PIS.

3-C PIS comprised of HABI (figure 1. 11), 2-mercaptobenzooxazole (MBO), a chain transfer agent, and 2,5-bis[[(4-diethylamino)phenyl]methylene]cyclopenta-none (DEAW) was used in experiments where several high-index organic monomers were incorporated into high optical quality acrylate oligomer-based formulations, irradiating at 546 nm^3. A 6-fold increase in Δn was achieved compared to an initial all-acrylate formulation. Samples prepared from these formulations have been used to write and read >200 high-quality holograms in a given volume of material.

Li *et al.*[117] described the sensitization of the homolysis of o-chlorohexaarylbisimidazole (o-Cl-HABI), electron acceptor, by bis(7-diethylaminocoumarin-3-yl) ketone (DEACK), electron donor. The radicals generated can initiate the polymerization of methylmethacrylate (MMA) when the system is irradiated with an Argon ion laser.

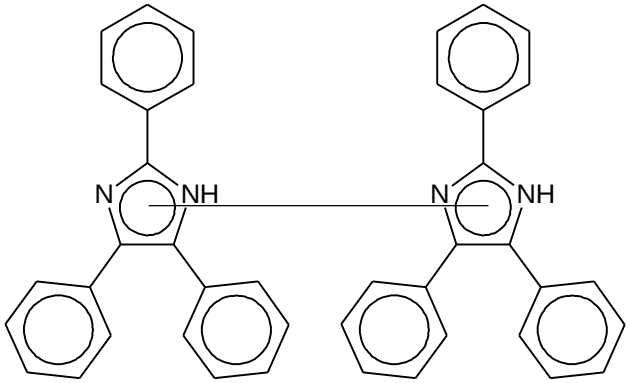

Figure 1. 11. Structure of HABI. This molecule can be used as a coinitiator in systems where an hydrogen abstraction takes place.

The free energy changes (ΔG_{el}) of the electron transfer process between different synthetic hexaarylbisimidazoles (HABIs) and ketocyanine dyes (JAWs) were determined[118]. The dependence of the rate of 1,1,1-tri(acryloxymethyl)propane photopolymerization, initiated with HABI + JAW systems in the presence of mercaptobenzoxazole, on the ΔG_{el} value and on the radiation wavelength (488 nm and 355 nm or 365 nm) was also studied. The authors report that the chemical structures of HABI and JAW do not affect considerably the rate of polymerization.

The sensitization mechanism in a photoinitiating system that consists of an aminostyryl sensitizing dye, 2-[p-(diethylamino)styryl]naphto[1,2-d]thiazole (NAS) (λ_{max} = 415 nm), and a radical generator, 2,2'-bis(2-chlorophenyl)-4,4',5,5'-tetraphenyl-1, 1'-bi-1H-imidazole (HABI) was investigated[119]. In a photopolymer bearing NAS/HABI system, an improvement of the photosensitivity was observed by the addition of coinitiator, 2-mercaptobenzothiazole (MBT), to the initiating system. Photochemical and photophysical behavior of the three-component initiating system, NAS/HABI/MBT, in a PMMA film was studied; it is considered that MBT can enhance the generation of the triplet state of NAS, which is hardly observed by direct excitation, and the mechanism of both singlet and triplet electron transfer from NAS to HABI is suggested. The same system had been studied previously using NPG instead of MBT obtaining similar results[120].

Four sensitizers that could be sensitive to He-Ne laser, NK-529, NK-3960, MCD and ECD, were synthesized by Zhang *et al.*[121]. The photoinitiating systems are composed of one of the four compounds above, 2- chlorohexaarylbiimidazole(2-Cl-HABI) and 3-mercapto-4- methyl-4H-1,2,4-triazole (MTA), which acted as sensitizer, initiator and hydrogen-donor respectively. Photopolymerization was initiated by free radicals which were produced by the electron transfer between the sensitizer and the initiator in the excited state. Comparing the monomer conversion of these four systems, the authors found: MCD >ECD >NK529 >NK3960. The system (MCD- HABI-

MTA) was used as a photoinitiating system of photopolymer holographic materials. The holographic material was composed of the above photoinitiating system, a binder, a mono- or multi-functional monomer, and other additives. Adding the third beam to expose the photopolymer plate simultaneously during the initial holographic exposure can increase the effective exposure sensitivity of the photopolymer plate. More than 80% of reflection grating diffraction efficiency can be obtained. The holographic gratings have a good physical and chemical stability under ambient conditions.

Coumarin derivates were also used for the polymerization of MMA[122]: the initiating systems contained 3-acetyl-7-(diethylamino)coumarin, 7-(diethylamino)-3-(2-benzimidazolyl)-coumarin or 7-(diethylamino)-3-(N-methyl-2-benzimidazolyl)coumarin as photosensitizer; 2-chlorohexaaryl-biimidazole as photoinitiator; and dodecyl mercaptan as H-donor coinitiator. When exposed to visible light, the biimidazole and coumarin undergo electron transfer from coumarin to biimidazole to produce free radicals. According to the authors, the three component system can be used, together with a binder and an active monomer to record holograms.

1. 5. Conclusion.

Three different types of photoinitiators were presented all along this chapter. The first ones, the Type I, proved to be very efficient, but their use is almost exclusively limited to UV irradiation. With Type II (or 2-C PIS), a wide variety of dyes become available to generate initiating radicals for polymerization, but the efficiency of these systems is not as high as for the Type I. To improve the efficiency of 2-C PIS, a third component is added to the formulation to form the so called 3-C PIS or PCIS. The development and study of these systems is the aim of this thesis work.

1. 6. References.

[1] Peiffer, R. W. Photopolymerization: Fundamentals and Applications, (Edited by A. B. Scranton, C. N. Bowman and R. W. Peiffer, **1997**), p. 1-14. American Chemical Society, Washington, DC.

[2] Allonas, X., C. Croutxe-Barghorn, J. P. Fouassier, J. Lalev_ee, J. P. Malval and F. Morlet-Savary, Lasers in Chemistry. Influencing Matter, (Edited by M. Lackner, **2008**), p. 1001-1027. Academic Press, New York, NY.

[3] Decker, C., J. Coat. Technol. **1997**, 59, p. 97-106.

[4] Holman, R., Eur. Coat. J. , **1985**, 9, p. 610-612.

[5] Sponsler, M. B., J. Phys. Chem., **1995**, 99, p. 9430-9436.

[6] Lochel, B., A. Maciossek, H. J. Quenzer and B. Wanger, J. Electrochem. Soc., **1995**, 143, 237-244.

[7] Wakasa, K., N. A. Chowdhury, R. Priyawan, Y. Yoshida, A. Ikeda, T. Hirose and M. Yamaki, J. Mater. Sci. Lett., **1996**, 15, p. 134-136.

[8] Shi, W. and B. R_anby, J. Appl. Polym. Sci., **1996**, 59, p. 1951-1956.

[9] Decker, C., Polymer Durability, Vol. 249 (Edited by R. L. Clough, N. C. Billingham and K. T. Grillen, **1996**), p. 319-334. American Chemical Society, Washington, DC.

[10] Akiyama, H., M. Momose, K. Ichimura and S. Yamamura, Macromol., **1995**, 28, p. 288-293.

[11] Chan, C. M., T. M. Ko and H. Hiraoka, Surf. Sci. Rep., **1996**, 24, p. 1-54.

[12] Fouassier, J. P., Photoinitiation, Photopolymerization, and Photocuring: Fundamentals and Applications. Hanser Gardner Publications, Munich, **1995**.

[13] Lalevee, J., X. Allonas, S. Jradi and J. P. Fouassier, Macromol., **2006**, 39, p. 1872–1879.

[14] Jurbergs, D., F.-K. Bruder, F. Deuber, T. Facke, R. Hagen, D. Honel, T. Rolle, M.-S. Weiser and A. Volkov, New recording materials for the holographic industry, **2009**, 72330K-72330K.

[15] Weiser, M.-S., F.-K. Bruder, T. Facke, D. Honel, D. Jurbergs and T. Rolle, Macromol. Symp., **2010**, 296, p. 133-137.

[16] Bruder, F.-K., R. Hagen, T. Rolle, M.-S. Weiser and T. Facke, Angew. Chem. Int. Ed., **2011**, 50, p. 4552-4573.

[17] Crivello, J. V. and K. Dietliker, Photoinitiators for Free Radical Cationic & Anionic Photopolymerisation. John Wiley & Sons, New York, **1999**.

[18] Green, W. A., Industrial Photoinitiators: A Technical Guide. CRC Press, Boca Raton FL., **2010**.

[19] Dietliker, K., A Compilation of Photoinitiators Commercially Available for UV Today. SITA Technology Limited, **2002**.

[20] Schilling M. L., Colvin V. L., Dhar L., Harris A. L., Schilling F. C., Katz H. E., Wysocki T., Hale A., Blyler L. L., Boyd C., *Chem. Mater*. **1999**, 11, 247-254.

[21] Davidenko N., Garcia O., Sastre R., *J. of Biomat. Sci., Polym. Ed.* **2003**, 14, 733-746.

[22] Moszner, N., U. K. Fischer, B. Ganster, R. Liska and V. Rheinberger, Dent. Mater., **2008**, 24, p. 901–907.

[23] Sandner, M. R., C. L. Osborn and D. J. Trecker, J. Polym. Sci., Part A: Polym. Chem., **1972**, 10, p. 3173-3181.

[24] Hutchison, J., M. C. Lambert and A. Ledwith, Polymer, **1973**, 14, p. 250-254.

[25] Fouassier, J.-P., D. Ruhlmann, Y. Takimoto, M. Harada and M. Kawabata, J. Polym. Sci., Part A: Polym. Chem., **1993**, 31, p. 2245-2248.

[26] Fouassier, J.-P., A. Erddalane, F. Morlet-Savary, I. Sumiyoshi, M. Harada and M. Kawabata, Macromol., **1994**, 27, p. 3349-3356.

[27] Costela, A., J. Dabrio, J. M. Figuera, I. García-Moreno, H. Gsponer and R. Sastre, J. Photochem. Photobiol., **1995**, A 92, p. 213-221.

[28] Allen, N. S., E. Lam, J. L. Kotecha, W. A. Green, A. Timms, S. Navaratnam and B. J. Parsons, J. Photochem. Photobiol., **1990**, A 54, p. 367-388.

[29] Kuhlmann, R. and W. Schnabel, Polymer, **1976**, 17, p. 419-422.

[30] Allen, N. S., E. Lam, E. M. Howells, P. N. Green, A. Green, F. Catalina and C. Peinado, Eur. Polym. J., **1990**, 26, p. 1345-1353.

[31] Catalina, F., J. M. Tercero, C. Peinado, R. Sastre, J. L. Mateo and N. S. Allen, J. Photochem. Photobiol., **1989**, A 50, p. 249-258.

[32] Allen, N. S., F. Catalina, P. N. Green and W. A. Green, Eur. Polym. J., **1986**, 22, p. 793-799.

[33] Amirzadeh, G. and W. Schnabel, Makromol. Chem., **1981**, 182, p. 2821-2835.

[34] Yates, S. F. and G. B. Schuster, J. Org. Chem., **1984**, 49, p. 3349-3356.

[35] Kayaman, N., A. Onen, Y. Yagci and W. Schnabel, Polym. Bull., **1994**, 32, p. 589-596.

[36] Allonas, X., C. Ley, C. Bibaut, P. Jacques and J. P. Fouassier, Chem. Phys. Lett., **2000**, 322, p. 483-490.

[37] Allonas, X., J. P. Fouassier, L. Angiolini and D. Caretti, Helv. Chim., **2001**, Acta 84, p. 2577-2588.

[38] Kucybaa, Z., M. Pietrzak, J. Pączkowski. L.-A. Linden, and J. F. Rabek, Polymer, **1996**, 37, p. 4585-4591.

[39] Jakubiak, J., X. Allonas, J. P. Fouassier, A. Sionkowska, E. Andrzejewska, L. A. Linden and J. F. Rabek, Polymer, **2003**, 44, p. 5219-5226.

[40] Allen, N. S., G. Pullen, M. Edge, I. Weddell and F. Catalina, Eur. Polym. J., **1995**, 31, p. 15-21.

[41] Williams, J. L. R., D. P. Specht and S. Farid, Polym. Eng. Sci., **1983**, 23, p. 1022-1024.

[42] Specht, D. P., P. A. Martic and S. Farid, Tetrahedron, **1982**, 38, p. 1203-1211.

[43] Allonas, X., J. P. Fouassier, M. Kaji, M. Miyasaka and T. Hidaka, Polymer, **2001**, 42, p. 7627-7634.

[44] Mallavia, R., A. Fimia, C. García and R. Sastre, J. Mod. Opt., **2001**, 48, p. 941-945.

[45]Mauguiere-Guyonnet, F., D. Burget and J. P. Fouassier, Prog. Org. Coat., **2007**, 59, p. 37-45.

[46] Mallavia, R., F. Amat-Guerri, A. Fimia and R. Sastre, Macromol., **1994**, 27, p. 2643-2646.

[47] Ibrahim, A., C. Ley, O. I. Tarzi, J. P. Fouassier and X. Allonas, J. Photopolym. Sci. Technol., **2010**, 23, p. 101-108.

[48] Tarzi, O. I., X. Allonas, C. Ley and J. P. Fouassier, J. Polym. Sci., Part A: Polym. Chem., **2010**, 48, p. 2594-2603.

[49] Costela, A., O. Garcia, I. Garcia-Moreno and R. Sastre, Macromol. Chem. Phys., **2004**, 204, p. 2233-2239.

[50] Padon, K. S. and A. B. Scranton, J. Polym. Sci., Part A: Polym. Chem., **2000**, 38, p. 2057-2066.

[51] Block, H., A. Ledwith and A. R. Taylor, Polymer, **1971**, 12, p. 271-288.

[52] Hageman, H. J., Prog. Org. Coat., **1985**, 13, p. 123-150.

[53] Burget D., Fouassier J. P., Amat-Guerri F., Mallavia R., Sastre R., *Acta Polym.* **1999**, 50, 337-346.

[54] Amat-Guerri F., Mallavia R., Sastre R., *Trends in Photochem. & Photobiol.* **1999**, 5, 103-116.

[55] Kucybała Z., Pietrzak M., Paczkowski J., *Chem. Mater*. **1998**, 10, 3555-3561.

[56] Pyszka I., Kucybala Z., Paczkowski J., *J. Polym. Sci. Part A: Polym. Chem*. **2003**, 41, 3048-3055.

[57] Gong Q., Huang M., Gu D., Gan F., *Guangzi Xuebao* **2005**, 34, 1714-1718.

[58] Cunningham A., Kunz M., *RadTech'98 North America UV/EB Conference Proceedings*, Chicago, Apr. 19-22, **1998**, 38-41.

[59] Valdes-Aguilera O., Pathak C. P., Shi J., Watson D., Neckers D. C., *Macromol.* **1992**, 25, 541-547.

[60] Sarker A. M., Polykarpov A. Y., De Raaff A. M., Marino T. L., Neckers D. C, *J. Polym. Sci: Part A Pol. Chem.* **1996**, 34, 2817-2824.

[61] Toba Y., Usui Y., Konishi T., Ito O., Uesugi T., *Macromol.* **1999**, 32, 6545-6551.

[62] Lan L. Y., Schuster G. B., *Tet. Lett.* **1986**, 27, 4261-4264.

[63] Chatterjee S., Gottschalk P., Davis P. D., Schuster G. B., *J. Am. Chem.. Soc.* **1988**, 110, 2326-2328.

[64] Chatterjee S., Davis P. D., Gottschalk P., Kurz B., Yang X., Schuster G. B., *J. Am. Chem. Soc.* **1990**, 112, 6329-6338.

[65] Kabatc J., Pietrzak M., Paczkowski J., *Macromol.* **1998**, 31, 4651-4654.

[66] Kabatc J., Pietrzak M., Paczkowski J., *J. Chem. Soc., Perkin Trans. 2*, **2002**, 287-295.

[67] Kabatc J., Paczkowski J., *Macromol.* **2005**, *38,* 9985-9992.

[68] Kabatc J., Jedrzejewska B., Paczkowski J., *J. Applied Polym. Sci.* **2006**, 99, 207-217.

[69] Kabatc J., Jedrzejewska B., Paczkowski J., *J. Polym. Sci. Part A: Polym. Chem.* **2006**, 44, 6345-6359.

[70] Jedrzejewska B., Kabatc J., Paczkowski J., *RadTech Europe* **2007** Conference Proceedings, Viena, Nov. 13-15, 2007.

[71] Kabatc J., Gruszewska M., Jedrzejewska B., Paczkowski J., *Polym. Bull.* **2007**, 58, 691-701.

[72] Gould, I. R., Shukla D., Giesen D., Farid S., *Helv. Chim. Acta* **2001**, 84, 2796-2812.

[73] Li J., Li, M., Song H., Yang, Y., Wang E., *Chinese J. Polym. Sci.* **1993**, 11, 163-170.

[74] Toba Y., Yasuike M., Usui Y., *J. Photosci.* **1998**, 5, 63-67.

[75] Jedrzejewska B., Tur M., Paczkowski J., J. of Photochem. and Photob. A: Chemistry, **2010**, 209, p. 32-40.

[76] Kabatc J. and Pączkowski J., *J. of Polym. Sci. Part A: Polym. Chem.* **2009**, 47, p. 4636-4654

[77] Kabatc J., Zadruzynska A., Czech Z., Kowalczyk A., *Dyes and Pigments*, **2011**, 92, p. 724-731.

[78] Jedrzejewska B., Pietrzak M., *J. of App. Polym. Sci.*, **2012,** 123, p. 3535-3544.

[79] Jedrzejewska B., Pietrzak M., Rafinski Z., *Polymer*, **2011**, 52, p. 2110-2119.

[80] Kaneko Y., Neckers D. C., *J. Phys. Chem. A* **1998**, 102, 5356-5363.

[81] Gao F., Yang Y.-Y., *Chinese J. of Polym. Sci.* **1999**, 17, 589-594.

[82] Wang E., He J.-H., Li M.-Z., Song H.-H., Li J., *J. Photopolym. Sci. and Tech.* **1992**, 5, 505-13.

[83] Li J., Li M., Chang Z., Wang E., *Ganguang Kexue Yu Guang Huaxue* **1993**, 11, 22-29.

[84] Feng K., Zang H., Martin D., Marino H. L., Neckers D. C., *J. Polym. Sci. Part A: Polym. Chem.* **1998**, 36, 1667-1677.

[85] Timpe H. J., Kronfeld K. P., Lammel U., Fouassier J. P., Lougnot D. J., *J. Photochem. Photobiol. A: Chem.* **1990**, 52(1), 111-122.

[86] Kawamura K., Kato K., *Polym. Adv. Tech*. **2004**, 15, 324-328.

[87] Garcia O., Costela A., Garcia-Moreno I., Sastre R., *Macromol. Chem. Phys.* **2003**, 204, 2233-2239.

[88] Suzuki S., Allonas X., Fouassier J. P., Urano T., Takahara S., Yamaoka T., *J. Photochem. Photobiol. A: Chem.* **2006**, 181, 60-66.

[89] Ortuño M., Marquez A., Gallego S., Neipp C., Fernandez E., *Opt. Mat.* **2007**, 30, 227-230.

[90] Fouassier, J. P., X. Allonas and D. Burget, *Prog. Org. Coat*., **2003**, 47, p. 16-36.

[91] Fouassier, J. P. and E. Chesneau, *Makromol. Chem.*, **1991**, 192, p. 1307-1315.

[92] Fouassier, J. P., F. Morlet-Savary, K. Yamashita and S. Imahashi, *Polymer 38*, **1997**, p. 1415-1421.

[93] Fouassier, J. P. and S. K. Wu, J. Appl. *Polym. Sci.*, **1992**, 44, p. 1779-1786.

[94] Fouassier, J.-P. and J. Lalevee, *RSC Advances*, **2012**, 2, p. 2621-2629.

[95] Allonas, X., J. P. Fouassier, M. Kaji and Y. Murakami, *Photochem. Photobiol. Sci.*, **2003**, 2, p. 224-229.

[96] Roffey, C. G., Photogeneration of Reactive Species for UV Curing. John Wiley & Sons, Chichester, **1997**.

[97] Grotzinger C., Burget D., Jacques P., Fouassier J. P., *Macromol. Chem. and Phys.* **2001**, 202, 3513-3522.

[98] Grotzinger C., Burget D., Jacques P., Fouassier J. P., *Polymer* **2003**, 44, 3671-3677.

[99] Kabatc J., Zasada M., Paczkowski J., *J. Polym. Sci. Part A: Polym. Chem.* **2007**, 45, 3626-3636.

[100] Kabatc J., Paczkowski J., *J. of App. Polym. Sci.*, **2010**, p. 2669-2675

[101] Kabatc J., *Polymer*, **2010**, 51, p. 5028-5036.

[102] Kabatc J., *J. of Photochem. and Photob. A: Chemistry*, **2010**, 214, p. 74-85.

[103] Kabatc J., Czechb Z., Kowalczyk A., *J. of Photochem. and Photob. A: Chem.*, **2011**, 219, p. 16-25.

[104] Padon K. S., Scranton A. B., *Polym. Mat. Sci. and Eng.* **2000**, 82, 27-28.

[105] Padon K. S., Scranton A. B., *J. Polym. Sci. Part A: Polym. Chem*. **2000**, 38, 3336-3346.

[106] Kim D., Scranton A. B., *J. Polym. Sci. Part A: Polym. Chem*. **2004**, 42, 5863-5871.

[107] Fouassier J. P., Chesneau E., *Makromol. Chemie* **1991**, 192(6), 1307-1315.

[108] Padon K. S., Kim D., Scranton A. B., *Polym. Preprints* **2001**, 42, 705-706.

[109] Padon K. S., Scranton A. B, *J. Polym. Sci. Part A: Polym. Chem*. **2001**, 39, 715-723.

[110] Gomez M. L., Avila V., Montejano H. A., Previtali C. M., *Polymer* **2003**, 44, 2875-2881.

[111] Kawabata M., Harada M., Takimoto Y., *J. Photopolym. Sci. and Tech*. **1988**, 1, 222-227.

[112] Harada M., Takimoto Y., Noma N., Shirota Y., *J. Photopolym. Sci. and Tech.* **1991**, 4, 51-54.

[113] Fouassier J. P., Ruhlmann D., Graff B., Takimoto Y., Kawabata M., Harada M., *J. Imag. Sci. and Tech.* **1993**, 37, 208-10.

[114] Timpe H.-J., Ulrich S., Decker C., Fouassier J. P., *Eur. Polym. J.* **1994**, 30(11), 1301-1307.

[115] Kim D., Stansbury J. W., *J. of Polym. Sci.: Part A: Polym. Chem.*, **2009**, 47, p. 3131-3141.

[116] Cook, Wayne D., and Fei C., *J. of Polym. Sci. Part A: Polym. Chem.*, **2011**, 49, p. 5030-5041.

[117] Li L., Yang W., Xu W., Yang Y., Zhang C., Li C., Mei W., *J. of Photopolym. Sci. and Tech.* **1996**, 9, 137-142.

[118] Bendyk M., Jędrzejewska B., Pączkowski J., Lindén L.-A., *Polimery* **2002**, n 9.

[119] Suzuki S., Perrier E., Urano T., Takahara S., Yamaoka T., *Polymer* **2005**, 46, 2238-2243.

[120] Suzuki S., Urano T., Miyagawa N., Takahara S., Yamaoka T., *J. Photopolym. Sci. and Tech.* **2001**, 14, 259-262.

[121] Zhang, C., Zhao J., He J., Li L., Yang Y., *Holographic Displays and Optical Elements II*, Proc. SPIE Vol. 3559, p. 81-87, 08/**1998**.

[122] Fang G., Xu J., Yang Y., *J. Photopolym. Sci. and Tech*. **1999**, 12, 339-342.

[123] Erddalane, A., J. P. Fouassier, F. Morlet-Savary and Y. Takimoto, *Polym. Sci., Part A: Polym. Chem.*, **1996**, 34, p. 633-642.

[124] Bi, Y. and D. C. Neckers, *Macromol.*, **1994**, 27, p. 3683-3693.

[125] Zhou, W. and E. Wang, *J. Photochem. Photobiol. A: Chem.*, **1996**, 96, p. 25-29.

[126] Kavarnos, G. J. and N. J. Turro, *Chem. Rev.,* **1986**, 86, p. 401-449.

[127] Kabatc, *J., Mat. Chem. Phys.*, **2011**, 125, p. 118-124.

[128] Kabatc, J. and K. Jurek, *Polymer*, **2012**, 53, p. 1973-1980.

[129] Kabatc, J. and J. Pazczkowski , *J. Photochem. Photobiol.*, **2006**, A 184, p. 184-192.

Chapter Two.

Photophysics of Astrazone Orange.

2. 1. Introduction.

Astrazone Orange (AO) is a cationic merocyanine dye widely used in PAN fibres dying process due to its low cost and high light absorption properties[1]. AO has many derivatives. The structure of the derivative studied in this work, AO R, is shown in figure 2.1.

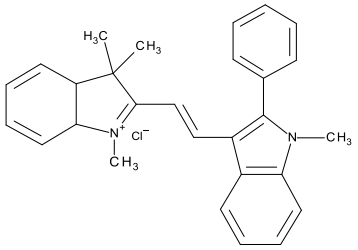

Figure 2.1 Chemical structure of AO-R.

The efficiency of AO R as a photosensitizer in 2- and 3-C PIS was first studied during Dr Ibrahim's thesis work. A quick analysis of the dye structure would suggest a simple fast dye isomerization as deactivation mechanism from the excited state, which would have make it difficult for any electron transfer reaction to have place. However, this dye showed to be rather efficient when combined with an electron donor as N-phenylglycine, NPG. This was not the case when combined with triazine S (TS), an electron acceptor (figure 2.2).

These results suggested that a more complicated photophysical process than expected had place after photon absorption. Hence, many studies were realized in order to have a complete description of the process.

In the first place, stationary UV-vis and fluorescence spectroscopy studies were performed with solutions of AO R in solvent of different viscosities. In second place, ultrafast spectroscopy and TCSPC studies were performed in different solvents as well in order to detect the primary intermediate species formed, followed by LFP studies.

Experimental results were compared with molecular modeling studies in order to come to a conclusion about the structures of the intermediate species involved and the deactivation mechanism for AO R.

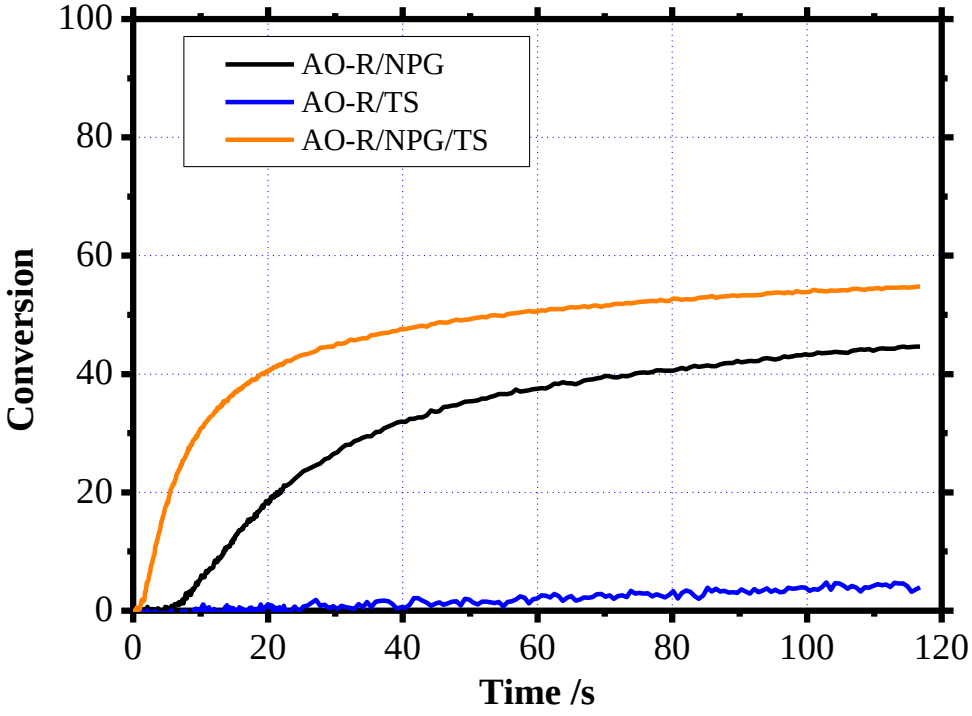

Figure 2.2. Conversion vs time results for PIS containing AO-R.

2. 2. Materials and methods.

Steady state UV-Visible spectra were obtained on a Cary 4000 spectrophotometer. Fluorescence and time correlated single photon counting experiments (TCSPC) were performed with a Horiba-Jobin-Yvon fluoromax 4 equiped with a single photon counting module. A 1 ns 473nm nanoled was used as pulsed source. Before comparison of measured spectra, they were all corrected in order to take into account the non-reciprocity of absorption and emission phenomena according to[2,3] in a transition dipole moment representation (TDM).

Femtosecond laser excitation wavelength was adjusted to 500 nm by mean of collinear 800 nm pumped CDP2017 (CDP corp) optical parametric amplifier. The 100fs laser pulses (800 nm) were provided by a Spectra-Physics Tsunami Ti:Sa oscillator coupled to a Spitfire pro Spectra-physics regenerative amplifier. Pump-probe measurements were performed on a CDP Excipro system. The resulting pump-probe cross-correlation of the setup was found to be about 200fs.

Astrazon Orange-R was purchased from TCI. Its structure was checked by NMR, and used as received. Solvents of spectrophotometric or HPLC grades were purchased from Sigma-Aldrich and used without further purification.

Laser flash photolysis (LFP) experiments were realized with a continuum Surelite YAG laser coupled to a continuum optical parametric oscillator SLOPO. The excitation pulses were adjusted to 500nm. LFP kinetics were recorded on an Applied Photophysics LKS80 system.

Quantum chemical (QM) calculations have been carried out using Gaussian 09.[4] Standard calculations for structural optimization were performed at the B3LYP/6-311G** level and electronic transitions (both absorption and emission) have been calculated by TDDFT (time-dependent density functional theory) at the same level of consistency.

Fluorescence emission was determined by calculating the relaxation of the excited state geometry followed by the emission state-specific solvation and by the emission to the final ground state[5,6] as implemented in Gaussian 09. Solvent was taken into account with the PCM model implemented in Gaussian 09.[7]

Vibrational frequencies have been checked to ensure that optimized conformations correspond to energy minima. Moreover, extra-calculations were performed with CAM-B3LYP, wB97XD and M062X DFT functionals and extended bases as 6-311++G(3df,3dp) and cc-pVTZ. These extra-calculations confirm the results found with the previous modest strategy (B3LYP/6-311G**). So, in the following discussion, interpretation is based on the results determined at the B3LYP/6-311G** level. Charge distribution was also investigated by the Mülliken and the electrostatic potential fit methods.

2. 3. Spectroscopic properties and solvent effect.

The evolution of the UV-Visible spectra of the dye in water, dimethyl sulfoxyde (DMSO), acetonitrile (MeCN), acetone and ethanol (EtOH) as a function of AO-R concentration were checked. All spectra present the same shape and evolve homothetically. This indicates that no aggregation occurs in the concentration range used (i.e. up to 2 10^{-4} M). Two bands could be seen in every studied solvent: a very intense one with a visible maximum around 500 nm (figure 2.3) and a small one in the UV below 300 nm. Furthermore, this allows to the determination of molar absorption coefficients in

the investigated solvents (table 2.1)[8,9]. It should be mentioned here that the dye was not soluble in low polar and non-polar solvents as THF, toluene and cyclohexane.

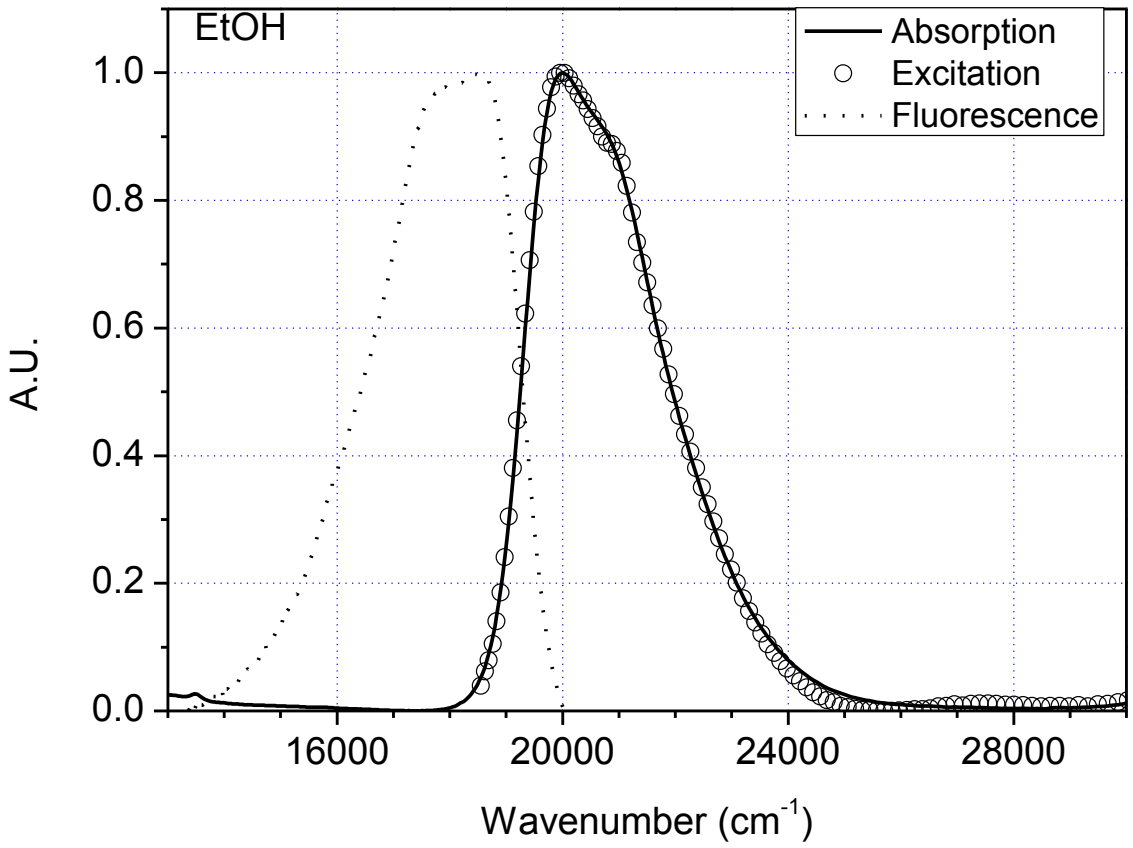

Figure 2.3. TDM representation of absorption (plain line), emission (dotted line) and excitation (circles) spectra of AO-R in EtOH.

All molar absorption coefficients are close to 50,000 $L.mol^{-1}.cm^{-1}$ (and up to 60,000 in EtOH), and in good agreement with molecular calculations (vide infra), which are relatively high values. Moreover, a small hypochromic effect is observed in the higher π^* solvents.

	D	π*	σ_{max}/nm	ε /L.mol^{-1}.cm^{-1}
H_2O	78.36	1.09	493	46424
DMSO	46.45	1.00	499	45912
MeCN	35.94	0.75	496	51517
Acetone	20.56	0.71	496	55561
EtOH	24.55	0.54	499	58192
Toluene	2.38	0.54	Not soluble	Not soluble

Table 2.1. Molar absorption coefficients of AO-R, dielectric constants D and π* Kamlet and Taft polarity parameter of solvents,[10,11] and maximum absorption wavelength λmax in nm.

Solvent	ν_{abs} /cm^{-1}	ν_{fluo} /cm^{-1}	Δν /cm^{-1}	E(S_1) /eV	Φ_{fluo}	τ(S_1)* /ps	τ_{rad} /ns	D	η /cP
Acetone	20141	18653	1488	2.38	2.6 10^{-3}	9.15	3.6	20.56	0.31
MeCN	20165	18620	1545	2.41	2.4 10^{-3}	7.6	3.2	35.94	0.37
H_2O	20285	18553	1732	2.38	3.3 10^{-3}	9.8	2.9	78.36	0.89
EtOH	20000	18556	1444	2.39	4.5 10^{-3}	13.2	3.5	24.55	1.07
DMSO	20022	18465	1557	2.38	12 10^{-3}	35.8	3.0	46.45	1.99
TEG	19932	18581	1351	2.38	31 10^{-3}	154	4.9	23.69	49

Table 2. 2. Photophysical experimental parameters of AO-R: maximum of absorption, emission and Stokes shift (Δν) after TDM correction (cm^{-1}), singlet state energy E(S1) (eV), fluorescence quantum yield Φ_{fluo}, singlet state and natural radiative lifetimes τ(S1) and τrad (in ps and ns respectively), dielectric constant D and solvent viscosity η (cP).

2. 4. Singlet state photophysics.

Very low intensity emission was detected in each solvent the dye is soluble in. The obtained transition dipole moment (TDM) representations of AO-R absorption, emission and excitation spectra in EtOH are displayed on figure 2.3.

Absorption and emission spectra are mirror images. Moreover, excitation and absorption spectra overlap almost perfectly, indicating that the excited state reached after light absorption should be very similar to the emissive state[12, 13]. The same behavior was obtained in all the other studied solutions and the maximum of absorption and emission, together with other parameters can be found in table 2.2.

The position of the emission and absorption maxima are not correlated to the solvent polarity as expected for a cationic molecule. Thus, it seems that neither polarity, nor hydrogen bonds play an important role in the steady state spectroscopic properties.

Fluorescence intensity increases with the solvent viscosity. Therefore, quantum yields of fluorescence were measured in all solvents (using Rhodamine 6G in EtOH as reference[12]). All quantum yields are very low (see table 2.2), in agreement with the low emission intensity observed. However, it can be seen that the quantum yield increases when going from less viscous solvents (e.g. acetone) to more viscous ones (e.g. DMSO) and even more in triethylene glycol (TEG). Knowing both the quantum yield of fluorescence and the singlet state lifetime, the determination of the natural radiative lifetime τ_{rad} was possible according to: $\Phi_f = \tau(S_1)/\tau_{rad}$[13]. The calculated values are listed in table 2.2. The radiative lifetimes in the different solvents are very similar and lay in the range of 3 to 5 ns (the deviations being easily explained by the possible experimental errors on the quantum yields calculations). The relatively long radiative lifetime in all the solvents associated to a very short lifetime of the first singlet state provides evidence for an excited state deactivation controlled by internal conversion (IC), intersystem crossing (ISC), charge transfer (CT), isomerization...[3, 12-14]

Moreover, the viscosity of the solvents seems to influence the photophysics of AO-R. Indeed, the higher emissions quantum yields and longer lifetimes are obtained in the most viscous DMSO and TEG solvents. This last remark indicates the involvement of structural changes in the present dye rather than internal charge transfer/recombination mechanisms due to the absence of dependence on the solvent polarity.[15,16]

2. 5. Primary events in AO-R.

Given the characteristic times scale of AO-R's singlet state, femtosecond pump-probe spectroscopy experiments were realized. An example of the spectro-temporal data obtained is displayed on figure 2.4. The excitation was realized at 500 nm in order to excite both the molecule in not too high vibrational levels (to prevent internal cooling of the molecule) and to gain visibility in the stimulated emission (SE) region.

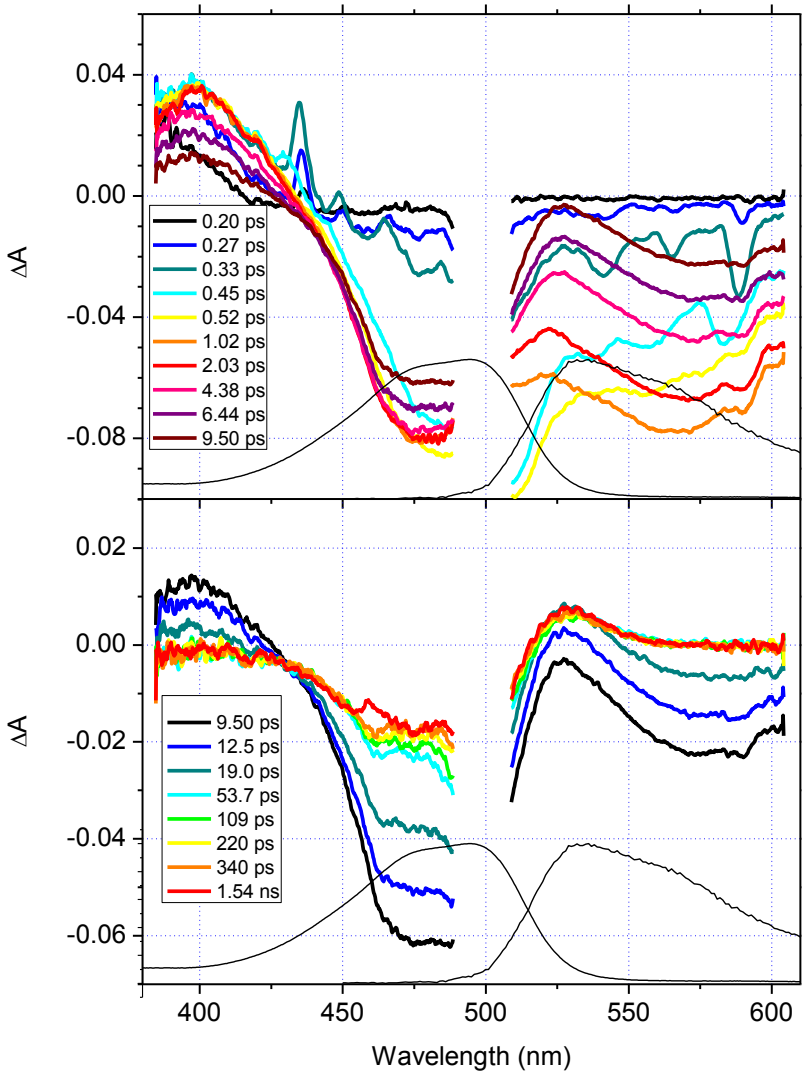

Figure 2.4. Pump-probe time resolved femtosecond spectroscopy of AO-R in MeCN. (Up) short time scale from 0.2 to 10 ps. (Down) longer time scale from 10 ps to 1.5 ns. In black the steady state absorption and emission spectra are recalled.

In all solvents the spectra show similar trends. In the blue region (i.e. up to 500 nm) of the time resolved spectra it is possible to observe: 1) a positive band centered around 400 nm whose amplitude monotonically decreases down to zero; 2) the negative bleaching band around 490 nm matching the steady state absorption of the dye (recalled as a black line in the bottom of the figure); and 3) that the bleaching never goes back to zero.

The red region of the spectra exhibits more complicated evolution: 1) at short time we can observe the stimulated emission band which is immediately overlapped by a growing positive peak around 530 nm; 2) at longer time scale the positive 530 nm band reach a final positive value while the SE band continue to increase up to zero with apparently the same kinetic as the positive 400 nm absorption band (see inset figure 2.5); and 3) together with the permanent negative bleaching, this is a strong indication of the fast formation of a photoproduct which do not return back to the ground state within the time window of our experiment (<4ns).

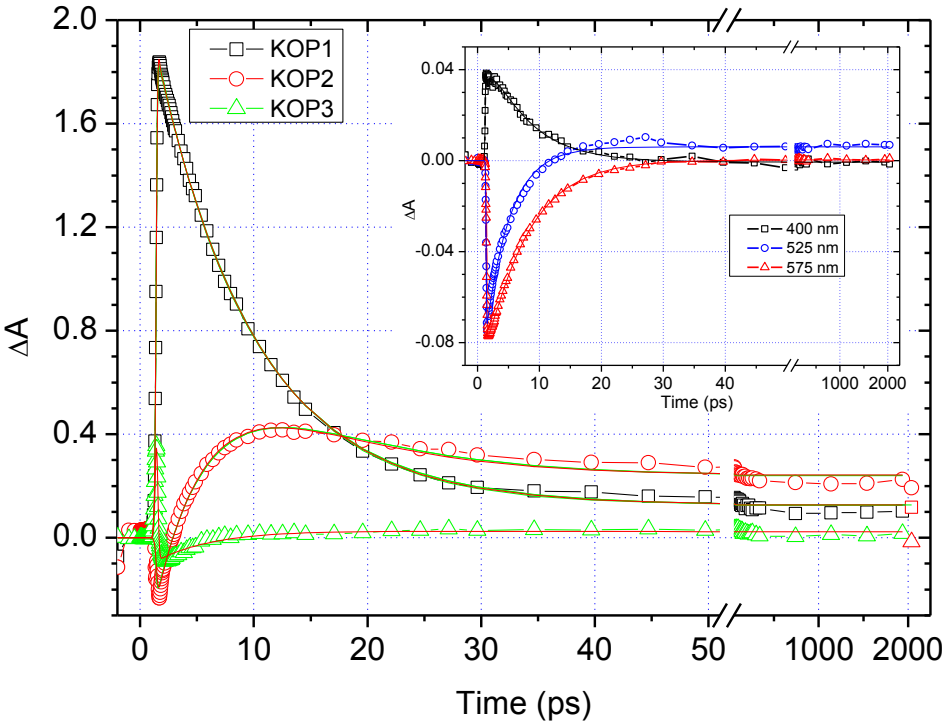

Figure 2.5. Orthogonal kinetics of AO-R in MeCN obtained by SVD of the spectro-temporal data. Inset: single wavelength at 400, 525 and 575 nm.

In order to get more insights into the kinetics, singular value decomposition (SVD)[17-19] and single wavelength kinetic analysis were performed. The first three orthogonal kinetics (KOP 1 to 3) in MeCN extracted from spectral-temporal data of figure 2.4 are displayed in figure 2.5 together with single wavelength kinetics at 400, 525 and 575nm as inset. The KOP were fitted with a sum of two

exponentials function plus a step. The corresponding lifetimes are given in table 2.3. It must be noted that a delayed growth of the KOP is observed in all the solvents. Moreover, the same delayed growth is also observed in the single wavelength kinetics. These last remarks indicate a sub 100fs phenomenon not fully resolved by the experimental setup. The obtained time constants in the different solvents are given in table 2.3, where t(SVD_1) and t(SVD_2) are the two time constants obtained by the SVD analysis. The kinetics at 400 nm and 575 nm were globally fitted with a monoexponential function and share the same time constant t(400/575), while the kinetics at 525 nm were fitted separately and needed up to two time constants t(525_1) and t(525_2) in DMSO and water due to non-exponential behavior.

	Acetone	MeCN	H_2O	EtOH	DMSO	TEG
η /cP	0.31	0.37	0.89	1.07	1.43	49
t(SVD_1)	5.42	5.69	2.54	8.14	1.43	11.8
t(SVD_2)	9.55	8.56	11.3	16.4	37.4	156
t(400/575)	9.15	7.56	9.8	13.2	35.8	153
t(525_1)	5.32	4.00	3.4	8.12	2.01	110
t(525_2)			12.4		27.8	

Table 2. 3. Kinetic parameters (time constants in ps) obtained by femtosecond pump-probe spectroscopy.

From table 2.3 it is obvious that the long time constant t(SVD_2) depends on the viscosity of the solvent going from around 9 ps in lower viscosity acetone and MeCN to a 153 ps in the highly viscous TEG. This behavior is in line with the increasing intensity of emission observed in fluorescence experiments. It can also be noticed that the short t(SVD_1) is very close to t(525_1).

The single wavelength kinetics at 400 and 575nm exhibits the same behavior and decay homothetically. This is confirmed by fitting the decays: a single exponential function with the same time constant (400/575) was enough to fit simultaneously both wavelengths kinetics. This strongly indicates that the transient absorption around 400 nm originates from the singlet excited state of AO-R. Moreover this monoexponential behavior exhibits a time constant t(400/575) which is very close to t(SVD_2) and bears the same viscosity dependence with solvent. Thus, in line with fluorescence observation and quantum yields measurements, t(SVD_2) reflects the lifetime of an emissive singlet excited state of AO-R. Moreover, it can be seen that this lifetime increases with the solvent viscosity (see table 2.3).

The rising band found around 530 nm is more difficult to interpret and exhibits strong non exponential behavior in DMSO and water. It can probably be argued that the overlap of absorption and emission bands of different species induces a complex kinetics. However it is clear that the rise time of this absorption is not correlated to the singlet state lifetime, as it grows much faster than S1 state decays (see inset in figure 2.5). Although the fitting time constants given in table 2.4 are indicative, they underline a quite viscosity-independent kinetics contrarily to t(SVD_2). Moreover, the signal becomes positive and permanent in the 3-4 ns timescale of the femtosecond setup (i.e. a step function) which, together with the permanent bleaching indicates the formation of a stable photoproduct. The time constant obtained from the fits are very close to t(SVD_1) and one could postulate that t(SVD1) mainly corresponds to the time formation of the photoproduct while t(SVD2) is related to the lifetime of AO-R excited singlet state S_1.

2. 6. Laser Flash Photolysis.

In order to indentify the photoproduct in the ns-µs timescale, Laser Flash Photolysis (LFP) experiments were performed in Ar saturated solution.

On figure 2.6, the µs LFP transient spectra of AO-R in Ar saturated MeCN can be seen. They are very similar in shape to the 1.54 ns spectra obtained in femtosecond pump-probe experiments: on the red side of the permanent bleaching a positive absorption band can be observed. The kinetics of the bleaching (at 450 nm) and the transient (at 550 nm) are given in the inset of the figure 2.6. A long lived transient was detected with lifetime longer than 180 µs. In order to check possible triplet state nature of this transient the same measurements were performed under air: neither the kinetics nor the spectra were modified by the presence of oxygen in the solution. At this stage, we can claim that the formation of a triplet state from AO-R is excluded.

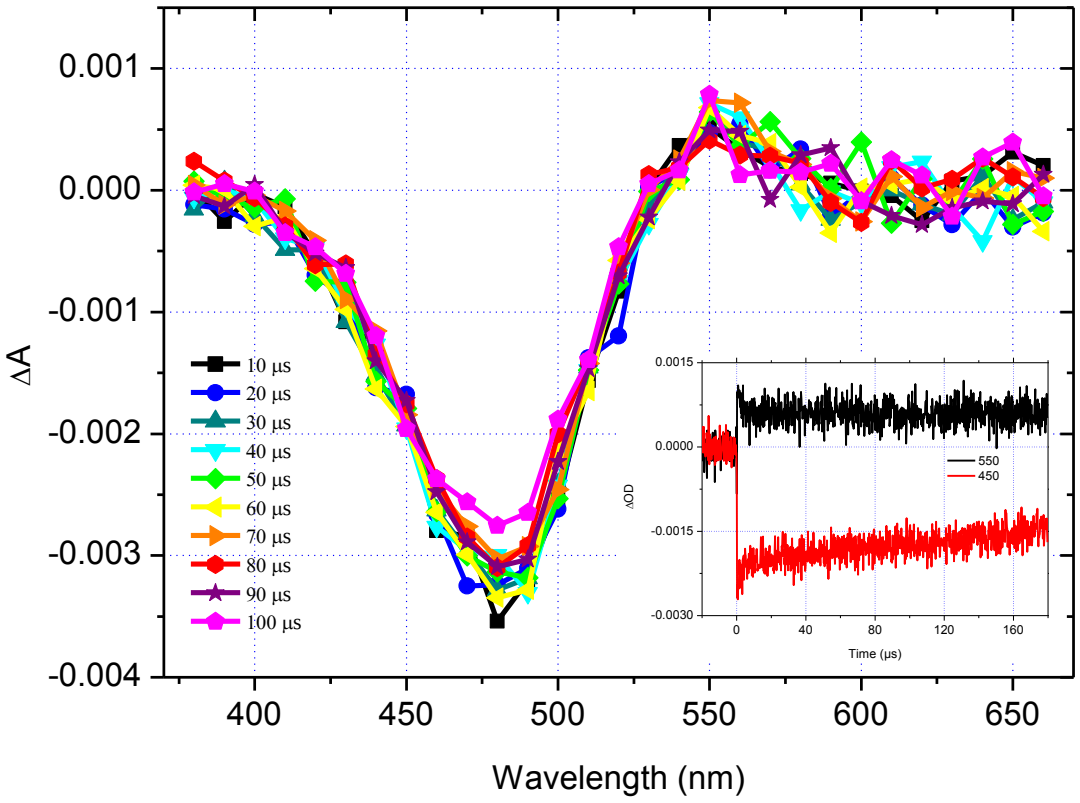

Figure 2. 6. Transient absorption spectra of AO-R obtained by laser flash photolysis (Ar saturated solution). Inset: kinetic at 550 and 450nm.

As a first conclusion, AO-R exhibits a very particular photophysics: no triplet state was detected in LFP, the radiative lifetime did not depend on the medium polarity, no steady state nor dynamic solvatochromism was observed and picosecond kinetics revealed viscosity dependent kinetics. In order to find out the subtle nature of the formed photoproduct quantum chemical calculations of AO-R in vacuum and in solvents have been jointly performed.

2. 7. Molecular modeling.

All of the work presented in this section, concerning the modeling of Astrazone Orange's eight conformers was made in the ground and excited state by the group of Patrice Bordat, from the university of Pau.

2.7.1. E and Z conformers.

Given the molecular structure of AO-R (figure 2.1), 8 possible conformers can be postulated: 4 entgegen (E) conformers and 4 zusammen (Z) conformers. The 4 (E) conformers come from the flip up/down or down/up of the two central hydrogens of the C-CH=CH-C moiety combined with a 180° flip of the phenyl ring moiety. The 4 (Z) conformers result from the C-CH=CH-C moiety making an elbow on the side of the dimethyl groups or on the side of the methyl-amino group, combined to a 180° flip of the phenyl ring moiety (conformers are displayed on Figure SI1).

The most stable conformer is displayed on figure 2.7 corresponding to an E conformer with the phenyl ring moiety on the same side as the dimethyl group. This (E) conformer will be called E1 in the following.

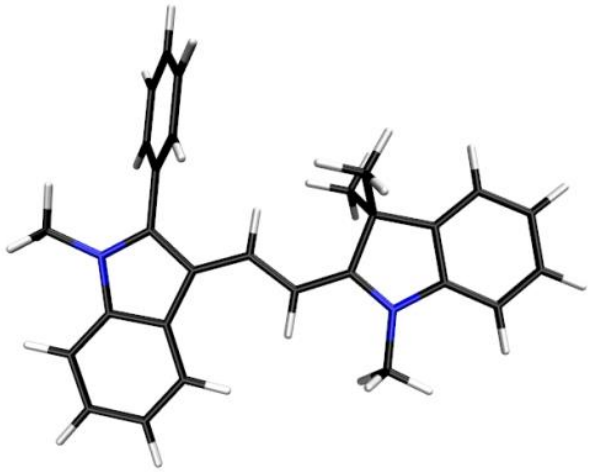

Figure 2. 7. Most stable (E) conformer (called E1) found from QM calculations.

In vacuum, other (E) conformers are 1.78, 2.12 and 3.68 kcal/mol above E1 (for E2, E2anti and E1anti respectively). Z conformers have much higher energies above E1: 8.41, 12.93, 14.37 and 17.57 kcal/mol (for Z1, Z2, Z4, Z3, respectively). Furethermore, QM calculations on all conformers in different solvents (acetone, MeCN, methanol (MeOH), EtOH, DMSO, water) have been carried out. Although the solvents lead to stabilization by about 17 to 35 kcal/mol depending on the nature of the solvent and on the nature of the conformers, the sequence of the conformers found in vacuum remains unchanged. So, the polarity of the solvent has a small influence on the conformers as it has been unambiguously demonstrated experimentally in the previous sections. A simple calculation using a Boltzmann distribution show that E1 represents 92.5 % of the ground state population at 20°C.

Figure 2.8 shows highest occupied (HOMO) and lowest unoccupied (LUMO) molecular orbitals of E1. The delocalization of both molecular orbitals combined to a strong overlap is in full agreement with a strong molar absorption coefficient and is expected to provide a visible absorption.

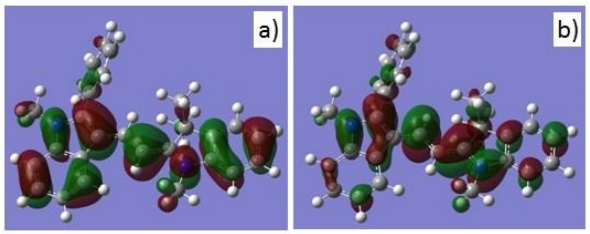

Figure 2. 8. a) HOMO and b) LUMO snapshots

Indeed, QM calculations give absorption for E1 at 441.65 nm in vacuum with oscillator strength of 0.8856. A second consequence is the delocalization of the net charge of +1e on the squeleton of AO-R. Indeed, from the Mülliken population analysis (as well as the ESP fit method), nitrogen atoms have a partial charge of about -0.48e, carbons' charges are in the [-0.3:+0.3]e range and hydrogens exhibit a partial charge of about +0.1e. A third consequence of the delocalization of the electronic density consists in the majority of the C-C bond lengths around 1.42 Å revealing a mixture of single and double bond characters. However, the central C-C bond length of the C-CH=CH-C moiety is 1.38 Å (even slightly lower with DFT functionals including electrostatic and/or dispersion corrections), highlighting the predominant double bond character of the center of AO-R.

	E1	E2	E1anti	E2anti	Z1	Z2	Z3	Z4
vacuum	441.6 (0.886)	439.2 (0.889)	454.8 (0.784)	453.5 (0.816)	463.23 (0.515)	482.7 (0.366)	515.3 (0.277)	489.2 (0.451)
Acetone	447.8 (1.090)	445.7 (1.069)	456.1 (0.991)	456.1 (1.035)	469.81 (0.611)	479.2 (0.464)	494.8 (0.281)	486.3 (0.594)
EtOH	447.7 (1.091)	445.5 (1.061)	455.9 (0.992)	455.8 (1.038)	469.78 (0.612)	479.1 (0.464)	494.6 (0.283)	486.1 (0.595)
MeOH	446.3 (1.082)	444.1 (1.061)	454.5 (0.983)	454.4 (1.028)	468.77 (0.605)	478.2 (0.457)	493.4 (0.277)	484.8 (0.589)
MeCN	446.8 (1.087)	444.6 (1.066)	455.0 (0.988)	454.9 (1.033)	469.17 (0.608)	478.5 (0.460)	493.4 (0.279)	485.2 (0.592)
DMSO	449.3 (1.110)	446.9 (1.087)	457.3 (1.010)	457.3 (1.056)	471.02 (0.622)	480.0 (0.473)	494.0 (0.287)	487.0 (0.608)
H_2O	446.1 (1.085)	443.9 (1.064)	454.1 (0.987)	454.1 (1.032)	468.69 (0.606)	477.9 (0.457)	492.0 (0.276)	484.4 (0.591)

Table 2. 4. First electronic transition (nm) and oscillator strength (in brakets) for all conformers in vacuum, acetone, acetonitrile, methanol (MeOH), ethanol, DMSO and water.

2.7.2. Electronic properties: absorption and emission.

We have also investigated the first absorption band of all 8 conformers in the 6 solvents mentioned previously. Results are collected in table 2.4. It can be seen that E1 and E2 have a similar absorption transition both in terms of maximum wavelength absorption and oscillator strengths. Then, E2anti and E1anti exhibit similar electronic transitions which are slightly red shifted by about 12 nm compared to E1. All (E) conformers have strong oscillator strengths. For (Z) conformers, the red shift is even more important from 22 to 60 nm. Nevertheless, absorption of (Z) conformers is weaker with oscillator strengths typically between 0.27 and 0.62. Another feature is that the solvents induce a small red shift of about 1-8 nm for all (E) conformers. For Z1, absorption wavelength is red shifted by 23 nm compared to E1 and the solvents further induce a red shift of 5 to 8 nm. The behavior of (Z) conformers is somehow more complex: the interaction of Z2, Z3 and Z4 with the solvents leads to an unexpected blue shift compared to vacuum by 3 to 5 nm (for Z2 and Z4) and 20 to 23 nm (for Z3 which is the most polar of Z conformers). However, the absorption wavelength for Z2, Z3 and Z4 is still red shifted by 35 and 50nm compared to E1 in the investigated solvents.

From tables 2.2 and 2.4, it can be seen that QM calculations underestimate the experimental absorption wavelength by about 50 nm. Nevertheless, QM calculations give an electronic transition for AO-R which is rather independent on the nature of the solvent as it has already been pointed out experimentally (Table 2.2). The trend discussed above is satisfactorily in agreement to the experimental data.

The first excited states of all 8 conformers in the solvents mentioned previously were also investigated. The relaxed excited state of E1, E1* is the most stable whatever the solvent. It is followed by E2*, E2anti* and E1anti* which are around 1.94, 4.42 and 6.07 kcal.mol^{-1} higher, respectively. This sequence is similar to the sequence of (E) conformers in the ground state. This is also true for the sequence of Z* conformers which presents the same order as the sequence found for the ground state of (Z) conformers: Z1*, Z2*, Z4* and Z3*. The energy difference between Z1* and Z3* is 5.14 kcal.mol^{-1} and Z1* is 10.82 kcal.mol^{-1} above E1*.

Fluorescence emission of AO-R in the different solvents mentioned previously has been calculated and the results are summarized in table 2.5.

Maximum emission wavelengths of (Z) conformers is not listed in table 2.5 because they exhibit either no or a very weak fluorescence emission out of the visible range. A possible explanation

of the non-fluorescence of (Z) conformers lies in the fact that (Z) conformers have a strong structural change between the ground state and the excited state as it is shown in Figure 2.8 for Z3.

	E1	E2	E1anti	E2anti
Acetone	545.61	541.67	571.81	570.57
EtOH	546.21	542.28	572.37	571.14
MeOH	546.92	542.98	573.02	571.82
MeCN	547.12	543.18	573.19	572.01
DMSO	547.62	543.72	573.67	572.52
H_2O	548.26	544.41	574.30	573.17

Table 2. 5. Maximum emission wavelengths (nm) for (E) conformers in acetone, acetonitrile, ethanol, methanol, DMSO and water.

On the contrary to (Z) conformers, the structures of (E) conformers in the ground states and in the excited states are very similar (see for example E1 and E1* displayed in figure 2.9). This result is in good agreement with the steady-state fluorescence and absorption results. Therefore, they present a strong fluorescence emission (with wavelengths given in Table 2.5). Once again, the sensitivity of the emission to the solvent is very weak as observed experimentally. Moreover, a close view to table 2.5 allows us to say that calculated emission of E1* is in good agreement with measured emission with only a deviation of 10 nm.

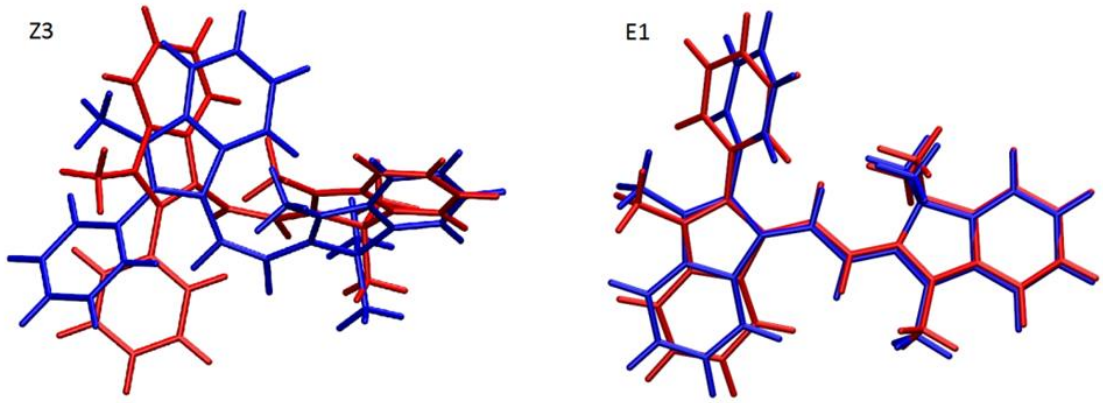

Figure 2. 9. Structures of Z3 (top) and E1 (bottom) in the optimized ground state (blue) and relaxed excited state (red).

2.7.3. Relaxation pathways of AO-R.

From experimental and computational results, a possible mechanism can be drawn explaining the tricky photophysics of AO-R. In figure 2.10, the position (relative to E1) of all optimized ground and excited conformers in MeCN is given. The blue arrow indicates the laser excitation energy used. It can be seen that E1* and E2* are very close. Thus, it can be postulated, as AO-R is in the E1 form in the ground state, that upon light absorption the Franck-Condon (FC) initial excited state reached has two relaxation pathways with unresolved sub-100 fs kinetics: either to the stabilized excited state E1* or towards the excited state of E2, E2*.

Taking into account the very weak fluorescence quantum yield determined experimentally, it is possible that a small fraction of the (FC) initial population decays towards the relaxed excited state E1* (giving then a fluorescence emission), while the other fraction of (FC) population is implied into the population of E2*.

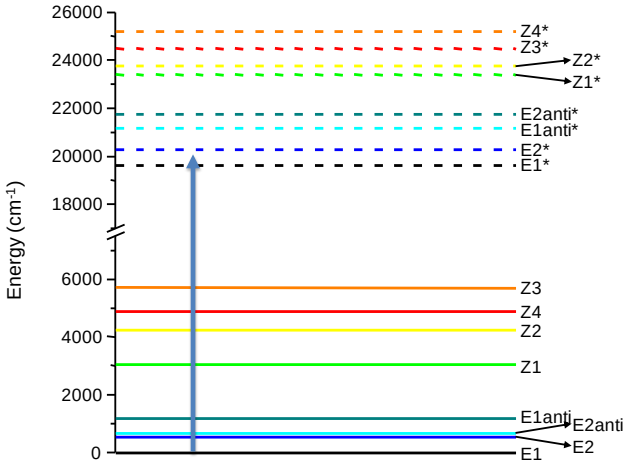

Figure 2. 10. Relative energy levels of the 8 optimized AO-R isomers in ground and relaxed excited state computed in acetonitrile.

Then the two populations evolve independently according to the decoupled experimental kinetics at 400/575 nm and 530 nm. Furthermore, QM calculations show that the central C=C bond in the C-CH=CH-C moiety is lengthen by 0.04 Å in the E2* excited states, implying a decrease of the double bond character and favoring isomerization from $E2^*$ to one (Z) isomer. The simplest isomerization in term of atoms movements occurs towards Z1 and is done in a quasi-constant molecular volume with small molecular rearrangement. This fact leads to a fast Hula-twist

isomerization reaction as observed elsewhere[20,21] and occurs in the 5-10 ps time scale giving rise to the positive peak observed around 535 nm and to low fluorescence intensity. Indeed, if E2* is fluorescent, its very short lifetime (<10 ps) and spectral recovery with E1* emission do not permit any observation. This postulated scheme is also supported by QM calculations as they indicate that (Z) isomers do not present fluorescence emission which is compatible with the experimental results. The postulated mechanism is displayed on figure 2.11.

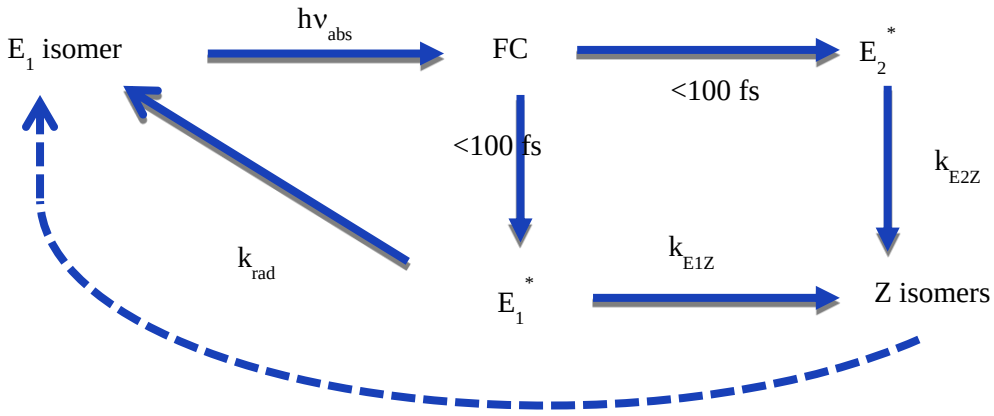

Figure 2. 11. Postulated mechanism explaining AO-R photophysics.

Keeping in mind that the radiative relaxation (k_{rad}) is almost constant whatever the solvent, the viscosity dependence of the lifetime of S1 (assigned to the relaxed excited state of E1, E1*) indicates that E1* deactivation arises from a competition between fluorescence and another route which would be viscosity dependent.[16-19] It is likely that E1* undergoes an isomerization involving more important rearrangement: the most simple route of isomerization is towards Z3 and this induces greater structural changes than the E2*→Z1 isomerization (see figure 2.11). This reaction induces a higher molecular reorganization which becomes viscosity dependent.[20,21] If it is postulated that Z3 isomer is formed with a rate constant $k(E_{1Z})$ which is solvent viscosity dependent (see proposed scheme on figure 2.12), $k(E_{1Z})$ will govern the emissive state lifetime according to:[22-25]

$$\tau_{S_1} = \frac{1}{k_{rad} + k(E_{1z})}$$

Therefore, k_{SZ} can be extracted from experiments. Taking into account that k_{rad} is in the ns time scale while singlet state lifetime τS_1) is in the ps time scale, $k(E_{1Z})$ is directly related to τS_1):

$$k(E_{1Z}) = \frac{1}{\tau_{S_1}} - k_{rad} \approx \frac{1}{\tau_{S_1}}$$

It is also important to mention that the possibility of the relaxed excited state E1* to give other isomer is in favor of a weak fluorescence quantum yield.

Once AO-R is in one of the (Z) states, a series of structural rearrangements possibly involving other (Z) and (E) conformers in order to go back to E1 can be proposed. First, the ground state of Z3 could thermally relax to the ground state of Z4, then to Z1 etc... Finally, the last step could be the thermal relaxation of E2 towards the ground state of E1. Whatsoever, as no experimental proofs are available one could also propose a direct relaxation to the ground state of E1.

2. 8. Conclusion.

In the light of the present work, AO-R shows a very complex photophysics which is partly explained by combining many complementary experimental and computational techniques. It appears that molecular modeling of AO-R is in a very good agreement with the experimental spectroscopic results allowing getting insights into its particular photophysics. It is demonstrated that 8 conformations are available for this cationic cyanine dye, and that the most stable (E) conformer, E1, represents more than 92% of the ground state population at 20°C. Associating computational results and experimental data permit to identify the formed photoproduct as one of the (Z) isomers and allow postulating a possible mechanism where two isomerizations could be involved: a very fast one, and a slower, viscosity-dependent second one, which governs fluorescence lifetime.

This complex photophysics, and particularly its viscosity-dependent behavior, explains the efficiency that Astrazone Orange R has shown as a photoinitiator.

2. 9. References.

[1] Kellett, H. *Journal of the Society of Dyers and Colourists,* **1968**, 84, p. 257-261.

[2] Angulo, G.; Grammp, G.; Rosspeinter, A. *Spectrochim. Acta, Part A* **2006**, 65, 727.

[3] Angulo, G. *EPA Newsletter* **2007**, 26.

[4] *Gaussian 09, Revision D.01, Gaussian, Inc., Wallingford CT*, **2009**.

[5] Scalmani, G.; Frisch, M. J.; Mennucci, B.; Tomasi, J.; Cammi, R.; Barone, V. *J. Chem. Phys*. 124, **2006**, 09107:1-15.

[6] Improta, R.; Barone, V.; Scalmani, G.; Frisch, M. J. *J. Chem. Phys.* **2006**, 125**,** 054103:1-9.

[7] Miertuš, S.; Scrocco, E.; Tomasi, *J. Chem. Phys.* **1981**, 55, 117.

[8] Suppan, P. *Chemistry and light*, RSC Cambridge UK **1994**

[9] Braun, A.M. ; Maurette, M.-T.; Oliveros, E. Technologie Photochimique; *Presses Polytechniques Romandes* Lausanne Switzerland **1986**.

[10] Marcus, Y. *The Properties of Solvents, Wiley Series in Solution Chemistry: Volume 4; John Wiley & Sons Ltd*, Chichester, England, **1998**.

[11] Kamlet, M. J.; Abboud, J.-L. M.; Abraham, M. H.; Taft, R. W. *J. Org. Chem.* **1983**, 48, 2877.

[12] Lakowicz, J.R. *Principles of fluorescence spectroscopy*, Kluwer Academic/Plenum publishers New York USA, **1999**.

[13] Valeur, B. *Molecular Fluorescence Principles and Applications*, WILEY-VCH Verlag GmbH Weinheim **2002**

[14] Turro, N.J.; Ramamurthy, V. ; Scaiano, J.C. *Modern molecular Photochemistry of Organic Molecules*, University science book, Sausalito California **2010**.

[15] Cornelissen-Gude, C.; Rettig, W.; Lapouyade, R. *J. Phys. Chem.* A **1997**, 101, 9673**.**

[16] Gude, C.; Rettig, W. *J. Phys. Chem. A* **2000**, 104, 8050.

[17] Ernsting, N. P.; Kovalenko, S. A.; Senyushkina, T. ; Saam, J. ; Farztdinov, V. *J. Phys. Chem. A* **2001**, 105, 3443.

[18] van Stokkum, I. H. M.; Larsen, D. S. ; van Grondelle, R. ; *Biochim. Biophys. Acta* **2004**, 1657, 82.

[19] Brazard, J.; Ley, C.; Lacombat, F.; Plaza, P.; Martin, M. M.; Checcucci, G.; Lenci, F. *J. Phys. Chem. B* **2008**, 112, 15182 – 15194.

[20] Liu, R.S.H.; Hammond, G.S. *Chem. Eur. J.* **2001**, 7, 4536.

[21] Liu, R.S.H. *Acc. Chem. Res.* **2001**, 34, 555.

[22] Yang, L.-Y. ; Harigai, M. ; Imamoto, Y.; Kataoka, M. ; Ho, T.-I. ; Andrioukhina, E. ; Federova, O. ; Shevyakov, S. ; Liu, R. S. H. *Photochem. Photobiol. Sci.* **2006**, 5, 874.

[23] Dellinger, B.; Kasha, M. *Chem. Phys. lett*. **1976**, 38, 9.

[24] Sun, Y.-P.; Saltiel, J.; Park, N.S.; Horburg, E.A. ; Waldeck, D.H. *J. Phys. Chem.* **1991**, 95, 10336.

[25] Malkin, S.; Fischer, E. *J. Phys. Chem.* **1964**, 68,1153.

Chapter Three.

Studies in 3-C PIS Mechanisms.

3. 1. Introduction.

In this chapter, main attention will be given to the different mechanisms that can take place in a PIS.

Three different approaches to the studies of these systems will be boarded. First, the classic LFP studies of 3-C PIS via LFP will be recalled from a previous work, with its advantages and limitations. In second place, the study of dye photolysis as a function of irradiation time will be shown and, last but not least, a mathematical model to obtain the concentration of different species involved in an ideal 3-C PCIS will also be presented and compared with experimental measurements.

3. 2. Materials and Methods.

All the polymerization experiments shown from now on in this work were carried out in a Vertex 70 FTIR, using the RT-FTIR technique. The monomer of study is SR 349 (figure 3.1), the same diacrylate used for experiments presented in chapter Two. Formulations contain a 0.1 wt% in dye, 1 wt% in each coinitiator and 10 wt% of DMSO in monomer and were stirred overnight before the realization of the experiments, unless specified otherwise. Samples with an optical density of around 1 at 1637 cm^{-1} (*i.e.* acrylates double bond absorption) were irradiated for 2 or 10 minutes with LED lamps of 390, 473 and 532 nm, depending on the PIS used.

To prevent the diffusion of oxygen into the sample under exposure, laminated experiments were carried out, placing the resin between two polypropylene films and two BaF_2 crystal windows. The thickness of the sample was adjusted using a 50 µm Teflon spacer.

The degree of conversion is calculated as:

$$Conversion\,\% = \frac{(A_{1637})_0 - (A_{1637})_t}{(A_{1637})_0}.100 \qquad (3.1)$$

where $(A_{1637})_0$ and $(A_{1637})_t$ correspond to the sample's initial Absorbance and the sample's absorbance at time "t" at 1637 cm^{-1} respectively. The rate of conversion (R_C) is calculated as:

$$R_C = \frac{\partial Conversion\%}{\partial t} \qquad (3.\ 2)$$

3. 3. Experimental proofs of PCIS behavior.

Many examples of PCIS were given in Chapter One. In this section, the PCIS behavior of some 3-C PIS for different wavelength of irradiation will be illustrated.

Three dyes were studied during this work. For 390 nm, the photosensitizer (PS) of choice was isopropyl thioxanthone (ITX), a very well-known photoinitiator that had showed great performance results in the past[1]; two pyrromethenic dyes, HMP and EMP were used for 473 and 532 nm respectively. The structures of these dyes can be seen in figure 3.1. The choice of these two dyes was made due to the extensive research made in our group regarding the mechanism of these type of compounds[2], where they have shown to be highly efficient in photoinitiation. These studies will be briefly explained in the following section. Figure 3.2 shows the UV spectra of these three dyes in acetonitrile.

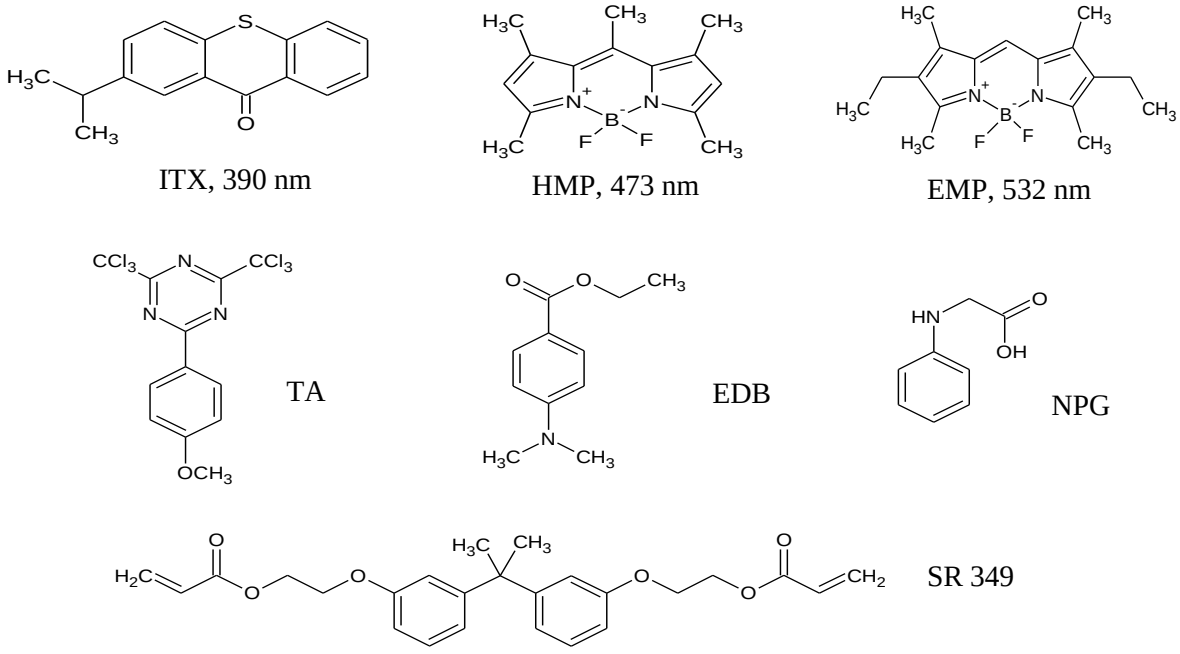

Figure 3.1. Chemical structures of the compounds used for these studies.

As coinitiators, amines ethyl-4-dimethylaminobenzoate (EDB) and N-phenylglycine (NPG) and triazine A (TA) were chosen, as their reactivity had already been studied by Tarzi *et al.*[2,3]. The structures of the coinitiators can also be seen in figure 3.1.

In the first place, 2-C PIS behavior was studied by using different combinations of dye/amine PIS. RT-FTIR results (figure 3.3) show that not all of the systems studied are suitable to initiate polymerization.

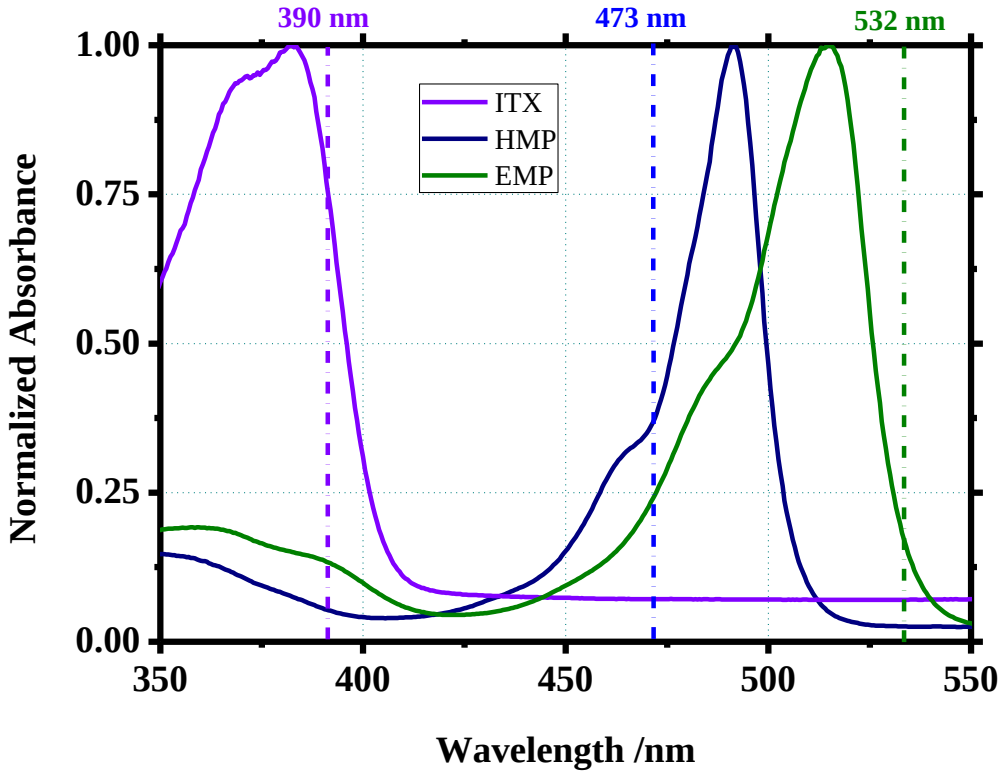

Figure 3.2. MeCN UV-vis spectra of the studied dyes and irradiation wavelengths for the different LED lamps used.

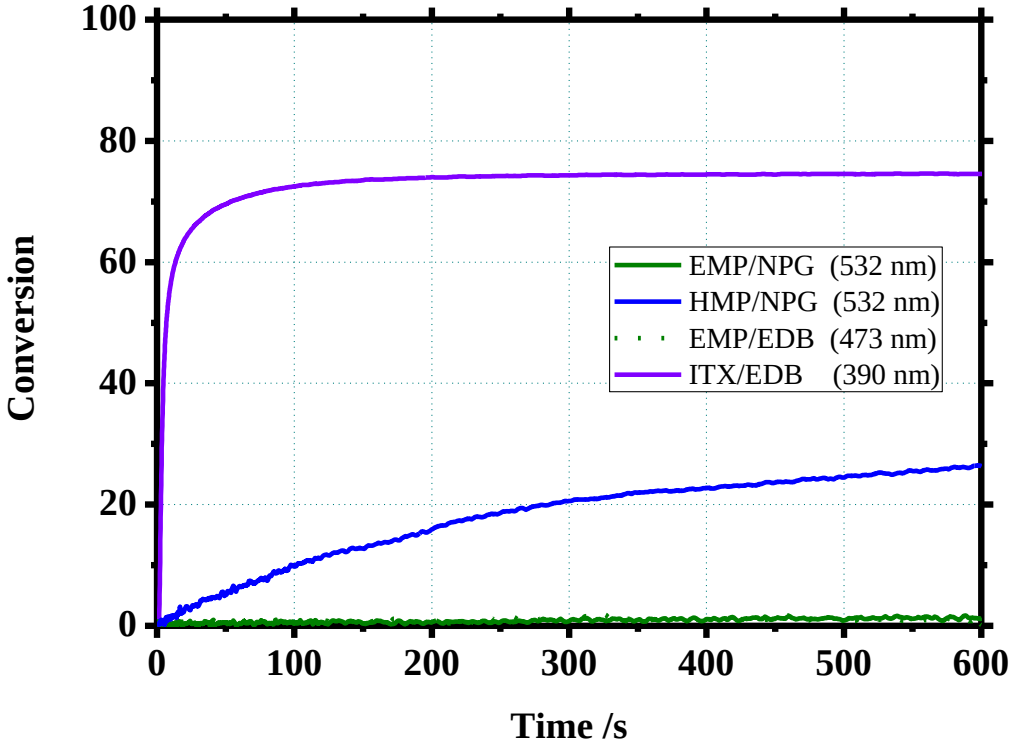

Figure 3.3. Monomer conversion vs. time for dye/amine PIS. ITX/EDB showed to be the most efficient with more than 70% conversion. EMP didn't show any polymerization with dye/amine systems.

Let's recall now that for initiating radical generation to happen, the co-initiator must be able to react with the excited state of the dye via an electron transfer reaction. This quenching of the excited state of the dye may not be efficient enough in the cases where no polymerization is registered.

As explained in Chapter One, amines are electron donors and, as seen in Chapter Two for Astrazone Orange, not all the dyes can easily undergo a reduction from their excited state. In these cases, dyes may react via oxidation with an electron acceptor instead. For this reason, dye/TA mixtures efficiency as 2-C PIS was studied under the same conditions. The RT-FTIR results can be seen in figure 3.4. In this case, it can be seen that all of the systems dye/TA can act as PIS. In other words, it is possible to find PIS suitable for all the studied wavelengths.

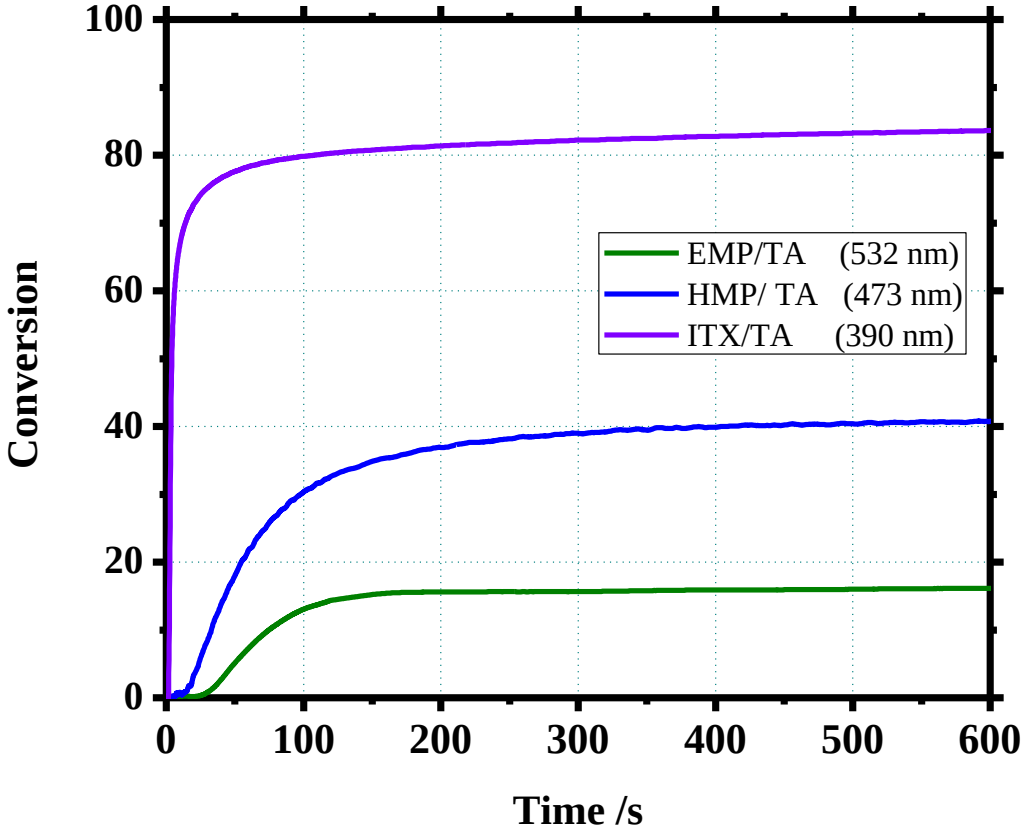

Figure 3.4. Monomer conversion vs time for dye/triazine PIS. All of the systems showed some degree of monomer conversion.

Of course, quenching becomes less efficient for thermodynamical reasons when using sources of irradiation of greater wavelengths (see section 3.4). To enhance the photoinitiating ability, 3-C PIS may be used instead of their 2-C counterparts in order to increase the efficiency, as shown in Chapter One but, before heading to the RT-FTIR results, let's take a little time to explain with more detail the advantages that the use of 3-C PIS may present over 2-C PIS.

Figure 3.5 shows typical mechanisms for 2- and 3-C PIS. In a dye/amine 2-C PIS (a), for instance, the dye is excited by an irradiation source and the excited state(s) generated reacts then with the co-initiator via an electron transfer reaction. The products of this reaction are an amino radical, which usually losses a proton in a further step to become the initiating radical of the polymerization reaction, and a dye radical. The dye radical is known to be involved in termination reactions in many cases.

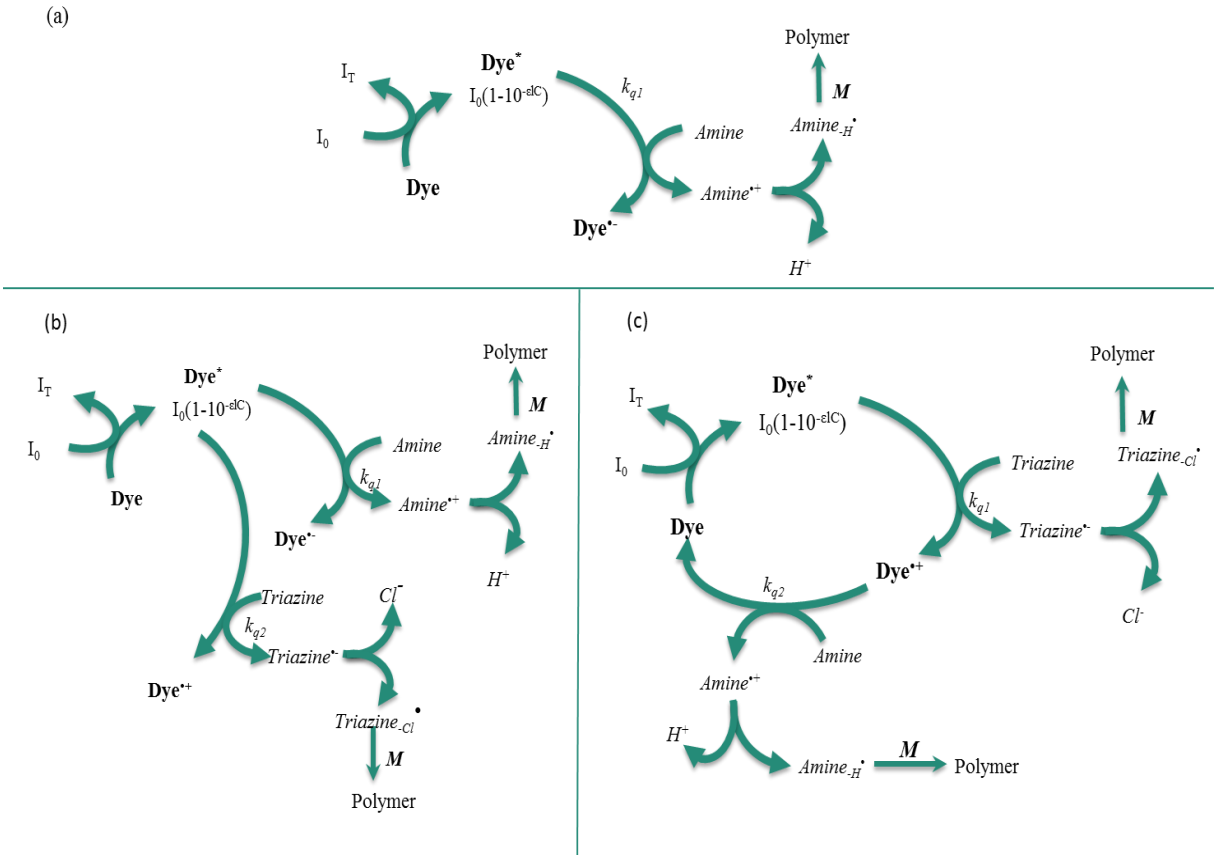

Figure 3.5. Examples of different possible mechanisms in PIS. (a) 2-C PIS dye/amine. (b) 3-C PIS where both co-initiators compete for the reaction with the excited dye and (c) 3-C PIS with PCIS behavior.

In 3-C PIS, as the amount of compounds and species in the formulation increases, there are many possible mechanisms that may take place, which can be summarized in a simple way in the two mechanisms shown in figure 3.5. In (b), the addition of a third compound (e. g. a triazine derivative) to the formulation only increases the efficiency of radical generation in the way that the excited state of the dye can be quenched by two different species. In this case, the replacement of a 2-C PIS for its respective 3-C PIS, may not result in a much more impressive efficiency increment than that obtained by simply using a more performing co-initiator or increasing the concentration of the co-initiator used in the first place.

This replacement of 2-C by 3-C PIS does not solve the main limitations presented by the former. Those limitations are the production of terminating dye radicals and the fact that radical production is limited by the amount of dye present in the formulation, which is normally between ten and twenty times smaller than that of the co-initiators. These problems are solved by adding a third component which will react with the dye radical instead of its excited state, as shown in figure 3.5 (c). When this is found, we are in the presence of a Photo-Cyclic Initiating System, PCIS.

The advantages of using PCIS instead of 2-C PIS are many. In the first place, the third component added will react with the dye radicals, decreasing the scavenging termination events in polymerization, thus resulting in greater monomer conversion. In second place, the ground state of the dye is regenerated, letting it available to reabsorb photons and reenter in a new reaction cycle. Thus, the production of radicals will no longer be limited by the amount of the dye in the formulations, but rather by the amount of co-initiators.

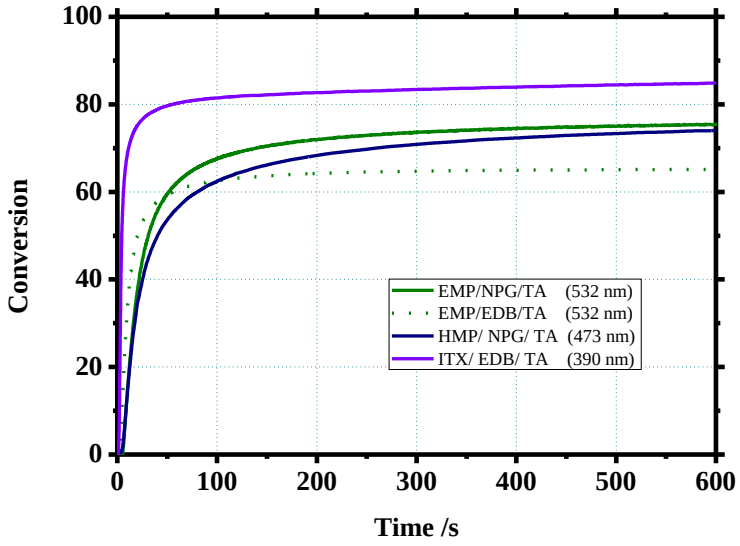

Figure 3.6. Monomer conversion vs. time for dye/triazine/amine PIS. More than 60% of monomer conversion was found for all the PIS.

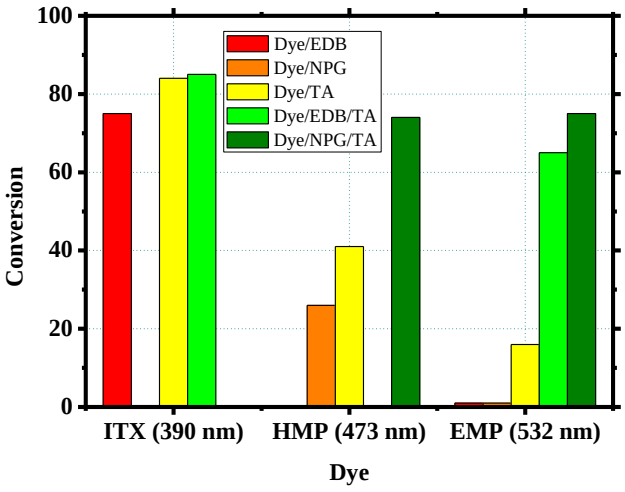

Figure 3.7. Monomer conversion for all the studied PIS. A clear PCIS behavior can be noticed for PIS containing EMP.

Of course, there are many possible processes that can take place in the reaction media. Another possibility, for example, could be to have a consecutive reaction like in (c), but where the dye ground state is not recovered. To go further, it could also be possible to have a competitive reaction for the excited state where the complementary co-initiator will react in a second step with the dye radical produced in order to regenerate the steady state, allowing the possibility of two competitive PCIS at the same time. This will be further discussed in section 3.7.

Now, going back to the PIS of study, RT-FTIR results obtained for 3-PIS can be seen in figure 3.6. Figure 3.7 compares the monomer conversion obtained for each PIS. Here, three different cases can be clearly distinguished. For ITX, both 2-C PIS shown great efficiency, meaning that both, TA and EDB, can react with ITX excited state, ITX*. In this case it can be concluded that mostly competitive reactions for the excited state of the dye take place when using the 3-C PIS ITX/EDB/TA.

Results obtained for EMP dye PIS, in contrast, clearly indicate the presence of a photocyclic behavior. EMP/amine PIS show no polymerization, indicating that neither EDB nor NPG are able to quench the excited state EMP*. For the PIS containing EMP/TA, however, around 16 percent of final conversion was found, meaning that EMP* can be quenched through an oxidative pathway. This is not surprising, since EMP is a cationic dye. For both 3-C PIS studied, EMP/EDB/TA and EMP/NPG/TA, an impressive increment of final conversion (65 and 75% respectively) and conversion rate (from less than 1 to 3 and 5 s^{-1}, respectively) are registered. Here, the presence of a PCIS is undeniable: the amines, which do not react with EMP* react, nevertheless, with EMP radicals. To conclude on whether the dye ground state is regenerated or not, requires further research and will be discussed in the following sections.

Regarding the PIS containing HMP, polymerization was found in both 2-C PIS and, although not as impressive as for EMP, an increment in final conversion can be noticed when using the 3-C PIS. For these PIS, however, it would be more difficult to conclude on whether there is a PCIS or competitive reactions.

3. 4. Thermodynamics of the PCIS.

As it was stated in the previous section, not every mixture of an acceptor, a donor and a dye will have photocatalytic behavior. In order to obtain it, the components should be carefully selected. Thus, a previous thermodynamic approach to the PCIS should be done. Figure 3.8 represents the different electron transfer reactions occurring in the oxidative PCIS.

The first reaction is the electron transfer reaction between the dye ground state and the coinitiator. Its reactivity is governed by the Gibbs free energy change $\Delta G_{ET}^{GS} = E_{ox}^{D} - E_{red}^{PS}$, where E_{ox} and E_{red} are the half-wave oxidation and reduction potentials for the donor and the acceptor, respectively. ΔG_{ET}^{GS} must be as endergonic as possible to prevent any dark reaction.

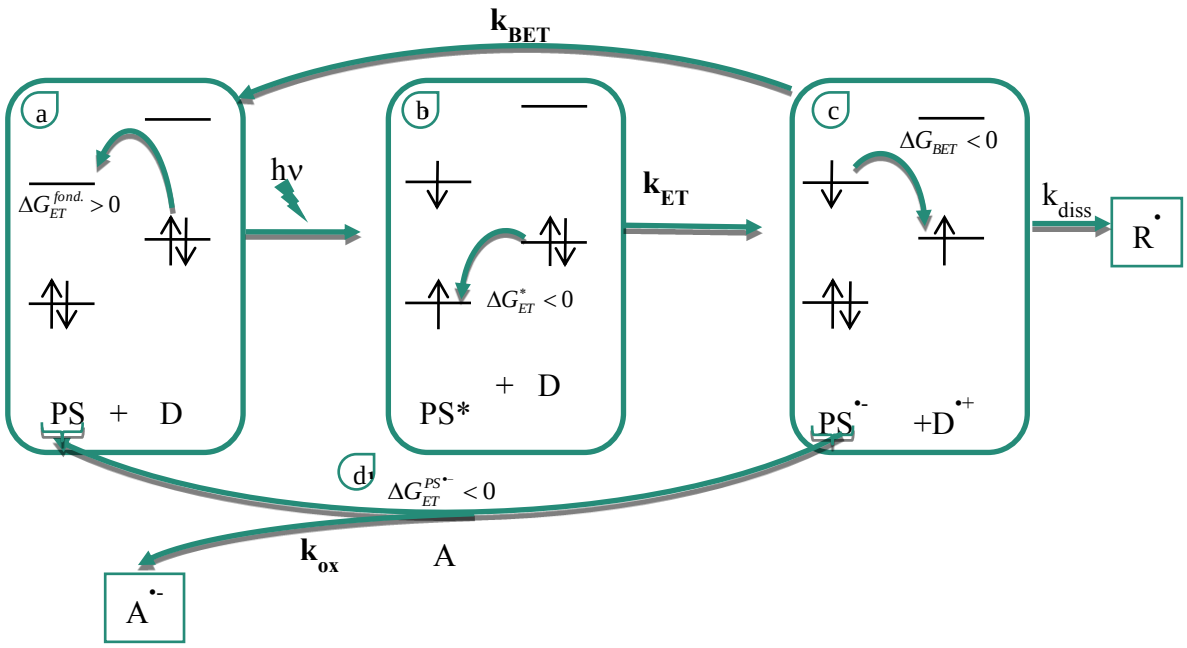

Figure 3.8. Thermodynamics of a reductive three-component PCIS, a) ground state reaction, b) excited state reaction, c) back electron transfer, d) PS regeneration.

After absorption of light, the PS goes into singlet or triplet excited states, in which it becomes both a better oxidant and reductor. As a consequence, electron transfer reaction can occur, for instance, with an electron donor D. The reaction must be as much exergonic as possible. The values of the Gibbs free energy change, ΔG_{ET}^{*}, for photoinduced electron transfer is given by the Rehm–Weller equation[4]: $\Delta G_{ET}^{*} = E_{ox}^{D} - E_{red}^{PS} - E^{*} + C$, where E* stands for the energy of the excited state. The Coulombic term C is usually neglected in polar solvent. ΔG_{ET}^{*} value will determine the rate of electron transfer and the dye and the electron donor must be chosen such that it is negative enough to obtain a high electron transfer rate constant.

For longer irradiation wavelengths (i. e. red light), the value of E* becomes smaller, which makes it more difficult to find an electron donor whit E_{ox}^{D} small enough to make the reaction exergonic.

The third electron transfer step is the unwanted back electron transfer BET within the contact ion pair (PS•-···D•+) which leads to initial reactants. ΔG_{BET} is given by $-\Delta G_{ET}^{GS} = -E_{ox}^{D} + E_{red}^{PS}$. This reaction is generally exergonic and the rate competes with the dissociation rate k_{diss} of the contact ion pair into free solvated species. In practice, BET reduce the overall radical generation quantum yields. Some new approaches allow to trigger this reaction[5,6].

The last step is the dye regeneration. In order for the cycle and for the catalytic behavior to occur, the corresponding Gibbs free energy change, $\Delta G_{ET}^{PS^{-\cdot}}$ should be negative. If one assumes that the reduction potential of $PS^{\bullet-}$ can be considered, in a row approximation, to be given by the oxidation potential of PS, then $\Delta G_{ET}^{PS^{-\cdot}} = E_{red}^{PS} - E_{red}^{A}$. Thus, in order to achieve efficient dye regeneration, the choice of the acceptor A should be carefully done to obtain an exergonic reduction of the oxidized PS.

This approach is also valid to an oxidative catalytic cycle where the PS first reacts with the acceptor A, and then its oxidized form is reduced by the donor D. This criterion was taken into account when selecting the 2- and 3-C PIS that will be presented further on in this thesis work.

3. 5. Mechanistic studies: the LFP approach.

The enhancement in the polymerization efficiency alone is not enough to prove the existence of a PCIS. Additional information like recovery of the dye after irradiation or the detection of the postulated species is desirable. A very effective way to achieve the detection of the intermediate

species is the study of solutions containing the PIS components by LFP. In this case, the PIS of study was EPP/EDB/TA, due to the fact that it had already shown the behaviour of a PCIS in polymerization[2]. The results here presented were performed by O. Tarzi in the sein of the LPIM and will be presented in this section as a way to illustrate how a PCIS behavior can be demonstrated by LFP studies.

EPP is a pyrromethene dye absorbing at 532 nm, whose structure is shown in figure 3.9. Its radical cation is easily detected at 400 nm according to Susuki[7]. In order to detect these species, solutions containing EPP alone, EPP with TA and EPP with both, TA and EDB, were studied by LFP at 400 nm. Also, in order to analyze the ground state dye recovery, these solutions were also studied at 520 nm, in order to register the bleaching of the dye. The solvent used for all of these solutions was MeCN. All of the samples were bubbled with argon 15 minutes previous to the LFP measurements.

The monitoring at 400 nm is shown in figure 3.9. Of course, the solution containing EPP alone shows not signal, but when TA is added to the solution, a permanent signal can be observed. This is a proof that EPP reacts with TA, generating the EPP cation radical and, in consequence, the TA anion radical. When EDB is also added to the solution, it can be seen that this signal disappears, suggesting that EDB reacts with EPP cation radical.

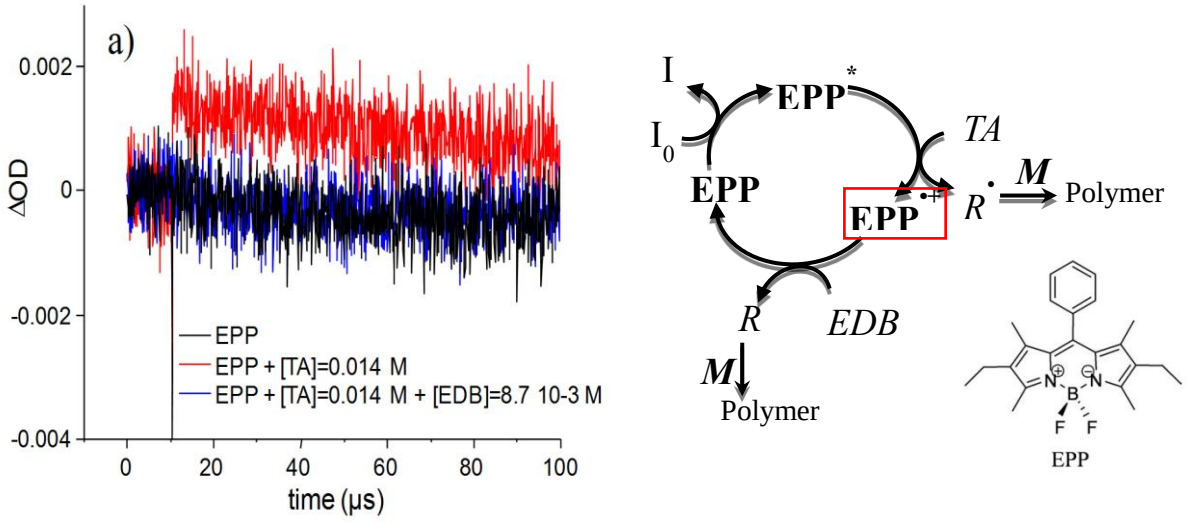

Figure 3.9. EPP radical cation monitoring at 400 nm. This species is generated after reaction with TA, but react rapidily in a further step with EDB.

The recording at 400 nm, however, does not give any evidence about the regeneration of the ground state of the dye. In order to obtain this information, the bleaching of EPP was studied at 520 nm. Figure 3.10 shows that, of course, the dye decays fully to its ground state in less than 10

microseconds. The same is observed when adding EDB to the solution, meaning that EDB does not react with the excited state of EPP. The solution containing EPP and TA, in the other hand, shows EPP bleaching, which is consistent with the apparition of the EPP cation radical observed at 400 nm. The bleaching observed when adding also EDB to the solution, however, is much smaller compared to the previous one. This shows that, somehow, a certain amount of EPP ground state dye is recovered after reacting with ta and EDB.

In the light of the experiments shown, LFP seems to be an effective method to prove the presence of a PCIS. Nevertheless, this method presents some disadvantages For example, the absorption of the intermediate species is not always known, which would require a complete previous study of the photophysics of the dye. With this in mind, a different approach to the PCIS studies was suggested.

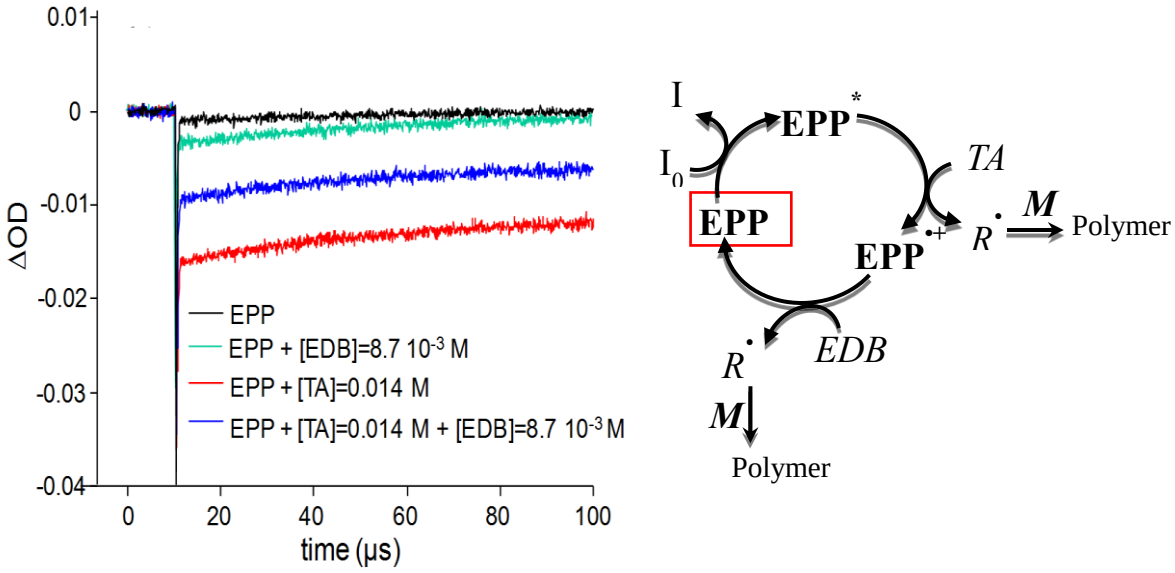

Figure 3.10. EPP bleaching monitored at 520 nm. The bleaching of the solution is greater for the solution containing TA than to the solution with TA and EDB, indicating that EPP ground state is being regenerated to some degree when the two species are present in solution.

3. 6. Mechanistic studies: the Dye Photolysis approach.

A much simpler method than LFP to prove PCIS behavior than LFP is to register dye photolysis as a function of the irradiation time. No change in absorbance should be registered when irradiating a solution containing the dye alone, provided that it is resistant enough to photobleaching.

In the case of an ideal PCIS, no changes should be noticed either for a solution containing the dye and one of the co-initiators, while a decay in the absorption value with time would be expected for a solution containing the dye and the other co-initiator, i.e., one of the co-initiators will react with the excited state of the dye, whereas the other will not. Finally, if there is a PCIS, the bleaching and recovery of the ground state dye is expected to be happening when the two co-initiators and the dye are in the solution: the co-initiator that didn't react with the excited state of the dye will now react with the dye radicals generated after reaction with the first co-initiator. As a result, no net change in absorbance during the irradiation process would be seen.

To perform such experiments, a set up as the one shown in figure 3.11 was built. All the solutions were prepared in MeCN and irradiated with a 532 nm LED lamp. The measurement of the transmitted intensity (I_T) as a function of time irradiation, as well of the LED lamp intensity (I_0) allowed to the calculation of the absorbance (A). All of the experiments were performed in Ar atmosphere. The studied PIS contained Rose Bengal (RB) as photosensitizer, ethyl 4-(dimethylamino)benzoate (EDB) as electron donor and triazine A (TA) as electron acceptor. The structures of these species can be seen in figure 3.12. This work was performed by Julien Christmann, as a part of his Master degree.

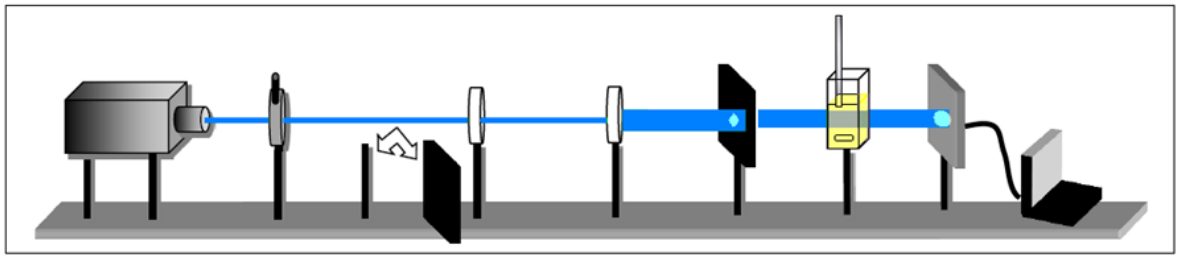

Figure 3.11. Assembly made to perform dye photolysis experiments. Changes in absorbance are recorded by monitoring the transmitted light intensity as a function of time.

In the first place, the evolution of the dye photolysis with time was registered for a MeCN solution containing RB/TA. Of course, for this system there is only one mechanism possible: the oxidation of the dye by TA. The photolysis was performed within a 1 cm width cell with the laser diode tuned to 9 mW/cm2 intensity. The initial dye concentration, $[RB]_0$, was 6.5 10^{-5} mol·L^{-1} (with ε = 31900 M^{-1}·cm^{-1} and a length, l, of 1 cm, this corresponds to an initial absorbance of around 0.2 at 532 nm) and the initial concentration of TA, $[TA]_0$, was 10^{-3} mol·L^{-1}. Thanks to the recording of the transmitted laser diode light, it was possible to calculate the optical density $A(t)$ of the sample, which was then used to calculate $[RB](t)$. This calculation can be seen in figure 3.12. A fast decrease of $[RB](t)$ occurs. This indicates that the dye is consumed during irradiation, due to the electron transfer

to TA. In about 100 s, the absorbance is almost zero indicating a complete consumption of the dye. It should be noted that no dye photolysis is observed for a solution of RB in MeCN alone under the same irradiation conditions.

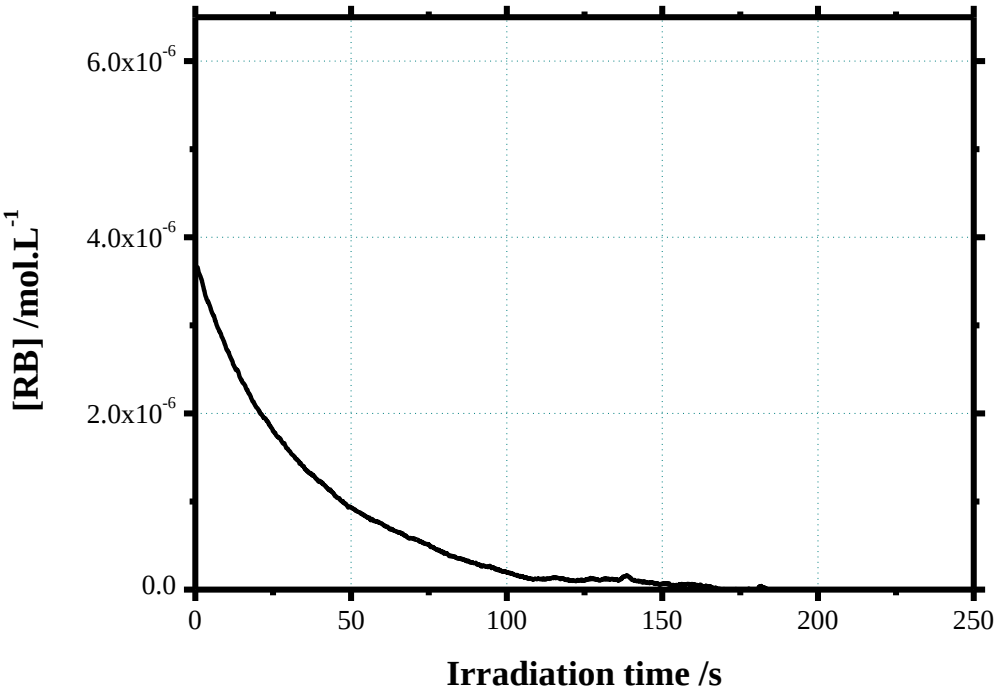

Figure 3.12. Photolysis of RB in a solution containing TA.

To quantify the consumption of the photosensitizer, PS, during the experiment, the photolysis quantum yield ($\Phi_{photolysis}$) was determined. $\Phi_{photolysis}$ is defined by the ratio of the initial number of PS molecules present in the solution (N_{PS}) to the total number of absorbed photons (N_{abs}), as expressed in equation expressed by the following equation:

$$\Phi_{photolysis} = \frac{N_{PS}}{N_{abs}} = \frac{V.[PS]_0}{V.\int I_{abs}dt} = \frac{[PS]_0}{\int I_{abs}dt} \quad (3.3)$$

where V is the volume of the irradiated solution. The absorbed photon concentration is given by:

$$\int I_{abs}dt = \int I_0\left(1 - 10^{-A(t)}\right)dt \quad (3.4)$$

where I_0 is the incident light intensity on the cell (9 mW·cm^{-3}, i.e., 4·10^{-5} einstein·s^{-1}·cm^{-3}). The experimental measurement of the absorbance $A(t)$ allows the calculation of $I_{abs}(t)$. Hence, the total concentration of absorbed photon is calculated as 3.43·10^{-4} mol·L^{-1} for RB/TA. Dividing the initial RB concentration by these values, a photolysis quantum yield of 0.19 for RB/TA is obtained.

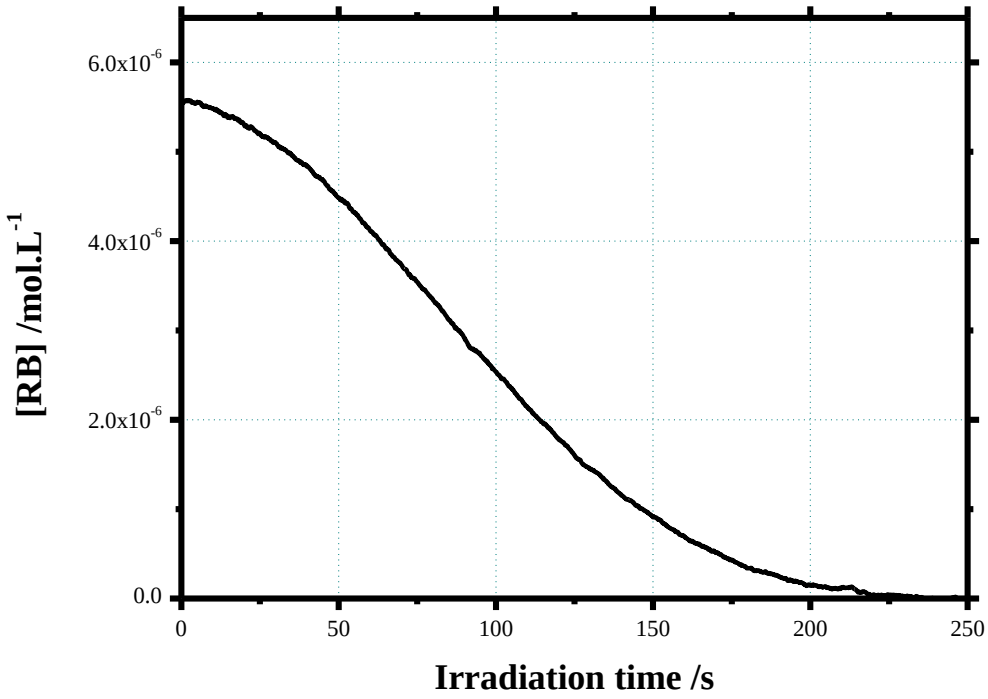

Figure 3.13. Photolysis of RB in a solution containing TA and EDB.

The same measurements made for the 2-C PIS RB/TA were made with a solution containing RB, TA and EDB. EDB was chosen as electron donor for the PCIS, because its reactivity toward ^{3}PS is low compared to that of TA. This ensures that ^{3}PS will react mainly with TA in an oxidative cycle. The solution was irradiated with the same laser diode and same output power.

The same values of $[RB]_0$ and $[TA]_0$ were utilized, and $[EDB]_0$ was fixed to 10^{-3} mol·L^{-1}. The experimental evolution of the [RB](t) can be seen in figure 3.13. The behavior is visibly different from that of RB/TA solution: the absorbance decreases slower at the beginning of the process, being almost constant for a couple of seconds. Then, the absorbance slowly decreases due to an increase of the photolysis rate with irradiation time. Only after 250 seconds the residual absorbance of the solution becomes zero: in the photocyclic system, the time required for complete consumption of the dye is two times longer than for Type II PIS. This confirms that there is dye regeneration within a photocycle exhibiting a photocatalytic behavior.

The longer experimental surviving time of RB in the PCIS is in qualitative agreement with the proposed schemes. To have a quantitative comparison between both systems, $\Phi_{photolysis}$ was also

determined for RB/TA/EDB. The total concentration of absorbed photons for the PCIS is 0.0139 $mol \cdot L^{-1}$. Dividing the initial RB concentration by this value leads to a photolysis quantum yield of $4.7 \cdot 10^{-3}$. This value is two magnitude orders smaller than that obtained for the RB/TA solution, and means that more than 210 photons are needed to bleach one dye molecule in the solution containing RB/TA/EDB, while only 5 photons are needed to bleach one RB molecule in the RB/TA solution. This clearly demonstrates the cyclic regeneration of the dye in the selected three component combination presented here. These experimental results confirm the photocyclic behavior of the selected 3-C system RB/TA/EDB.

3. 7. Mechanistic studies: Modelization.

All the processes that could be involved in a PIS (and that were discussed in this chapter) are summarized in figure 3.14, where where I_{abs} is the number of absorbed photons per second; k_{de1}, k_{de3} are the rate constants of singlet and triplet state deactivation to the ground state, respectively; k_{ISC} the rate constant of the intersystem crossing from ^{1}PS to ^{3}PS; ^1k_q/A, ^3k_q/A, (^1k_q/D, ^3k_q/D) the bimolecular electron transfer rate constant of the singlet and triplet excited state of the PS by the acceptor A (donor D), respectively; k_{red} and k_{ox} are the rate constants of reduction and oxidation of $PS^{\bullet+}$ and $PS^{\bullet-}$, respectively.

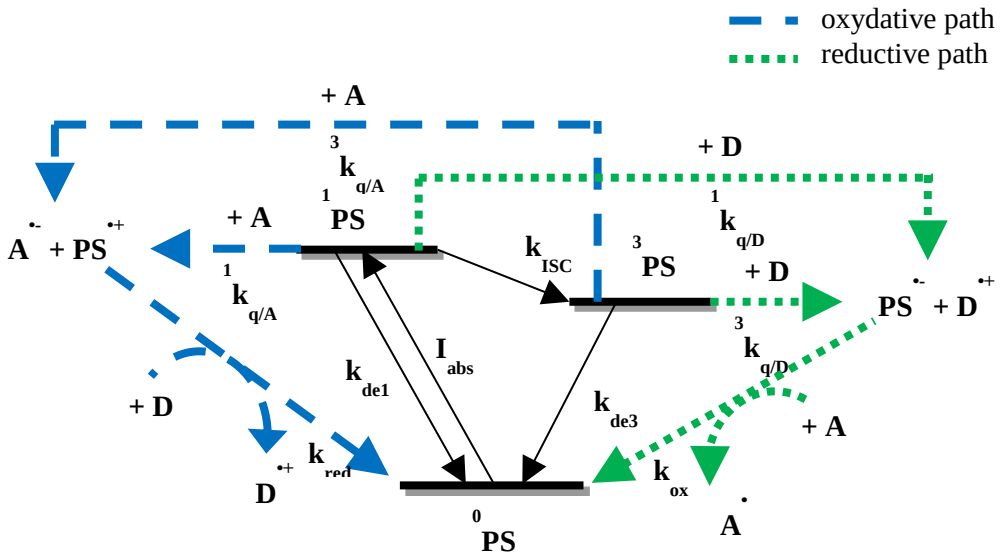

Figure 3.14. Diagram of all the possible reactions having place in a 3-C PIS. Black figures represent the photophysics of the PS.

The time evolution of all the species involved are determined by the following equations 3.5 to 3.11. This System of differential equations can be numerically solved in order to simulate the concentration profiles of all the species with time.

$$\frac{d[{}^0PS]}{dt} = -I_{abs} + k_{de1}[{}^1PS] + k_{de3}[{}^3PS] + k_{redox/A}[PS^{\cdot -}][A] + k_{redox/D}[PS^{\cdot +}][D] \quad (3.5)$$

$$\frac{d[{}^1PS]}{dt} = I_{abs} - k_{de1}[{}^1PS] - k_{ISC}[{}^1PS] - {}^1k_{q/A}[{}^1PS][A] - {}^1k_{q/A}[{}^1PS][D] \quad (3.6)$$

$$\frac{d[{}^3PS]}{dt} = k_{ISC}[{}^1PS] - k_{de3}[{}^3PS] - {}^3k_{q/A}[{}^3PS][A] - {}^3k_{q/D}[{}^3PS][D] \quad (3.7)$$

$$\frac{d[PS^{\cdot -}]}{dt} = {}^1k_{q/D}[{}^1PS][D] + {}^3k_{q/D}[{}^3PS][D] - k_{\underline{redox}}[PS^{\cdot -}][A] \quad (3.8)$$

$$\frac{d[PS^{\cdot +}]}{dt} = {}^1k_{q/A}[{}^1PS][A] + {}^3k_{q/A}[{}^3PS][A] - k_{\underline{redox}}[PS^{\cdot +}][D] \quad (3.9)$$

$$-\frac{d[D^{\cdot +}]}{dt} = \frac{d[D]}{dt} = -{}^1k_{\underline{q}}[{}^1PS][D] - {}^3k_{\underline{q}}[{}^3PS][D] - k_{\underline{redox}}[PS^{\cdot +}][D] \quad (3.10)$$

$$-\frac{d[A^{\cdot -}]}{dt} = \frac{d[A]}{dt} = -{}^1k_{\underline{q}}[{}^1PS][A] - {}^3k_{\underline{q}}[{}^3PS][A] - k_{\underline{redox}}[PS^{\cdot -}][A] \quad (3.11)$$

In order to simulate the photocyclic behavior, the different rate constants involved in the proposed mechanism were measured by time resolved spectroscopies (laser flash photolysis for triplet excited states and time correlated single photon counting for excited singlet states). The experimental quenching rate constants and their corresponding ΔG_{ET} are given in Table 3.1. As it was not possible to measure k_{red} and k_{ox}, a value of $2 \cdot 10^3$ $M^{-1} \cdot s^{-1}$ was estimated to perform the computations. This is justified by the fact that the radical recombination in the type II systems observed by laser flash photolysis occurs in the millisecond timescale. The last rows of Table 3.1 contain the calculated Gibbs free energy of the dye regeneration redox reaction. These slightly endergonic values (0.42 and 0.12 eV) are in agreement with low k_{red} and k_{ox} rate constants, as used for computation. The measured electron transfer rate constants are in line with the ΔG, confirming the low reactivity of ^3PS toward EDB. Intersystem crossing rate constant k_{ISC} was obtained from the triplet state quantum yield and singlet state lifetime according to [8]:

$$\varphi_0^T = \frac{k_{ISC}}{k_{de1} + k_{ISC}} = k_{ISC}\tau_0^S \quad (3.12)$$

Quencher	ΔG_{ET} /eV, k_q /$M^{-1}s^{-1}$				
	^{0}**RB**	^{1}RB	^{3}RB	$RB^{\cdot+}$	$RB^{\cdot-}$
EDB	2.07	-0.10, $9.0\ 10^8$	0.27, $4.5\ 10^4$	0.42, -	
TA	1.77	-0.40, $6.0\ 10^9$	-0.03, $1.7\ 10^7$		0.12, -

Table 3.1. Thermodynamic and kinetic parameters of the PCIS simulation.

With this RB concentration, and in absence of any quencher, the triplet state lifetime was measured around 80 µs, leading to k_{de3}= $1.25{\cdot}10^4$ $M^{-1}{\cdot}s^{-1}$. The following parameters were used to perform the computation: the continuous incident light intensity I_0 was fixed to 9 $mW{\cdot}cm^{-2}$ at 532 nm (i.e., $4{\cdot}10^{-5}$ $Einstein{\cdot}L^{-1}{\cdot}s^{-1}$). The initial PS (i.e., RB) concentration was fixed to $[RB]_0 = 6.50{\cdot}10^{-6}$ M, with ε = 31900 $M^{-1}{\cdot}cm^{-1}$ and a cell length of 1 cm this corresponds to an absorbance of 0.2 at 532 nm, in line with the experiments. The initial concentration of the quenchers were fixed at $[TA]_0 = 10^{-2}$ M and $[EDB]_0 = 10^{-3}$ M for TA (acceptor A) and EDB (donor D). The calculations were performed by Master's student Julien Christmann.

Figure 3.15 shows the changes in RB, $RB^{\bullet+}$, TA, and $TA^{\bullet-}$ concentrations for RB/TA system. Two remarks can be made from this result. First, the ground state of the dye is quickly bleached: in about 4 seconds it has completely disappeared. Second: the final $TA^{\bullet-}$ concentration, i.e., the maximum number of initiating radicals produced is equal to the initial ground state RB concentration. The final triazine concentration remains almost constant because of the large excess of TA in the solution.

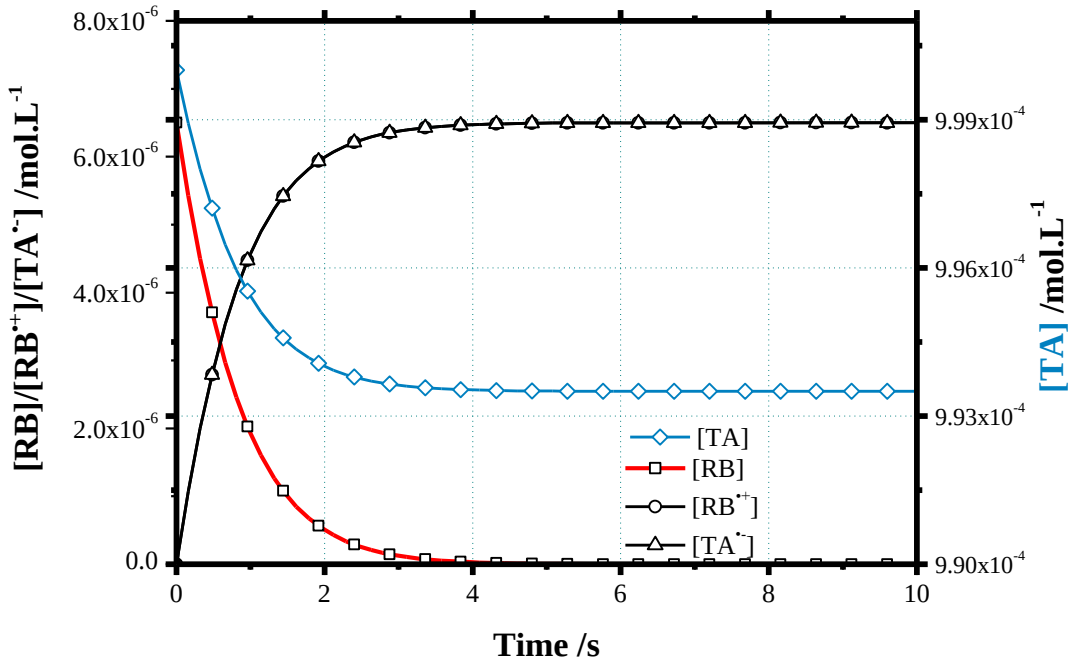

Figure 3.15. Calculated concentration profile for a solution containing RB and TA. The radical generation is limited by the amount of PS.

The same conclusion can be drawn for the RB/EDB calculation. the only different would be found in the calculated rates due to the lower reactivity of EDB with TA excited states (i.e., *k*q/D). Under these conditions the limiting component for radical generation in these type II PIS is the concentration of the dye.

In the photocyclic system, the initial pseudo first-order reaction rates are equal to $^3kq/A[TA]_0 = 1.7 \cdot 10^5\ s^{-1}$ for TA (acceptor A) and $^3kq/D[EDB]_0 = 4.5 \cdot 10\ s^{-1}$ for EDB (donor D). This means that the oxidative photocycle preferentially occurs, at least until $^3kq/A[TA] > 3kq/D[EDB]$. The plot of $\log(^3kq/A[TA])$ and $\log(^3kq/D[EDB])$ in Figure 3.16 shows that it is the case for the first 310 seconds of the reaction: during this period it can be assumed that the oxidative pathway is the main reaction.
The evolution of [RB], [TA] and [EDB], also displayed on figure 3.16, is also very interesting. Two major differences with Type II PIS can be outlined: first, the acceptor TA reacts completely (i.e., its final concentration is zero). Second, the ground state RB concentration, presents only a slight decrease during the first 200 seconds. This first part of the cycle can be explained by the reduction of the oxidized dye $RB^{\bullet+}$ by EDB leading to a recovery of the dye ground state. As soon as no more TA is available (around 250 seconds), [RB] decays faster to zero. In this second part the photocatalytic system is reduced to a conventional Type II system, where the dye is consumed during its reaction

with the excess of amine EDB. Only one TA equivalent of EDB is lost during the first part of the cycle, and [EDB] reduces to $0.9 \cdot 10^{-2}$ M. During the second part of the reaction, a small $6.5 \cdot 10^{-6}$ M is consumed (i.e. the initial RB concentration, cf. type II PIS).

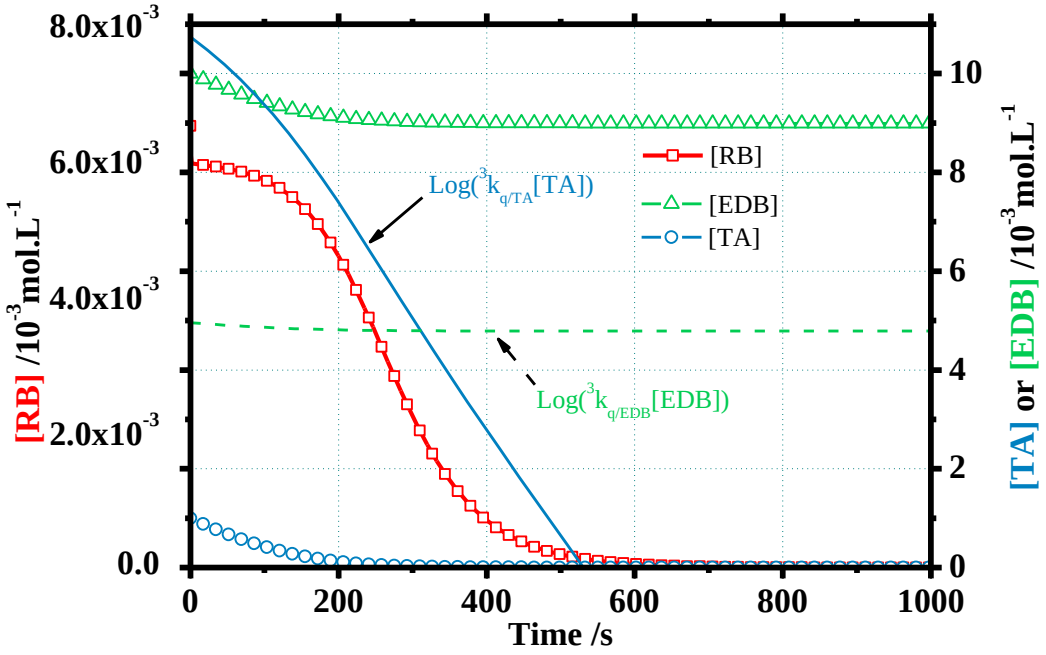

Figure 3.16. Calculated concentration profiles for a solution containing RB, TA and EDB. Radical generation is first limited by TA, then by the PS

On figure 3.17, the evolution of $EDB^{\bullet+}$ and $TA^{\bullet-}$ concentrations are displayed together with RB. In the first part of the cycle (before 300 s) both radical curves are similar. Then, as soon as TA is consumed, no more $TA^{\bullet-}$ is produced and a final concentration of $1 \cdot 10^{-3}$ M is reached. At this stage the $EDB^{\bullet+}$ also reaches $1 \cdot 10^{-3}$ M. From this point on, the excess of EBD reacts with RB leading to a small additional $6.5 \cdot 10^{-6}$ M for $EDB^{\bullet+}$ and to the bleaching of the dye.

Thus, the computed final total radical concentration is formally equal to $2.0065 \cdot 10^{-3}$ M. Once more, the advantages of photocyclic systems over the 2-C PIS are shown: 1. the dye is constantly regenerated; 2. the final radical concentration is much higher for PCIS; 3. under the studied conditions, the limiting component is no more the dye, but the co-initiator of lowest concentration, in this case, the acceptor TA. All this phenomena explain the synergistic effect observed in some free radical polymerization.

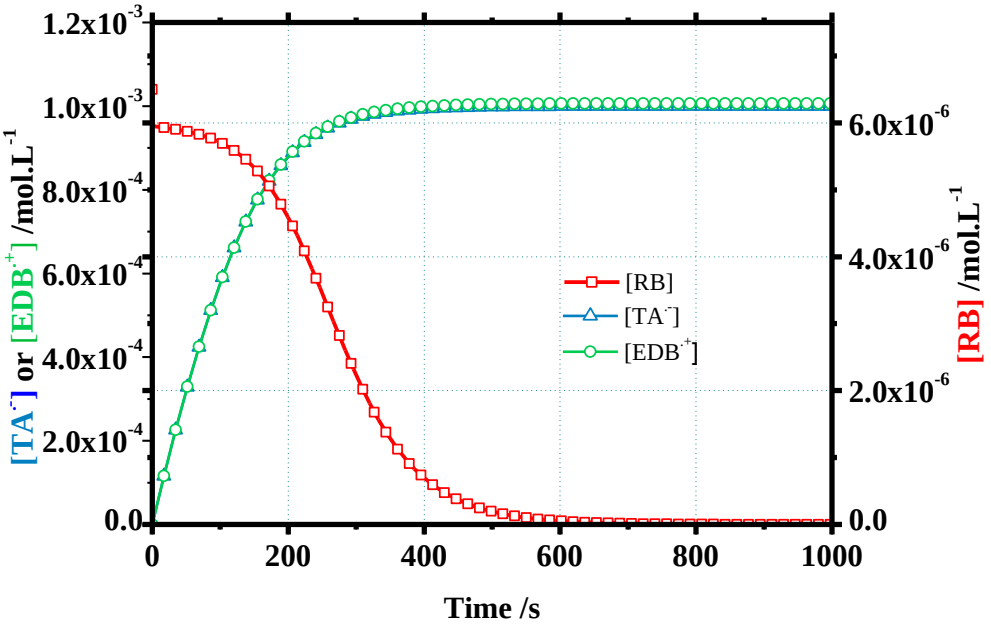

Figure 3.17. TA and EDB calculated radical concentration profile for a solution containing RB, TA and EDB. EDB radical final concentration is only slightly higher than TA radical final concentration.

The radical quantum yield is defined by the ratio of the number of produced radical to the total number of absorbed photons (N_{abs}) and can be expressed as follows:

$$\Phi_{rad} = \frac{N_{rad}}{N_{abs}} = \frac{V.([A^{\cdot -}] + [D^{\cdot +}])}{V \int I_{abs} dt} = \frac{[A^{\cdot -}] + [D^{\cdot +}]}{\int I_{abs} dt} \quad (3.13)$$

The calculated quantum yields for Type II RB/TA and photocyclic RB/TA/EDB PIS are given in table 3.2. In Type II PIS both quantum yields are equal because the amount of radicals formed is equal to the amount of dye photolysed. For photocyclic system, in contrast, the photolysis quantum yield is two orders of magnitude smaller: more than 600 photons are needed to bleach one dye molecule. Φ_{rad} value is almost the same for both systems over the complete modelization time scale. However, this value would be expected to be higher if only the part where the PCIS is still active would have been considered to make the calculation.

	RB/TA	RB/TA/EDB
$\Phi_{photolysis}$	0.475	$1.55.10^{-3}$
Φ_{rad}	0.475	0.478

Table 3.2. Quantum radical yields for the calculated 2- and 3-C experiments.

The fact that the shape of the concentration profiles obtained with calculations is the same than the one observed experimentally is an indicative that the system actually behaves as a PCIS. Nevertheless, it can be seen from the experimental results that the consumption of the dye takes more time than the one calculated for the Type II PIS, while it is faster for the photocatalytic system. This is confirmed by comparing the experimental photolysis quantum yields to the computed values: the experimental photolysis quantum yield is higher for real photocatalytic system RB/TA/EDB, while the opposite stands for RB/TA. This may be due to the fact that the bleaching of the dye is not only a direct consequence of the electron transfer reaction but could also be attributed to secondary reactions between the radicals and the dye-derivate intermediates. As a consequence, the experimental efficiency of the photocycle is lower than the simulated one.

3. 8. Conclusion.

PIS for different visible sources of irradiation were found. When the wavelength became longer, more efficient PIS are required. In this case, PCIS are the best choice.

Different types of mechanisms for PIS were presented and discussed. Their study was approached in three different ways. LFP approach was recalled from a previous work to show how the mechanism of a PCIS can be detected.

A method for measuring dye photolysis was also presented and a powerful mathematical model was developed in order to calculate the physical parameters involved in the PIS mechanism.

3. 9. References.

[1] Charlot, V, A. Ibrahim, X. Allonas, C. Croutxé-Barghorn and C. Delaite., *Pol. Chem.*, *Vol 5* (**2014**), p. 6236–6243.

[2] Tarzi, O. I., X. Allonas, C. Ley and J. P. Fouassier, *J. Polym. Sci., Part A: Polym. Chem.,* **2010**, 48, p. 2594-2603.

[3] Ibrahim, A., C. Ley, O. I. Tarzi, J. P. Fouassier and X. Allonas, *J. Photopolym. Sci. Technol.*, **2010**, 23, p. 101-108.

[4] Rehm, D.; Weller, A. *Isr. J. Chem.* **1970,** *8, p.* 259–271.

[5] Kawamura, K.; Schmitt, J.; Barnet, M.; Salmi, H.; Ley, C.; Allonas, X. *Chem.–Eur. J.* **2013,** *19, p.* 12853–12858.

[6] Kawamura, K.; Ley, C.; Schmitt, J.; Barnet, M.; Allonas, X. *J. Polym. Sci., Part A: Polym. Chem.* **2013,** *51, p.* 4325–4330.

[7] Suzuki, S.; Allonas, X.; Fouassier, J. P.; Urano, T.; Takahara, S.; Yamaoka, T. J. Photochem *Photobiol A: Chem* **2006**, 181, p. 60–66.

[8] Turro, N. J.; Ramamurthy, V.; Scaiano, J. C. *Modern molecular photochemistry of organic molecules;* University science book: Sausalito, California, **2010**.

Chapter Four.

Pulsed Laser Polymerization.

4. 1. Introduction.

So far, all the polymerization experiments shown in this work were performed using the so called Continuous Wave (CW) irradiation mode. As it was explained in Chapter Three, this irradiation mode produces continuous excitation of the PS all along the polymerization process, allowing to the manifestation of PCIS behavior.

The irradiation can also be provided by a pulsed laser, in which is commonly known as Pulsed Laser Polymerization (PLP). This irradiation mode makes it possible to separate initiation from propagation and termination steps, since the duration of the laser pulse and, thus, the initiating radicals generation, is commonly around 10 nanoseconds, which is not enough time for propagation and termination reactions to occur. It means that most (if not all) of the propagation and termination steps have place only after the initiation reactions have finished. Thanks to this, propagation and termination coefficients were successfully calculated for various systems, by combining Single Pulse-PLP (SP-PLP) technique with PLP-SEC[1], -ESR[2-5] and -MALDI-MS[6,7].

PLP experiments, as it will be presented and discussed in this chapter, are characterized by the necessity of a certain number of pulses irradiating the sample before any polymerization could be noticed by RT-FTIR technique. As the detection limit of this method is around 0.5 of monomer percentage conversion in the conditions used during this work, this pulses can be defined as pulses with less 0.5% conversion per pulse and will be noted as P_{in} (i.e. "inhibition pulses"). This amount of pulses depends on the PIS chosen, the pulse energy, the monomer pot age, and many other factors.

With the existence of P_{in} being the main limitation in the efficiency, a great amount of work was devoted to the understanding of this phenomena. Hence, this chapter aims to make a first approach to the study of how the different parameters involved can affect the efficiency of PLP. To achieve this, five samples of SR 349 containing 1 wt% of TPO as PI and 10 wt% of DMSO were irradiated with a sequence of pulses of 1, 2, 3, 4 and 5 mJ energy respectively, according to the scheme presented in the following section. The results obtained were critically analyzed.

In addition to the analysis of experimental results, a mathematical model was developed to generate a tool capable to predict PLP efficiency by only knowing certain physicochemical properties of the systems as composition, viscosity, radical quantum yield, irradiation energy; and basic

polymerization reaction kinetics. The aim of the development of such model is to allow to the calculation of kinetic constants, k_p and k_t from the PLP experiments and, eventually, the calculation of photophysical properties of the PIS.

4. 2. Experimental set up.

Contrarily to the CW mode, were irradiation is provided by a LED lamp and the beam is directed to the sample via optical fiber, in PLP experiments the laser beam is directed to the sample with a prism (figure 4.1). This allows to the use of greater energy per pulse values, and decreases energy fluctuations, improving the reproductibility of results. The irradiation source was a nanosecond pulsed Nd:YAG laser (Continuum minilite), which has two different wavelengths that can be used to irradiate the samples: 355 and 532 nm.

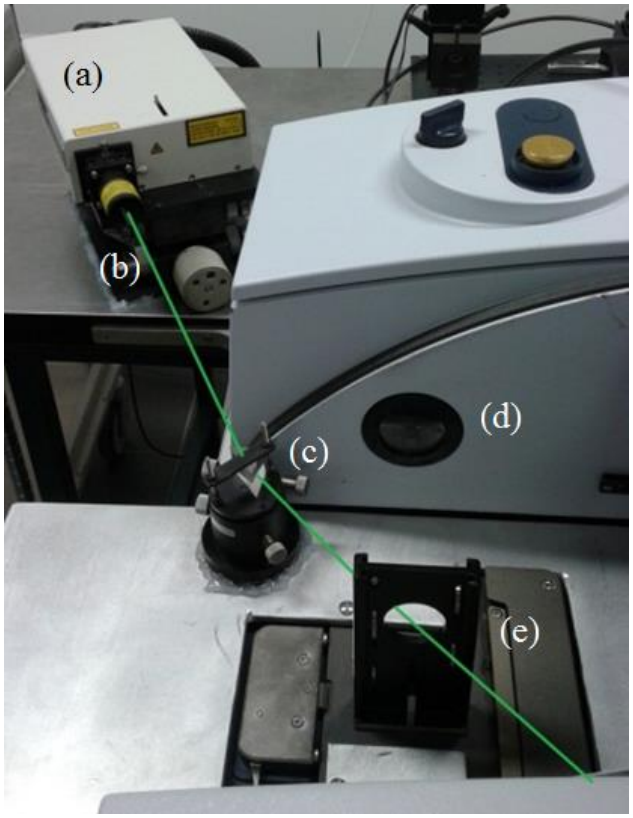

Figure 4.1. Experimental set up for PLP experiments. (a) LASER, (b) beam trajectory, (c) prism, (d) Vertex70®, (e) sample holder.

During Dr. Haja Tar's thesis[8], the ideal conditions to perform PLP experiments were studied. Seven seconds of dark time between two irradiation pulses was found to be enough to consume all the initiating and growing chain radicals, i.e., no polymerization was noticed after a dark time period of seven seconds. The samples were, then, irradiated with a sequence of 30 pulses, using a dark time between two successive irradiation pulses of 7.5 seconds. It was found during Dr. Tar's work, that this amount of pulses is enough to collect relevant information about the efficiency of the PIS. Scheme 4.1 illustrates the method described.

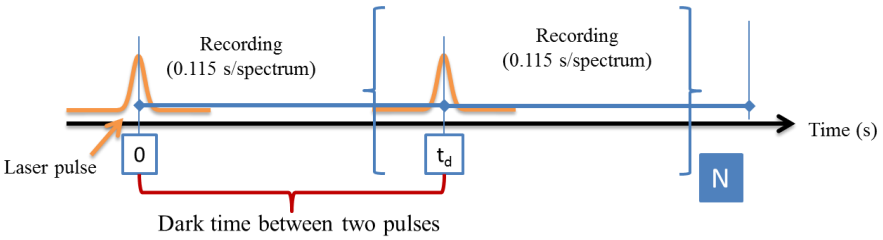

Scheme 4. 1. PLP experiments sequence. N was chosen to be 29, giving a total pulse number of 30 and t_d is 7.5 seconds.

For a better understanding of the results presented all along this chapter and the following ones, a typical plot of monomer conversion vs. time for a PLP experiment is shown in scheme 4.2. Each arrow represents a laser irradiation pulse on the sample. P_{in} stands for inhibition pulses as explained in the introduction. An explanation of this phenomenon will be suggested further in this chapter. $\Delta C\%_i$ is the monomer conversion percentage reached between the pulses i and i+1 for a given experiment and $\Delta C\%_{max}$ is the maximum conversion percentage reached in an experiment by only one pulse, regardless the pulse number.

Analogously to CW mode, $R_{c\,i}$ can be defined as the maximum conversion rate obtained for a given pulse, and $R_{c\,max}$ as the maximum conversion rate obtained in one experiment.

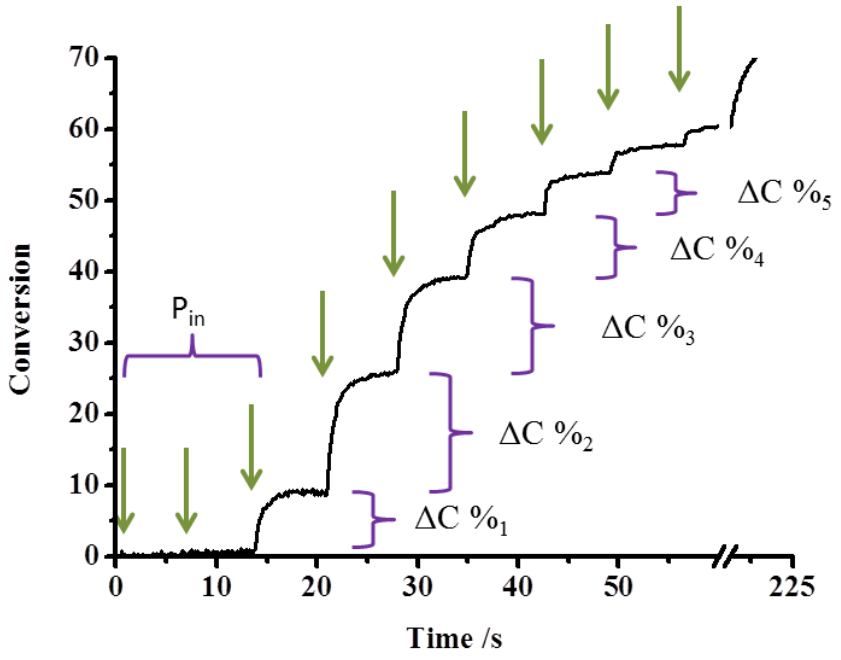

Scheme 4. 2. Typical conversion vs. time plot for a PLP experiment. P_{in} is the number of inhibition pulses and $\Delta C\ \%_i$ is the monomer conversion reached in the ith pulse.

4. 3. TPO, a simple yet efficient Type I PI.

As it will be seen in Chapter Five, the efficiency varies enormously depending on the PIS chosen. For this reason, the selection of the PI is crucial before carrying out any PLP experiment.

As the objective of this work is the understanding of the mechanisms having place in PLP, a simple, well-known type I PI was chosen. The advantage of this type of PI is that there are not intermediaries in the radical generation process, and their generation mechanism is very simple.

Diphenyl(2,4,6-trimethylbenzoyl)phosphine oxide, also known as TPO, is a very well-known type I PI that was widely used for many polymerization applications[9,10] . Its structure is shown in figure 4.2 and it can be decomposed in two initiating radicals after irradiation.

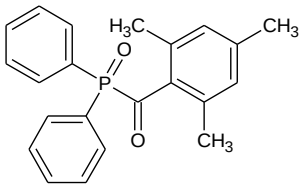

Figure 4.2. Structure of Diphenyl(2,4,6-trimethylbenzoyl)phosphine oxide, TPO.

TPO's UV spectrum in MeCN (figure 4.3) presents two absorption bands in the near UV region: one with its maximum at 296 nm, and the other with maximum at 380 nm. The fusion of these two peaks results in a continuous absorption band from 280 to 420 nm, which makes it suitable to be used as a PI with a 355 nm irradiation source, as it is the minilite pulsed Nd-YAG LASER used to perform all the PLP experiences presented in this thesis.

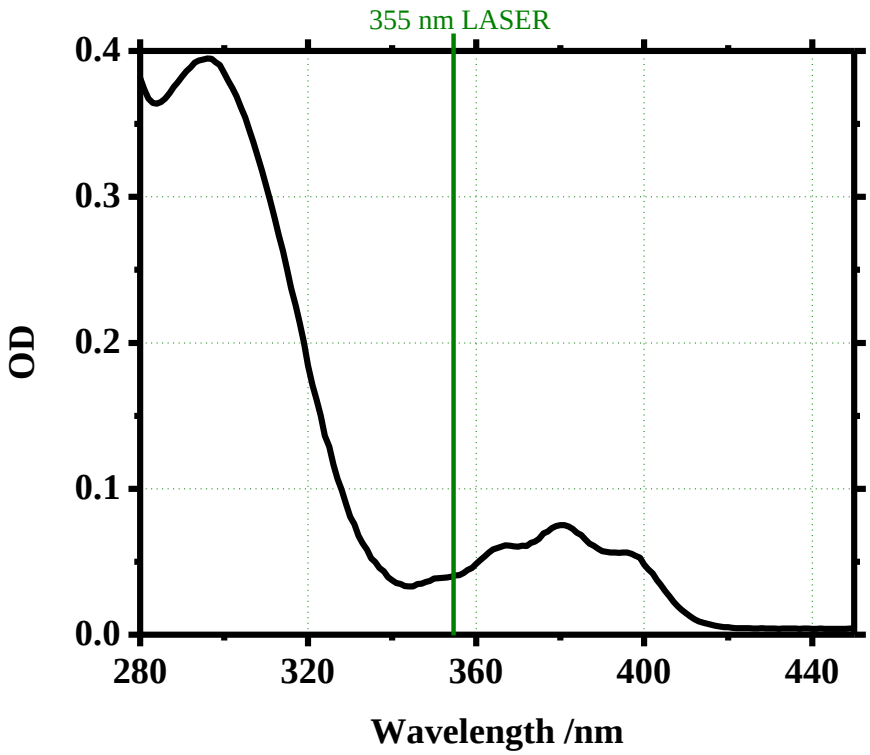

Figure 4.3. TPO's absorption spectrum in MeCN.

TPO overcome a homolytic rupture after light absorption, generating two different radicals, whose structures can be seen in figure 4.4. The addition of both radicals to acrylate monomers was proven and studied by J. Lalevée *et al.*[16] These properties will be mentioned again in section 4.8.

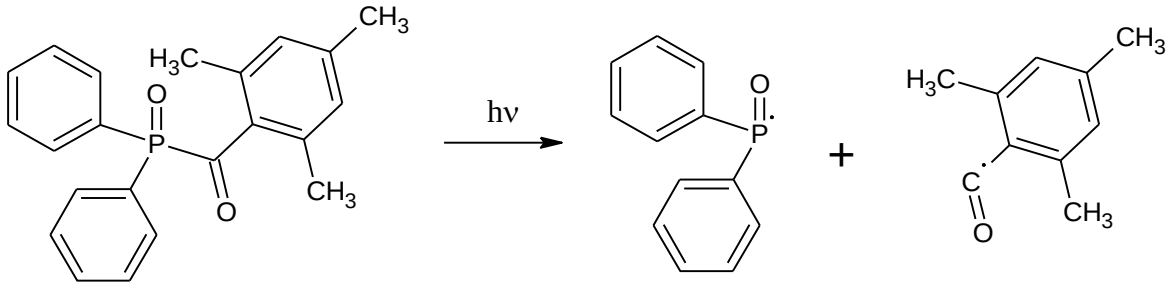

Figure 4.4. Decomposition of TPO after light irradiation.

4. 4. The effect of pulse energy in polymerization efficiency.

The energy of the pulsed laser was regulated in order to obtain pulses of 1, 2, 3, 4 and 5 mJ to irradiate the samples, as described in the introduction. The samples were SR 349 solutions containing 1 wt% of TPO as PI and 10 wt% of DMSO to help the PI dissolution.

The studies that will be presented in this section will allow to the obtaining of a response curve. The expected result would be to have an increase in efficiency as the energy pulse increase: the number of photons emitted increases with the pulse energy, and so should the number of photon absorbed, which is translated into higher radical generation and higher conversion values. However, other situations are imaginable: the absorption of the sample could be in a saturated regime; in which case an increase in the number of photons received would not increase photon absorption; also, the bleaching of the PI may be increased, giving place to a faster consumption of the PI instead of an increase in the number of initiation radicals generated. A situation where too many radicals are generated can also be pictured, in which case recombination initiating radicals or primary radical recombination could be favored over initiation and propagation processes, decreasing the polymerization efficiency.

Figure 4.5 shows the monomer conversion as a function of the time for the five samples. No monomer conversion was found for the sample irradiated with 1 mJ pulses. It can also be seen that polymerization's efficiency increases with the pulse energy as expected. The round-shaped curves obtained after each pulse (i.e, every 7.5 seconds) are related to the values of k_p and k_t, as will be further discussed in section 4.8.

A more interesting analysis can be made from figure 4.6, where conversion per pulse is plotted as a function of the pulse number. As a general remark, all the curves follow the same pattern: first, there is a certain number of P_{in} that can be seen at the beginning; then, there is a quick increase of the value of conversion per pulse (ΔC%) until the reach of a maximum value ($\Delta C\%_{max}$) is observed Finally, a decrease in ΔC% until the end of the experiment can be seen.

When comparing the five curves, several tendencies can be observed when increasing the pulse energy: the reaching of $\Delta C\%_{max}$, is delayed to lower pulse numbers; the number of P_{in} decreases and the increase and decrease in ΔC% with pulse number becomes sharper.

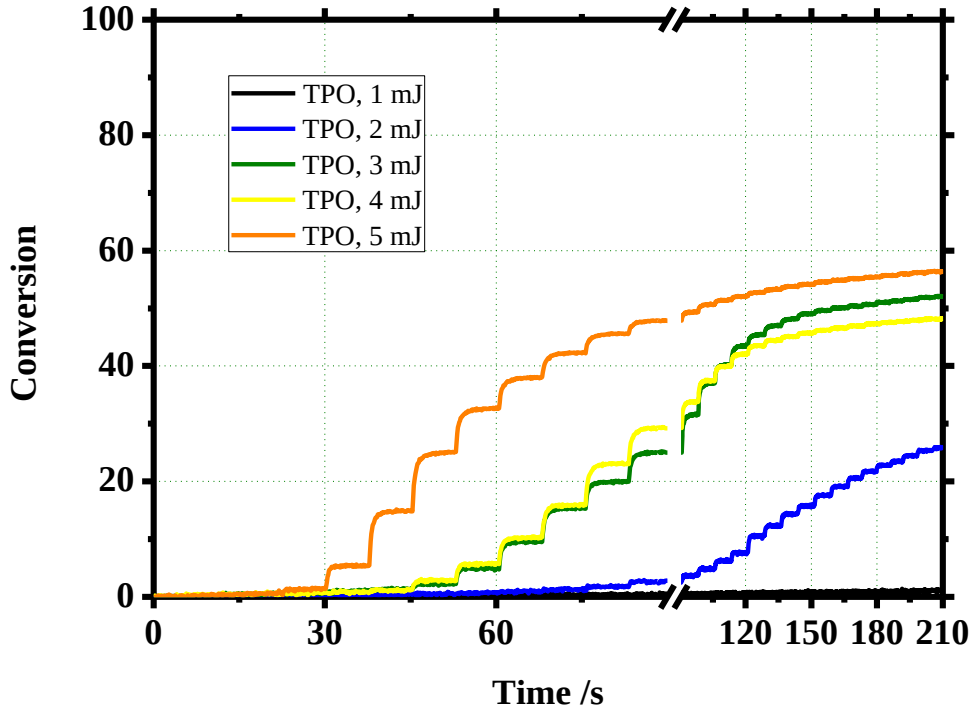

Figure 4. 5. Monomer conversion as a function of time for TPO samples irradiated with 1 to 5 mJ pulses. Dark time between pulses was set up around 7.5 s. Polymerization efficiency increases with energy pulse.

As higher values of ΔC% are expected when using higher pulse energies, a similar reasoning can be done in order to explain the decreasing in P_{in}. Formulations have inhibitor species, as dissolved

oxygen, that will not allow polymerization to be initiated until they are totally consumed from the media. Hence, the radicals generated whit the first pulses are going to be used to consume these species. Of course, the more energetic the pulses, the more radicals per pulse will be generated and so, all the inhibitor molecules will be consumed with a smaller quantity of pulse. Therefore, the P_{in} number will decrease as the energy of the pulse increases.

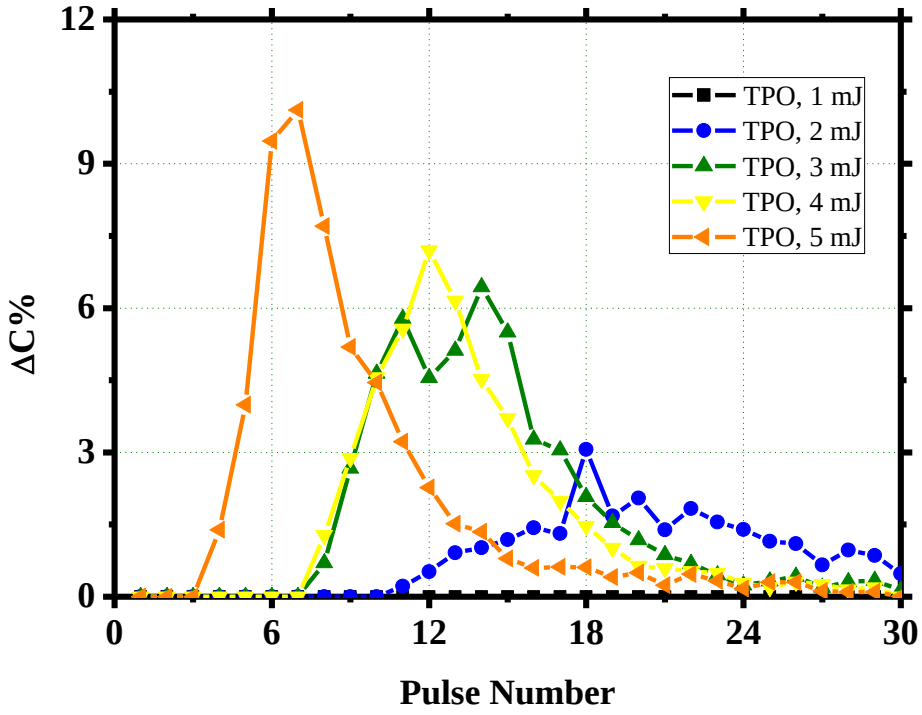

Figure 4. 6. Monomer conversion as a function of pulse number for TPO samples irradiated with 1 to 5 mJ pulses. Curves present similar pattern, which is delayed to earlier stages when increasing the pulse energy.

Of course, monomer's physical properties also play an important role in the polymerization efficiency, due to the fact that the samples' viscosity is modified as the polymer networks are developed in the media. The polymerization process involves bimolecular radical recombinations (e.g. the bimolecular termination) which are diffusion-limited. As diffusion constant is a function of viscosity and this is, at times, function of the monomer conversion, the dependence of efficiency with monomer conversion is evident.

As the viscosity of the media increases, k_t value becomes smaller, but k_p remains constant for longer before it also decreases as a consequence of media jellification. The point where k_t decreases but k_p still remains constant is known as the auto acceleration of the polymerization reaction

(Trommsdorff's effect) and it takes place between 10 and 20 percent of monomer conversion for polyfunctional monomers like SR 349. $\Delta C\%_{max}$ values would be expected, then, to be found within this region. In order to find the autoacceleration region for SR 349, the monomer conversion per pulse was plotted as a function of the monomer conversion. This can be seen in figure 4.7. The exact monomer conversion at which $\Delta C\%_{max}$ is found may vary due to a combination of parameters related to the monomer and photoinitiator nature and is not easy to determine from the plot here presented. This subject will be boarded again in Chapter Six.

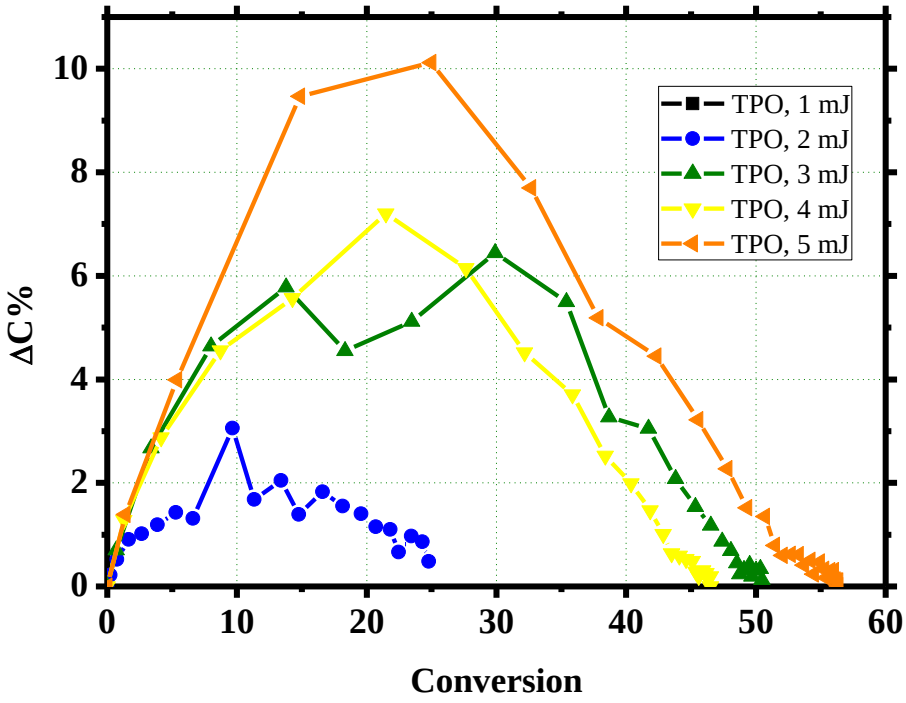

Figure 4. 7. ΔC% as a function of Monomer conversion. The value of $\Delta C\%_{max}$ is reached at different values of monomer conversion for each sample.

4. 5. Inhibition dose.

As it was said in the previous section, the formulations are known to have many inhibitor substances in small concentration which are added in order to prevent polymerization in the monomer pot. Oxygen is also a very well-known inhibitor in radical reactions. Assuming the fact that there is a

maximum inhibitor's concentration that enables polymerization to be initiated, the P_{in} number can be thought as the amount of energy needed to consume the inhibitor species. If this is true, P_{in} will decrease as the pulse energy increases, which is indeed, the case (figure 4.8).

An interesting yet ambitious point on this regard would be to find a way to quantify this inhibitor concentration. A simple, indirect way to do this is to multiply the quantity of inhibition pulses by the pulse energy, obtaining what can be called *Inhibition dose*. This amount can be defined as the energy with which a sample must be irradiated before any monomer conversion could be noticed by RT-FTIR method.

Figure 4.9 shows the inhibition dose for each sample. Letting alone the value for 1 mJ experience, this value can be considered as constant and close to 19 mJ. The differences found experimentally can be attributed to small fluctuations in energy among pulses and the difficulty to find an accurate value of inhibition dose, due to the fact that P_{in} is a discrete amount.

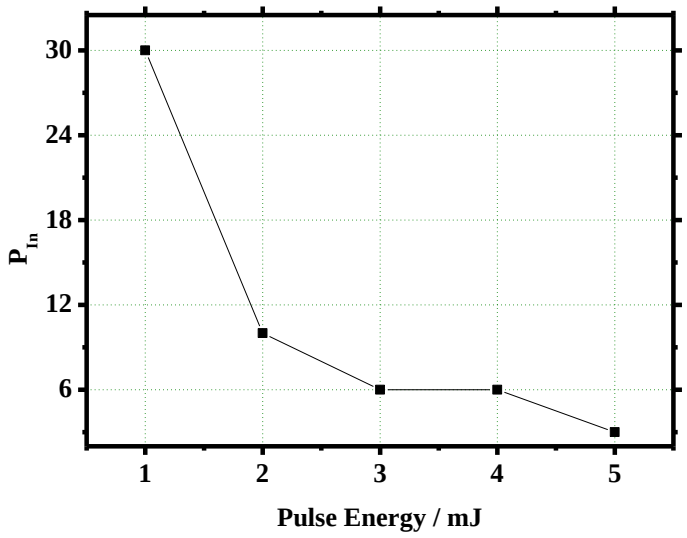

Figure 4. 8. P_{in} vs Pulse energy. The number of P_{in} decreases when the energy per pulse increases, as expected.

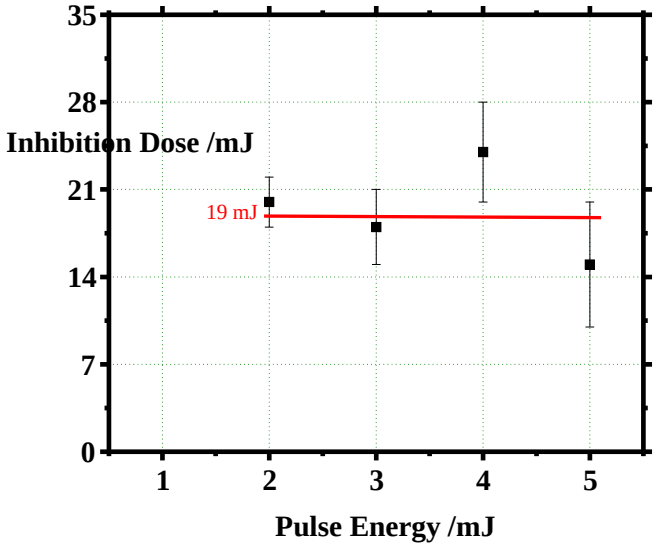

Figure 4. 9. Inhibition dose vs Pulse energy. With the first data point left aside, inhibition dose can be considered to be constant and around 19 mJ.

The results presented in the previous paragraphs are not surprising when thinking of the amount of energy of irradiation as an amount of radicals generated: as the inhibitor's concentration is the same in all the samples, the amount of radicals needed to erase them from the formulation will be the same, and so will be the energy dose required to generate them.

The 1 mJ case is particular. Since no polymerization at all was detected, it is difficult to determine the real inhibition dose: as the amount of radicals generated after these pulses is very small, more pulses will be needed to overcome the inhibition pulses period. After these inhibition pulses, the photoinitiator's concentration will be smaller due to bleaching, which would give place to even smaller amounts of initiating radicals and smaller values of conversion per pulse.

4. 6. R_C and ΔC% analysis.

A PLP experiment can be characterized by each pulse's R_C and ΔC% values, i. e. $R_{C\ i}$ and $\Delta C\%_{\ i}$ for the ith pulse of that experiment. In this section, the effect of energy pulse over these two parameters will be analyzed more in detail.

In first place $R_{C\ max}$ values were plotted vs. pulse energy. Figure 4.10 shows clearly that there is a linear correlation between these two parameters. This correlation, however, indicates that there is a threshold in energy. In other words, there is a pulse energy under which no polymerization would be registered. For the studied system, this pulse energy would be around 0.5 mJ if linear response is considered. Nevertheless, as no polymerization was found with pulses of 1 mJ energy, it could be an indication of non-linearity when using low energy pulses, being the apparent linear correlation an approximation only valid for the higher irradiation energies used.

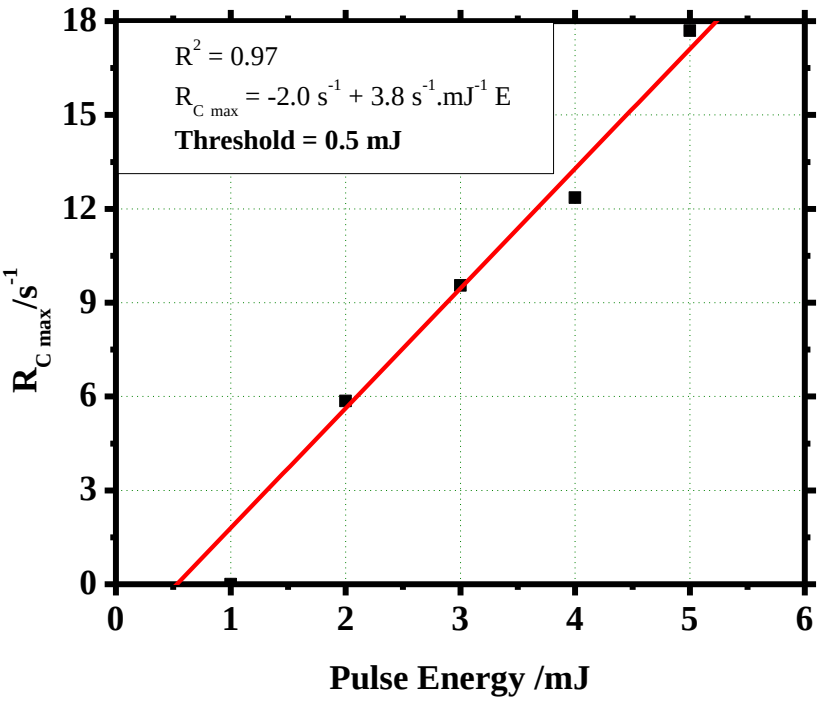

Figure 4. 10. $R_{C\ max}$ vs pulse energy. Linear correlation was found, with a threshold value smaller than that observed empirically.

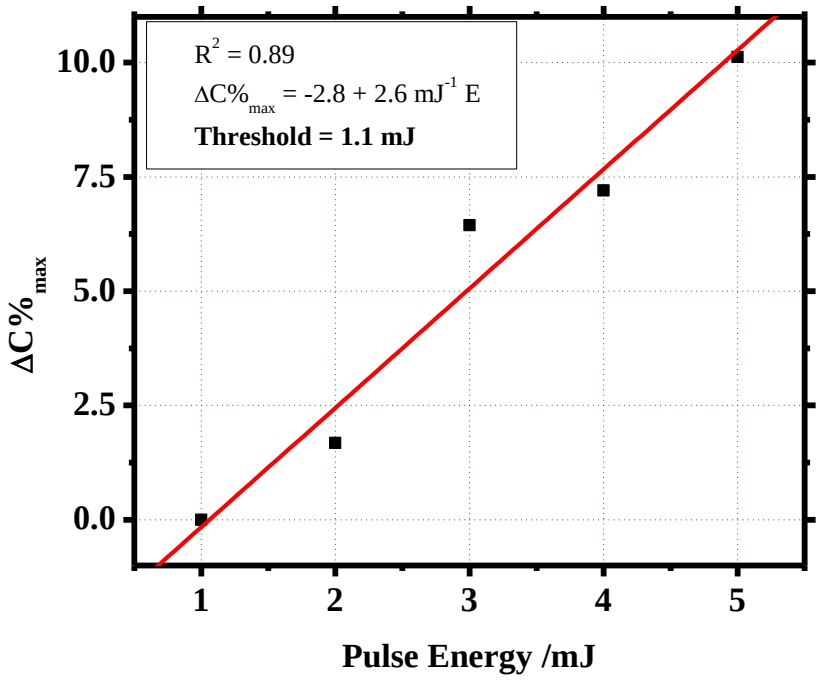

Figure 4. 11. ΔC $\%_{max}$ vs pulse energy. Linear correlation was found as for $R_{C\,max}$.

The same analysis was made for ΔC% $_{max}$ values (figure 4.11). A linear correlation was also found between these two parameters but, in this case, the calculated threshold is above 1 mJ. This fact is consistent with the absence of polymerization registered with 1 mJ energy pulses. However, the possibility of non-linearity response at low energy pulses may place the threshold to even higher values of pulse energy.

From the results shown in figures 4.10 and 4.11, it becomes clear that there is a linear correlation between R_{Cmax} and $\Delta C\%_{max}$. To go a step further, not only these values, but every R_{Ci} of every measurement was paired with its correspondent $\Delta C\%_i$ value. The result is shown in figure 4.12. It is remarkable to see that there is a linear correlation between these two parameters, regardless of the monomer conversion, formulation viscosity, pulse energy, and inhibitor concentration in the medium. Such a result has two primary consequences. The first one is that the conversion per pulse reached is limited by the conversion rate for that pulse, being this, limited by viscosity, photoinitiator's efficiency, irradiation energy, etc. The second consequence is that any treatment made over R_C can also be performed over ΔC%. This result is particularly useful, taking into account the fact that ΔC% is easier to calculate and can be determined with better precision than R_C.

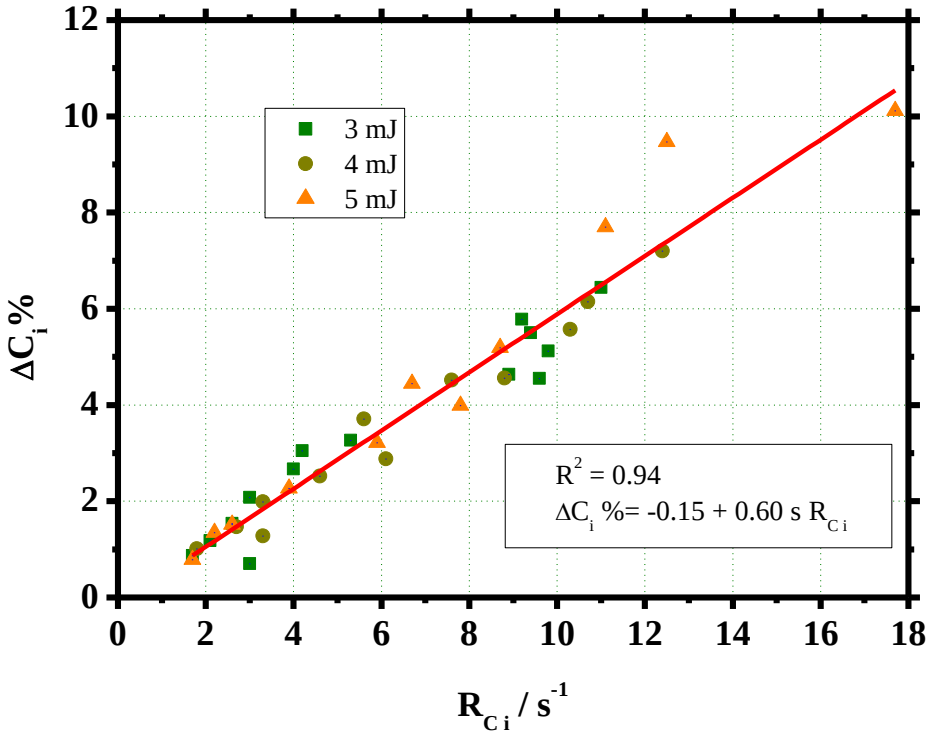

Figure 4. 12. $\Delta C\%_i$ vs R_{Ci}. A linear correlation was found regardless of viscosity, conversion, monomer concentration and irradiation energy.

4. 7. Studies on termination mechanism.

Previous sections of this chapter were devoted to analyze the results obtained from the response curves realized in order to know how the different parameters that characterize PLP experiments are affected by the energy of the pulses used. This section, on the other hand, aims to the acquisition of mechanistic evidence, especially regarding termination. With this in mind, a well-known model for the study of CW termination mechanism[11-13] will be briefly explained.

Photopolymerization can be considered as a three stage reaction, as described in the scheme 4.3: in the photoinitiation process, radicals are generated from light absorption by the photoinitiator or photosensitizer. Then, these radicals will react with the monomer to create growing chains in the propagation state. This growth is finally stopped in the termination stage, which can be differentiated into three types: monomolecular, bimolecular or by primary radical termination.

1-Photoinitiation:

$$[A] \xrightarrow{h\nu} 2R^{\bullet}$$

$$R^{\bullet} + M \xrightarrow{k_i} RM_1^{\bullet}$$

2-Propagation:

$$RM_n^{\bullet} + M \xrightarrow{k_p} RM_{n+1}^{\bullet}$$

3-Termination:

Bimolecular

$$RM_n^{\bullet} + RM_p^{\bullet} \xrightarrow{k_{tB}} RM_{n+p}$$

Radical trapping (monomolecular):

$$RM_n^{\bullet} \xrightarrow{k_{tM}} \text{occlusion/ scavenging}$$

Primary Radical Termination:

$$RM_n^{\bullet} + R^{\bullet} \xrightarrow{k_{tPRT}} RM_nR$$

Scheme 4. 3: Typical three-stage polymerization mechanism.

Following the description showed, considering long chain length and steady state approximation, the dependence of polymerization rate, R_P, with light intensity is given by equations (4.1) to (4.3), if the termination reaction is bimolecular, monomolecular or by primary radical termination respectively.

$$R_p = \left(\frac{\alpha k}{k_{tb}}\right)^{0.5} I_0^{0.5}[M] \quad (4.1)$$

$$R_p = \frac{\alpha k}{k_{tm}} I_0[M] \quad (4.2)$$

$$R_p = \frac{k_i k_p}{k_{tPRT}}[M]^2 \quad (4.3)$$

By taking logarithms for each member, it leads to equation (4.4) for every termination mechanism and, thus, by plotting ln (R_p) as a function of ln (I_0), the value of the slope can give information about the termination reaction.

$$\ln(Rp) = \underline{\beta} \ln(I_0) + c \quad (4.4)$$

When applying this model to PLP, there are several points to pay attention to. First, the fact that time irradiation is negligible compared to the polymerization time. It means that the reaction is very likely to be produced far from the steady state approximation conditions. Another limitation is the fact that, contrary to CW mode, it is not possible to compare conversion rates values for one given

monomer conversion at different irradiation energies, precisely due to the discontinuity of the irradiation.

With the last statement in mind, ln ($R_{C\ max}$) was plotted as a function of ln (Pulse energy). Figure 4.13 shows that there is a linear correlation between these two parameters, with a slope value of 1.3. The challenge here is to understand what the meaning of this value is.

Staying with the CW model previously explained, this would mean that termination process occurs mainly via scavenging (including reaction with inhibitor species, as oxygen) or radical trapping rather than via second-order radical recombination. But if the approximation of the termination model used are still valid on PLP or not, is still to be determined. Further studies on this subject will be presented in Chapter Six.

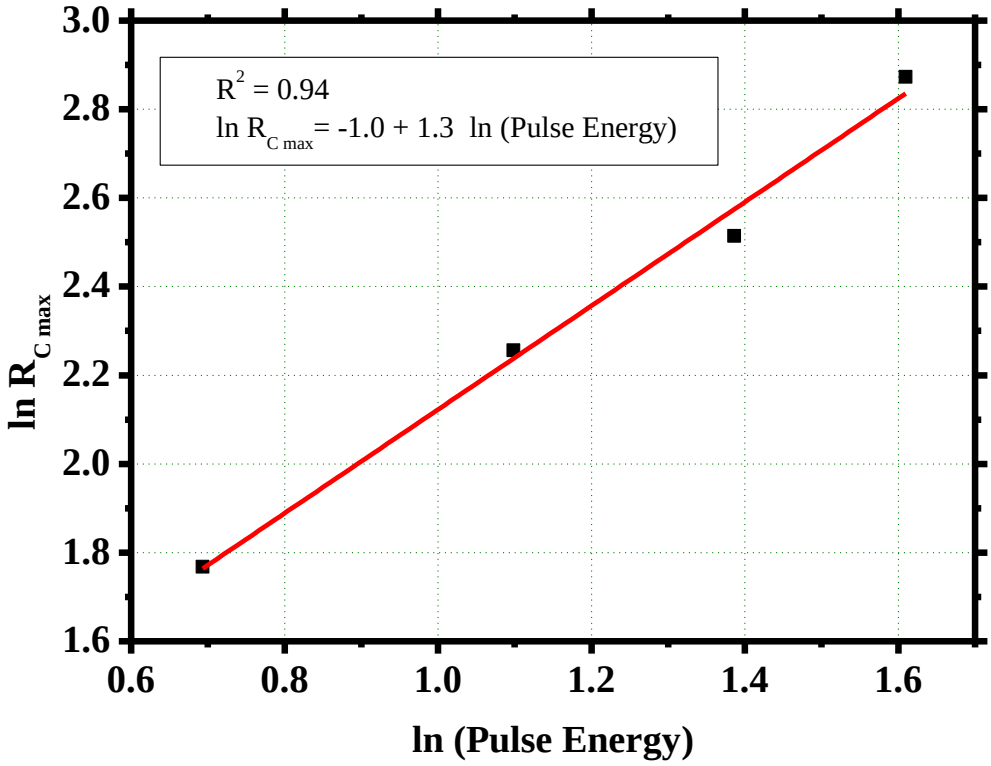

Figure 4. 13. ln ($R_{C\ max}$) was plotted as a function of ln (Pulse energy). A linear correlation with a slope of 1.3 may indicate scavenging or pseudo-first order termination mechanism.

4. 8. PLP modeling.

To the light of the results presented in the previous sections, a PLP model was developed in order to have a complete understanding of the conditions that give place to the presence of P_{in} at the beginning of the PLP experiments and to be able to predict the reactivity of a given system under PLP conditions. There are two main questions concerning the inhibition aspect. The first one would be whether P_{in} are just due to the presence of high concentration of inhibitor species or if there are other factors in game and, the second one, is how could this situation possibly be overcame.

The most ambitious reason to develop such model is that it could be used for both, the prediction of the efficiency of a photoreactive resine only by knowing some of the sample's parameters as absorption, irradiation energy, radical quantum yield of the PIS, rate constants and photophysical properties, and, in the other way to calculate physical constants from the experimental results.

The model here presented has, then, the aim to unveil those questions, but also the aim to remain a simple, yet useful tool that could serve as a first approach to the resolution of the problem. It begins with a polymerization scheme (scheme 4.4) similar to that presented in section 4.7, but with some differences.

In first place, a certain amount of initiating radicals ($R^{\cdot}$) is considered to be generated instantaneously after a pulse arrives to the sample. These radicals can react among them in a bimolecular recombination; with the monomer which is the initiation step (M) or with any inhibitor species (Inh) present in the sample. Once it reacts with the monomer, it generates a living chain. This living chain can react with an Inh molecule again or with another R in which is known as primary radical termination (PRT), leading to inactive species, or it can react with another monomer giving place to the propagation step. The reactions mentioned can happen to any living chain, whatever the amount of monomers are attached to it. All of them are considered to be equally reactive. Living chains can also react among them in the bimolecular termination step. All the living chains are regrouped regardless the number of M molecules they are constituted of and will be noted as $RM^{\cdot}$.

An interesting discussion can be made regarding whether to include monomolecular termination in this model or not. Although it was studied and demonstrated by Andrzejewska *et al*[14] that monomolecular termination is not negligible, especially in multifunctional monomers, which is

the case of SR 349, it was preferred not to take this phenomena into account to make the first calculations for simplicity. Further in this section the convenience of including this termination type to the calculations will become evident.

$$R^{\cdot} + R^{\cdot} \rightarrow R_2 \qquad k_{R\text{-}R}$$

$$R^{\cdot} + M \rightarrow RM^{\cdot}(M^{\cdot}) \qquad k_i$$

$$RM_n^{\cdot}(M_n^{\cdot}) + R^{\cdot} \rightarrow RM_nR\ (M_nR)$$

$$R^{\cdot} + Inh \rightarrow RInh^{\cdot} \qquad k_{PRT}$$

$$RM_n^{\cdot}(M_n^{\cdot}) + Inh \rightarrow RM_nInh^{\cdot}\ (M_nInh^{\cdot}) \qquad k_{inh}$$

$$RM_n^{\cdot}(M_n^{\cdot}) + M \rightarrow RM_{n+1}^{\cdot}\ (M_{n+1}^{\cdot})$$

$$RM_n^{\cdot} + RM_m^{\cdot} \rightarrow RM_{n+m}R \qquad k_{inh}$$

Scheme 4. 4. Polymerization reactions for the PLP model.

The differential equations that define the kinetic behavior of the system described above are those given by equations (4.5) to (4.8), where k_{inh}, k_{PRT} and k_t are considered diffusion-controlled in a first approach.

$$\frac{\partial[R]}{\partial t} = -k_{R-R}[R]^2 - k_i[R][M] - k_{PRT}[RM][R] - k_{inh}[R][Inh] + [R]_0 \qquad (4.5)$$

$$\frac{\partial[RM]}{\partial t} = -k_t[RM]^2 + k_i[R][M] - k_{inh}[RM][Inh] - k_{PRT}[RM][R] \qquad (4.6)$$

$$\frac{\partial[M]}{\partial t} = -k_i[R][M]\ - k_p[RM][M] \qquad (4.7)$$

$$\frac{\partial[Inh]}{\partial t} = -k_{inh}([R] + [RM])[Inh] \qquad (4.8)$$

4. 8. 1. Calculations.

To perform the calculations, initial conditions (see 4.8.2) were input in a Mathematica® notebook altogether with the differential equation system. The notebook allows the calculation of one pulse at a time. After the first calculation, final monomer conversion and inhibitor concentration were reinjected and kinetics constants and initiating radicals' concentration were obtained to perform a second calculation. A dark time of 7.5 seconds between pulses was used, as in the experimental part, which means that 7.5 seconds calculations were performed for each pulse. Initiating radicals were considered to be generated immediately after pulse irradiation (i.e., 0 seconds).

4. 8. 2. Initial conditions.

The TPO experiments discussed above in this chapter were taken as reference to perform the calculations. The 5 mJ experience (figure 4.4) was chosen for being the one with more reliably calculated ΔC%, since bigger values bring to smaller relative errors Also, it covers a wider range of monomer conversion values, since the final conversion of this experiment is bigger than for the others.

The initial monomer concentration in the formulations can be easily calculated and is around 2.5 mol L^{-1}. Diffusion constant was calculated using equation 4.9. The viscosity of the formulation containing 10 wt% DMSO was measured and it turned out to be equal to 270.7 cp, resulting in an initial k_{diff} value of 2.4 10^7 L mol^{-1} s^{-1}. This diffusion constant will control the processes of bimolecular termination, primary radical termination and inhibition, as stated above.

$$k_{diff} = \frac{8RT}{3\eta} \quad (4.9)$$

Initiating radicals' concentration was obtained according to equation 4.11, where h is the Planck's constant; c is the speed of light; λ is the irradiation wavelength, 355 nm; N_A is the Avogadro's number; Φ_R is the radical quantum yield, which is 0.73 for TPO; E is the pulse energy (5 mJ); and A_λ and V are the absorbance and volume of the sample, respectively.

$$[R\cdot] = \frac{\Phi_R \lambda E\,(1 - 10^{-A_\lambda})}{hCN_A V} \quad (4.11)$$

Samples are protected from oxygen diffusion as explained in Chapter Three. The volume of irradiation is 5 μL. The absorbance of a sample was measured and is approximately 0.06 at 355 nm. The concentration of each of both initiating radical species generated after the first irradiation pulse is,

then, 2.78 10^{-4} mol L^{-1}. However, the decrease in photoinitiator's concentration after each pulse due to radical generation causes a smaller production of radical concentration with each pulse. The new initial PI concentration can be easily calculated as $[PI]_{i+1}=[PI]_i - [R^{\cdot}]_I$, and the new radical concentration can be recalculated with equation 4.11. These values can be then input in the Mathematica® notebook to be used in the calculation of the following pulse.

The structures of both radicals generated from TPO photolysis are shown in figure 4.4. Both addition constants, k_{add}, were measured by J. Lalevée *et al.*[17] and were estimated for SR 349 as1.10^5 and 3.10^7 L mol^{-1} s^{-1} in this work. The initiating rate constants are then given by equation 4.12.

$$k_i = \frac{k_{add} k_{diff}}{k_{add} + k_{diff}} \quad (4.12)$$

The initial value of k_p was estimated to be 2 10^4 L mol^{-1} s^{-1} from Andrzejewska's work[14]. A further modification to this value will be made from experimental data obtained and it will be explained in the following subsections. Finally, the initial inhibitors' concentration, $[inh]_0$, was estimated to be around 1 10^{-3} mol L^{-1}.

Table 4.1 summarizes all the initial conditions used to make the calculations.

Parameter	Initial value
$\mathbf{K_{i\,1}, k_{i\,2}}$	1.10^5 , 3.10^7 L mol^{-1} s^{-1}
$\mathbf{k_p}$	2 10^4 mol L^{-1} s^{-1}
$\mathbf{K_t = k_{PRT} = k_{inh} = k_{R\text{-}R} = k_{diff}}$	2.4 10^7 mol L^{-1} s^{-1}
$\mathbf{[M]_0}$	2.5 mol L^{-1}
$\mathbf{[Inh]_0}$	1.10^{-3} mol L^{-1}
$\mathbf{[R^{\cdot}]_0}$	2.78 10^{-4} mol L^{-1}

Table 4.1. Initial parameters used to perform the calculations.

4. 8. 3. Inhibition pulses.

According to the modeling results, in the first pulses all reactions take place in less than 0.1 seconds. These are the pulses corresponding to the inhibition regime seen experimentally (figure 4.5). However, from the 4th pulse on, it can be seen that reaction occurs in longer periods of time. This will be discussed further in the following subsections.

In figure 4.14, the conversion per pulse obtained, ΔC%, is shown together with the inhibitor concentration. It can be seen that, as long as the inhibitor concentration remains high, ΔC% values are below 0.5% of conversion, i. e., these are inhibition pulses according to the definition given above. Furthermore, it can be seen that the polymerization's efficiency increases once that most of inhibitor was already consumed as it was stated before. Propagation and termination steps are less important while there are still inhibitors in the sample: the main process having place is a competence for the initiating radicals between monomer and inhibitors.

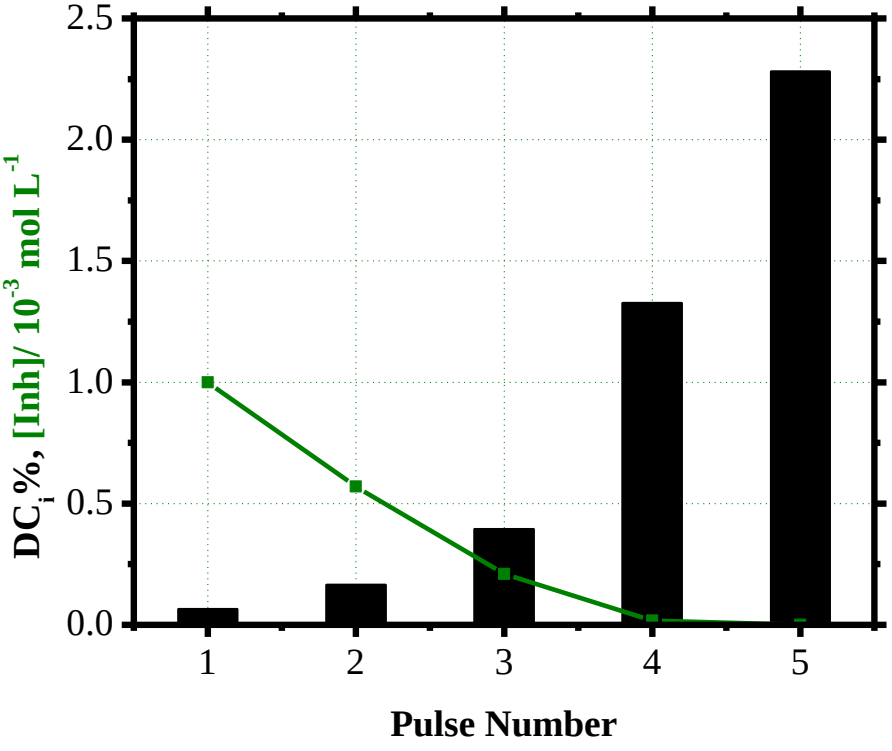

Figure 4. 14. Inhibitor concentration (green line) and monomer conversion per pulse (black bars) as a function of the pulse number. It can be seen that ΔC% values increase when the inhibitor concentration decreases.

4. 8. 4. Curve fitting.

The initial values used, although giving a satisfying explanation to the presence of P_{in}, are not in agreement with the value of ΔC% obtained in pulse number 5. At this point, it can be argued that formulation's viscosity has increased greatly from the starting point, and so that k_{diff} and, in consequence, k_t, have decreased. Figure 4.15 shows the monomer conversion calculated for the 5th pulse by making variations only in k_{diff} (k_t). It can be seen that the value of ΔC% increases as the value of k_{diff} decreases.

A first approach would suggest that the value of k_{diff} lies between 0.3 and 0.4 . 10^7 L mol^{-1} s^{-1}, but a deeper analysis of the conversion curves indicates that a deeper treatment of the results has to be done in order to obtain a better estimation of the kinetic constants values.

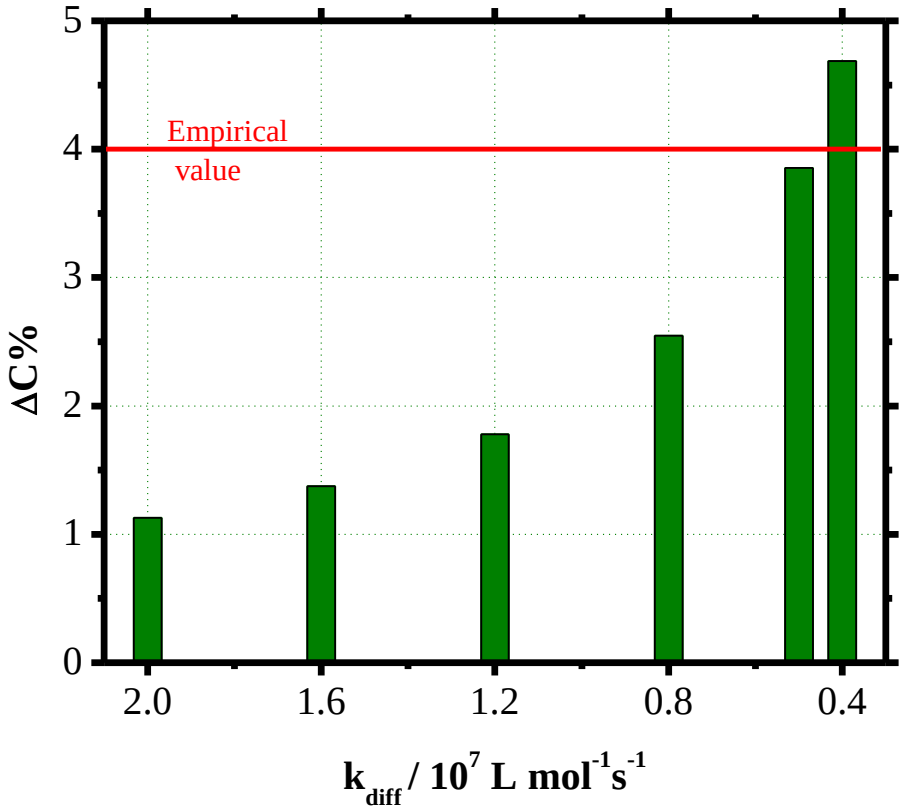

Figure 4. 15. ΔC% obtained for the fifth pulse for different values of k_{diff}.

Figure 4.16 shows the conversion profile for different values of rate constants compared to the experimental one. Blue and green curves are obtained when using the two smaller values of k_{diff} shown in figure 4.15. it can be seen that despite the ΔC% values are close to the one obtained experimentally, the shapes of the curves are far for representing the real conditions.

Green and yellow curves show the effect in monomer conversion that has place when increasing k_p value only, leaving k_{diff} unchangded. It can be seen that the effect is similar to that obtained with the decrease of k_{diff}. However, when comparing these curves to the one obtained experimentally, it can be seen that the slope of these curves at the end of the calculation is bigger than the experimental one. This difference suggests that a competitive reaction to propagation is having place that is not being taken into account in the model. Indeed, by introducing monomolecular termination to the calculation (orange curve), the shape of the curve fits much better the data. The addition of this termination step to the calculation is in agreement with Andrzejewska's work.[14] The value of the monomolecular termination constant, $k_{t,m}$, was found to be around $1s^{-1}$. This value is not expected to be highly influenced by viscosity and will be considered constant for the following pulses.

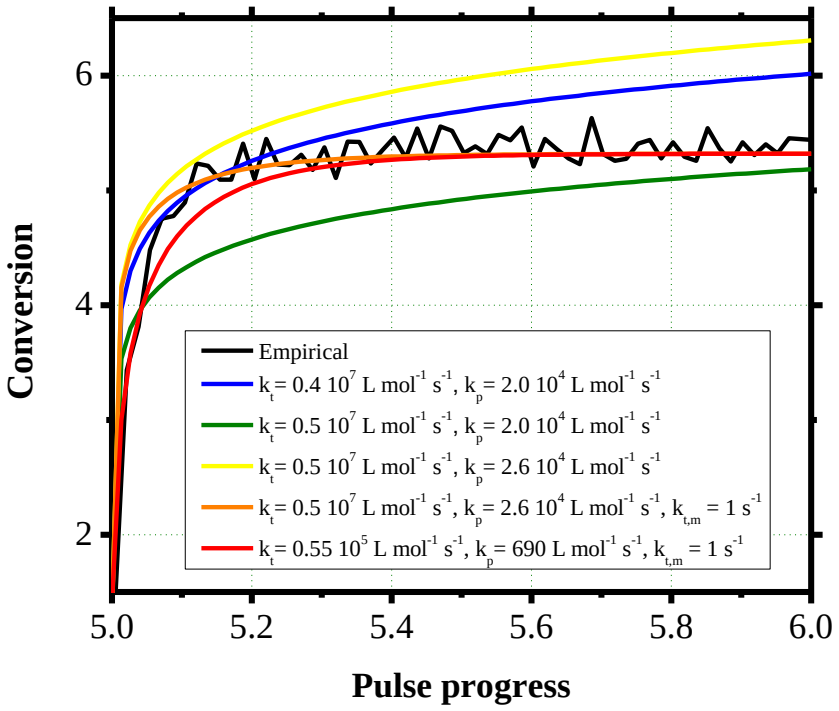

Figure 4. 16. Different parameters used to model the 5th pulse. Orange and red curves consider monomolecular termination, which fits better the experimental data.

Furthermore, by analyzing the curvature of the experimental curve, it can be seen that the initial parameters chosen are very high compared to the observed experimentally: the propagation reaction finishes much in advance for the calculated curve, which means that the process is actually much slower, i.e., the k_p and k_t values are smaller.

In order to find better parameters that could fit this behavior, the values of k_p and k_t were decreased to fit the shape of the experimental curve. The red curve shows the results obtained when using 0.55 10^5 L mol^{-1} s^{-1} for k_t and 690 L mol^{-1} $s^{-1}$for k_p. It can be seen that this curve fits the experimental data much better than the previous one.

The same reasoning was repeated to fit the conversion curves for the rest of the pulses (from 6^{th} to 15^{th}). The final calculated curve is shown together with the experimental one in figure 4.17. It can be seen that the curves fit adequately the experimental data, which is really impressive for such a simple model.

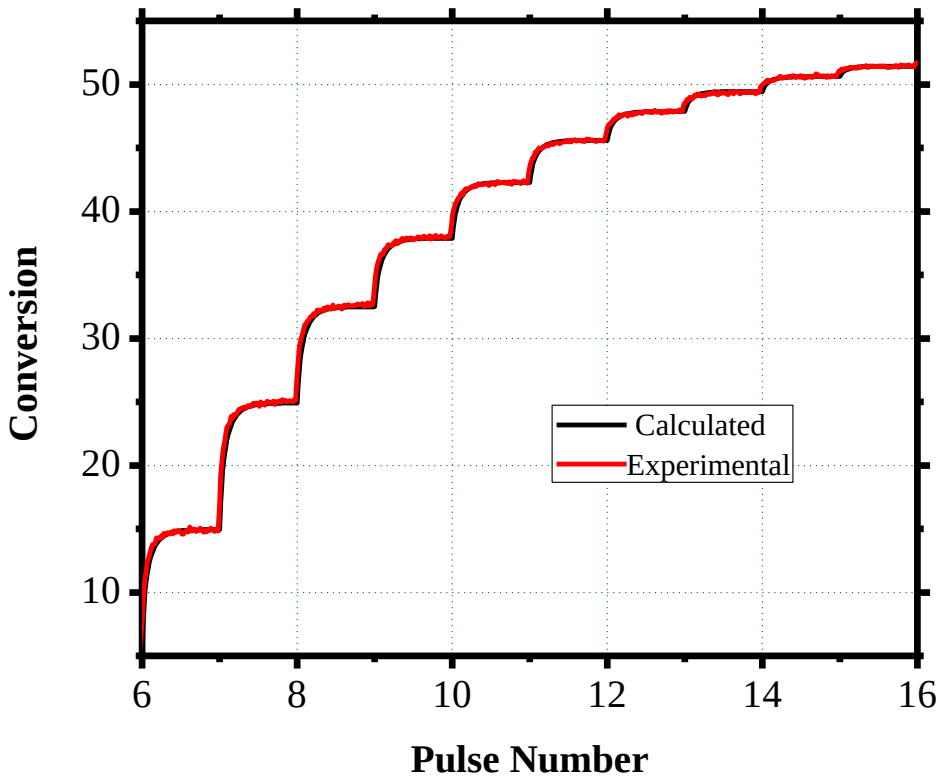

Figure 4. 17. Experimental and calculated curve for pulses 6 to 16. An impressively good curve fitting was found despite the simplicity of the model.

4. 8. 5. Reevaluation of the initial conditions.

One of the most important results obtained after fitting the model to the experimental curve is that the variation of the values of k_p and k_t with monomer conversion was determined. Figures 4.18 and 4.19 show the variation of k_p and k_t with monomer conversion, respectively.

It can be seen that the initial values are orders of magnitude bigger than those found for the pulses 4 and on. These results suggest that the initial values chosen for k_t and k_p should be reevaluated. It has to be considered that the bibliographic values of these parameters present a wide variation from monomer to monomer and that the first values used were only estimative. It has to be also remarked that the initial values of k_t and k_p are not of big importance during the inhibition pulses regime, since the main processes having place at that point are inhibition and initiation processes as stated above.

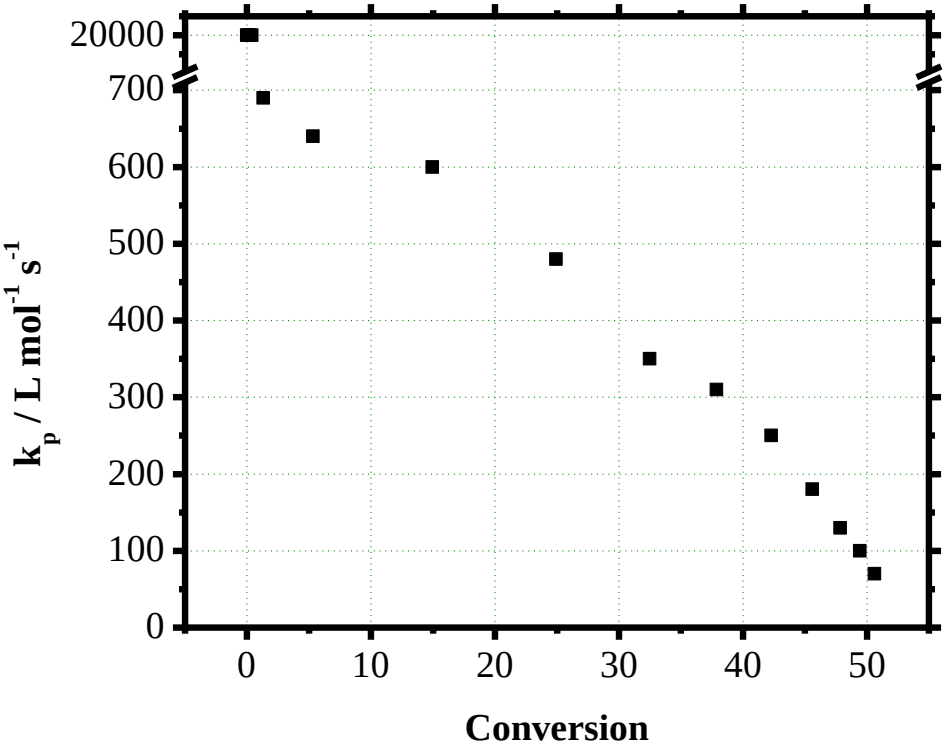

Figure 4. 18. Variation of k_p with monomer conversion obtained by the fitting of conversion curve.

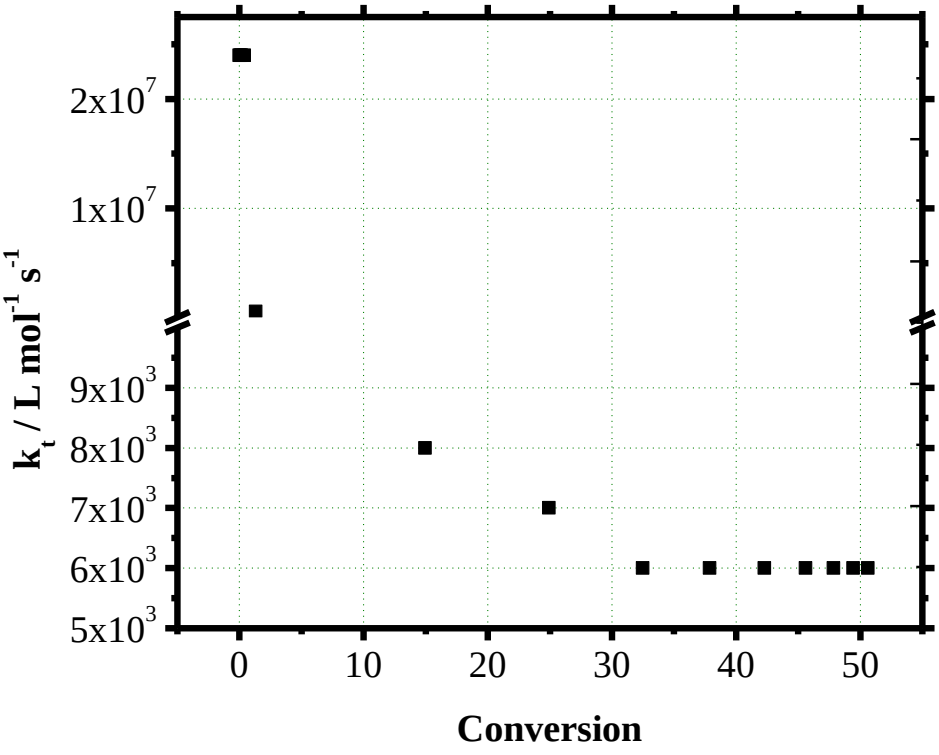

Figure 4. 19. Variation of k_t with monomer conversion obtained by the fitting of conversion curve.

According to Buback[15], k_p can be considered as the sum of two contributions: the difussional-control constant, $k_{p,\ D}$ and the chemical-control constant, $k_{p\ 0}$. According to the same paper, the difussional-control contribution is generally accepted to vary with the inverse of the relative viscosity, η_r, which gives the overall expression of k_p shown in equation 4.13, where $k_{p,D}^0$is the diffusional propagation constant in pure monomer.

$$\frac{1}{k_p} = \frac{1}{k_{p,0}} + \frac{\eta_r}{k_{p,D}^0} \quad (4.19)$$

From figure 4.19, the value of $k_{p,0}$ (i.e., propagation without difussion), can be estimated to be around 690 L mol^{-1} s^{-1} by observing the obtained trend, which is in agreement with the literature[14] . The value of $k_{p,D}^0$ can be determined from the intercept value of the tangent line from the plot of log (k_p) vs. conversion, as explained in reference 15. This plot can be seen in figure 4.20 and the value of $k_{p,D}^0$ obtained was $1.10^{8.5}$ L mol^{-1} s^{-1}, which is also in agreement with the reference[15].

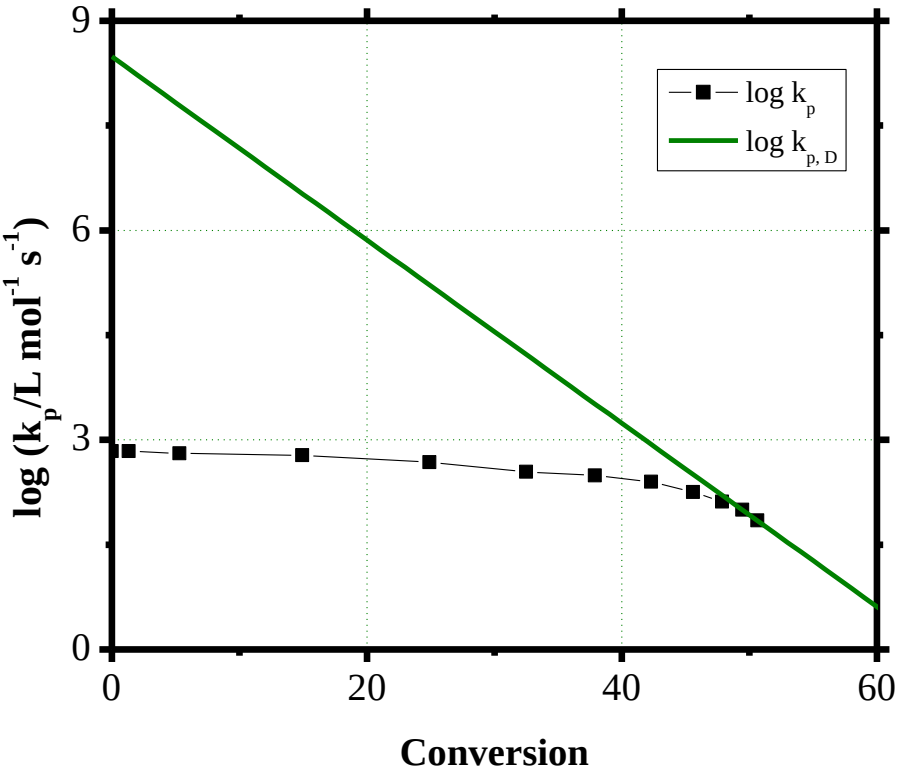

Figure 4. 20. Logarithm of k_p as a function of monomer conversion. The tangential curve at high conversion can be used to calculate the value of $k_{p,D}^0$, which was found to be $1.10^{8.5}$ L mol^{-1} s^{-1}

In summary, the new initial value of k_p is 690 L mol^{-1} s^{-1}, which is in agreement with literature[14] and with Buback's model. Of course, if k_p initial value is reevaluated, the same has to be done for k_t. In order to do this, calculations were made with the new initial values to find the best value of k_t that fits the experimental data as already explained above. This value turned out to be $5.5\ 10^5$ L mol^{-1} s^{-1}.

Furthermore, these parameters allow to calculating the variation of η_r with conversion can be calculated from equation 4.19, which was a hard challenge to the date, due to experimental difficulties.

The plot of η_r vs. monomer conversion can be seen in figure 4.21. The increase of viscosity value with conversion is rather impressive and it indicates that most of the polymerization process having place is diffusion controlled. The lower part of what should be a rather sigmoidal growth can be identified in the plot: a very slow increase can be seen in the beginning and a sudden fast increase is

noticed around 50% of conversion. Of course, this abrupt growth has to reach a plateau once the media is completely jellified.

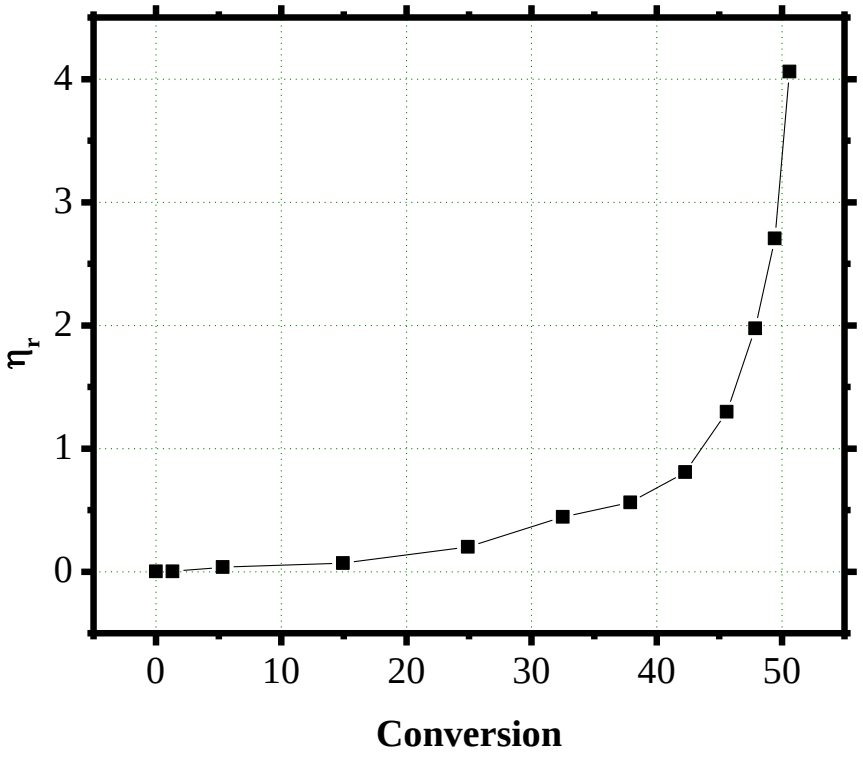

Figure 4. 21. Relative viscosity as a function of monomer conversion. The lower part of what seems to be a sigmoidal behavior can be appreciated.

Regarding termination reaction, Buback considers termination as the sum of diffusional reaction and what is known as "reaction diffusion". The diffusional part has, at times, contributions of translational and segmental diffusion and chemical reaction, as it can be seen in equation 4.20. k_{TD} and k_{SD} have analogous behavior to k_{PD}

$$\frac{1}{k_{t,D}} = \frac{1}{k_{TD}} + \frac{1}{k_{SD}} + \frac{1}{k_{CR}} \quad (4.20)$$

Furthermore, the reaction diffusion term can be calculated from eqution 4.21. The concept of reaction diffusion is that radical sites came into contact through propagational growth of the chain ends.

$$k_{t,RD} = C_{RD} k_p \left(1 - \frac{conversion\%}{100}\right) (4.21)$$

Then, considering k_{CR} and k_{SD} >> k_{TD}, overall bimolecular termination reaction constant can be described as in equation 4.22[15]. This approximation is generally valid in resins that undergo big viscosity changes with conversion, for conversions that are not too small.

$$k_t = \frac{k_{t,D}^0}{\eta_r} + \frac{C_{RD}\left(1 - \frac{conversion\%}{100}\right)}{\frac{1}{k_{p,0}} + \frac{\eta_r}{k_{p,D}^0}} (4.22)$$

From equation 4.22, the value of k_t at zero conversion is approximately $k_{t,D}^0 + C_{RD} k_{p,0}$. $k_{t,D}^0$ can be estimated as equal to $k_{diff\ 0}$, i.e. 2.4 10^7 L mol^{-1} s^{-1}, and so, the value of C_{RD} can be calculated using the equation 4.22 and the data previously obtained for different conversion values. The values of this parameter for different conversion values were calculated and are shown in figure 4.22.

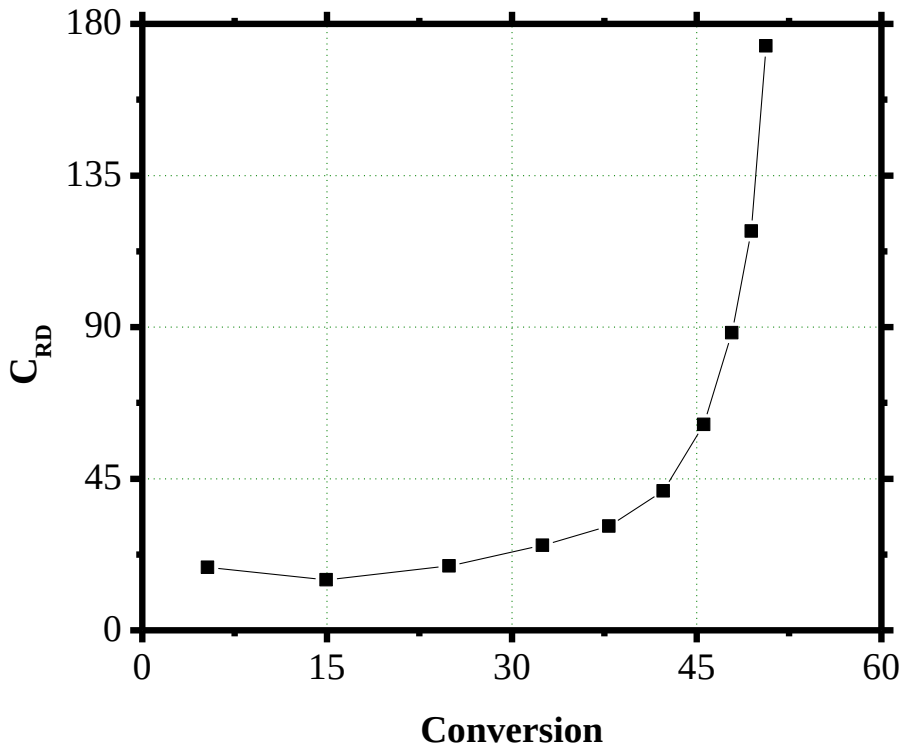

Figure 4. 22. Progression of C_{RD} with monomer conversion. The reaction diffusion mechanism for bimolecular termination becomes more important as radicals' diffusion is hindered due to the high viscosity of the media.

It can be seen that the chemical diffusion termination mechanism becomes more important with conversion. This is reasonable since, at high conversion, molecules are trapped in a jellified media and chemical diffusion of the radical is more probable than the physical translation of a living radical into another one.

4. 8. 6. Analysis of ΔC% as a function of conversion.

Figure 4.7 showed the value of ΔC% as a function of conversion. In figure 4.23, these values are compared with the calculated ones. It can be seen that there is an almost perfect overlap between both curves. Furthermore, the values of kp/kt are also shown. The value of kp/kt is very small at low conversions and reachs a maximum at the conversion value where $\Delta C\%_{max}$ is found. Then, this ratio decays again at higher conversions, which is consistent with smaller values of ΔC%.

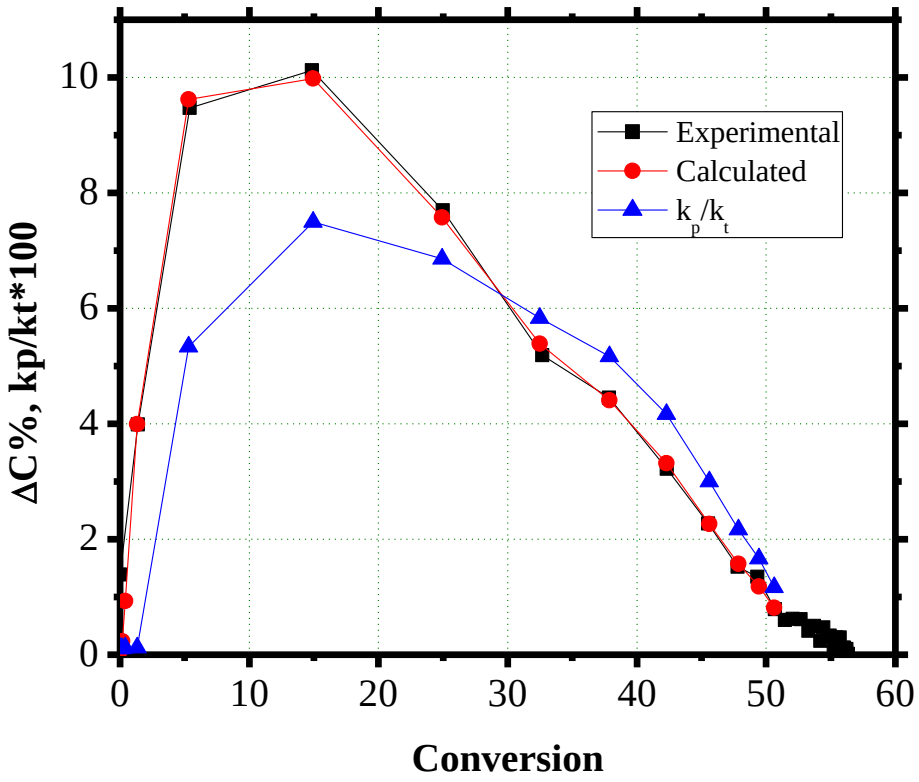

Figure 4. 23. Experimental and calculated ΔC% values as a function of the monomer conversion. In blue, the value ok k_p/k_t ratio is also displayed.

4. 9. Conclusion.

An introduction to Pulsed Laser Polymerization studies was presented. The main characteristics of these experiments were shown and explained.

In the first part, the effect of the pulse energy in polymerization efficiency was studied, finding that, as expected, the efficiency increases with pulse energy. A linear correlation between $R_{C\,i}$ and $\Delta C\%_i$ was found. The fact that this correlation is independent of monomer conversion, energy pulse and inhibitor concentration is astonishing and has two consequences: one, the $\Delta C\%$ values are limited by the conversion rate and two, any analysis of $\Delta C\%$ is equivalent to the analysis of $R_{C\,i}$. This is a big advantage since conversion values are easier to calculate than conversion rates.

The inhibition pulse phenomenon and the concept of inhibition dose were introduced and explained. Polymerization can't be initiated (or, at least, not noticed) until all the inhibitor species present in the sample are totally consumed.

A very powerful, yet simple model was developed to study PLP mechanisms. The study of the conversion curve vs. time for a sample irradiated with 5 mJ energy pulses lead to the determination of k_p and k_t values and its dependence with the monomer conversion for SR 349.

Finally, by using Buback's model, it was possible to corroborate these values and also to calculate the variation of η_R with conversion, which was a difficult challenge to the date. A rather sigmoidal behavior was found.

4. 10. References.

[1] S. Beuermann, M. Buback, "Rate Coefficients of Free-radical Polymerization Deduced from Pulsed Laser Experiments", *Prog. Polym. Sci.*, **2002**, 27, p. 191–254.

[2] J. Barth, M. Buback, "SP-PLP-EPR Investigations into the Chain-Length-Dependent Termination of Methyl Methacrylate Bulk Polymerization", *Macromol. Rapid. Commun*., **2009**, 30, p. 1805-1811.

[3] J. Barth, M. Buback, "SP-PLP-EPR – A Novel Method for Detailed Studies into the Termination Kinetics of Radical Polymerization", *Macromol. React. Eng.*, **2010**, 4, p. 288-301.

[4] J. Barth, M. Buback, "SP-PLP-EPR Study into the Termination Kinetics of Methacrylic Acid Radical Polymerization in Aqueous Solution", *Macromolecules*, **2011**, 44, p. 1292-1297.

[5] J. Barth, W. Meiser, M. Buback, "SP-PLP-EPR Study into Termination and Transfer Kinetics of Non-Ionized Acrylic Acid Polymerized in Aqueous Solution", *Macromlecules*, **2012**, 45, p. 1339-1345.

[6] R. X. E. Willemse, A.M. Van Herk, "Determination of Propagation Rate Coefficients of a Family of Acrylates with PLP-MALDI-ToF-MS", *Macromol. Chem. Phys.*, **2010**, 211, p. 539-545.

[7] C. Boukaftane, A.M. Van Herk, "PLP and MALDI-ToF Determination of Propagation Rate Coefficients of Fast-Polymerizing Acrylates with Heterocyclic Side-Chains: Tetrahydrofurfuryl Acrylate and (R)-α-Acryloyloxy-β,β-dimethyl-γ-butyrolactone", *Macromol. Chem. Phys.*, **2011**, 212, p. 96-101.

[8] H. Tar Thesis, C. Ley, X. Allonas, "*Development of New Photoinitiating Systems for Free Radical Photopolymerization*", UHA. **2013**

[9] M.Wozniak, T. Graule, Y. de Hazan, D. Kata, J. Lis, "Highly loaded UV curable nanosilica dispersions for rapid prototyping applications", *Journal of the European Ceramic Society*, *Vol. 29, Issue 11*, August **2009**, p. 2259–2265.

[10] H. Arikawa, H. Takahashi, T. Kanie, S. Ban, "Effect of various visible light photoinitiators on the polymerization and color of light-activated resins", *Dental Materials Journal*, **2009**, 28, No. 4, p 454-460.

[11] J. V. Kelly, F. T. ONeill, J. T. Sheridan, C. Neipp, S. Gallego, and M. Ortuno *J. Opt. Soc. Am. B* **2005**, 22, p. 407-416.

[12] G. Odian, *Principles of Polymerization*, 4th Edition, John Wiley & Sons, Inc., Hoboken, New jersey, **2004**, p. 832.

[13] E. Andrzejewska, "Photopolymerization kinetics of multifunctional monomers", *Progress in Polymer Science* **2001**, 26, p. 605-665.

[14] E. Andrzejewska, M. B. Bogacki, "Monomolecular and bimolecular termination in the polymerization of di(meth)acrylates", *Macromol. Chem. Phys.* **1997**, 198 p. 1649-1664.

[15] M. Buback, "Free-radical polymerization up to high conversion. A general kinetic treatment", *Makromol. Chem.* **1990**, 191, p. 1575-1587.

[16] J. Lalevée, X. Allonas, S. Jradi, J-P. Fouassier, "Role of the Medium on the Reactivity of Cleavable Photoinitiators in Photopolymerization Reactions", *Macromolecules*, **2006**, 39, p. 1872-1879.

Chapter Five.

PLP With Visible Light.

5. 1. Introduction.

PLP mechanisms were studied in the previous chapter for an UV PI, TPO. However, one of the main objectives of this thesis is the development of PIS that are suitable to use under visible irradiation. In order achieve this, a wide variety of PIS capable of absorbing 532 nm light were irradiated in order to compare their reactivity and to develop further PIS whose efficiency is much higher in PLP.

Since PIS decomposition kinetics plays an important role in the analysis of the results[1], 2- and (mostly) 3-C PIS were studied in order to study if there were any difference with the type I PI system that was studied in Chapter Five. It was previously shown in Chapter Four that 2-C PIS are usually less efficient than 3-C PIS in CW mode; this is the reason why the studies shown within this chapter will be centered mostly in 3-C PIS.

The efficiency of different families of PIS in PLP was studied and compared. Figure 5.1 shows the structures of all the compounds involved. The results obtained were critically analyzed and will be presented in the following sections. The wavelength of irradiation used for these experiments was 532 nm and the same conditions used in Chapter Four apply. Pulse energy was set to 10 mJ for all the experiments, as they are the standard conditions used within our collaboration with Bayer Material Science.

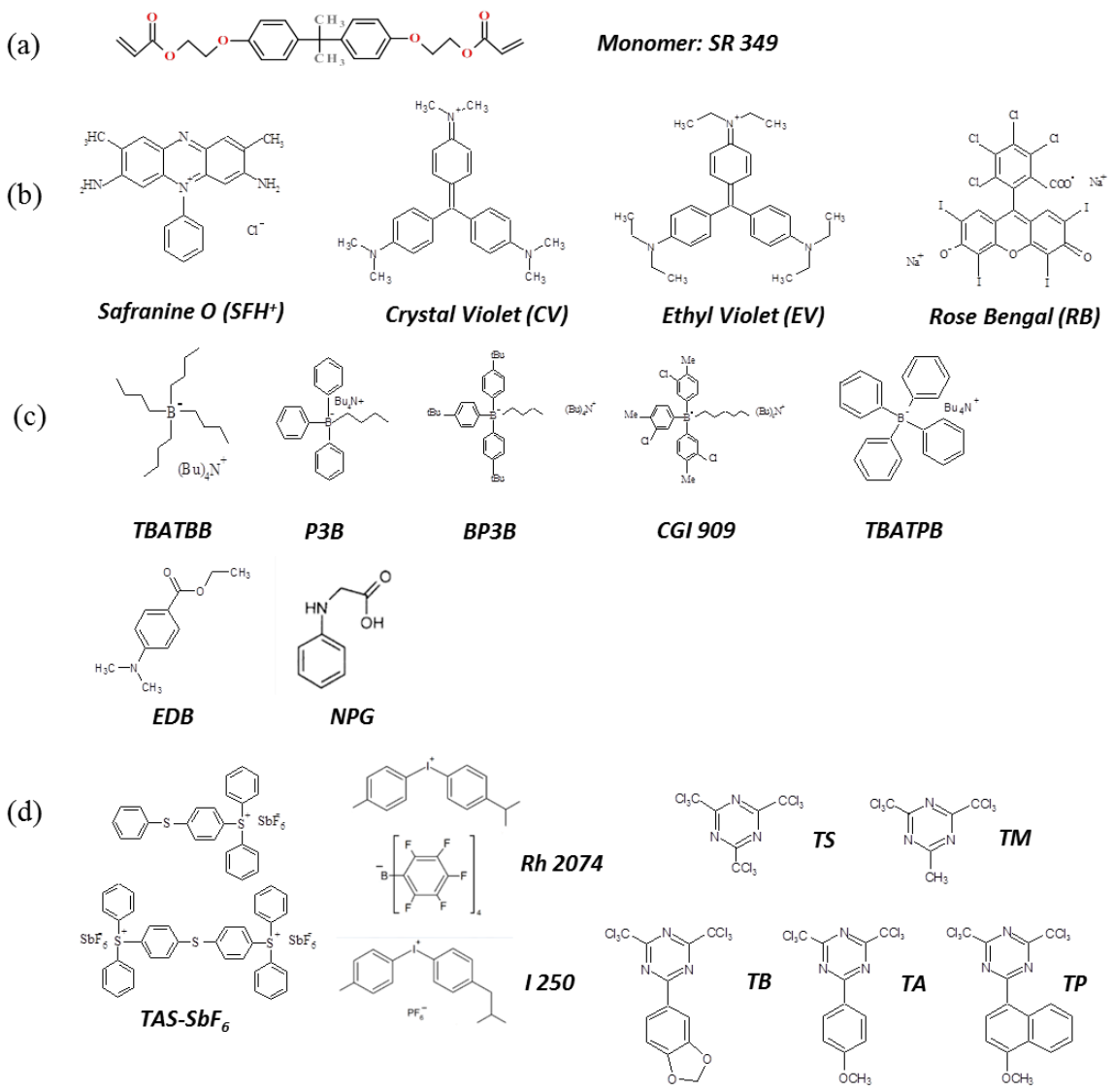

Figure 5. 1. Chemical structure of the substances used for the studies shown in this chapter. (a) monomer, (b) dyes, (c) electron donors, (d) electron acceptors.

5. 2. 2- vs 3-C PIS in PLP. SFH^+/ Borate salts/ Electron acceptor.

It was shown in Chapter Four that 3-C PIS are usually more efficient than their 2-C counterparts in CW mode. Before heading to other measurements, a comparison between 2- and 3-C PIS in PLP should also be done. To make this comparison, PIS containing safranine O (SFH^+) and Borate salts were compared with 3-C PIS containing different kinds of electron acceptors.

SFH^+/Borate salt PIS were chosen for this work due to the high performance they have shown in the works of Haja Tar[2] and Ahmad Ibrahim[3]. Four borate salts, TBATBB, P3B, BP3B and CGI909 were used as electron donors and SFH^+ as green light photosensitizers. The results of these experiments can be seen in figure 5.2. Main parameters are displayed in table 5.1 for an easier interpretation.

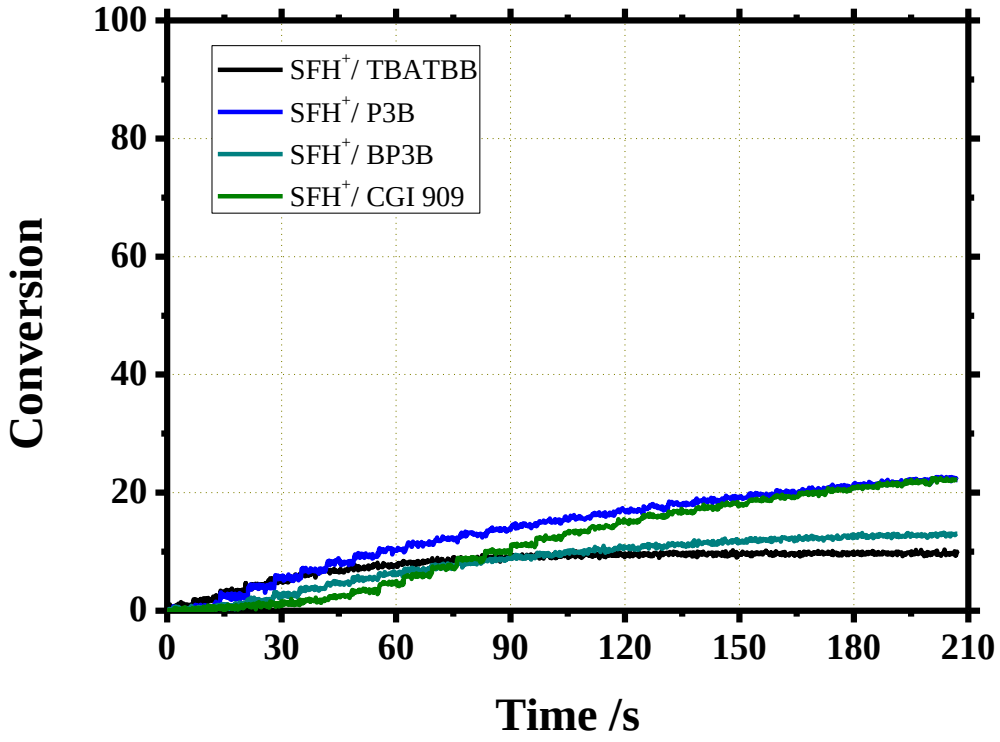

Figure 5. 2. Conversion vs. time plot for SFH^+/ Borate salts 2-C PIS. Efficiency for these systems is extremely low.

PIS	$R_{C\ i\ max}$	P_{in}	$\Delta C\%_{max}$	Final Conversion
SFH^+ / TBATBB	n. m.	1	1.7	10
SFH^+ / P3B	n. m.	1	1.7	22
SFH^+ / BP3B	n. m.	1	1.3	13
SFH^+ / CGI 909	n. m.	4	1.4	22

Table 5. 1. Main experimental parameters obtained for SFH^+/ Borate salts 2-C PIS.

It can be seen that the conversion reached with these PIS is extremely low even after 20 pulses of irradiation. This can be attributed to a low efficient quenching of the SFH^+ excited state by the borate salts involved.

In order to improve this low efficiency, different additives were added to the 2-C PIS in order to find an efficient 3-C PIS: sulfonium and iodonium salts and HABI and triazine derivatives. The efficiency obtained for the 3-C PIS was critically analyzed and is presented in the following subsections.

5. 2. 1. SFH^+/ Borate salts/ Sulfonium salts.

The first compound studied as an electron acceptor in the PIS was TAS-SbF_6 (Figure 5.1), a sulfonium salt. This compound showed satisfactory results in Tar's thesis work[2]. That is the reason why it was decided to study its efficiency in PLP. Conversion as a function of time can be seen in figure 5.3 and main parameters in table 5.2.

PIS	$R_{C\ i\ max}$	P_{in}	$\Delta C\%_{max}$	Final Conversion
SFH^+ / TBATBB/ TAS-SbF_6	n. m.	1	1.4	17
SFH^+ / P3B/ TAS-SbF_6	n. m.	2	2.7	23
SFH^+ / BP3B/ TAS-SbF_6	n. m.	3	1.4	18
SFH^+ / CGI 909/ TAS-SbF_6	n. m.	9	1.6	22

Table 5. 2. Main experimental parameters obtained for SFH^+/ Borate salt/ TAS-SbF_6 3-C PIS.

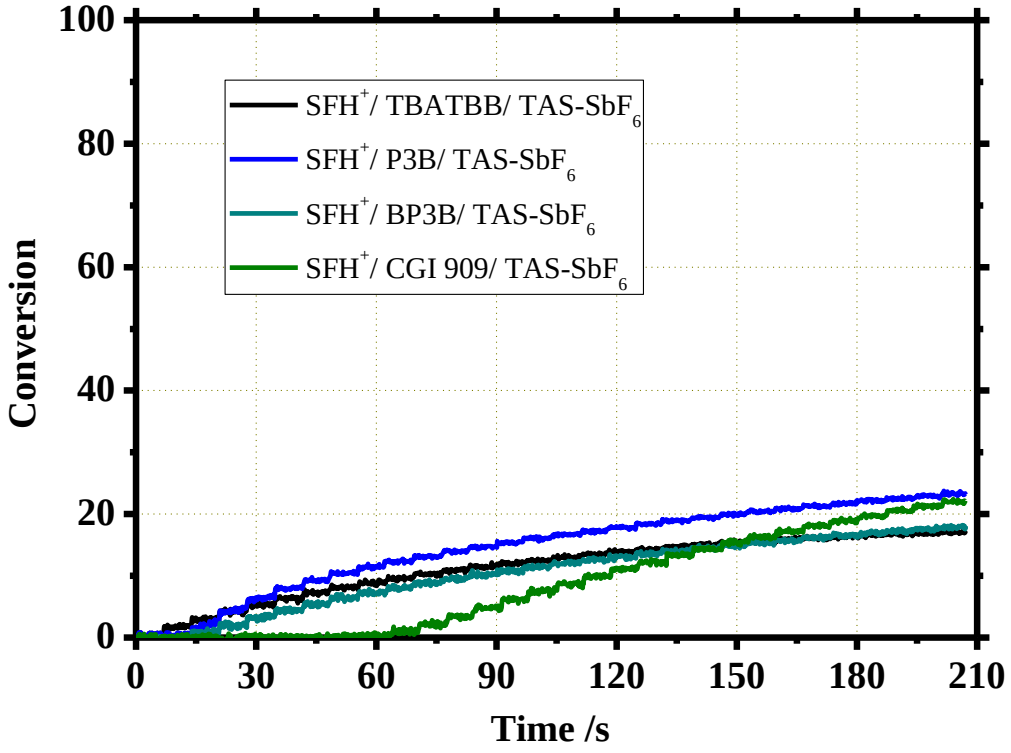

Figure 5. 3. Conversion vs. time plot for SFH^+/ Borate salt/ TAS-SbF_6 3-C PIS. The addition of sulfonium salts does not entail any improvement in the efficiency of polymerization compared with the SFH^+ / Borate salt 2-C PIS.

It can be seen that, in this case, the addition of TAS-SbF_6 does not improve the efficiency of SFH^+/ Borate salt 2-C PIS. This result discards, of course, the possibility of a PCIS among the three components of the PIS and shows that the sulfonium salt does not react with safranine O radicals. However, the reactivity of this family of compounds has not yet been studied and the mechanistic evidence to the date is not enough to conclude on its influence in the efficiency of polymerization.

5. 2. 2. SFH^+/ CGI 909/ Electron acceptors.

The efficiency of electron acceptors from other families was also studied in 3-C PIS. CGI 909 was chosen as a reference among the four borate salts shown above to make the first experiments due to its medium-level reactivity. The studies were later extended to other borate salts. The electron acceptors included five triazine derivatives and two iodonium salts whose structures can be seen in

figure 5.1. The synergistic behavior in this type of 3-C PIS compared to its 2-C counterpart was already demonstrated by Ibrahim during his thesis[3].

The experiments were carried out not only in PLP mode conditions, but also in CW mode, and the results obtained in both methods were compared.

5. 2. 2. 1. Triazine derivatives.

Regarding triazine derivatives, the efficiency of 3-C PIS containing five different ones (TA, TB, TM, TP and TS) was studied in both, CW and PLP mode. In the first place, conversion vs. time plot results are shown in figure 5.4 for CW mode. It can be seen that the efficiency of five PIS is similar. However, the triazine derivatives can be grouped in the least reactive ones: TB and TM; two derivatives where an intermediate value of final conversion was found, TP and TS; and TA, which shows the highest final conversion within this group (table 5.3).

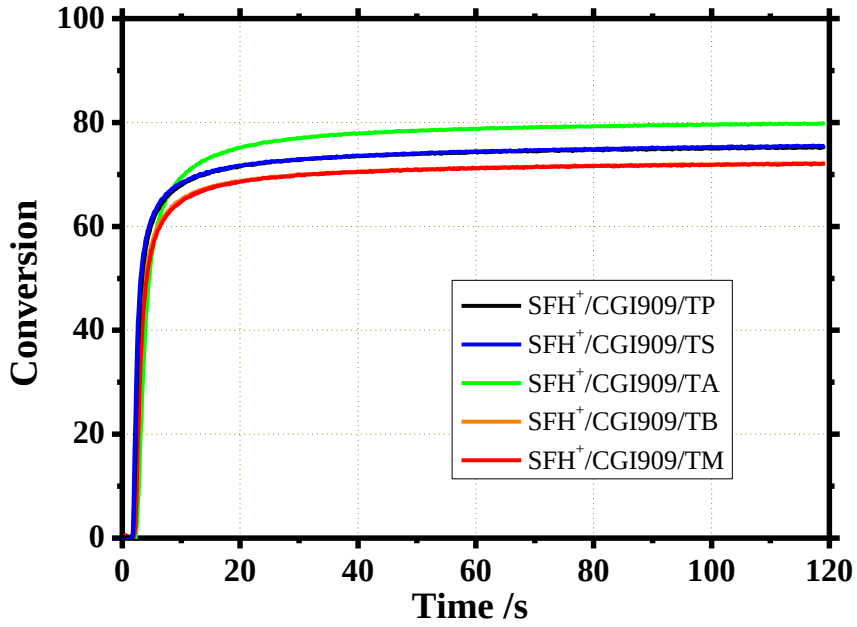

Figure 5. 4. Conversion vs. time plot for SFH^+/ CGI 909/ Triazine derivative 3-C PIS in CW mode. Similar efficiency was found.

PIS	Final conversion	$R_{C\ max}$
SFH^+ / CGI 909/ TP	75	53
SFH^+ / CGI 909/ TS	75	57
SFH^+ / CGI 909/ TA	80	31
SFH^+ / CGI 909/ TB	72	43
SFH^+ / CGI 909/ TM	72	40

Table 5. 3. Main experimental parameters obtained for SFH^+/ CGI 909/ Triazine derivative 3-C PIS in CW mode.

PLP mode experiments were also performed using the five PIS containing triazine derivatives. Conversion vs. time plot for these measurements can be seen in figure 5.5 and the main parameters calculated can be found in table 5.4.

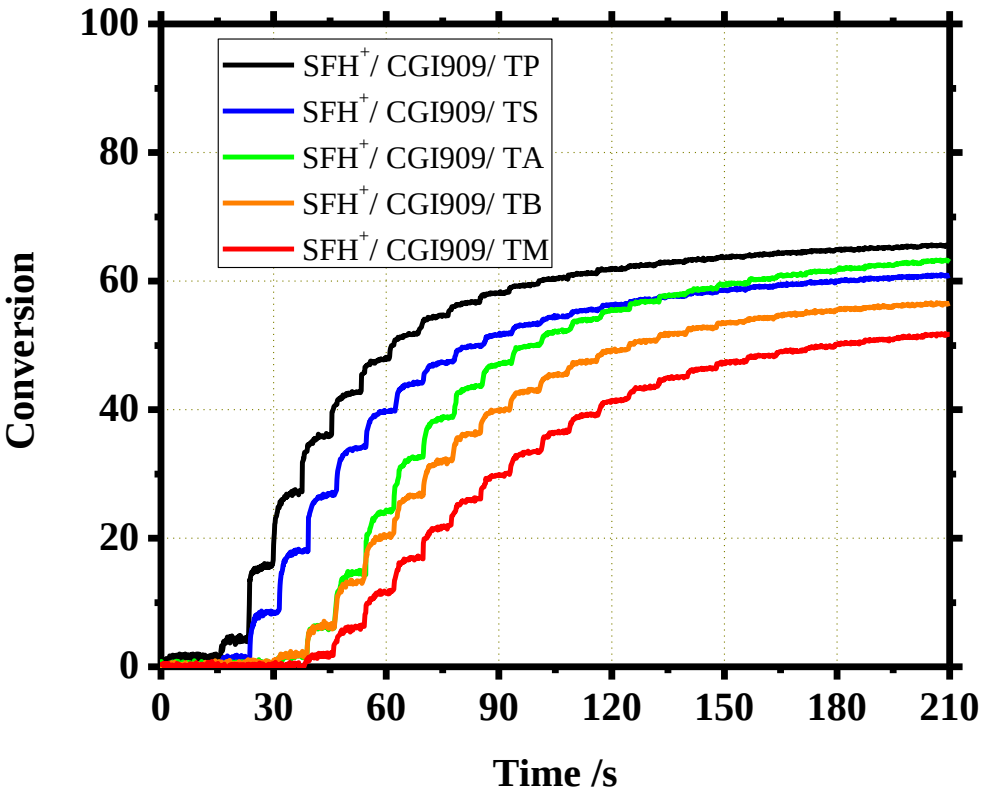

Figure 5. 5. Conversion vs. time plot for SFH^+/ CGI 909/ Triazine derivative 3-C PIS in PLP mode. The small differences found in CW mode are outlined in PLP.

PIS	$R_{C\ i\ max}$	P_{in}	$\Delta C\%_{max}$
SFH^+ / CGI 909/ TP	37	2	11
SFH^+ / CGI 909/ TS	16	2	9
SFH^+ / CGI 909/ TA	11	4	9
SFH^+ / CGI 909/ TB	10	4	7
SFH^+ / CGI 909/ TM	10	5	5

Table 5. 4. Main parameters obtained for SFH^+/ CGI 909/ Triazine derivative 3-C PIS in PLP mode.

The five PIS show different reactivities in PLP mode. As in CW mode, TP and TS showed to be the most efficient triazine derivatives, while TB and TM were the least efficient ones. TA shows an intermediate reactivity which seems to increase at the end of the experiment.

Figure 5.6 shows a plot of $\Delta C\%_i$ as a function of the pulse number for the five PIS. The progression of the curves shown is identical to that seen in Chapter Four: at first, inhibition pulses are found. Then, polymerization starts to be noticed and reactivity increases rather quickly with the pulse number. In the third zone, the maximum value of conversion per pulse ($\Delta C\%_{max}$) is reached. Finally, reactivity decreases until the end of the experiment.

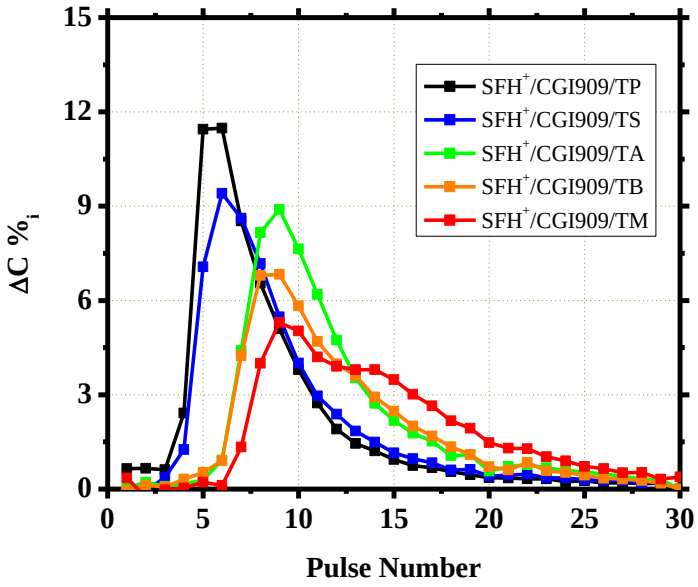

Figure 5. 6. $\Delta C\%_i$ vs. pulse number plot for SFH^+/ CGI 909/ Triazine derivative 3-C PIS in PLP mode. Four different regions can be distinguished in the curves: inhibition, reactivity increasement, reach of maximum and reactivity decreasement.

As a general rule, it can be stated that most efficient PIS present curves in which the polymerization process occurs within a small number of pulses while less efficient systems present a slower progression all along the experiment. Also, the more efficient a PIS is, the smaller the quantity of P_{in} is found. This means that the "inhibition dose" for more efficient PIS is smaller, which is not surprising because more efficient radical generation will consume the inhibitor species present in the samples within less pulses as it was already demonstrated in Chapter Four.

5. 2. 2. 2. Iodonium salts.

The effect of the addition of iodonium salts, Rhodorsil © 2074 and Irgacure © 250 (Rh 2074 and I 250, respectively) in the efficiency of polymerization was also studied. Both iodonium salts have very similar molecular structures. Their main difference, thus, is found in their counter-ion. The efficiency of these 3-C PIS had already been studied in CW mode by Dr. Ahmad Ibrahim[3]. A similar final conversion value has been observed by him in both cases. Regarding the conversion rate, however, I 250 had shown almost twice the rate shown by Rh 2074, meaning that the PIS SFH^+/CGI 909/I 250 is more efficient than SFH^+/CGI 909/Rh 2074.

Having these previous results in mind, PLP experiments were carried out for both PIS. In figure 5.7 it can be appreciated that both PIS have approximately the same final conversion, but the PIS containing I 250 presents a much bigger $\Delta C\%_{max}$ value. Also, the maximum conversion rate is bigger for SFH^+/ CGI 909/ I 250. The exact values of these parameters can be seen in table 5.5. The values found imply that PIS that show higher conversion rate values have also higher values of $\Delta C\%_{max}$. This observation will be boarded in following sections.

PIS	$R_{C\ i\ max}$	P_{in}	$\Delta C\%_{max}$	Final Conversion
SFH^+ / CGI 909/ I 250	22	3	16	71
SFH^+ / CGI 909/ Rh 2074	9	4	7	70

Table 5. 5. Main experimental parameters obtained for SFH^+/ CGI 909/ Iodonium salts 3-C PIS.

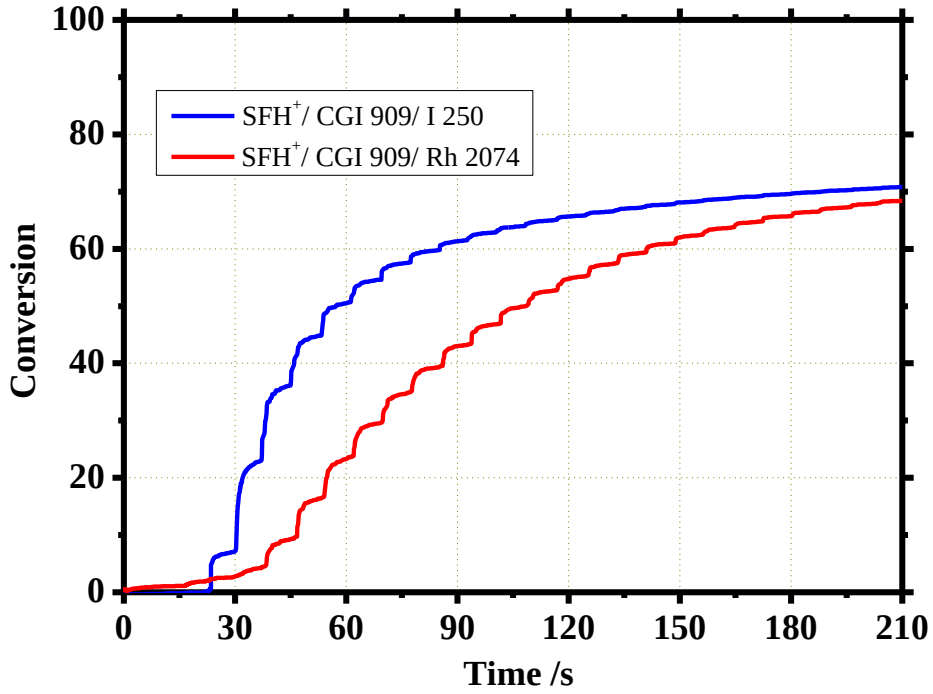

Figure 5. 7. Conversion vs. time plot for SFH^+/ CGI 909/ Iodonium salt 3-C PIS. Final conversion is almost the same for both PIS, but I 250 has a bigger $\Delta C\%_{max}$.

5. 2. 3. SFH^+/ Borate salts/ Electron acceptors.

Once the efficiency of PIS containing CGI 909 was studied, this borate salt was replaced by TBATPB, P3B or BP3B in the formulations in order to study and compare their reactivity. Once more, triazine derivatives and iodonium salts were used as electron acceptors. For the former, only TS, TP and TA were used since they showed higher reactivity among the five derivatives used in 5.2.2.1.

5. 2. 3. 1. Triazine derivatives.

The efficiency as PIS of systems containing SFH^+, borate salts and triazine derivatives TA, TS or TP were studied. Experiments were performed in PLP and CW mode as well in order to compare the efficiency of the PIS in both irradiation modes.

Figure 5.8 shows the conversion vs. time plots for the nine PIS studied in CW (right) and PLP (left), and table 5.6 summarizes the calculated experimental parameters.

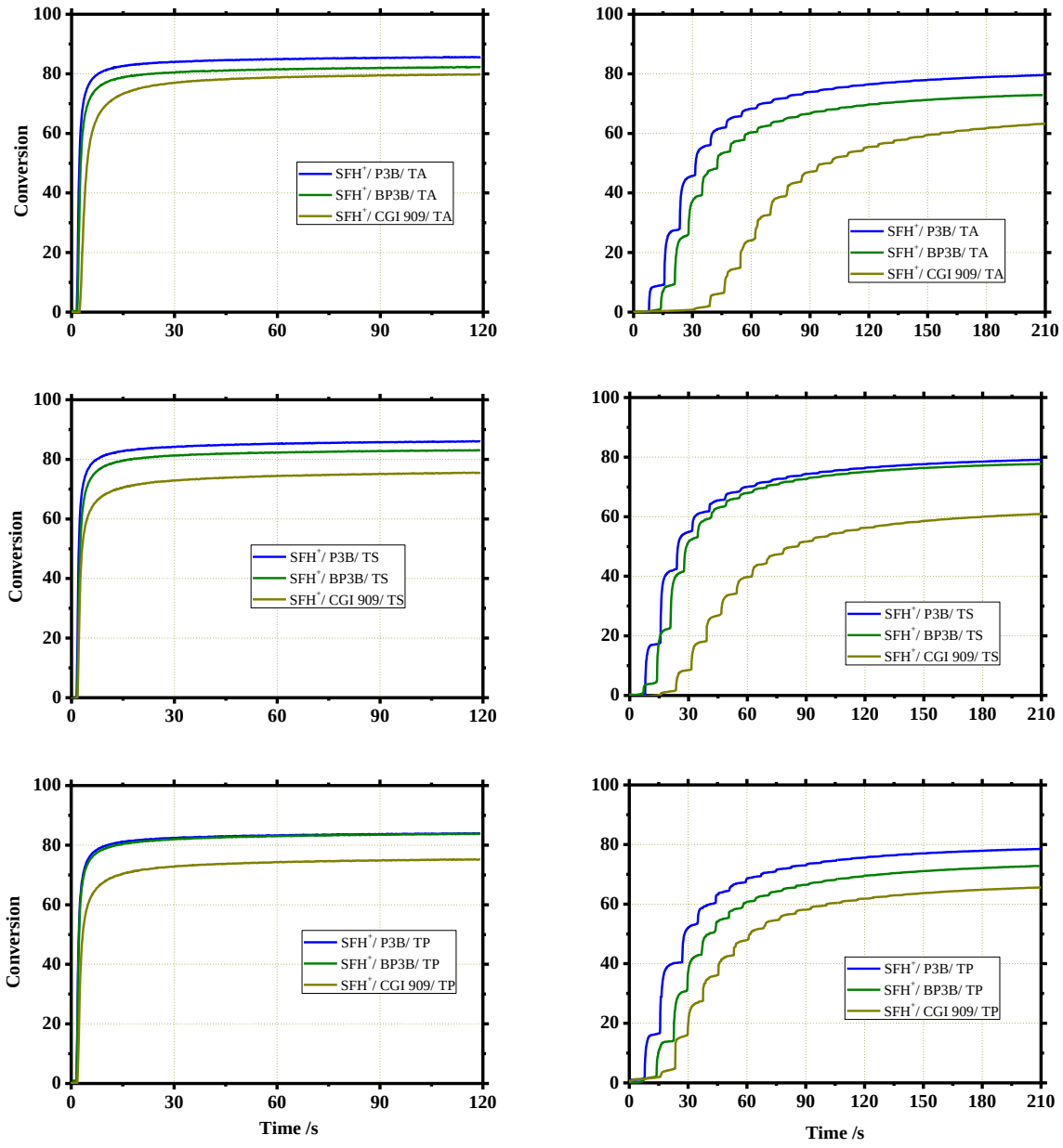

Figure 5. 8. Monomer conversion vs. time plot for SFH^+/ Borate salt/ Triazine derivative 3-C PIS in CW (Right) and PLP mode (Left). From top to bottom: TA, TS and TP.

It can be seen that, for each triazine derivative, the reactivity of P3B and BP3B PIS is quite similar, while CGI 909 presents lower efficiency in the three cases. When changing to PLP mode, differences in efficiency are outlined as it was shown for the SFH^+/CGI 909/triazine derivatives, thought it seems that the effect observed depends on the triazine. By analyzing PIS containing TP, for example, it can be seen that no difference in reactivity was found between P3B and BP3B in CW mode, while a difference of around 3% of monomer conversion was found for the PIS containing TS. This trend observed in CW mode is reversed in PLP mode, where almost no difference in reactivity was found for PIS containing TS, whereas a difference in final conversion of around 5% was found for PIS containing TP.

The differences in efficiency found between CW and PLP mode is related to the pulse duration. In CW mode, as irradiation is continuous, the excited state of the dye is continuously regenerated in 3-C PCIS, thus, the quenching efficiency from the co-initiators became less important to the global efficiency. However, in PLP, the duration of the laser pulse is shorter than the duration of a photocyclic reaction between the dye and the co-initiators and the quenching efficiency becomes more important, since dye's excited state will not be regenerated until the following pulse arrives and the efficiency obtained in any given pulse will strongly depend in the quantum yield of radical formation for the PIS used.

PIS	$R_{C\ i\ max}$	P_{in}	$\Delta C\%_{max}$	**Final Conversion (CW)**	**R_{Cmax} /s^{-1} (CW)**
SFH^+ / P3B/ TA	30	1	18	86	84
SFH^+ / BP3B/ TA	20	2	16	82	63
SFH^+ / CGI 909/ TA	20	4	9	80	31
SFH^+ / P3B/ TS	43	1	25	86	90
SFH^+ / BP3B/ TS	30	1	18	83	70
SFH^+ / CGI 909/ TS	22	3	9	75	57
SFH^+ / P3B/ TP	38	1	19	84	89
SFH^+ / BP3B/ TP	25	1	17	84	81
SFH^+ / CGI 909/ TP	12	2	21	75	53

Table 5. 6. Main experimental parameters obtained for SFH^+/ Borate salt/ Triazine derivative 3-C PIS in PLP and CW mode.

5. 2. 3. 2. Iodonium salts.

Figure 5.9 illustrates the SR 349 conversion as a function of the time for the PIS containing the four different borate salts with I 250 (left) and Rh 2074 (right). CW experiments were not performed during this thesis, as they had already been studied by Dr Ibrahim during his thesis work.

P3B and BP3B are, among the four borate salts studied, the most efficient ones and present similar reactivity, as it can be expected from their similar chemical structure (figure 5.1). TBATPB, in contrast, presents the lowest efficiency. The reason for this can be attributed to the lower stability of phenyl radicals compared with butyl ones. It is normally accepted that the radical borate salt loses an alkyl or aryl radical group which is the actual photoinitiator radical[3]. The dissociation of the butyl radical present in P3B, BP3B and CGI 909 from the borate radical will probably occur more easily than that of a phenyl group, due to its higher stability. Thus, as TBATPB only has arylic substituents, the difference in efficiency is explained.

Another remarkable result is that no inhibition pulses were found for SFH^+/ P3B/ I 250 nor SFH^+/ BP3B/ Rh 2074 PIS, which makes it a good candidate to develop efficient PLP experiments. Table 5.7 summarizes the main parameters for all the PIS.

PIS	$R_{C\ i\ max}$	P_{in}	$\Delta C\%_{max}$
SFH^+/ TBATPB/ I 250	n. m.	17	3
SFH^+/ P3B/ I 250	30	0	19
SFH^+/ BP3B/ I 250	45	1	27
SFH^+/ CGI909/ I 250	22	2	16
SFH^+/ TBATPB/ Rh 2074	8	21	2
SFH^+/ P3B/ Rh 2074	32	1	19
SFH^+/ BP3B/ Rh 2074	34	0	19
SFH^+/ CGI909/ Rh 2074	9	4	7

Table 5. 7. Main experimental parameters obtained for SFH^+/ Borate salt/ Iodonium salt 3-C PIS in PLP mode.

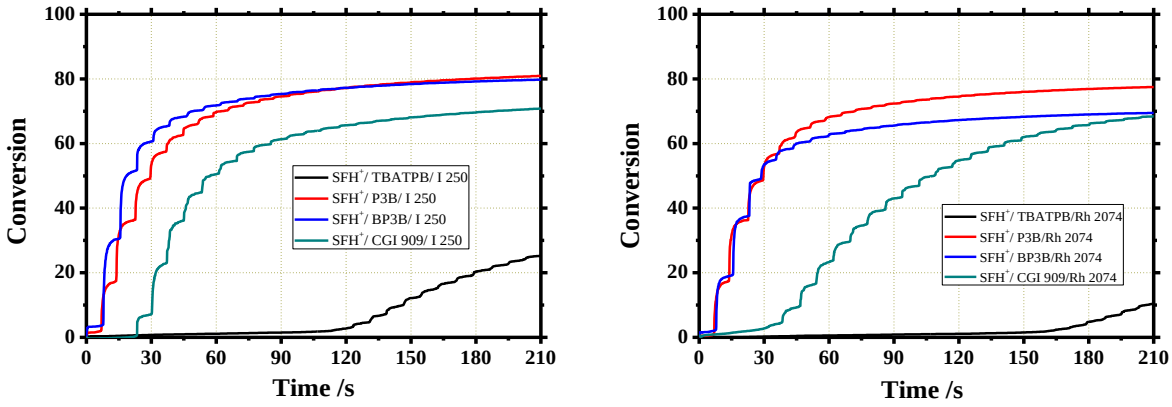

Figure 5. 9. $\Delta C\%_i$ vs. pulse number plot for SFH^+/ Borate salt/ Iodonium salt 3-C PIS in PLP mode. Left: I 250, right: Rh 2074. P3B and BP3B are the most efficient borate salts, TBATPB, the least.

5. 3. Dye effect in the PIS efficiency.

The reactivity of different dyes, Rose Bengal (RB), Crystal Violet (CV) and Ethyl Violet (EV) in PLP was also studied. RB had already been used in PLP experiences in Dr. Tar thesis work. Low or none conversion had been found when combining it with borate salts in PLP. The main reason for this can be attributed to a very inefficient quenching due to coulombic repulsive interactions between them, since both, RB and borate salts present negative electric charges. The quenching constant rates for these reactions were measured by Ibrahim *et al.*[4]

CV and EV themselves had been used in formulations in CW mode by Dr. Ibrahim. These dyes present very short lifetime excited states in non-viscous media[5]. However, as the decay of these species involves the rotation of an aromatic ring, its excited state lifetime increases in highly viscous media (e. g. an acrylate media as in the formulations studied), making a bimolecular quenching possible. This, together with the greater absorption molecular coefficient of these dyes (Table 5.8), makes them interesting candidates to be used as photosensitizers in PIS.

Dye	ε, 532 nm /M^{-1} cm^{-1}
SFH^+	26 10^3
CV	90 10^3
EV	117 10^3
RB	28 10^3

Table 5. 8. Molar extinction coefficients for the four dyes used, at 532 nm

Figure 5.10 shows the conversion vs. time plots in PLP for Dye/ Borate salt/ TA PIS. It can be seen that CV and EV have similar efficiency, while for PIS containing RB, no polymerization is observed. SFH^+ is the most efficient dye among the PIS studied. The effect of the dye in efficiency is, then, a combination of its excited state lifetime, its absorption coefficient, and the efficiency of quenching by the co-initiator: It must absorb the wavelength of irradiation to generate excited states, these excited states must have a long lifetime, so that the bimolecular quenching from the co-initiator is possible, and the quenching has to be effective, which means that the dye must be relatively easily oxidized or reduced. Of course, the last statement becomes more difficult for higher wavelengths. This is the main difficulty that visible light-induced polymerization must overcome. Table 5.9 summarizes the parameters obtained.

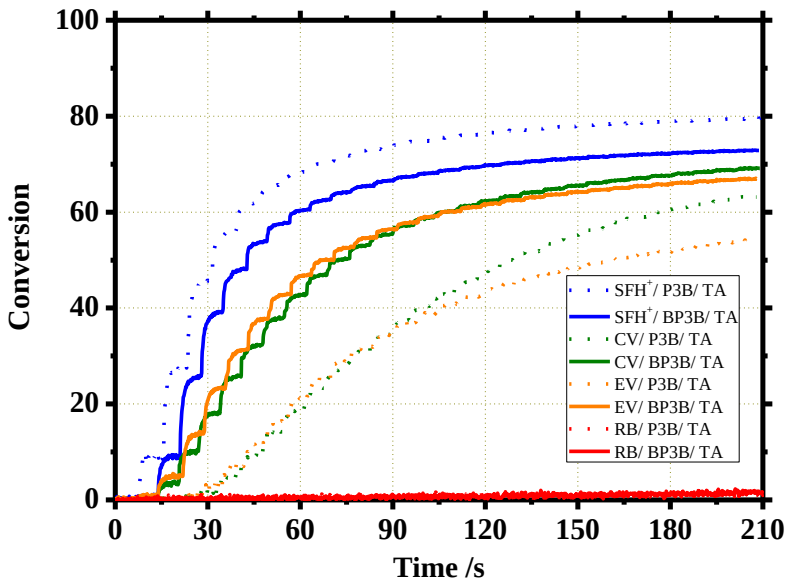

Figure 5. 10. Monomer conversion vs. time plot for Dye/ Borate salt/ TA 3-C PIS in PLP mode.

No studies for CV and EV PIS were made to determine which type of mechanism takes place in the photoinitiating process. However, Dr Ibrahim's work suggests the presence of a PCIS-like mechanism.

PIS	$R_{C\ i\ max}$	P_{in}	$\Delta C\%_{max}$
SFH^+/P3B/TA	32	1	24
SFH^+/BP3B/TA	22	2	16
CV/P3B/TA	4	4	4
CV/BP3B/TA	16	2	8
EV/P3B/TA	10	3	5
EV/BP3B/TA	14	1	9
RB/P3B/TA	n. m.	n. m.	0
RB/BP3B/TA	n. m.	n. m.	0

Table 5. 9. Main experimental parameters obtained for Dye/ Borate salt/ TA 3-C PIS in PLP.

5. 4. Amines as electron donors.

Amines have also been widely used as co-initiators. Some of its main applications in polymerization were presented in chapter 1. Its efficiency as co-initiators in PLP mode was also studied. As these compounds are not negatively charged, their efficiency as RB^{-*} quenchers is expected to be better than that of borate salts. To study this, formulations containing amines and RB were prepared and exposed to continuous and pulsed laser irradiation. Amines used in these experiments were NPG and EDB. As electron acceptors, I 250 and Rh 2074 were chosen.

Conversion vs. time plots for CW and PLP mode can be found in figures 5.11 and 5.12 respectively. It can be seen that in CW mode, only NPG PIS are able to initiate polymerization. These results suggest that RB quenching by EDB is not efficient enough. The Rehm–Weller equation, already presented in chapter four, $\Delta G^*_{ET} = E^D_{ox} - E^{PS}_{red} - E^* + C$, states that the smaller the oxidation energy of the electron donor, E^D_{ox}, the more exergonic the quenching of the excited state will be. The values of oxidation energy are 930 and 1070 mV for NPG and EDB respectively, which explains the higher efficiency of NPG in PIS.

When analyzing PLP mode results, however, only RB/NPG/Rh 2074 shows significant monomer conversion. It has already been seen in previous section that Rh 2074 is more reactive than I 250. Conversion rates, maximum conversion per pulse and number of inhibition pulses are summarized in table 5.10.

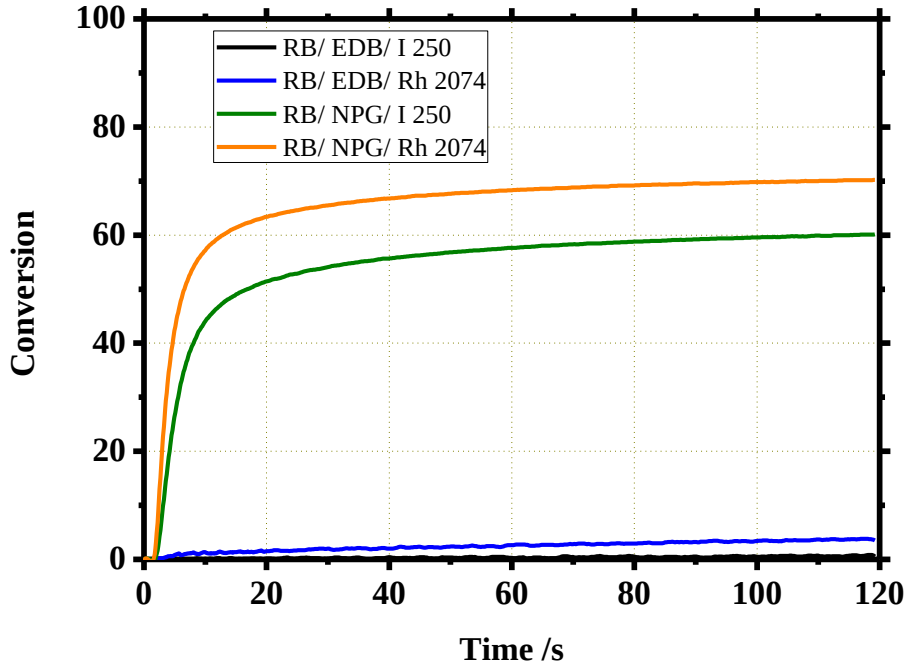

Figure 5. 11. Monomer conversion vs. time plot for RB/ Amine/ Iodonium salt 3-C PIS in CW mode. EDB is not an efficient coinitiator under these conditions.

PIS	$R_{C\ i\ max}$	P_{in}	$\Delta C\%_{max}$	**Final Conversion (CW)**	**R_{Cmax} /s^{-1} (CW)**
RB/ EDB/ I 250	n. m.	n. m.	0	0	0
RB/ EDB/ Rh 2074	n. m.	n. m.	0	0	0
RB/ NPG/ I 250	n. m.	4	0.5	60	10
RB/ NPG/ Rh 2074	n. m.	3	4.2	70	18

Table 5. 10. Main experimental parameters obtained for RB/ Amine/ Iodonium salt 3-C PIS in PLP and CW.

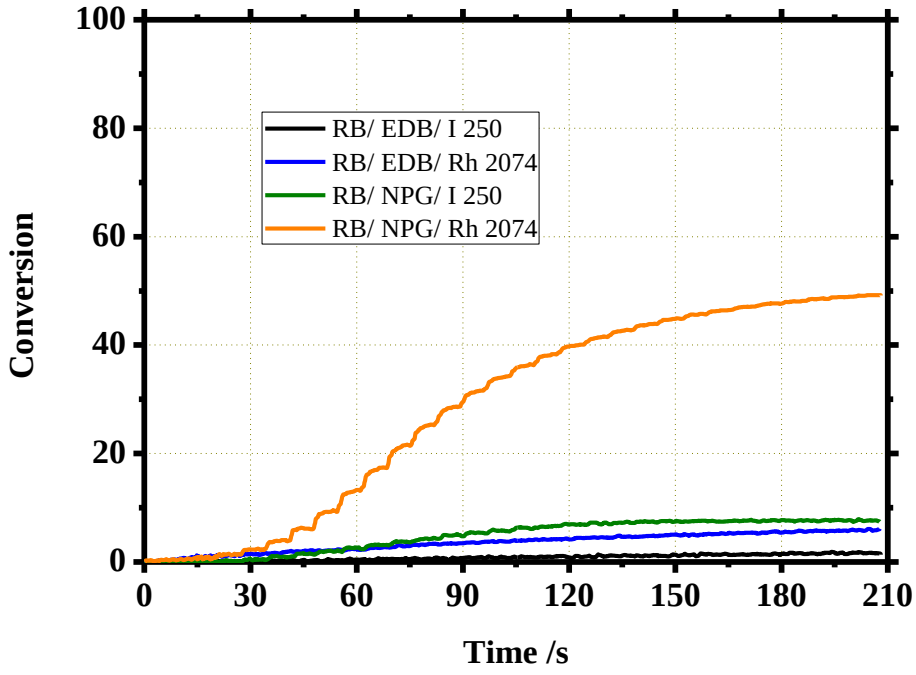

Figure 5. 12. Monomer conversion vs. time plot for RB/ Amine/ Iodonium salt 3-C PIS in PLP mode. Under these conditions, the only efficient PIS was RB/ NPG/ Rh 2074.

PIS	$R_{C\ i\ max}$	P_{in}	$\Delta C\%_{max}$	**Final Conversion (CW)**	**R_{Cmax} /s^{-1} (CW)**
SFH^+ / NPG/ I 250	n. m.	5	2.4	66	16
SFH^+ / NPG/ Rh 2074	n. m.	4	3.0	68	17
SFH^+ / NPG/ TA	n. m.	4	2.4	49	6.8
SFH^+ / NPG/ TP	n. m.	4	2.2	58	10
SFH^+ / NPG/ TS	n. m.	4	3.5	66	14

Table 5. 11. Main experimental parameters obtained for SFH^+/ NPG/ Electron acceptor 3-C PIS in PLP and CW.

PIS with SFH^+ amine were also studied. In this case, only NPG was used. As electron acceptors, TA, TP, TS, Rh 2074 and I 250 were added to the formulations. CW and PLP monomer conversion vs. time plots are shown in figures 5.13 and 5.14 respectively and the characteristic parameters obtained are shown in table 5.11.

In CW mode, PIS containing iodonium salts or TS showed the highest efficiency. The final monomer conversion in these cases was higher than 60%. In PLP mode, different behavior is noticed. TP and TA present almost the same final conversion, while TS PIS shows higher efficiency than I 250. The most efficient PIS among this group, however, is SFH^+/ NPG/ Rh 2074.

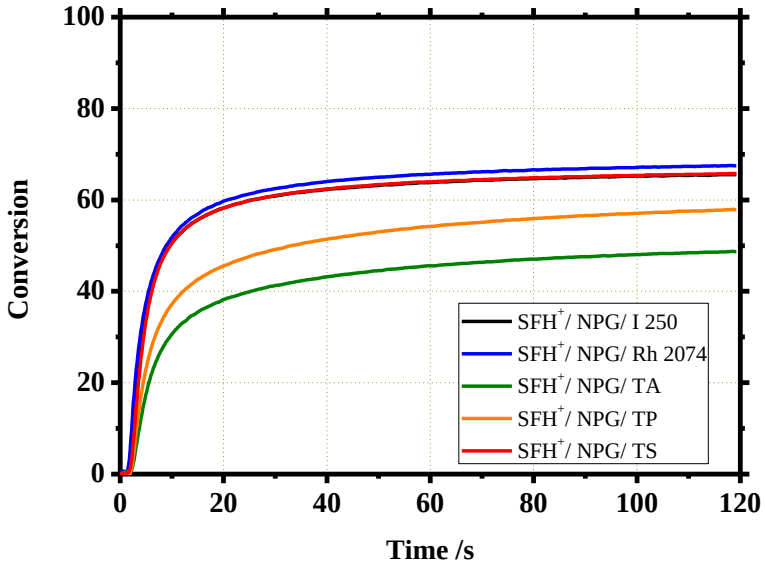

Figure 5. 13. Monomer conversion vs. time plot for SFH^+/ NPG/ Electron acceptor 3-C PIS in CW mode. PIS containing iodonium salt and PIS containing TS are the most efficient among this series.

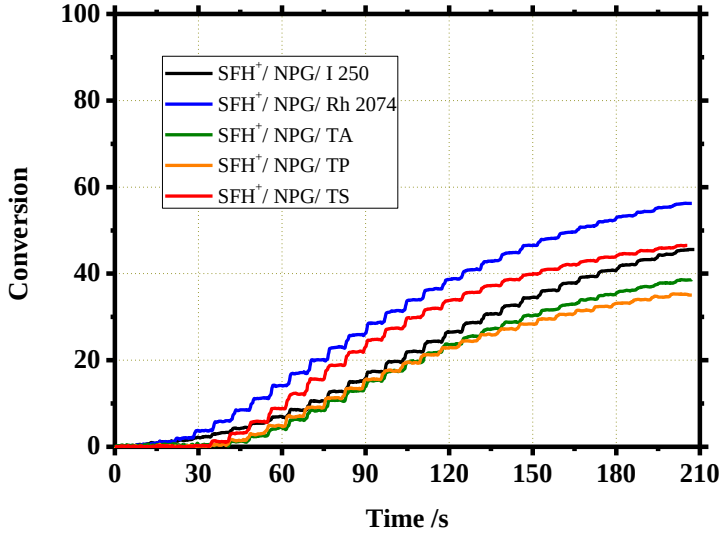

Figure 5. 14. Monomer conversion vs. time plot for SFH^+/ NPG/ Electron acceptor 3-C PIS in PLP mode. SFH^+/ NPG/ Rh 2074 is the most efficient PIS among this series.

5. 5. PLP vs. CW mode.

As it was already explained in Chapter Four, the main advantages a 3C-PIS has over a 2C-PIS, is the regeneration of the ground state of the dye via reaction with a redox additive (Figure 5. 15), eliminating radicals that favor the termination of the polymerization, while generating new radicals capable of initiating polymerization. As the dye is regenerated in these kind of mechanisms, often 3C-PIS are designated as photocatalytic systems, even if it photocyclic initiating systems (PCIS) is a more accurate description.

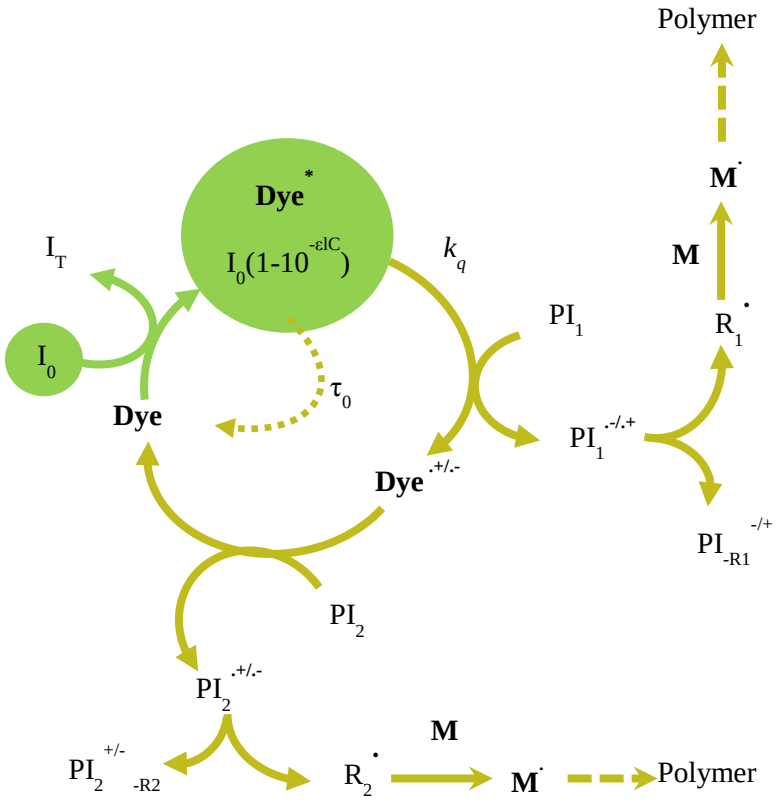

Figure 5. 15. Photoinitiation mechanism for 3C-PIS under continuous irradiation.

Basically, in a PCIS, the dye absorbs a certain amount of photons, given by its concentration, C, its molar extinction coefficient, ε, and the energy dose, I_0. The excited state generated is then quenched by a donor coinitiator (*e. g.* a borate salt). The efficiency of the quenching is given by k_q.

This quenching reaction generates a radical that will further react with the monomer initiating, thus, the polymerization reaction. The reduced dye radical species is then quenched by an electron acceptor redox additive (*e.g.* triazine derivatives or iodonium salts) to regenerate the ground state of the dye and one more initiating radical. Under continuous irradiation of PCIS, the ground and excited state are, thus, continuously regenerated. Furthermore, two radicals are produced in one cycle, leading to the possibility of having radical quantum yields greater than one.

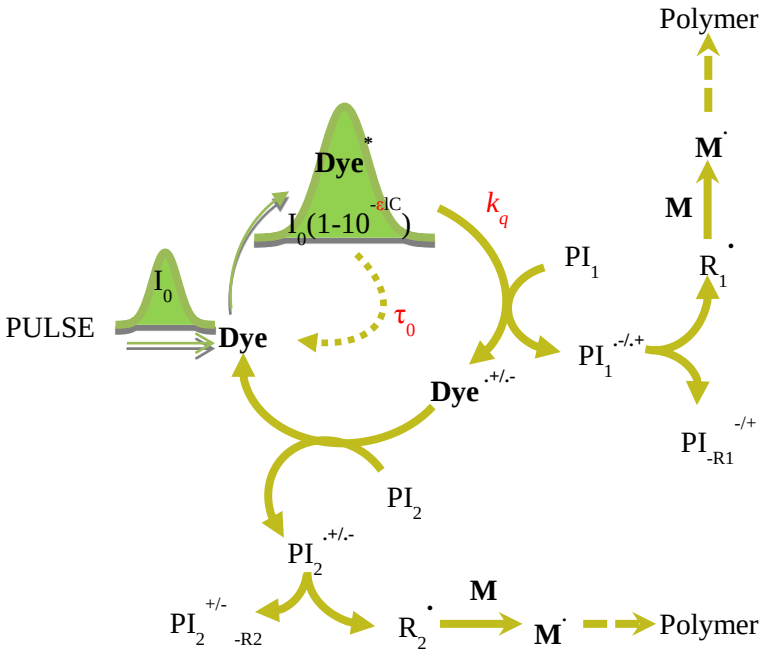

Figure 5. 16. Photoinitiation mechanism for 3C-PIS under PLP mode.

In PLP (figure 5.16), the same basic mechanism takes place. The main difference lies in the time of irradiation. The regeneration of the dye's ground state via PCIS, takes some milliseconds and thus, in order to excite the dye molecules again, the irradiation must last longer. This is not the case in PLP where pulse has a shorter duration (10 nanoseconds) than the time required for one or more

cycles to be completed. Then, only the ground state will be regenerated, and the cycle won't continue until a new pulse of irradiation arrives after the dark time.

In other words, in PLP a high molar absorption of the dye and a long decay time to the ground state are needed in order to generate a quantity of excited state of the dye as high as possible. Moreover, high quenching efficiency is needed in order to generate a greater amount of radicals (higher quantum yields) suitable to initiate the polymerization reaction.

In order to find a correlation between the performance of a PIS in CW and PLP mode, $R_{C\ i\ max}$ values obtained in PLP mode were plotted vs. $R_{C\ max}$ values obtained in CW for the PIS studied. This plot is shown in figure 5.17. A linear correlation was found between both parameters, which enhances the idea that $R_{C\ max}$ is related to the quantum radical generation of the PIS.

Figure 5.18 shows the values of $\Delta C\%_{max}$. A linear correlation was also found between these two parameters, which is not surprising since it has been shown in Chapter Five that there is a linear correlation between $\Delta C\%_i$ and $R_{C\ i}$ in PLP mode. Once more, the fact that the analysis of any of these two variables is equivalent is put in evidence. Also, it can be seen that there is less dispersion in plot 5.18, since, as it was already explained, $\Delta C\%$ is easier to calculate than R_C, and the error in the determination is also smaller.

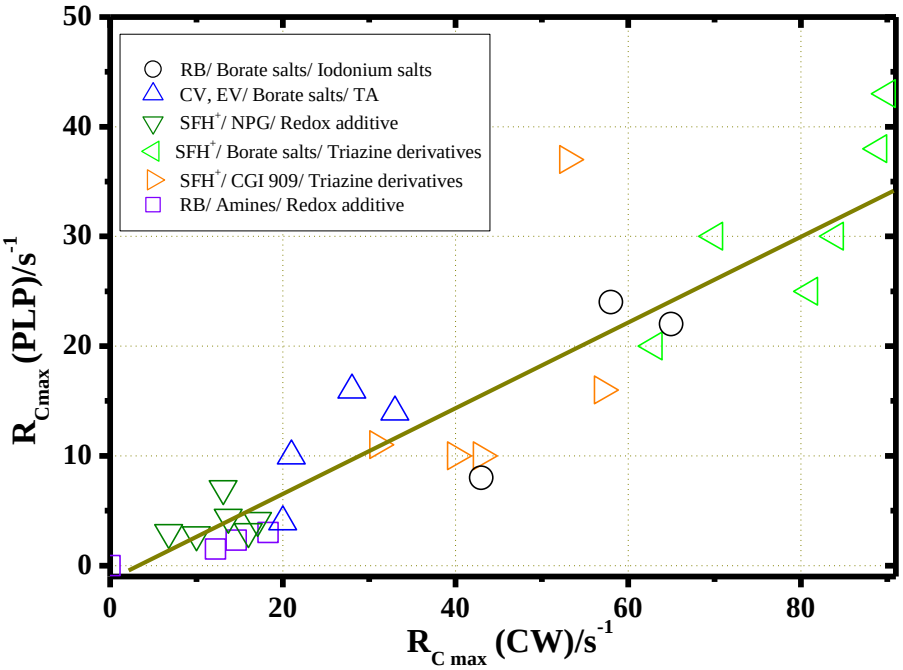

Figure 5. 17. $R_{C\ i\ max}$ values in PLP mode vs. $R_{C\ max}$ (CW). Linear correlation was found. Each group of PIS is represented with a different symbol.

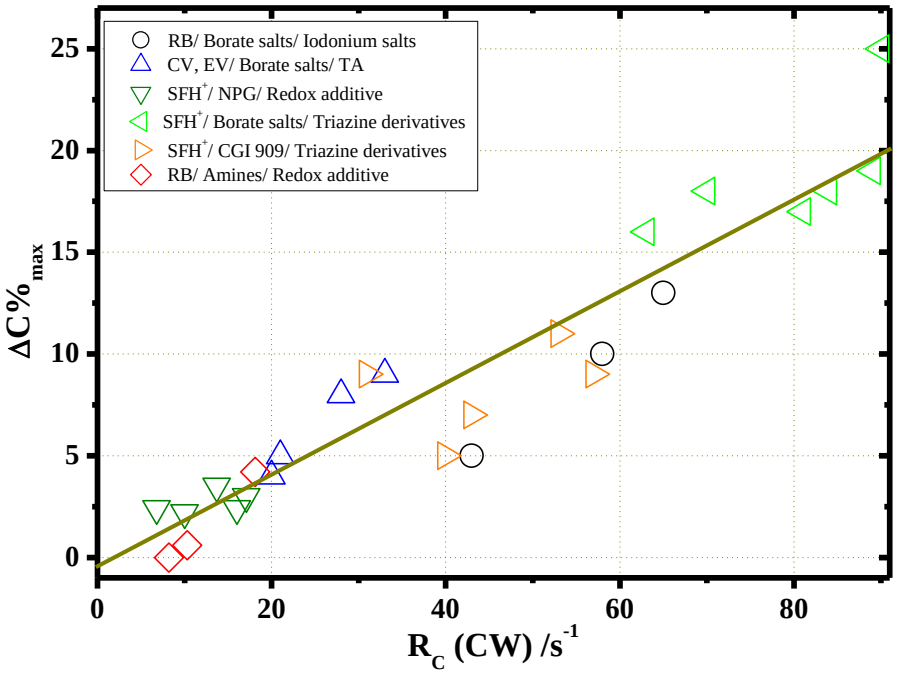

Figure 5. 18. $\Delta C\%_{max}$ values in PLP mode vs. $R_{C\ max}$ (CW). Linear correlation was found. Each group of PIS is represented with a different symbol.

5. 6. Conclusion.

The results shown in this chapter provide a panorama of PLP, presenting a big amount of results that contribute to the understanding of PLP. A wide scanning of different PIS was made in PLP and the parameters that influence their efficiency were analyzed.

Two efficient PIS for PLP were found in which no pulse of inhibition was observed: SFH^+/ P3B/ I 250 and SFH^+/ BP3B/ Rh 2074.

Differences between CW and PLP modes were put in evidence and a possible explanation for them was given. Also, a correlation between the efficiency of the different PIS in both modes was also found.

5. 7. References.

[1] M. Buback, A. Kuelpmann, " A Suitable Photoinitiator for Pulsed Laser-Induced Free-Radical Polymerization", *Macromol. Chem. Phys.*, **2003**, 204, p. 632-637.

[2] H. Tar Thesis, C. Ley, X. Allonas, "*Development of New Photoinitiating Systems for Free Radical Photopolymerization*", UHA **2013**.

[3] A. Ibrahim Thesis, C. Ley, X. Allonas, "*Development of Photoinitiating Systems for Free Radical Photopolymerization Usable for Laser Imaging*", UHA **2011**.

[4] A. Ibrahim, X. Allonas, C; Ley, K. Kawamura, H. Berneth, FK Bruder, T. Facke, R. Hagen, D. Honel, T. Rolle, G. Walze, MS Weiser, "High Performance Photoinitiating Systems for Holography Recording: Need for a Full Control of Primary Processes", *Chem. Eur. J.*, **2014**, 20, p. 15102–15107.

[5] D. Magde, M. W. Windsor, "Picosecond internal conversion in crystal violet", *Chemical Physics Letters*, **1974**, 24, p. 144-148.

Chapter Six.

Viscosity Effect in Polymerization.

6. 1. Introduction.

In Chapters Four and Five, PLP was presented as an alternative irradiation method to CW. The former chapter, shown mechanistic studies of polymerization reaction, especially by analyzing the effect of the energy pulse in monomer conversion. The latter was devoted to analyze the effect of using different PIS in the polymerization efficiency.

It was seen in Chapter Four that the viscosity of the formulation changes drastically with monomer conversion. This is one of the main concerns in industrial processes[1] . As the bimolecular termination is limited by diffusion and this is, in terms, viscosity-dependent, the amount of ΔC% obtained reaches a maximum between 10 and 30% of monomer conversion.

The original aim of the work that will be presented in this chapter was to obtain higher values of monomer conversion in PLP experiments. The idea was that, by diluting the formulations, the jellification process would be retarded to higher conversions, thus, allowing to achieve higher degree of final conversion. However, the exact opposite effect was surprisingly found in PLP.

The effect of viscosity in PLP efficiency was studied for a 3-C PIS, SFH^+/ CGI 909/ TS. This PIS was chosen because it was used as a reference to compare reactivity in the work performed for our industrial partners. In order to do these studies, four formulations were prepared by changing the monomer/solvent ratio as it will be further explained. Furthermore, this effect was not only studied in PLP, but also in CW and the results obtained using both irradiation modes were compared.

6. 2. Viscosity measurements.

To properly study the effect of formulation's viscosity in PLP and CW modes, the first step is to prepare formulations with different solvent/ monomer ratios. During this work, reference PIS SFH^+/ CGI 909/ TS was added to formulations containing 0, 5, 10, 15 and 20 wt% of DMSO in SR 349. It should be noted here that the increase of DMSO content in formulations slightly modifies the

monomer concentration. However, the viscosity variation is much bigger in relative terms than the variation in monomer concentration and so the effect produced by the latter can be considered negligible.

Formulations viscosities were measured at 25°C. Values obtained were plotted as a function of DMSO's wt% and are shown in figure 6.1. An exponential-like decrement in the value of viscosity, η, can be observed. As diffusion constant, k_{diff}, is inversely proportional to η, formulation containing 20% wt DMSO has the fastest diffusion process over all the studied formulations.

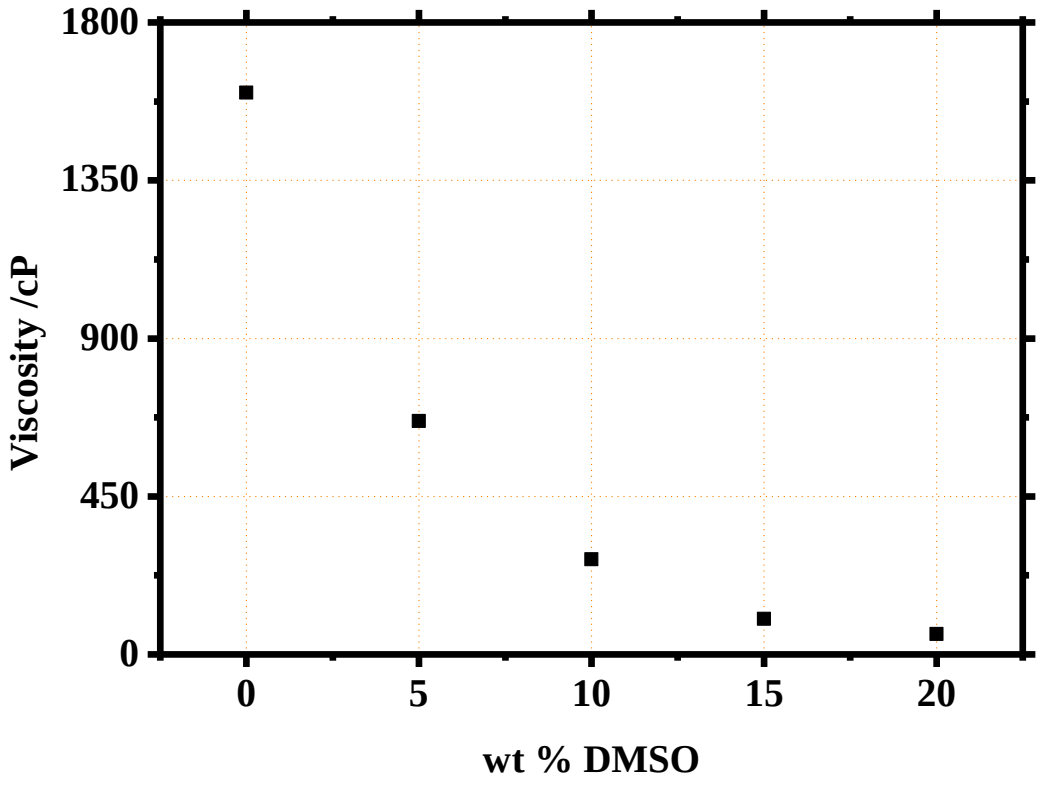

Figure 6.1. Viscosity (in cP) of the formulations as a function of DMSO's wt%.

6. 3. Viscosity effect in PLP mode.

PLP experiments were performed for all the five formulations prepared. Formulation containing 0 wt% in DMSO, didn't show any polymerization, probably due to solubility issues[2] . For this reason, this formulation will not further be mentioned on in this chapter.

Different values of pulse energy were used, from 2 to 14 mJ, in order to observe the effect of laser energy on system response for every viscosity value. Termination regime was studied by using classical CW model presented in Chapter Four, with all the precautions already explained about the conclusions that may be taken from it. Furthermore, the variation of maximum rate conversion per pulse ($R_{C\ max}$) and maximum conversion per pulse ($\Delta C\%_{\ max}$) with pulse energy and viscosity (η) were critically analyzed.

6. 3. 1. Conversion curves.

Before heading to a more detailed analysis, conversion curves are presented in this section.

Experimental results displayed on figure 6.2 show that, whatever the viscosity, no polymerization was found in any case when using 2 mJ pulses of irradiation. This is a similar case than the observed to 1mJ experiences performed with TPO in Chapter Four. It is clear that overall efficiency (i.e. maximum per pulse rate and conversion) increases with pulse energy, as expected. On the other side, the polymerization efficiency decreases when the viscosity decreases (i.e. DMSO %wt increase): both conversion rate and per pulse conversion are lower for less viscous formulations.

This reactivity order is the opposite of the one desired at first, but it can be explained as follows: as the initial formulation viscosity increases, propagation steps become faster, while inhibition and bimolecular termination, which are diffusion-controlled, are much slower. It has been discussed in Chapter Four that the values of $\Delta C\%$ obtained are basically the result of the ratio between k_p and k_t, as these processes are completely separated from initiation. The combination of these effects, then, results in smaller values of $\Delta C\%$ for less viscous samples.

However, the effect of viscosity may also have a component related to the change in the photophysical properties of the PIS used, as it was already mentioned in this thesis that sometimes, the photophysical behavior of the components of a PIS are strongly dependent on the viscosity of the media[3], but these effects will be considered negligible given the nature of the studied PIS.

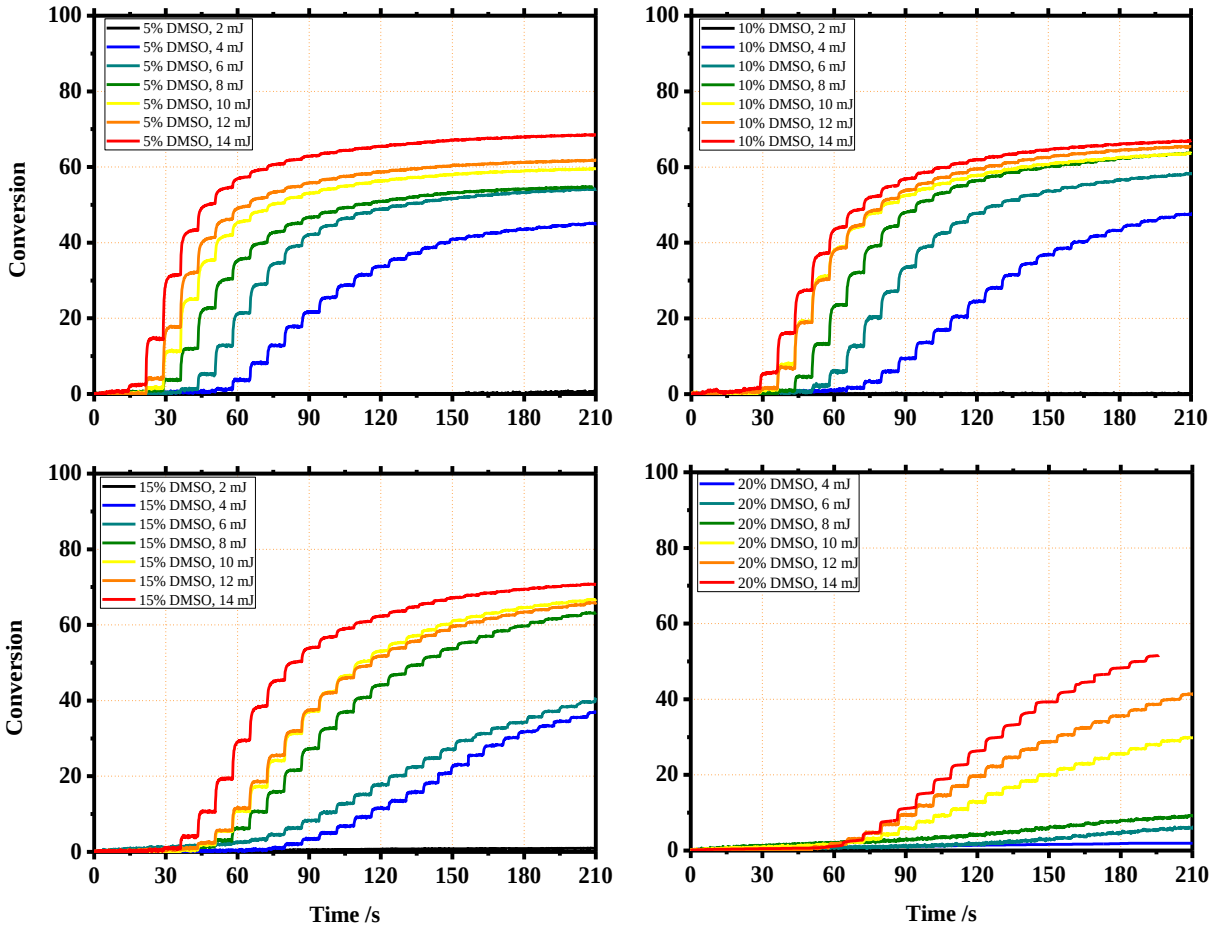

Figure 6. 2. Conversion curves for formulations containing 5, 10, 15 and 20 DMSO's wt%.

The comparison in efficiency of the four samples can easily be seen in the ΔC% vs pulse number curves (figure 6.3). $\Delta C\%_{max}$ value is smaller and delayed to longer irradiation pulse numbers when decreasing pulse energy or viscosity. This viscosity-dependent efficiency indicates that diffusion-controlled bimolecular-termination is still more important over monomolecular termination: the greater the viscosity the slower the diffusion would be and, in consequence, the smaller the value of k_t, resulting, in aftermaths, in a greater monomer conversion.

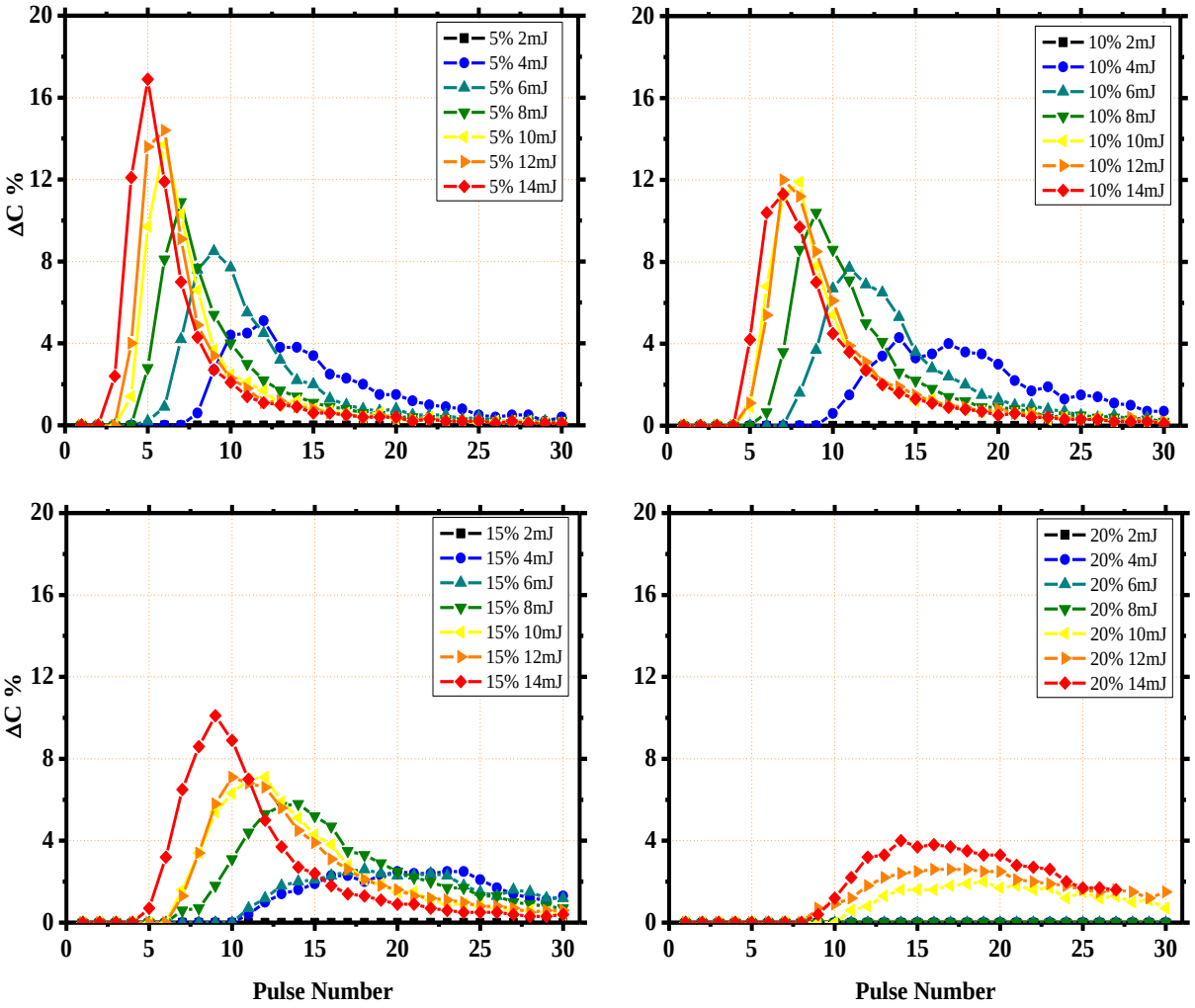

Figure 6. 3. Per pulse conversion, ΔC %, as a function of the pulse number.

6. 3. 2. Intensity effect and termination mechanism studies.

$\Delta C\%_{max}$ and $R_{C\ max}$ were plotted against pulse energy for the four formulations studied, in order to obtain a response curve for each one. Plots are shown in figures 6.4 and 6.5 respectively. As already found for TPO in Chapter Four, linear correlations were found for the four formulations in both cases. The slope value of the linear regressions made for each curve increases with viscosity confirming that reactivity increases with it, as observed on conversion curves.

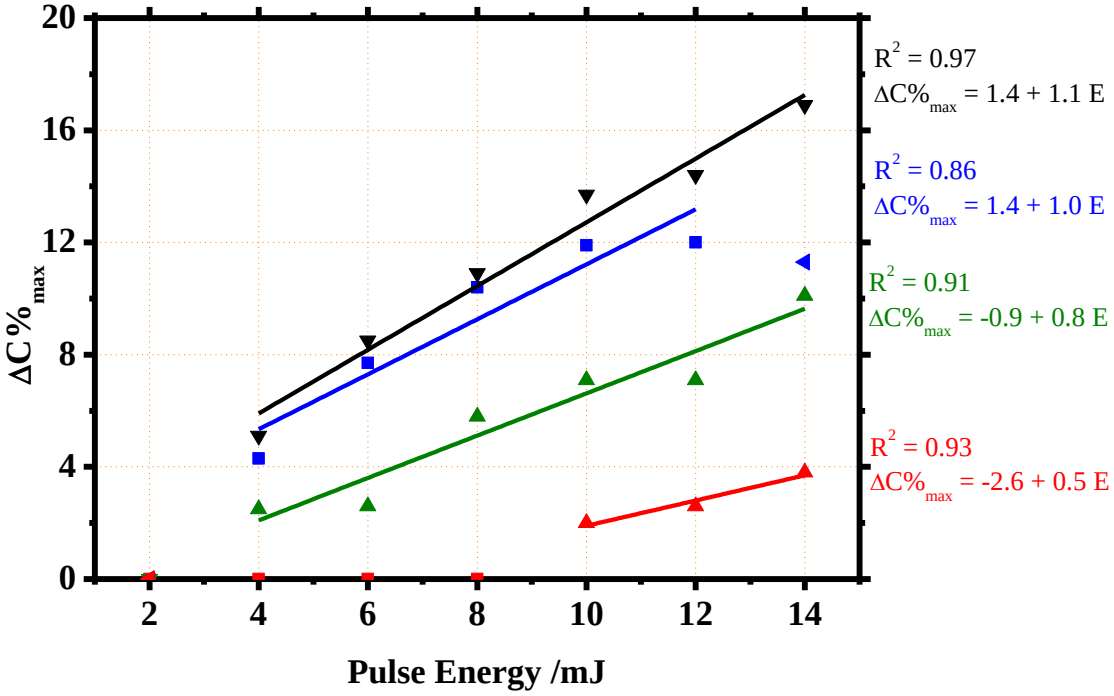

Figure 6. 4. ΔC% $_{max}$ response curve for all the formulations studied. Linear correlation was found.

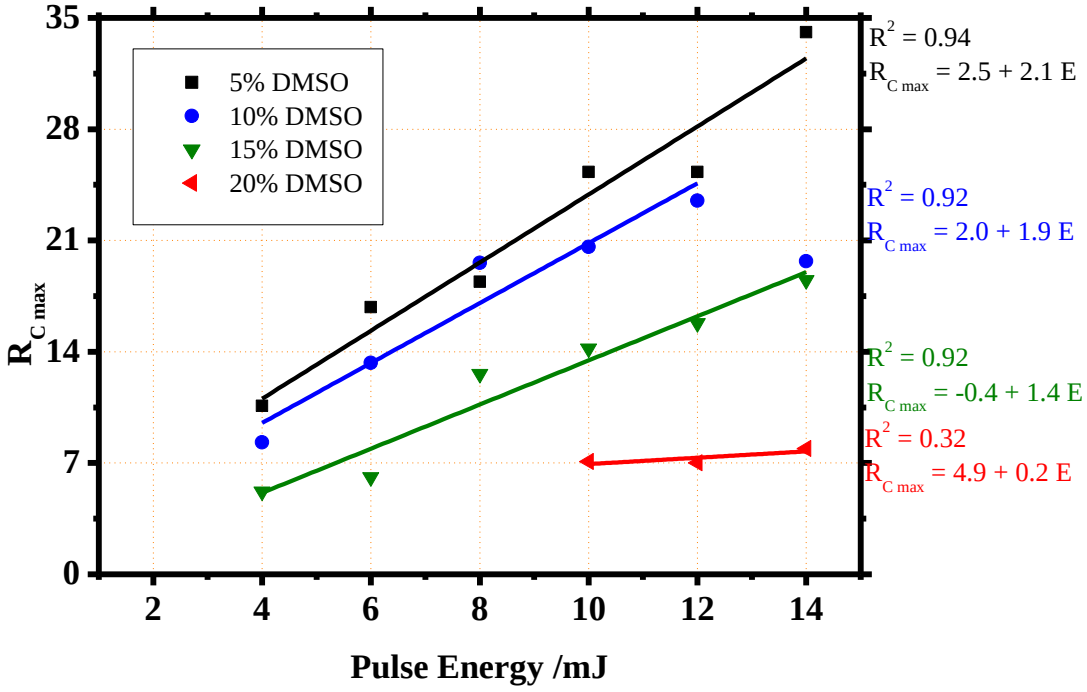

Figure 6. 5. $R_{C\ max}$ response curve for all the formulations studied. Linear correlation was found.

The model formerly developed for CW mode explained in section 5.7, was also applied to these systems. Thus, ln ($R_{C\ max}$) was plotted as a function of ln (Pulse energy) for all of the four formulations (figure 6.6). Similar slope values were found for all the systems. The fact that the slope value is close to the unity in 5, 10 and 15 wt% DMSO would suggest that termination process is predominately monomolecular, in contrast with the diffusional-controlled bimolecular termination behavior explained in 6.3.1. However, since the model applied is only valid under certain conditions, it is possible that not all of them are met in PLP, as already explained in Chapter Four. The smaller slope value for 20% DMSO formulation can be attributed to lack of data to obtain a reliable linear regression.

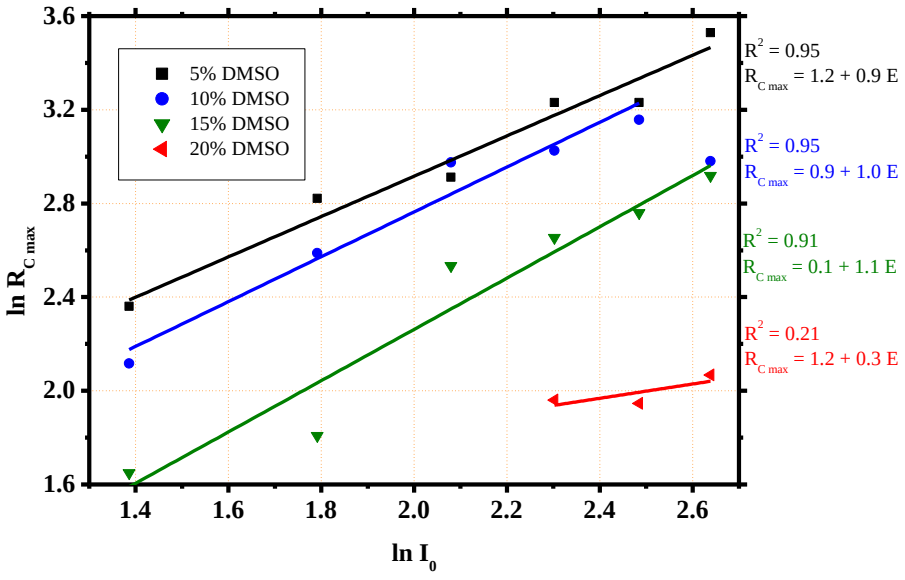

Figure 6. 6. ln $R_{C\ max}$ vs ln I_0 plot. The slope values indicate monomolecular termination.

6. 3. 3. Inhibition dose.

The presence of P_{in}, is noticed in all of the samples. Their amount decreases with pulse energy, as can be seen in figure 6. 7. For 20 % DMSO formulation, low values of ΔC_i % make it difficult to find the number of P_{in}, especially for low pulse energy measurements. At 2 mJ per pulse, as no polymerization was observed, the number of pulse inhibition was fixed to 30 for all the formulations,

which is the total number of pulses in the experiment. For the same reason, in 20 wt% DMSO formulations, as no polymerization was detected during experiment, P_{in} was fixed at 30 for 2, 4, 6 and 8 mJ pulse energy.

The amount of energy required for polymerization to start (i.e. to be detectable) in any sample, can be calculated as the pulse energy times the number of inhibition pulses P_{in}, and it is called "inhibition dose", as presented in Chapter Four. In figure 6.8, the inhibition dose for each formulation is plotted as a function of the pulse energy. Inhibition dose remains constant for every formulation, but it is smaller in less viscous formulations. This decrease can be explained by the fact that inhibition and bimolecular termination reactions are diffusion-controlled and, thus, the more viscous a formulation is, the slower the inhibition reaction becomes, favoring the propagation steps to have place instead and increasing the polymerization efficiency.

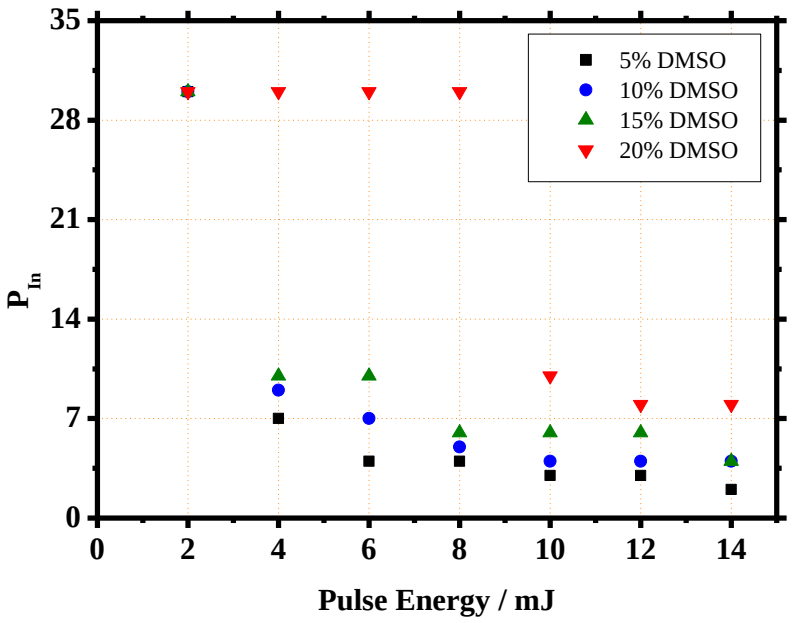

Figure 6. 7. P_{in} as a function of the energy pulse for all the formulations studied.

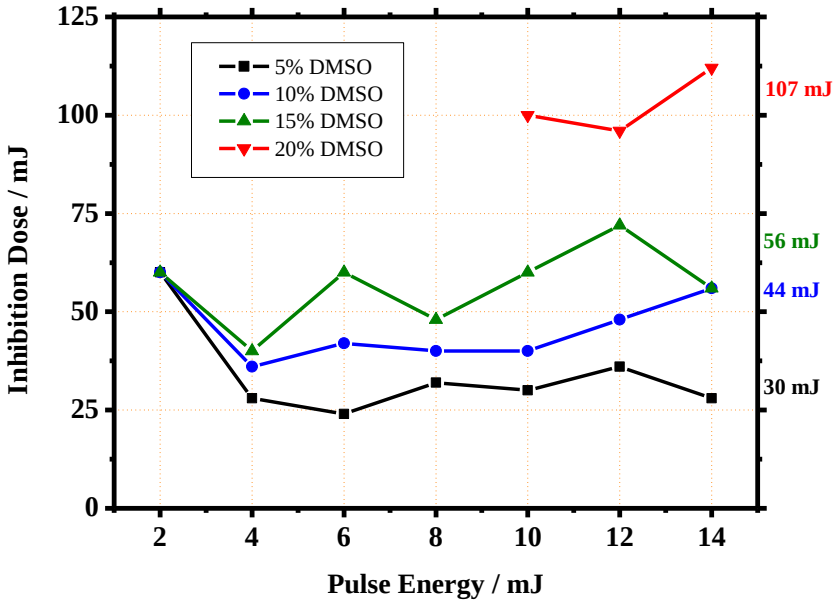

Figure 6. 8. Inhibition dose as a function of the energy pulse for all the formulations studied. The viscosity dependence indicates diffusion-controlled inhibition processes.

6. 3. 4. Correlation between ΔC_i % and $R_{C\,i}$.

Per pulse conversion (ΔC_i %) values were plotted against their respective per pulse rates $R_{C\,i}$ for every pulse in all the experiments (figure 6. 9). A linear correlation was found, independently of the formulation, pulse energy or initial monomer conversion, showing that, for PLP, any analysis of ΔC_i % or $R_{C\,i}$ is equivalent. This is not a minor fact, as the values for ΔC_i % are much simpler to calculate that those of $R_{C\,i}$. The absolute values of the former are also more reliable, as their determination is less affected by the signal to noise relation.

More interestingly, the slope value of the linear regression obtained for this data is 0.52 s, which is almost the same value obtained for TPO considering the experimental errors.

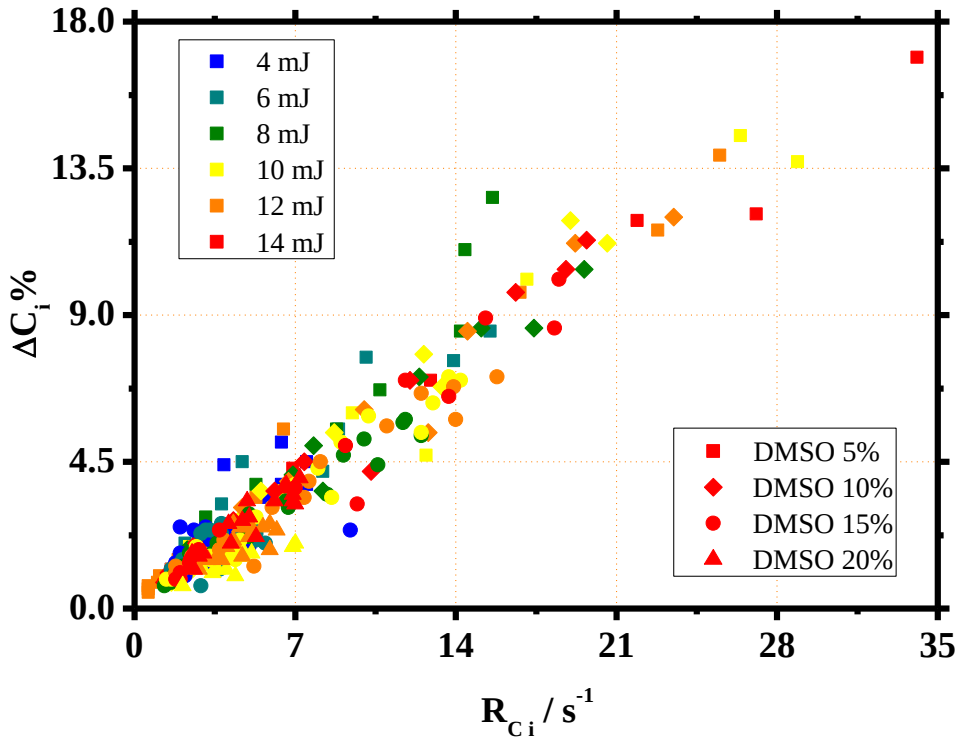

Figure 6. 9. Per pulse conversion ΔC_i % vs per pulse rates $R_{C\,i}$. A linear correlation was found independently of the formulation, pulse energy or initial monomer conversion.

6. 3. 5. Analysis of the viscosity effect.

Formulations with higher viscosity showed to be more efficient than less viscous ones. It was already said in Chapter Five that diffusional rate constants are proportional to η^{-1}. In order to find a correlation between viscosity and efficiency, $R_{C\,max}$ was plotted against η^{-1}. Figure 6.10 shows linear correlation between these two parameters for the pulse energy range studied.

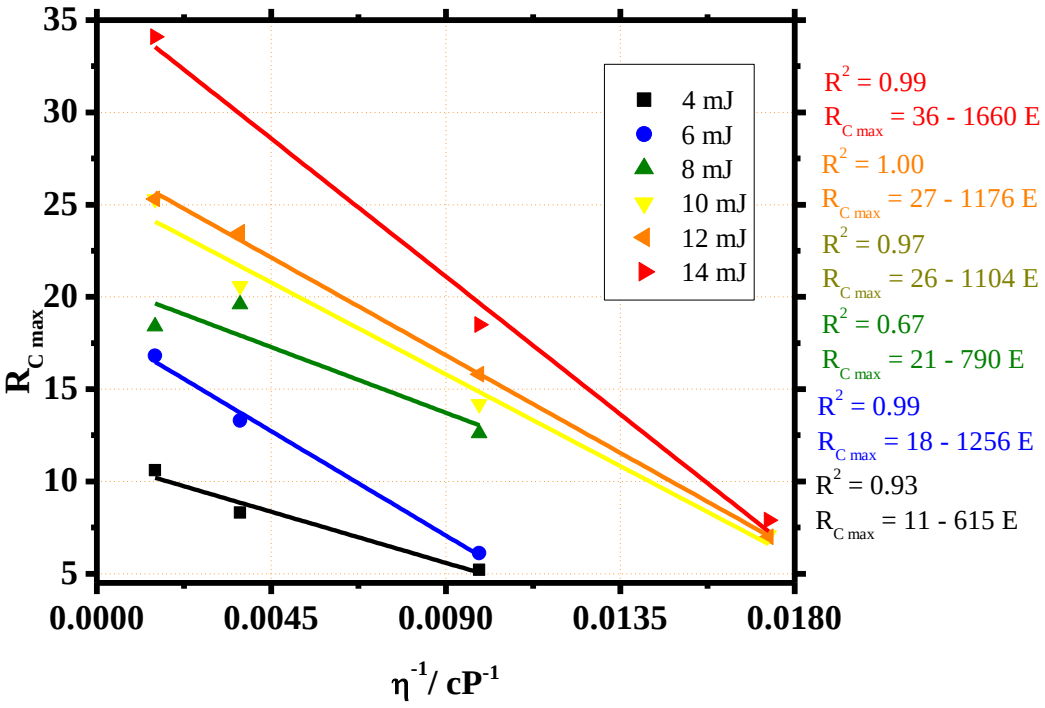

Figure 6. 10. $R_{C\ max}$ vs η^{-1}. Linear correlation was found for all the formulations.

Analyzing this result in more detail, the formula of the linear equation for the relation found can be written as in equation 6.1, where $\frac{\partial R_C}{\partial \eta^{-1}}(E)$ is the variation of R_C with viscosity, as a function of the irradiation energy and $R_{C\,(\eta \to \eta_0)}$ is the hypothetical value of R_C that would be found in a formulation whose viscosity would be equal to that of the pure monomer. The minus sign is added in order to define $\frac{\partial R_C}{\partial \eta^{-1}}(E)$ as a positive number.

$$R_C = -\frac{\partial R_C}{\partial \eta^{-1}}(E)\frac{1}{\eta} + R_{C\,(\eta \to \eta_0)} \quad (6.1)$$

It was previously shown in section 6.3.2 that $R_{C\ max}$ presents a linear correlation with pulse energy. The intercept values of the linear regressions shown in figure 6.10 are the hypothetical conversion rates that would be found for a formulation whose viscosity approachs the monomer viscosity. This is the physical interpretation of $R_{C\,(\eta \to \eta_0)}$. Then, if the values of $R_{C\,(\eta \to \eta_0)}$ of each

formulation are plotted against viscosity, a linear response should be obtained, as for the other values of R_C. Figure 6.11(right) shows that this is indeed the case.

The analysis of the slope's value dependence with pulse energy (Figure 6.11 left) is not so evident and requires additional research.

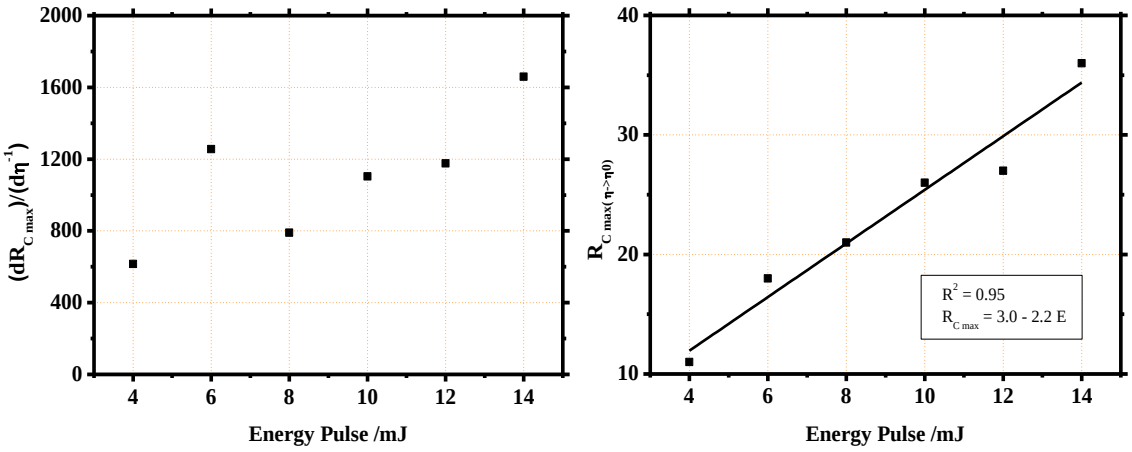

Figure 6. 11. Variation of the regression parameters from equation 6.1 as a function of pulse energy.

An analogue analysis can be made by replacing $R_{C\ max}$ by $\Delta C\%_{max}$. Figure 6.12 shows the linear regression for $\Delta C\%_{max}$ vs η^{-1} curves. This time, the regression equation is given by (6.2).

$$\Delta C\%_{max} = -\frac{\partial \Delta C\%_{max}}{\partial \eta^{-1}}(E)\frac{1}{h} + \Delta C\%_{max\ (\eta \to \eta_0)} \quad (6.2)$$

As it was shown in a previous section, R_{Ci} and ΔC_i % are linearly correlated. Thus, the same behavior is expected in this case. Working with ΔC_i % values are easier to calculate than R_{Ci}, and the values can be obtained with more precision. Figure 6.13 shows the analysis of the slope and intersection values obtained from the regressions. As expected, the same behavior is observed for R_{Cmax} and $\Delta C\%_{max}$.

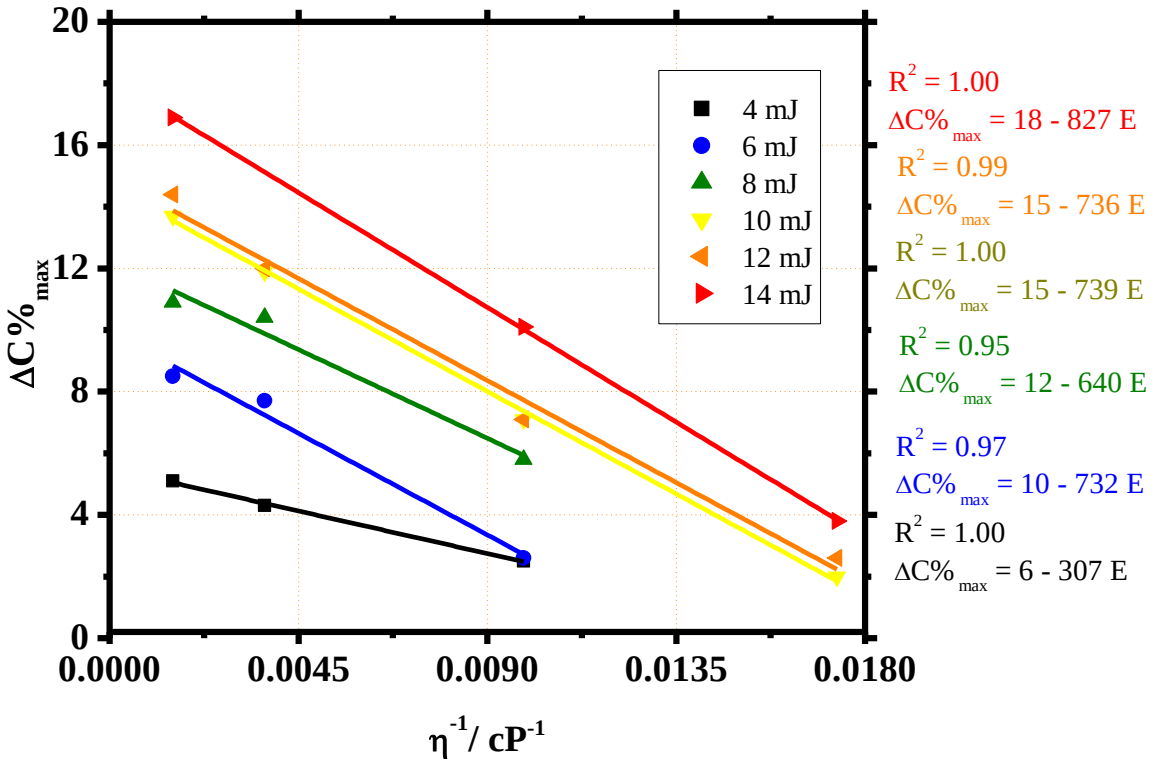

Figure 6. 12. $R_{C\,max}$ vs η^{-1}. Linear correlation was found for all the formulations.

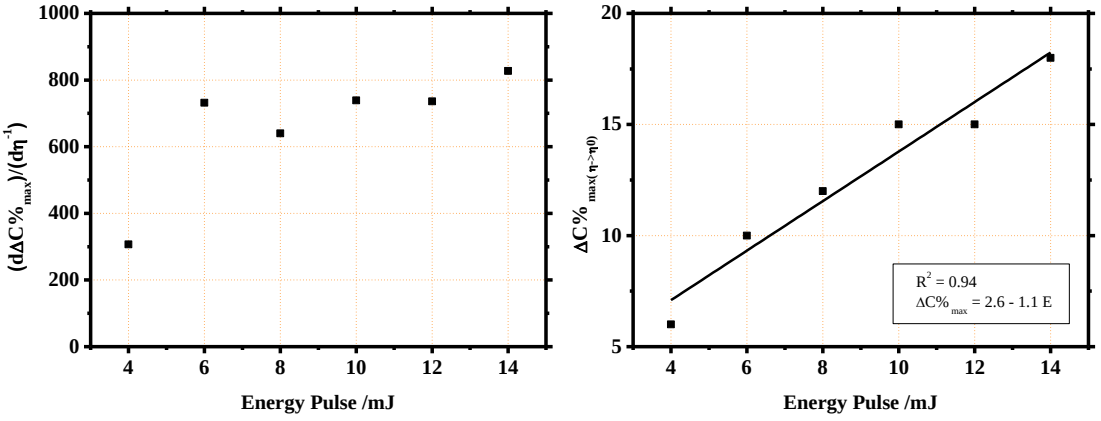

Figure 6. 13. Variation of the regression parameters from equation (6.2) as a function of pulse energy.

6. 3. 6. Effect of monomer conversion on ΔC %.

The fast increment in ΔC % after the first inhibition pulses can be attributed to high increment of the viscosity of the formulation due to the polymer formation, as it was already explained above. At higher conversions, however, the monomer concentration is smaller, and polymerization rate decreases, resulting in smaller values of ΔC %. The values of k_p also start to decrease from certain conversion values as shown in Chapter Four, which also causes the values of ΔC % to be smaller. Among these effects, there must be an intermediate conversion value where polymerization rate reaches a maximum value. To determine this value, ΔC % was plotted vs the total monomer conversion before a new laser pulse arrives to the sample. Results are shown in figure 6.14.

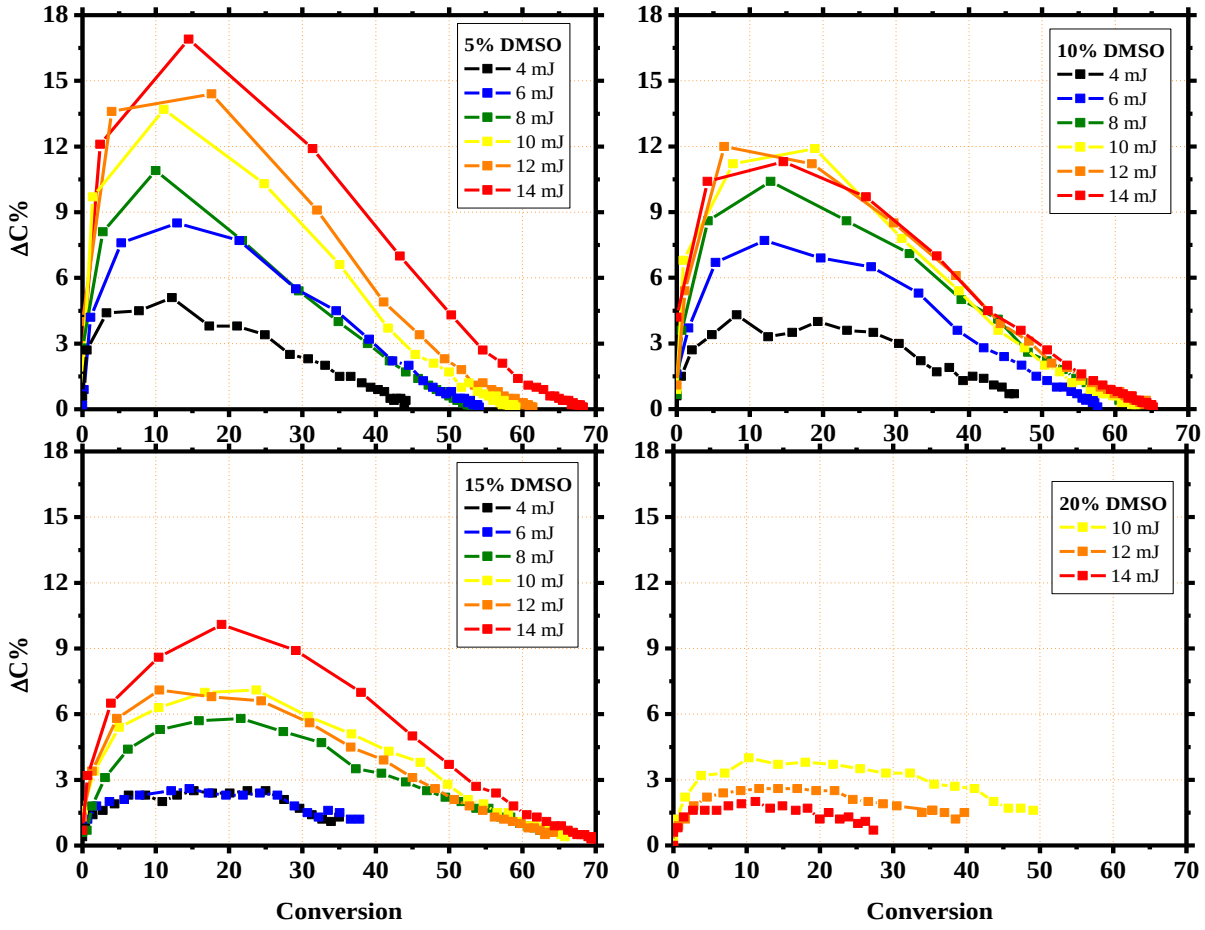

Figure 6. 14. ΔC_i % vs conversion plots for all the studied formulations. Maximum position is difficult to determine.

The determination of the exact position of this maximum in the plots may not be an easy task, since data is discontinued and no mathematical function was developed yet in order to be able to predict it at the moment. As a first approximation, it can be estimated to be between 10 and 20 % of monomer conversion. This fact was also seen in Chapter Five for TPO, where it was determined that this point is reached at the conversion value where k_p/k_t reachs its maximum. In these systems, as the initial viscosity varies from one system to another, this point may also vary from formulation to formulation

6. 4. Viscosity effect in CW mode.

Analogue studies to those presented in previous section were performed in CW mode. Several differences were found, which will be presented all along this section.

6. 4. 1. Conversion curves.

At first sight, by looking at the conversion (figure 6.15) and conversion rate (figure 6.16) curves, 10% DMSO seems to be the more efficient above the four formulations, with higher conversion rates. However, the highest final monomer conversion was slightly reached for 20% DMSO formulation, as it was expected at first for PLP. A deeper analysis may clarify these contrasting results.

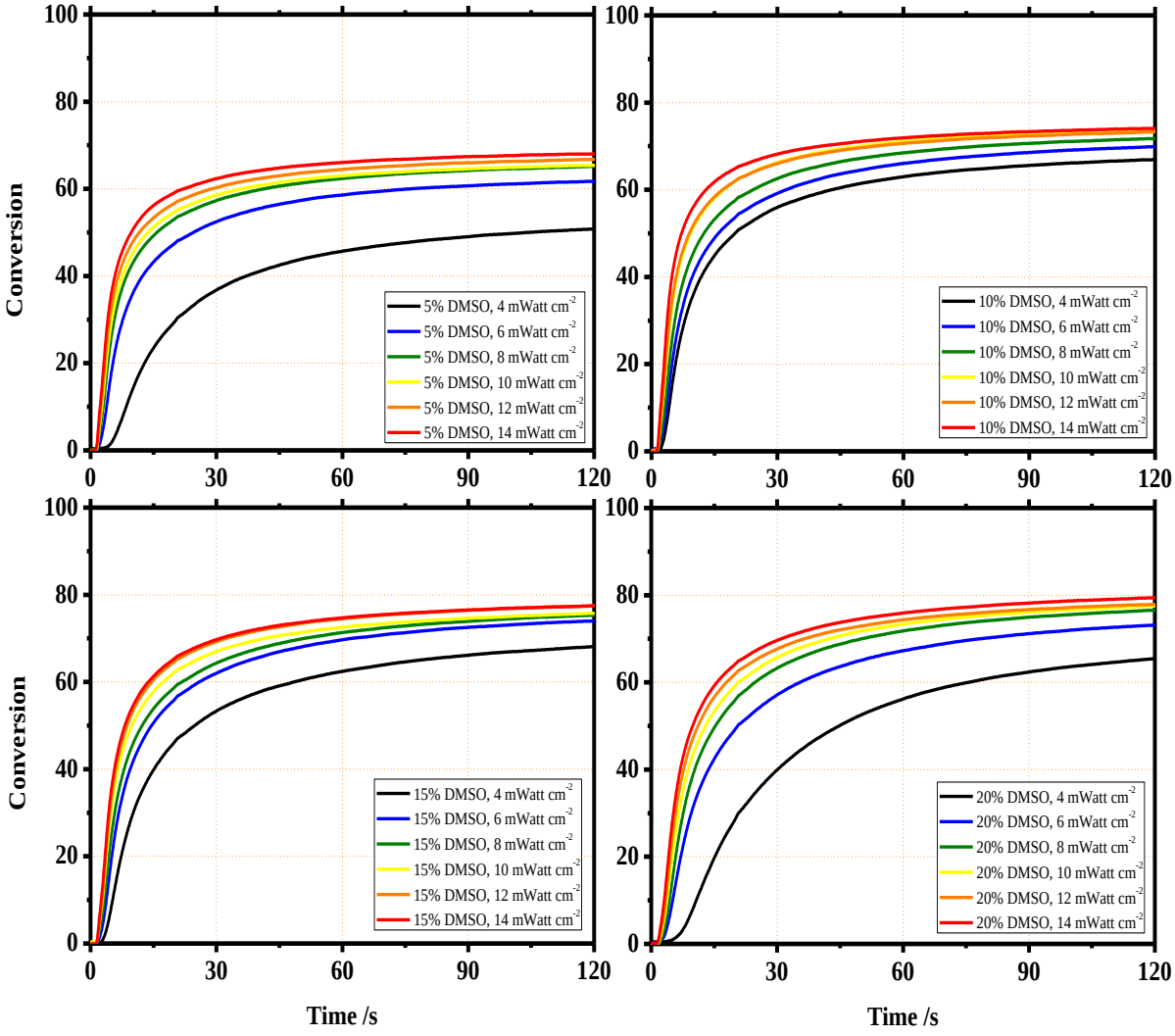

Figure 6. 15. Conversion vs time curves in CW mode for all the studied formulations.

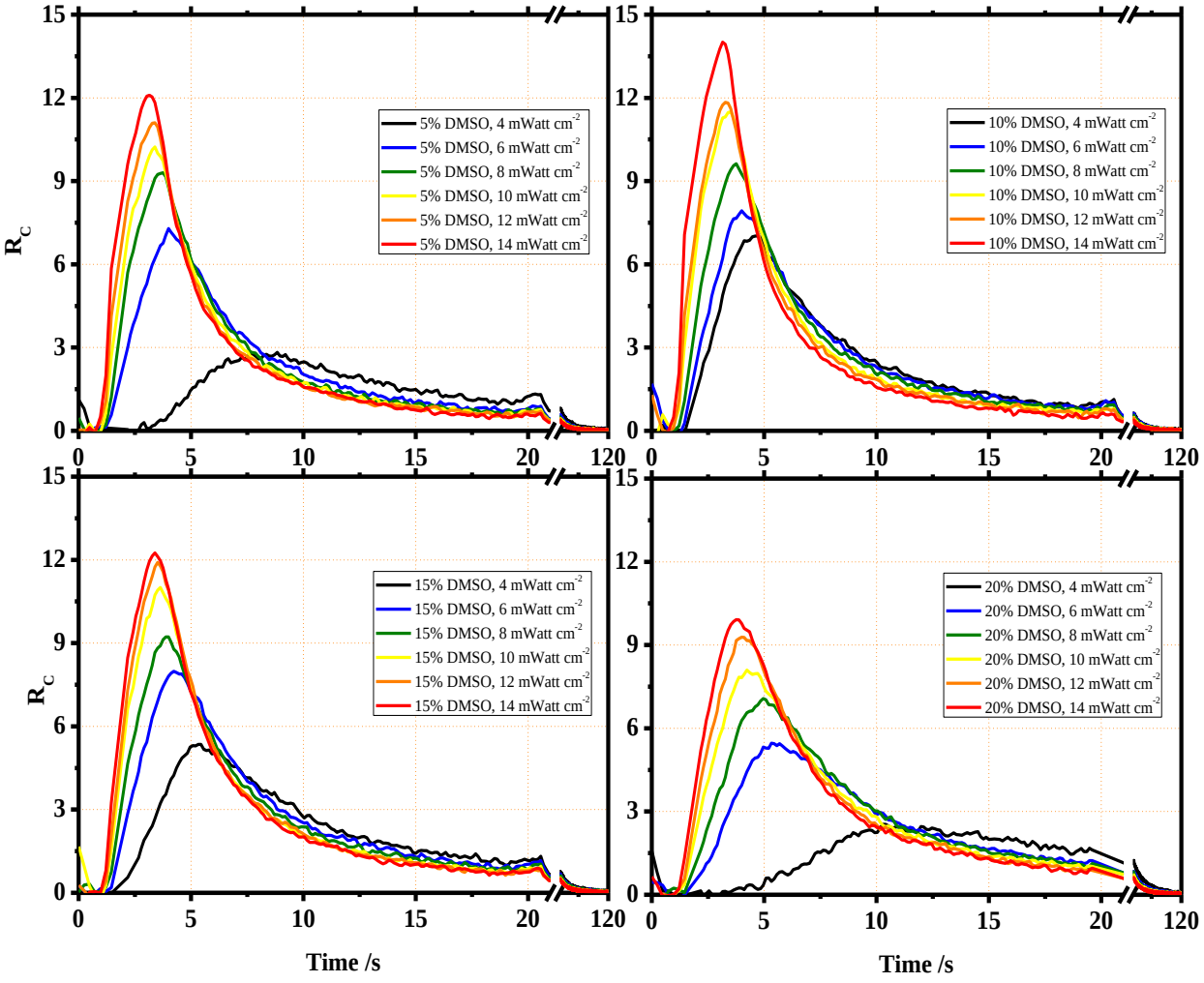

Figure 6. 16. Conversion rate vs time curves in CW mode for all the studied formulations.

6. 4. 2. Response curves and termination mechanism studies.

To begin with the analysis of the results obtained, the final monomer conversion was plotted versus the irradiation energy for each formulation. The results can be seen in figure 6.17. It can be concluded from here that the final monomer conversion increases with DMSO wt%, i.e. decreases with viscosity. This behavior was initially expected for PLP as well: as the initial viscosity of the formulation is much smaller, the jellification point of the system will be retarded to higher values of monomer conversion, allowing to the obtainment of higher values of final conversion.

As it was previously made for PLP, the following step was to analyze the response curves for maximum conversion rate, $R_{C\ max}$. Plot is shown in figure 6.18. Here, formulation containing 20%

DMSO has the lowest values of conversion rate, whereas the highest ones are for 10% DMSO. This indicates the presence of two different effects that have opposed consequences on the efficiency of polymerization.

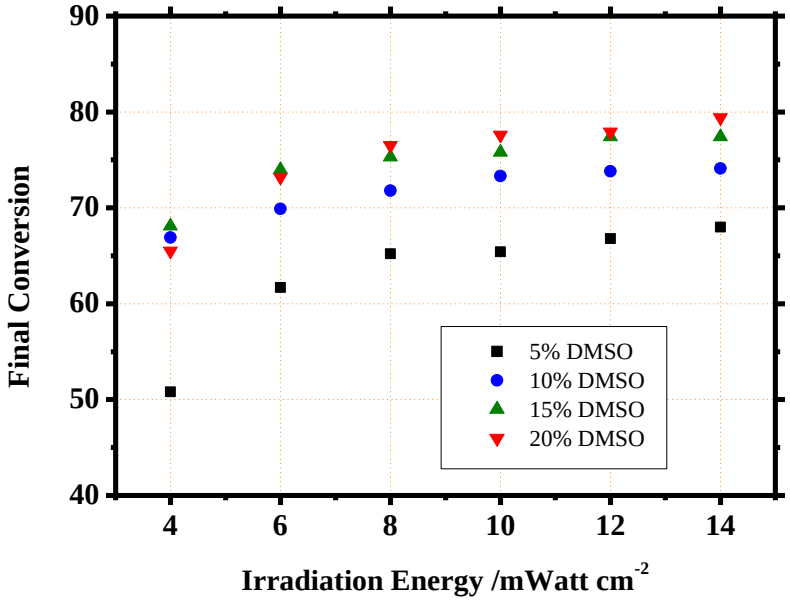

Figure 6. 17. Response curve for final conversion in CW. Higher monomer conversion are found in lower viscosity formulations.

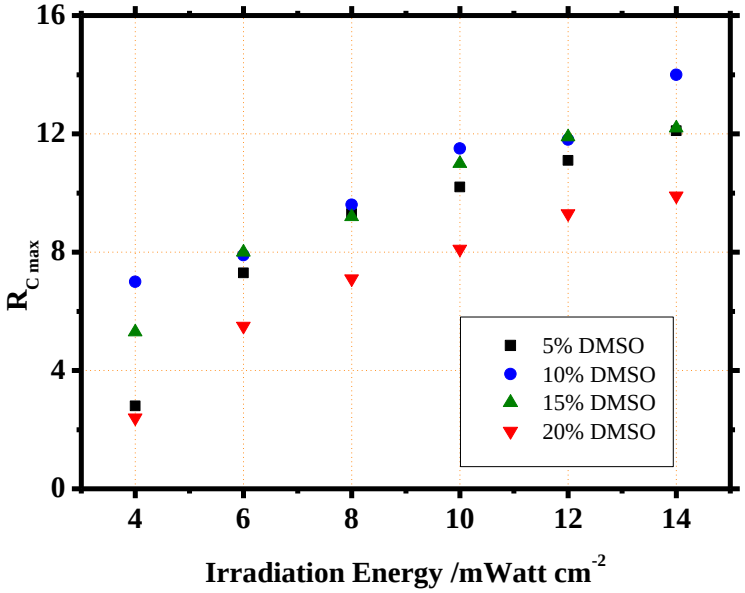

Figure 6. 18. Response curve for conversion rate in CW. Higher values were registered for intermediate viscosity formulations.

The first conclusion that can be remarked from plots 6.17 and 6.18 is that, contrarily to the effect noticed in PLP, R_C and final conversion are not correlated in CW mode. Furthermore, the order in this case seems to be rather the opposite. A possible explanation to the effect observed will be proposed further in this chapter.

The following step is to study the termination mechanism, by applying the model presented in section 4.7. 2 mJ pulse experiments were not considered to calculate the linear regressions. The slope values obtained (figure 6.19) lay around 0.5, which indicates bimolecular termination. The same results had been found in studies previously presented in Dr. Ibrahim's thesis[4] . It is also important to remark that the approximations of the model are all valid in CW polymerization. This result is yet another strong indication that the approximations of this method are not valid in PLP since, as irradiation only affects initiation, termination mechanism should be the same independently of the irradiation mode used.

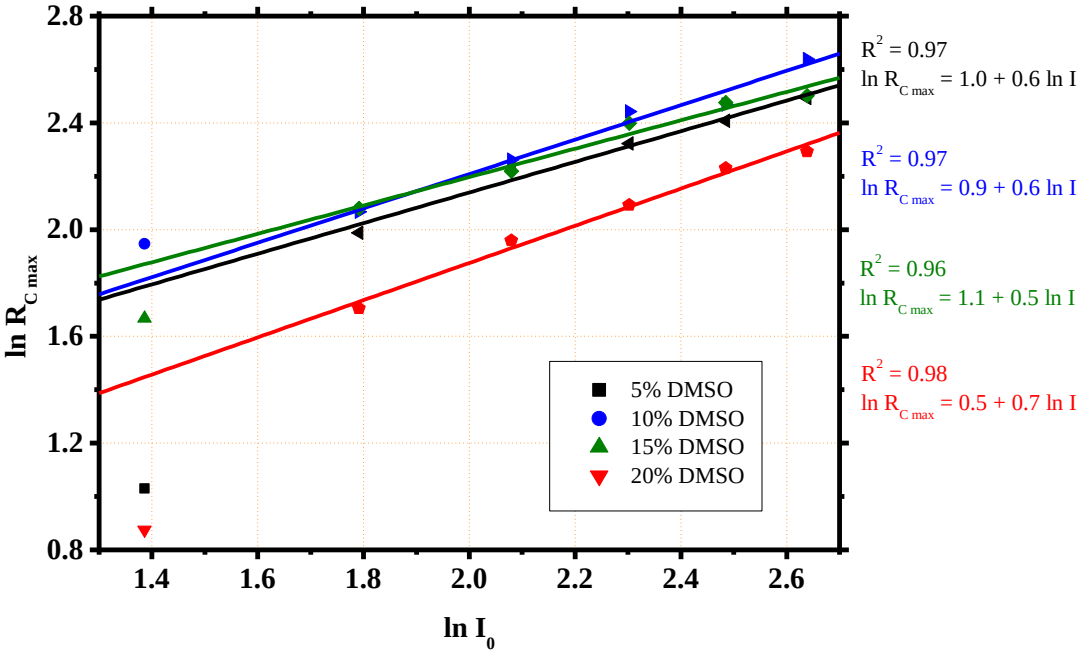

Figure 6. 19. ln $R_{C\,max}$ vs ln I_0 plot. The slope values indicate bimolecular termination.

6. 4. 3. Analysis of the viscosity effect.

In figure 6.20, the maximum conversion rate is plotted as a function of η^{-1} for different irradiation energies. The maximum value is obtained in all cases for the formulation containing 10% DMSO. For less viscous formulations (10, 15 and 20 wt% DMSO), the conversion rate increases with viscosity, as expected. For 5% DMSO, however, $R_{C\ max}$ is smaller than for 10 wt% DMSO formulation.

This is probably due to an earlier jellification of the media, since the initial viscosity of the 5% DMSO formulation is relatively higher than the others. This fact may cause auto acceleration to stop earlier than for the rest of the samples, resulting on smaller values of $R_{C\ max}$.

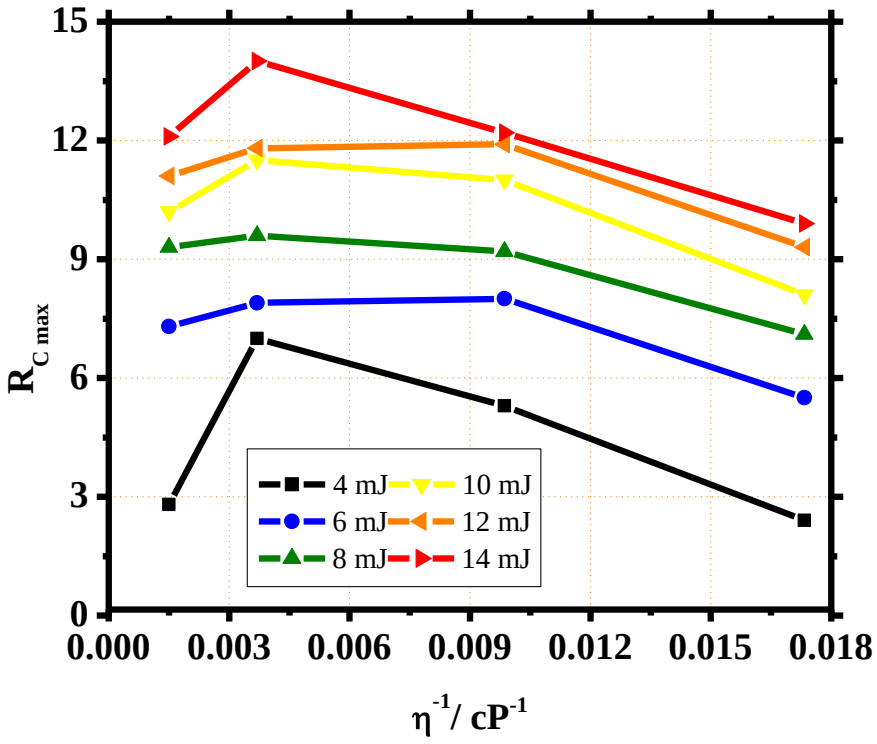

Figure 6. 20. $R_{C\ max}$ vs η^{-1}. The maximum can be found for 10% DMSO formulation, indicating the presence of two contrasting effects.

6. 4. 4. $R_{C\ max}$ as a function of conversion.

To reinforce the conclusion made in the previous section, the influence of conversion in the value of $R_{C\ max}$ was studied. Figure 6.21 shows that the bigger $R_{C\ max}$ values are found at bigger conversion values. The conversion value where $R_{C\ max}$ is found increases with pulse energy as well. It is interesting to remark that the variations noticed on the curves are much more pronounced for CW than for PLP.

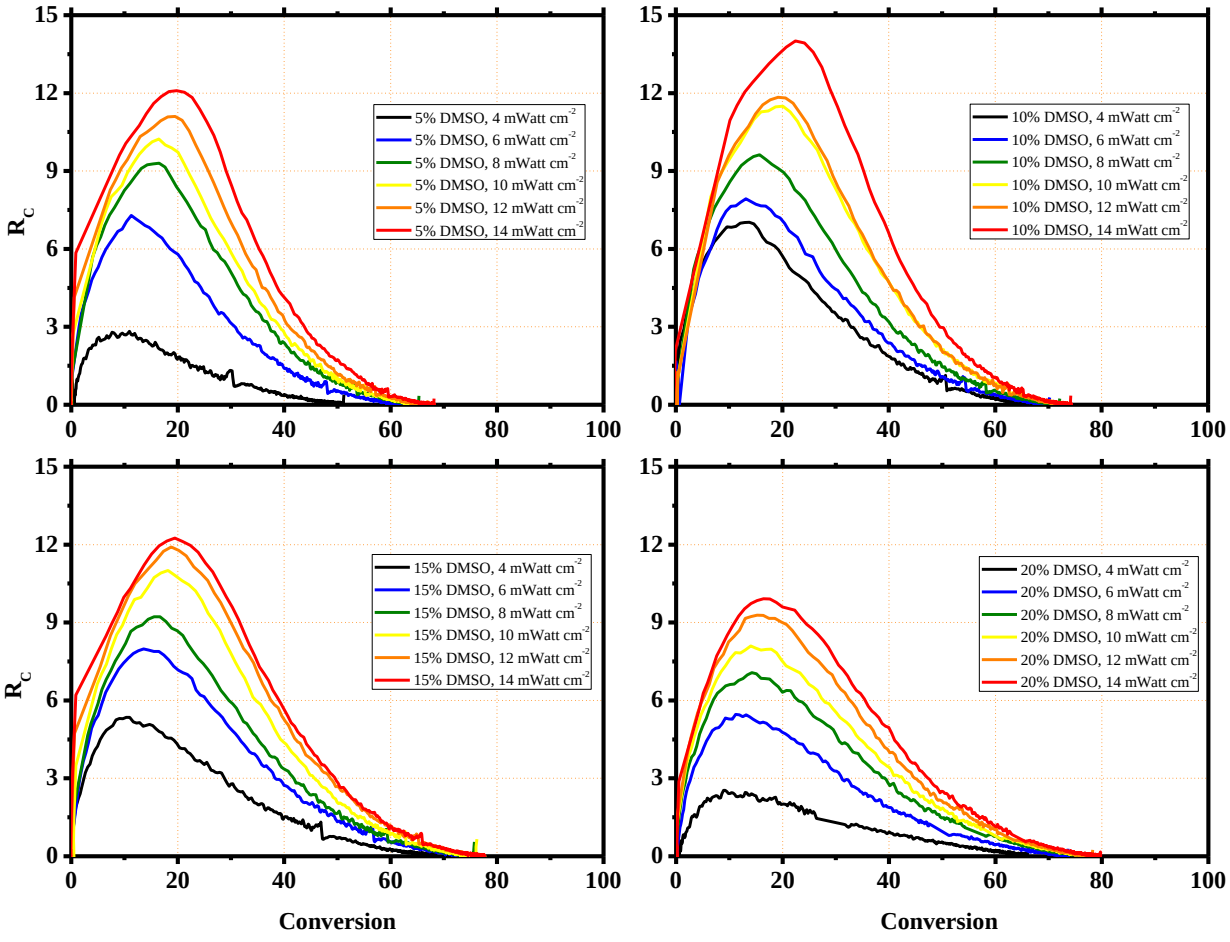

Figure 6. 21. R_C as a function of monomer conversion. Greatest rate conversions are found at higher monomer conversion values.

With these results in mind, two complementary analyses were made in order to study the viscosity's effect. First, the monomer conversion where $R_{C\ max}$ was reached was plotted as a function of the irradiation energy (figure 6.22). These conversion values increase linearly with irradiation energy for all the four formulations. Another interesting result was found when plotting the conversion where $R_{C\ max}$ was reached as a function of the $R_{C\ max}$ value (figure 6.23). The results show a linear correlation between these two parameters.

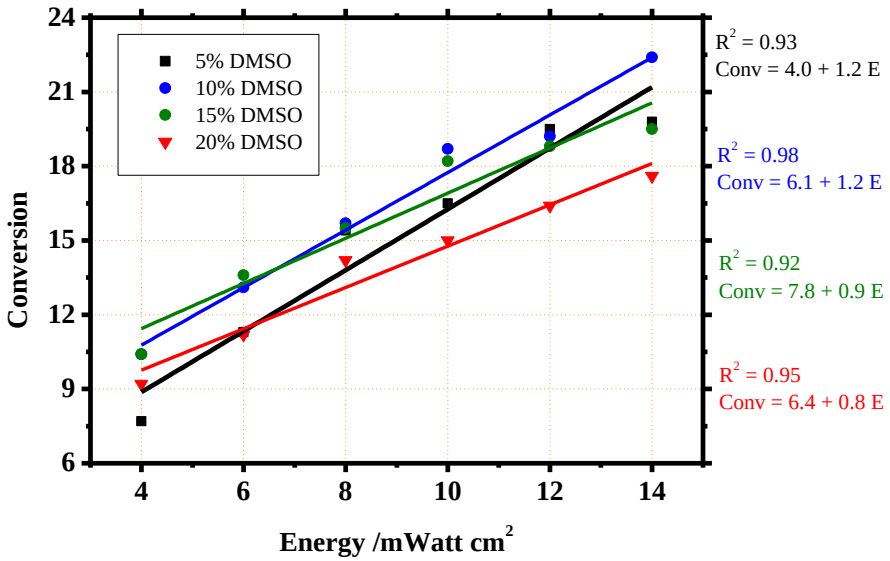

Figure 6. 22. Conversion as a function of the energy irradiation. Linear correlation was found.

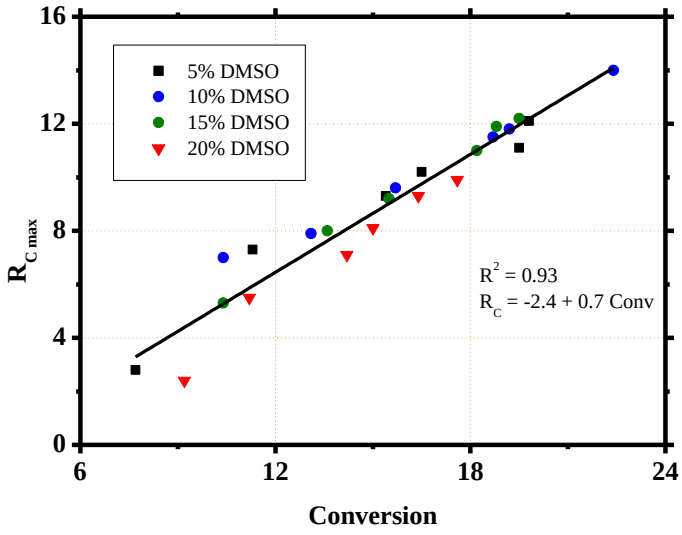

Figure 6. 23. $R_{C\ max}$ as a function of monomer conversion where it's reached. Linear correlation was found, showing that $R_{C\ max}$ values are limited in systems jellifying at smaller conversion values.

Increasing the irradiation energy, increases the values of $R_{c\ max}$ reached. Higher values of R_{Cmax} will, in turns, appear at higher values of monomer conversion. Furthermore, formulations that are too viscous show smaller values of $R_{C\ max}$. Bimolecular termination reactions are faster in less viscous media, as diffusion constant depends on viscosity. Thus, the values of $R_{C\ max}$ reached in less viscous formulations are expected to be smaller. The reason why the higher the $R_{C\ max}$ is, the higher conversion it is reached, is probably due to the rheological properties of the media.

It is interesting to remark that this effect is not as marked in PLP as it is in CW. This difference can be attributed to the fact that in PLP, the irradiation is stopped between two pulses and the system is allowed to reach equilibria before a new pulse arrives, which is not the case under CW mode.

6. 5. Conclusion.

Different viscosity effects were found in PLP and in CW.

Regarding conversion, final conversion was found to be higher for samples with lower viscosities in CW mode. However, for PLP experiments the exact opposite trend was found. This behavior was attributed to the initial values of k_p and k_t and to the big influence these parameters have in $\Delta C\%$ values, since in PLP mode, initiation process is completely separated from propagation and termination.

In CW, in contrast, the influence of k_p and k_t is not the only effect to take into account, since initiation process is present all along the experiments. In this case, the higher final conversion values obtained for less viscous samples can be attributed to a delayed jellification of the media in terms of conversion, which allows polymerization to proceed longer than in more viscous media.

Sections 6.3 and 6.4 were devoted to discuss the studies made under PLP and CW irradiation modes conditions, respectively. Several differences were found between both irradiation methods. The aim of this section is to remark those differences.

Maybe the most relevant difference is the influence of R_C in monomer conversion. In PLP, $\Delta C_i\%$ is directly proportional to $R_{C\ i}$, whereas in CW, final conversion is not so strictly related to R_{Cmax}. The reason for this lies in the irradiation time. In PLP, all the initiating radicals are generated in

a short time (10 ns), and polymerization's efficiency depends strongly in the amount of primary radicals generated right after the pulse arrives to the sample. In CW, in contrast, as the sample is irradiated all along the experiment, initiating and primary radicals can be generated at any time, and thus, polymerization is no limited by the amount of radicals generated instantaneously at one time.

The conversion where the maximum efficiency is reached for a sample does not seem to be affected by its efficiency in PLP, contrarily to the effect observed in CW. The reason why correlation between the maximum conversion rate values and the conversion at which they are found for each experiment are strictly linear was not determined yet. This relation may be a complex mixture of effects depending on formulation viscosity, PIS efficiency, irradiation energy and inhibitors' concentration.

6. 6. References.

[1] H. U. Moritz , *Chem. Eng. Techno,* **1989**, 12, p. 71-87.

[2] Fouassier, J. P., *Photoinitiation, Photopolymerization, and Photocuring: Fundamentals and Applications.* Hanser Gardner Publications, Munich, **1995**.

[3] D. Magde, M. W. Windsor, "Picosecond internal conversion in crystal violet", *Chemical Physics Letters*, **1974**, 24, p. 144-148.

[4] A. Ibrahim Thesis, C. Ley, X. Allonas, "*Development of Photoinitiating Systems for Free Radical Photopolymerization Usable for Laser Imaging*", UHA **2011**.

Conclusions.

The photopolymerization process was investigated all along of this thesis work: from the fundamental studies made to study the photophysical properties of a photoinitiator, to the study of propagation and termination steps via PLP.

The photophysics of Astrazone Orange R was studied and a deactivation mechanism was postulated. It was demonstrated that the conformer E1 represents more than 92% of the ground state population of AOR at 20°C. An isomerization reaction takes place from the excited state, which is viscosity-dependent and governs the fluorescence lifetime. This process makes AOR a very efficient photoinitiator in highly viscous media.

The possibility of a synergistic effect in 3-C PIS was analyzed for different systems. Suitable PIS were found for photopolymerization with visible light at different wavelengths. Some of them present photocyclic behavior. Two different approaches to the study of PCIS behavior were presented: the LFP approach, where generation of radicals and dye bleaching are recorded, and the dye photolysis approach, where the recording of dye photolysis is compared with a mathematical model that allows to the calculation of photolysis and radical generation quantum yield.

In the second half of this work, Pulsed Laser Polymerization mechanism was studied. A model was developed in order to calculate the values of k_p and k_t of the process and its progression with monomer conversion. With these data and by applying Buback's model, it was possible to estimate the changes of viscosity with conversion from PLP-RT-FTIR studies. It was also shown that monomolecular termination process has to be taken into account to obtain a complete description of the process.

The efficiency of many PIS absorbing in the green region of the electromagnetic spectra in PLP was studied. Their efficiency was analyzed and compared. The most efficient PIS among all the studied turned out to be SFH^+/ P3B (or BP3B)/ Triazine derivatives (or iodonium salts).

Finally, the effect of the initial viscosity formulation was studied in CW and in PLP. In PLP, efficiency and conversion per pulse increase with initial viscosity, while in CW, the highest final conversion was found for the less viscous systems. In PLP, conversion and conversion rate are directly related, because, as initiation is separated from propagation and termination, conversion is strongly dependent in the ratio k_p/k_t, which is bigger in highly viscous media. However, in CW, as initiation process is continuously present in the sample, this effect is not so marked. The highest final conversion in this case is, then, attributed to a delayed jellification of the media in terms of conversion, since the samples are more diluted.

There are many perspectives on this work.

Photopolymerization is a technique with a huge potential to develop in the following years to come, with many applications in the development of materials to be used to improve new technologies. In this way, the study of the complex reactions having place in a PIS is yet to be fully understood, and mechanisms to be clarified.

The further development of the two models presented during this work will help to obtain many physical properties of the systems that were of difficult access to the date. These are propagation and termination coefficient rates and its variation with monomer conversion, and the variation of viscosity in a polymerization system.

The work here presented may be just the first step into the development of new techniques that can improve the current approaches to the study of photopolymerization mechanisms, where a much more detailed control of the physical parameters, may lead to the synthesis of new materials with very specific properties.

The study of Astrazone Orange, for instance, may be continued in order to find the better way to take profit of its viscosity dependent photophysics, which can be very useful in polymerization, as it was demonstrated all along these six chapters. The synthesis of alternative derivatives and its effect on its photophysics may lead to a much more efficient dye to use in polymerization.

(French version)

Le processus de photopolymérisation a été étudié tout au long de ce travail de thèse.

La photophysique de l'Astrazone Orange R a été étudiée et son mécanisme de désactivation a été démontré. Le comphorméère E1 represente plus de 92% de la population de l'état fondamental de l'AOR à 20°C. Une réaction d'isomérization a lieu depuis l'état excité, laquelle dépend de la viscosité et régule la fluorescence. Ce procès fait de l'AOR un photoamorceur très efficace dans le milieu visqueux.

La possibilité d'un effet synergique dans les 3-C PIS a été analysée. Des PIS utilisables pour la polymérisation avec différentes longueurs d'onde ont été trouvés. Deux façons différentes à l'étude des PCIS ont été présentées : celle du LFP, et celle de la photolyse du colorant.

Dans la deuxième partie de ce travail, les mécanismes de PLP ont été étudiés. Un modèle a été développé pour le calcul des constants de vitesse de propagation et terminaison et sa dépendance avec la conversion du monomère.

L'efficacité de plusieurs PIS pour polymérisation avec de la lumière verte a été étudiée. Son efficacité a été analysée et comparée.

Finalement, l'effet de la viscosité initiale sur l'efficacité de la polymérisation a été étudié en CW et PLP.

Plusieurs perspectives se sont dégagées de ce travail.

La photopolymérisation est une technique ayant un très grand potentiel devant être développée dans les prochaines années. Plein d'applications sont possibles dans l'industrie des matériaux donc l'étude des réactions qui ont lieu dans un PIS doivent toujours être clarifiés.

Le développement des deux modèles présentés dans ce travail pourrait faciliter le calcul de plusieurs propriétés des systèmes qui sont difficilement accessibles à l'heure actuelle.

Le travail présenté est juste le premier pas dans le développement de nouvelles techniques qui pourrait améliorer les études existantes des mécanismes de photopolymerisation.

Les études sur l'AOR devraient être continuées pour pouvoir trouver une façon de profiter de son complexe photophysique. La synthèse des dérivâtes d'AOR pourrait donner lieu à des photoamorceurs beaucoup plus efficaces pour la polymérisation.